Coastal Risk Assesment for Ebeye

Technical report

Deltares

Coastal Risk Assessment for Ebeye

Technical report

Alessio Giardino
Kees Nederhoff
Matthijs Gawehn
Ellen Quataert
Alex Capel

1230829-001

Deltares

Title
Coastal Risk Assessment for Ebeye

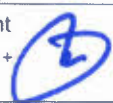| Client	Project	Reference	Pages
The World Bank	1230829-001	1230829-001-ZKS-0001	142

Keywords
Coastal hazards, coastal risks, extreme waves, storm surges, coastal erosion, typhoons, tsunami's, engineering solutions, small islands, low-elevation islands, coral reefs

Summary
The Republic of the Marshall Islands consists of an atoll archipelago located in the central Pacific, stretching approximately 1,130 km north to south and 1,300 km east to west. The archipelago consists of 29 atolls and 5 reef platforms arranged in a double chain of islands. The atolls and reef platforms are host to approximately 1,225 reef islands, which are characterised as low-lying with a mean elevation of 2 m above mean sea level. Many of the islands are inhabited, though over 74% of the 53,000 population (2011 census) is concentrated on the atolls of Majuro and Kwajalein.

The limited land size of these islands and the low-lying topographic elevation makes these islands prone to natural hazards and climate change. As generally observed, small islands have low adaptive capacity, and the adaptation costs are high relative to the gross domestic product (GDP).

The focus of this study is on the two islands of Ebeye and Majuro, respectively located on the Ralik Island Chain and the Ratak Island Chain, which host the two largest population centres of the archipelago. In particular, the client (The World Bank) has approached Deltares for the development of a coastal hazard assessment for these two islands. The following hazards are analysed as part of the study: waves, storm surges, typhoons and tsunamis. The direct impacts (inundation and coastal erosion) are evaluated specifically for the island of Ebeye. The analysis is carried out for different return periods and expected climate change scenarios and sea level rise. The hazard assessment is then used as a basis to carry out the coastal risk assessment, where information on hazards is combined with information on exposure and vulnerability. The output from the risk assessment allows the determination of weak spots where adaptation measures may be required at present or in the future and for which a conceptual design and cost-estimate is presented. Also, the developed method is used to test the effectiveness of each of these measures, in achieving the predefined objective in terms of risk reduction. This is a very effective strategy for reducing the total investment costs and maximizing the future benefits of the interventions.

Version	Date	Author	Initials	Review	Initials	Approval	Initials
	October 2017	Alessio Giardino		Ap van Dongeren (Executive Summary + Chapter 1, 2, 3, 4, 5, 6, 10, 11 + Appendix A, B)		Frank Hoozemans	
		Kees Nederhoff		Dirk-Jan Walstra (Chapter 7)			
		Matthijs Gawehn		Mark de Bel (Chapter 8 and 9)			
		Ellen Quataert		Marcel van Gent (Chapter 8 and 9 + Appendix C)			
		Alex Capel					

State
final

Deltares

Title
Coastal Risk Assessment for Ebeye

Client	Project	Reference	Pages
The World Bank	1230829-001	1230829-001-ZKS-0001	142

Deltares

Contents

Appendices

1 Executive Summary

The Republic of the Marshall Islands (RMI) consists of an atoll archipelago located in the central Pacific Ocean, stretching approximately 1,130 km north to south and 1,300 km east to west. The archipelago consists of 29 atolls and 5 reef platforms arranged in a double chain of islands named Ratik and Ralik (Owen at al., 2016). The atolls and reef platforms are host to approximately 1,225 reef islands, which are characterised as low-lying with a mean elevation of 2 m above mean sea level.

The limited land size of these islands and the low-lying topographic elevation makes these islands prone to natural hazards originating from the sea. Moreover, the impact of those hazards is likely to increase dramatically in the future considering the effect of sea level rise and climate change.

The World Bank has approached Deltares to carry out a hazard assessment for the two islands of Ebeye and Majuro and to perform a relative coastal risk assessment for the island of Ebeye (Figure 1.1). The coastal risk assessment is the basis for identifying priorities areas of interventions. For those areas where the estimated risks are higher, a conceptual design and an indicative cost estimate of suitable coastal protection measures is proposed.

Figure 1.1   Aerial view of the two islands of Ebeye (left figure) and of the DUD (Delap-Uliga-Djarrit) main population centre of the island of Majuro (right figure).

The **hazard** assessment includes the assessment of the impact of the following hazards: extreme waves from the ocean and the lagoon side, extreme water levels (including the effects of tides, inverse barometric effects, wind stress and ENSO effects), typhoons and tsunamis. Extreme events, with different return periods, and for different time horizons (i.e. accounting for the effect of sea level rise and climate change) have been estimated.

The first step, in order to carry out the hazard assessment, consisted in collecting the necessary input **data**: bathymetric data, topographic data, water levels, wind and waves. In particular, measured data were not available at Ebeye at the start of the current project. Therefore, a variety of data sources were used to achieve the scope of the project: measurement data collected at nearby locations, data from global models and field data collected during the field visit. It is highly recommended that more detailed data is to be collected before detailed design and implementation of the proposed solution, in order to reduce the uncertainties in the flooding maps and optimize the design, with a possible reduction of the estimated construction costs.

Figure 1.2 shows the results of a preliminary topographic survey over the island of Ebeye. The figure shows how most of the island is located approximately between 0 m and 3 m, with the higher part of the island located at the ocean side and lower at the lagoon side, as consistent with literature data at other similar atoll islands. As a result of the island topography, it follows that, although hazards from the lagoon are generally lower than those from the ocean side, houses and infrastructures located at the lagoon side may also be subjected to flooding because of their very low topographic location.
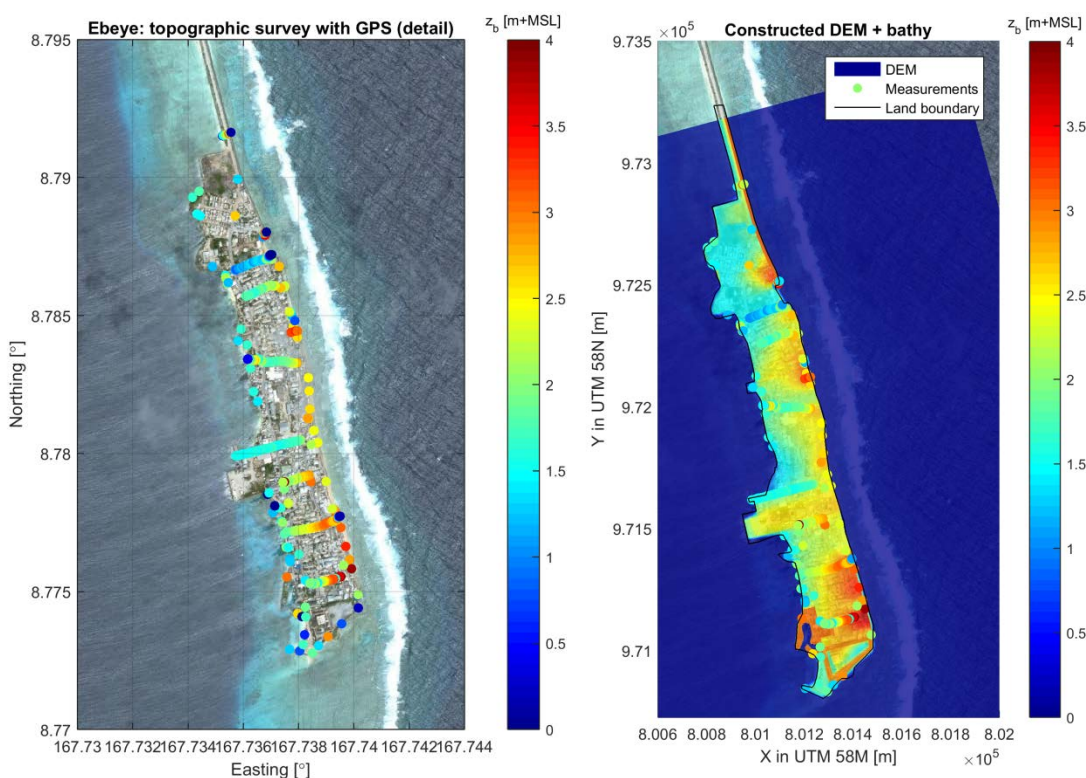
Figure 1.2   Measured topographic point (left figure) and interpolated digital elevation map (right figure).

The results from the **hazard** quantification have shown that the main source of hazards is: large swell waves and typhoons, both reaching the islands from the ocean. Tsunamis are estimated to be a minor source.

Swell waves are waves that are generated by far-away storms and travel across oceans. These waves typically have long wave periods (the time difference between the individual crests of waves) and can reach offshore wave heights of up to 4 meters for extreme events

with a return period of 50 years. Since they are not associated with local storms they can impact islands like those in RMI on sunny days without any other warning.

Pacific typhoons generally develop around the Marshall Islands, with an occasional full impact on the islands. Only 30 tracks were found over the Marshall Islands between 1979 and 2015, with a wind speed larger than 18 m/s (the threshold for storm with an intensity of tropical storm or higher; Figure 1.3).

On the other hand, most of the tsunami waves that have been recorded from the past large events from mega thrust earthquakes (e.g. 2011 Tohoku tsunami) resulted in minor impact (i.e. inundation) at the RMI. For example, offshore tsunamis waves generated by the Tokoku event in 2011 were estimated at less than 1 m in the RMI and occurred at low tide therefore not causing remarkable damages (Hess et al., 2015; Robertson and Hwang, 2015).
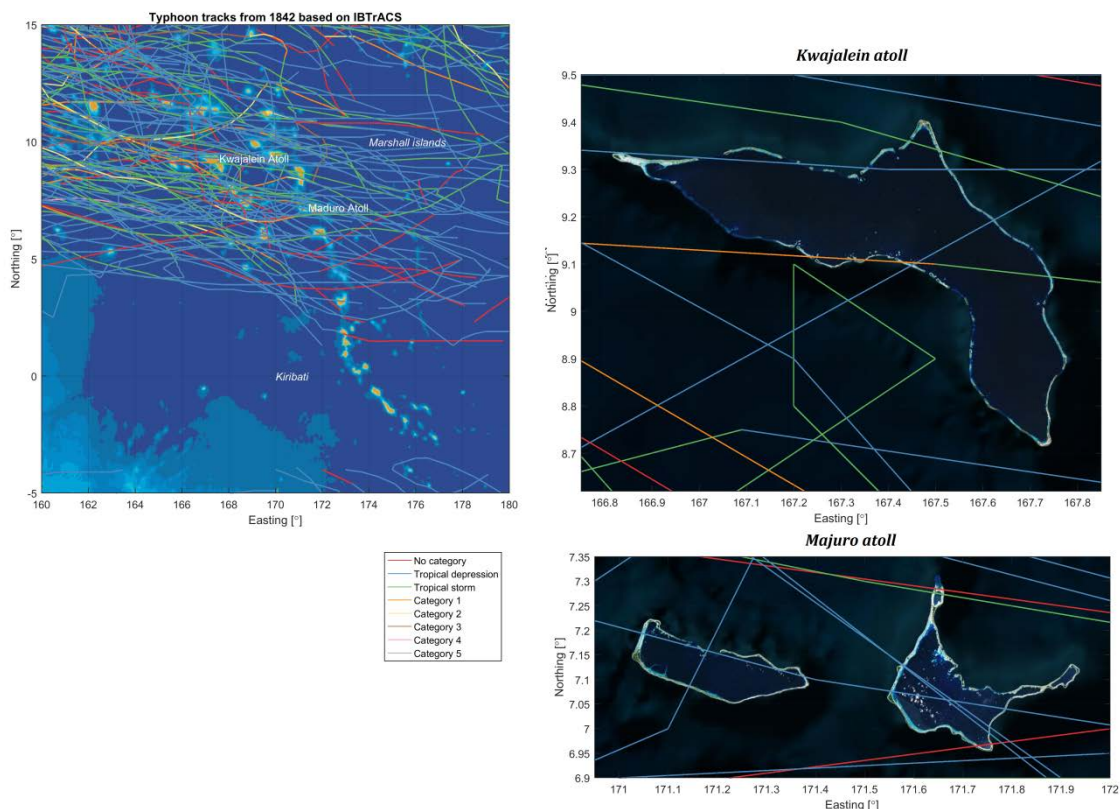
Figure 1.3   Typhoon tracks from 1945 across the study area per category based on IBTrACS database (https://www.ncdc.noaa.gov/ibtracs/. Left upper panel: area of interest around RMI. Right upper panel: zoom on Kwajalein atoll. Right lower panel: zoom on Majuro. Colours indicate Saffir-Simpson hurricane scale)

Offshore hazards were translated into **impacts** over the island by means of numerical modelling calculations, supported by the XBeach code (Roelvink et al., 2009) and simple calculations freely available via the SimpleCoast website (http://www.simplecoast.com/). In particular, the following impacts were considered: flooding and coastal erosion.

According to model results, swell waves are the main source of **inundation** when considering more frequent events (return periods lower than 30 year). On the other hand, the major but less frequent inundations (return periods larger than 30 years) are caused by typhoon events.

Wind waves from the lagoon can also result in flooding of the low-lying areas located at the lagoon side (e.g. area between the North Camp and the port). This observation is also supported by information collected from local inhabitants.

The largest flooding events (i.e. return period of 10 years of larger) from the ocean may lead to inundation of the entire island, with water crossing the entire island and reaching the lagoon from the ocean side. This already occurs in the present situation. Figure 1.4 and Figure 1.5 show two examples of computed flooded maps for events with a return period of 10 years, in the present situation and in the year 2100. The same information is summarized in Table 1.1. The table provides an overview of the percentage of inundated areas, flooded by more than 20 cm of water, for different return periods, and considering different time horizons under sea level rise scenarios RCP 4.5 (reduced CO_2 emissions) and RCP 8.5 (business-as-usual).

It is noteworthy that the inundation area for the lower return periods (5 years) is likely to increase with a factor 3-4 from the present situation to the situation in 2100, depending on the RCP scenario. On the other hand, the increase in flooding extension for events with the highest return periods (50 years) is likely not to increase considerably as the situation is already critical in the current situation. This essentially means that the island is likely to get flooded more frequently when no adaptation option is implemented, due to the increase in water depth and wave height approaching the coast.

Deltares
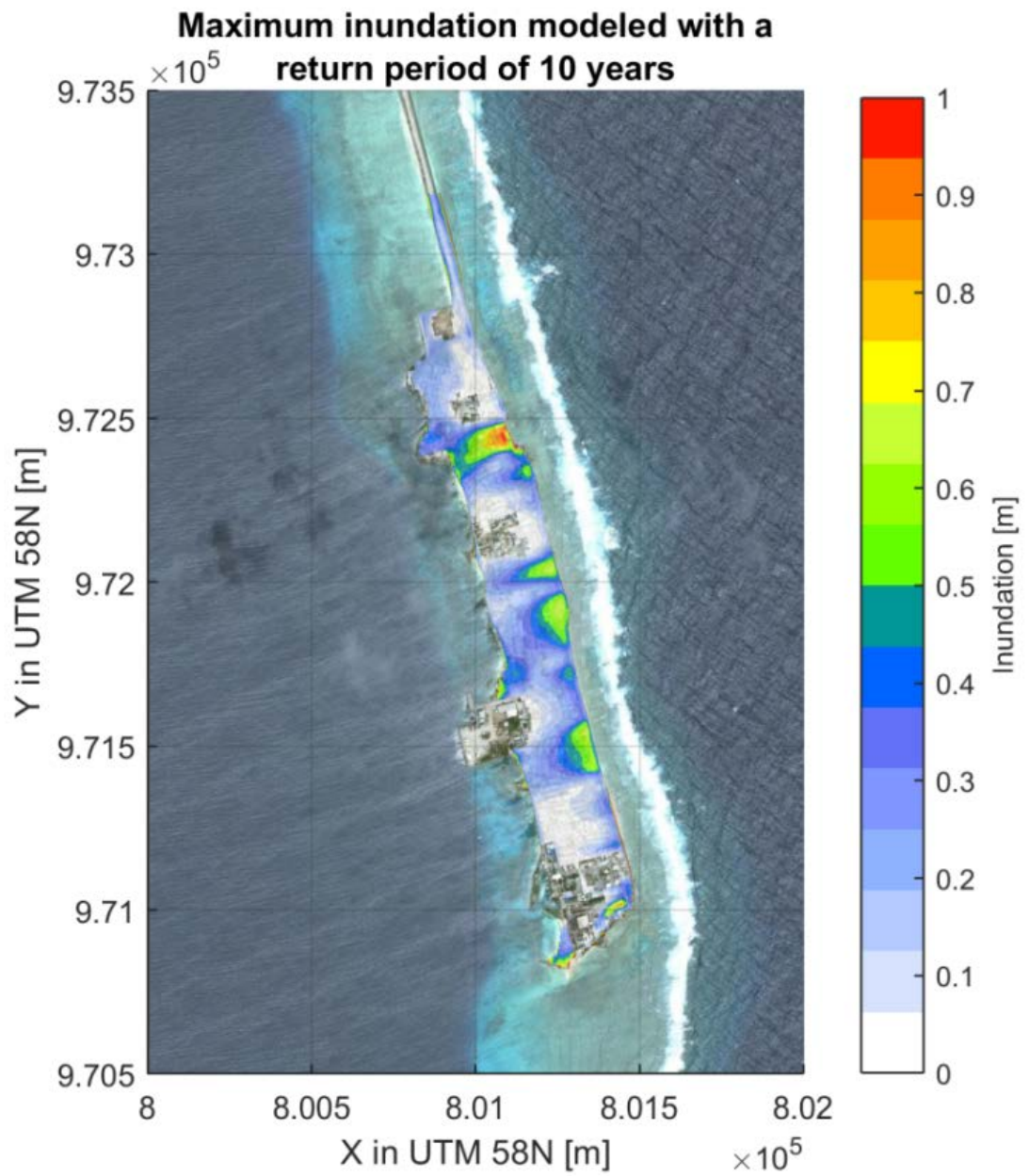
Figure 1.4   *Inundation map showing the maximum impact of coastal hazards for the current situation, and considering a return period of 10 years.*
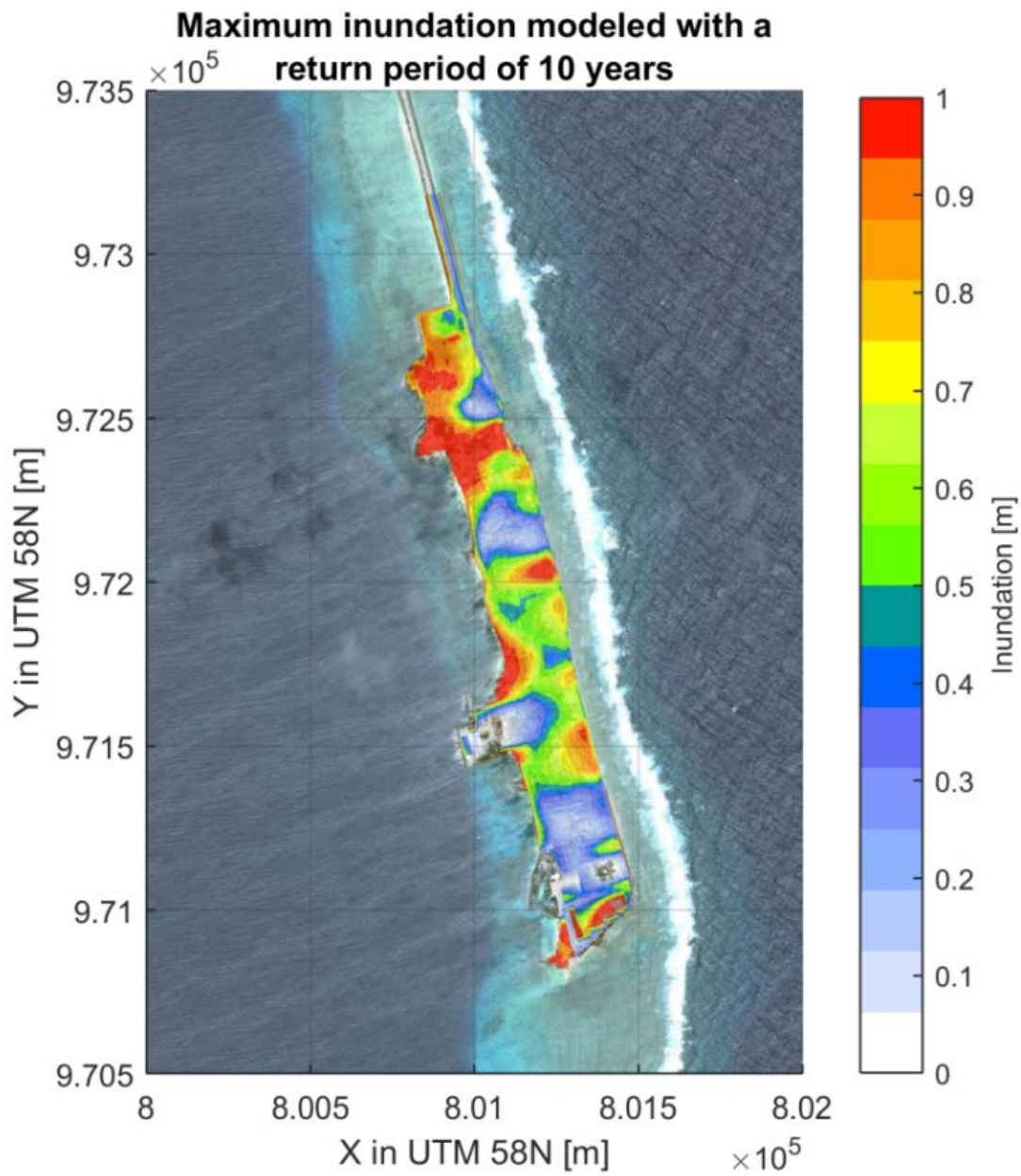
Figure 1.5   Inundation map showing the maximum impact of coastal hazards for sea level rise scenario RCP 8.5
2100, and considering a return period of 10 years.

Table 1.1 *Percentage of maximum island inundation with return periods 5, 10, 30 and 50. The % relative to the island area is given for a minimum inundation depth of 20 cm.*

[%] of island inundation (>20 cm)				
RP [yr]	Current SLR = 0 m	RCP 4.5: 2030 SLR = 0.12 m	RCP 4.5: 2050 SLR = 0.23 m	RCP 4.5: 2100 SLR = 0.53 m
5	21.7	30.1	41.0	61.1
10	30.2	40.7	47.9	66.2
30	69.9	76.4	80.7	87.0
50	90.0	93.4	93.3	94.0
RP [yr]	Current SLR = 0 m	RCP 8.5: 2030 SLR = 0.13 m	RCP 8.5: 2050 SLR = 0.26 m	RCP 8.5: 2100 SLR = 0.78 m
5	21.7	33.0	43.1	74.0
10	30.2	41.4	50.3	78.2
30	69.9	76.7	82.2	91.8
50	90.0	93.4	93.4	94.1

In a similar way, overtopping rates have been computed at two sections of the rock revetment which protect the northern part of the island and the causeway from the ocean side. In particular: one section at the newly constructed revetment with a measured crest level of approximately 3.1 m above mean sea level, and one section at the old revetment, with a crest level of approximately 2.2 m (see Figure 1.6). Discharge volumes (also defined as overtopping rates) in the current situation, at the two sections, and for different return periods, are shown in Figure 1.7. On the same figure, the threshold value of 50/l/s/m is also indicated, representing the serviceability limit state.

The Figure shows how this limit is over exceeded at both sections of the revetment already in the current situation, for events with a return period of 1 year or larger. Especially, the overtopping rates at the poorly-constructed revetment are extremely high (few thousand l/s/m).

Figure 1.6 *Left picture: well-constructed revetment. Right-picture: poorly constructed revetment.*
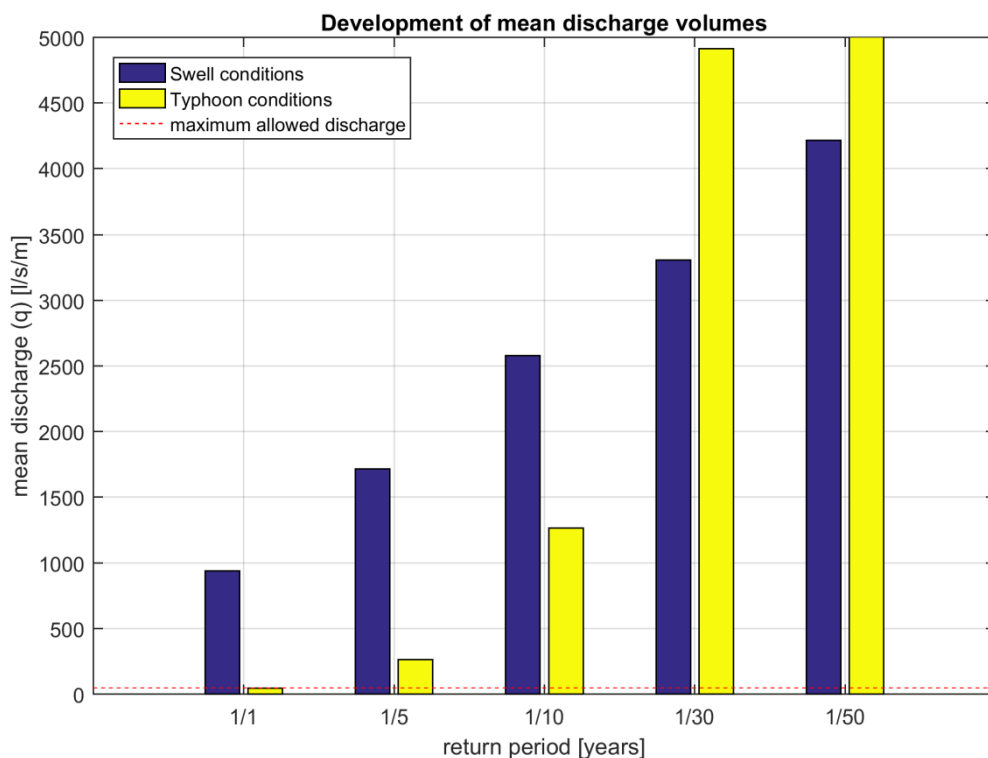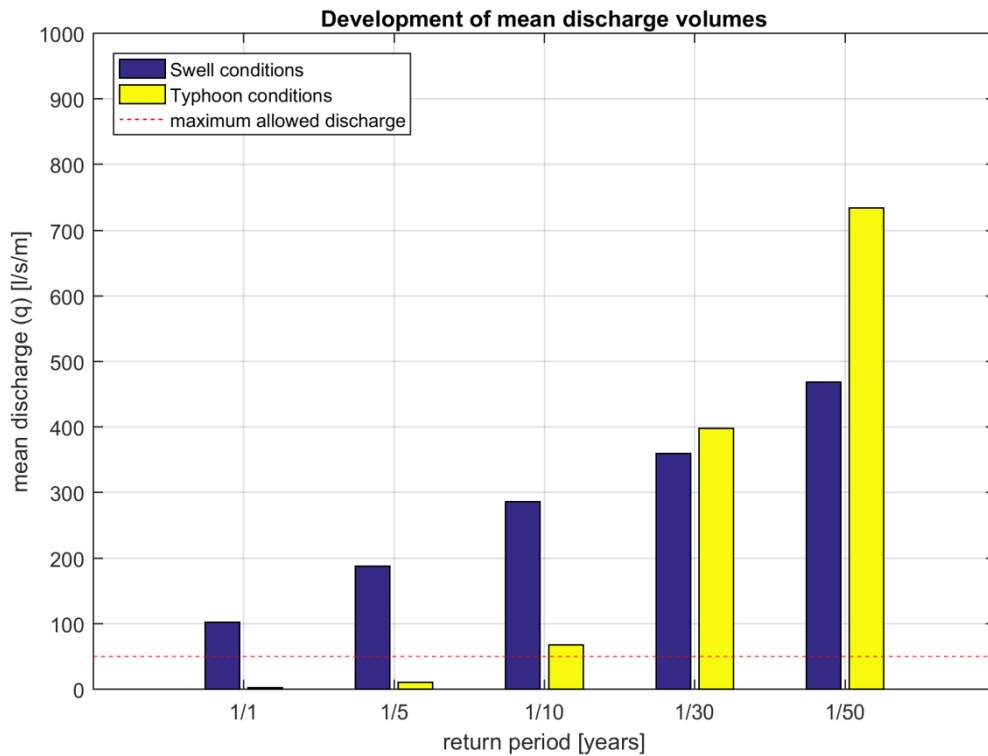
Figure 1.7   Mean overtopping discharge based on the EurOtop Overtopping Manual (2007) as a function of the return period, forced with nearshore XBeach values for different return periods and contributions. Upper panel for the well-constructed revetment. Lower panel for the poorly constructed revetment. The horizontal red dashed line indicates the serviceability limit state of 50 l/s/m. Both figures refer to the present condition.

Coastal erosion is in general a complex phenomenon which can be the result of many different causes, some of them naturogenic and others anthropogenic, acting at different temporal and spatial scales. In this study, only the effect of storm-induced erosion and area loss due to sea level rise were assessed. The assessment was carried out by means of simple relations, without the use of any morphological model. Sea level rise is likely to lead to a coastal retreat, of a magnitude depending on the actual sea level rise rate and provided that there is a sufficient accommodation space to allows for this retreat. Figure 1.8 shows the coastal retreat for two representative profiles on the island.

The information on flooding levels and coastal erosion, are then combined with the information on exposure (Figure 1.9) and vulnerability over the island, in order to produce a full risk assessment.
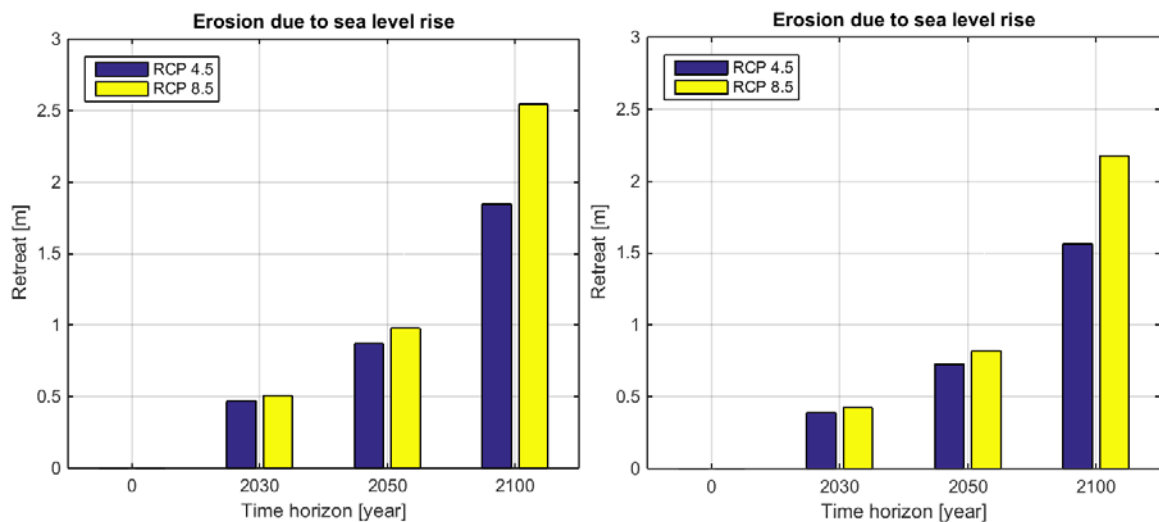
Figure 1.8 Coastal horizontal retreat due to sea level rise for transect 3 (left panel) and transect 6 (right panel). The definition of transects is shown in Section 7.3.2 of the report. Retreat values are shown for each time horizon and climate change scenarios RCP 4.5 (blue bars) and RCP 8.5 (yellow bars).
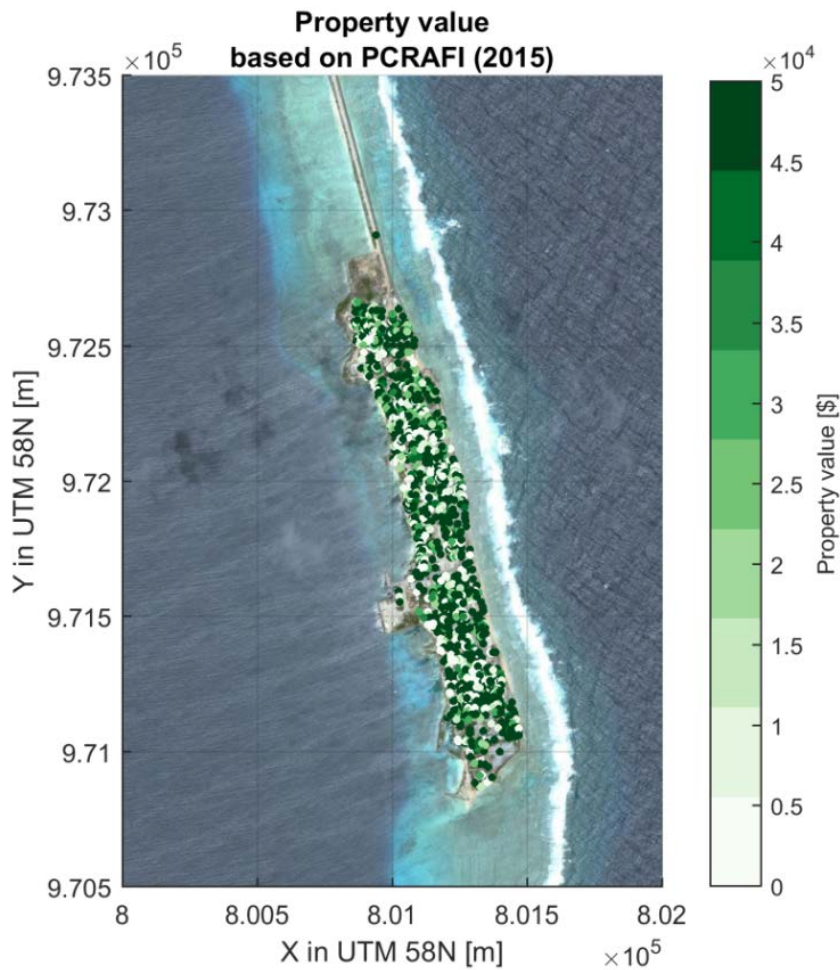
Figure 1.9   Exposure data (property values) for Ebeye island (PCRAFI, 2015).

The results from the coastal risk assessment are shown in Figure 1.10, indicating risks based on expected annual damages (EAD) for the current situation and in the future under RSP scenario 8.5. The results from the risk assessment indicate that, in general, risks on the ocean side are higher than on the lagoon side. Those risks are likely to increase in the future due to sea level rise. The risk assessment was used as a basis to identify the location of possible interventions.

Two hot-spots can be visible in the present situation, both located at the ocean side: one in the north and one in the central part of the island. These two locations stand out as locations at higher risks due to a combination of: high exposure and low topographic elevation.
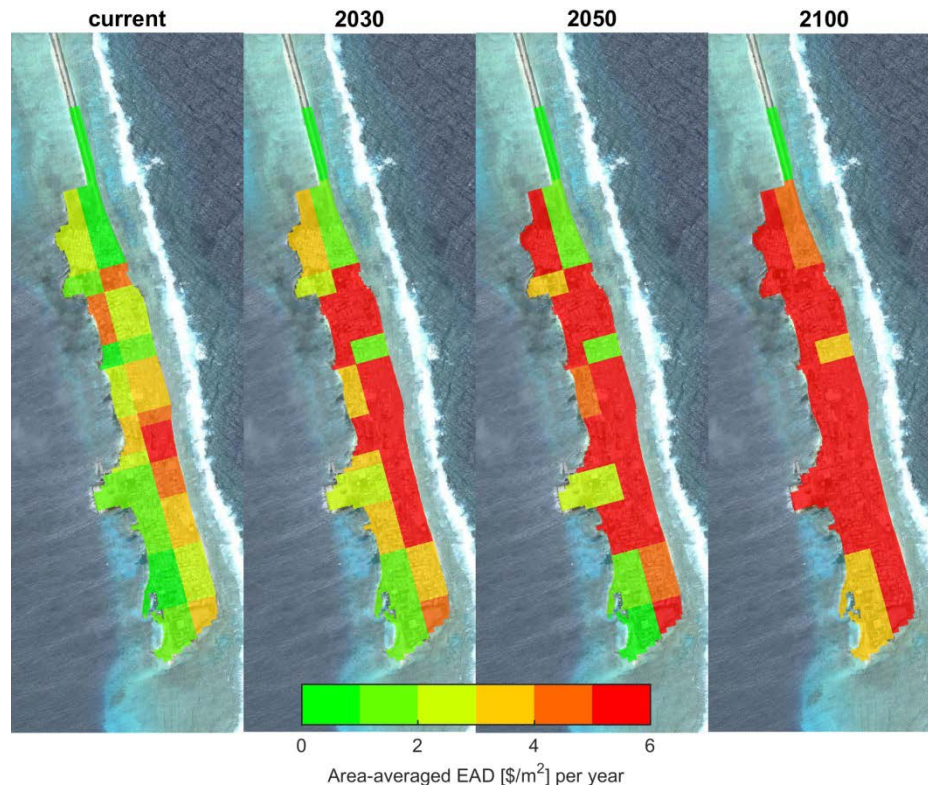
Figure 1.10 EAD in USD/m2 per area in RCP 8.5 for all time horizons.

Conceptual designs of possible solutions have been proposed based on information on: local wave climate, hydraulic performance, accessibility to shore, maintenance costs, flexibility and durability. A revetment type of solution appears the most suitable type of intervention for the Ebeye situation. Different conceptual designs of the revetment have been proposed. Our preferred solution is a revetment combined with a berm in front of it, which may be more flexible also in case of sea level rise and, therefore, higher waves approaching the coast (Figure 1.11). This design, even when these more critical conditions will occur, will still promote wave breaking due to the presence of the berm in front of the revetment. Therefore, the solution can be considered flexible and easily adaptable, with minimal effort, to these more severe conditions. The recommended construction scheme, in order to reduce cost, is based on the use on the use of single-layer cubes, instead of rocks.
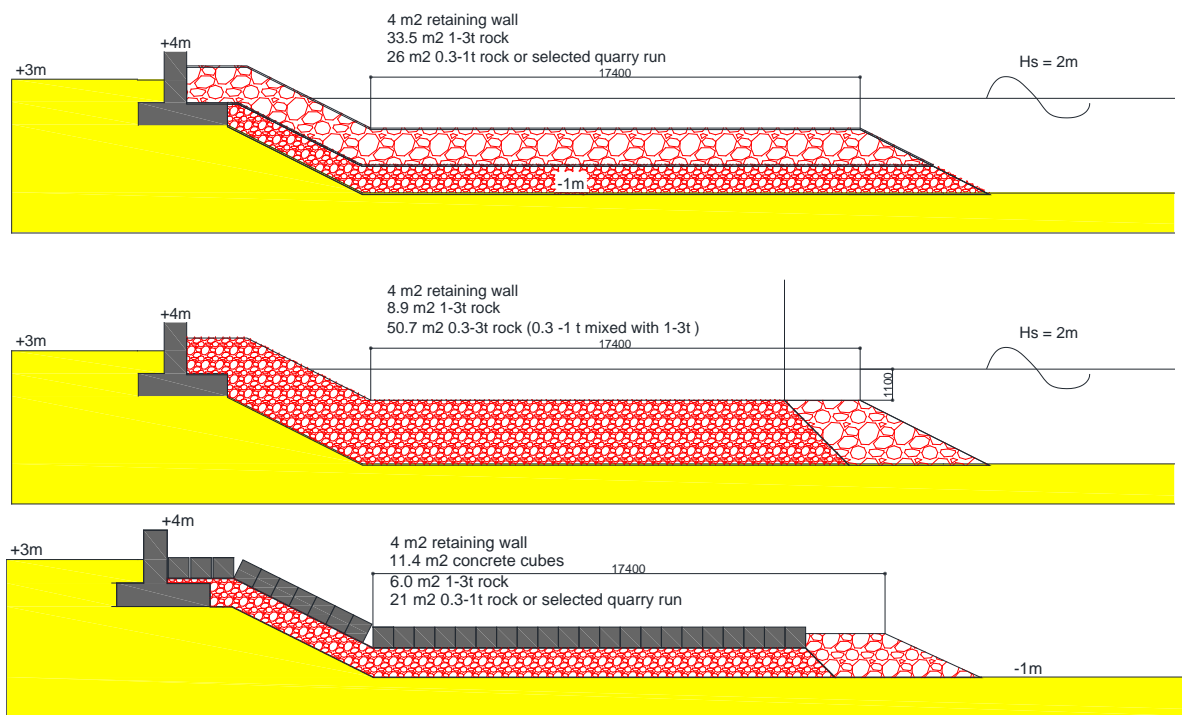
Figure 1.11 Durable berm type solutions, adaptable to conditions in case of sea level rise.

Ranges of costs per linear meter for the construction of suitable revetment designs have been provided. These costs range between 16,000 up to 25,000 USD per linear meter, according to the material used for construction (respectively single-layer cubes or rocks). These values provide a first-order indication and they assume the use of imported aggregates for constructions. Costs may vary largely depending on the material and methods used for construction. Also, costs will depend on the final design of the structure.

The final price per linear meter and the available budget will determine the length and location of the structure which can be built. Four options have been evaluated in the study, depending on the available budget (Figure 1.12):

    a)   Revetment protecting the complete coastline at the ocean side
    b)   Revetment protecting only the two hot-spots
    c)   Revetment protecting the central part of the island
    d)   Revetment protecting the causeway

The effectiveness of the four different options in terms of reduction in expected annual damages (EAD) has been tested by means of the same risk analysis procedure as used for the determination of the hot-spot locations in the reference situation. The results are summarized in Table 1.2 for solutions at different locations and for two different designs: a standard revetment and a revetment with berm.
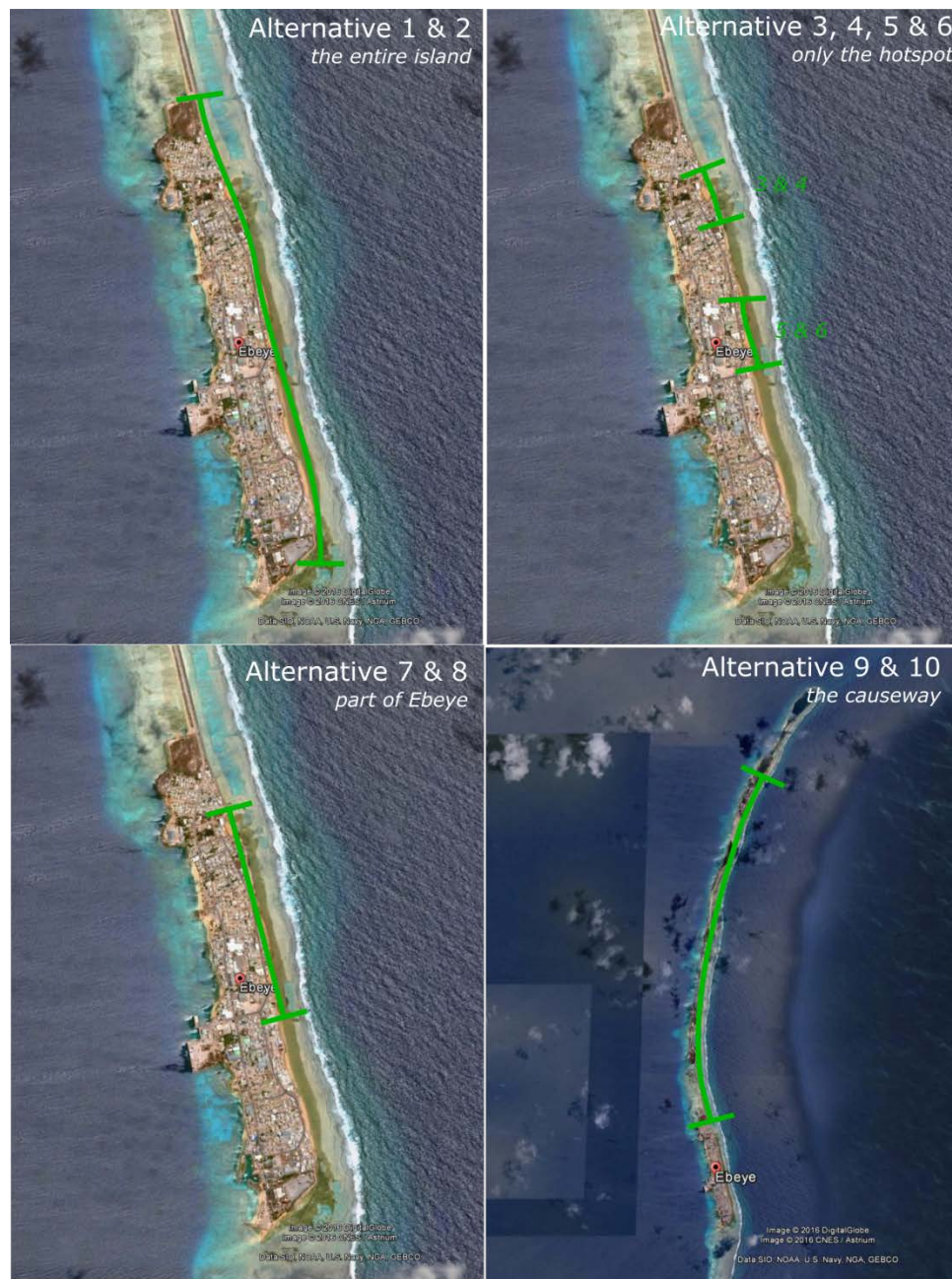
Figure 1.12 Different proposed locations for the adaptation options

Deltares

Table 1.2   Adaptation options with costs and benefits.

#	Location	Revetment type	Length [km]	Costs [million $]	Decrease EAD [million $]	Decrease EAAP [people]	Ratio Decrease EAD/Costs [%]
1	Entire island of Ebeye	Standard	2000	$28.0	$0.71	3256	3%
2	Entire island of Ebeye	Berm	2000	$32.6	$0.70	3335	2%
3	Hotspot location 1	Standard	260	$3.6	$0.51	629	13%
4	Hotspot location 1	Berm	260	$4.2	$0.54	959	12%
5	Hotspot location 2	Standard	260	$3.6	$0.29	440	7%
6	Hotspot location 2	Berm	260	$4.2	$0.30	631	6%
7	Hotspot location 1 +2 and in between	Standard	1060	$14.8	$0.73	3437	5%
8	Hotspot location 1 +2 and in between	Berm	1060	$17.3	$0.70	3311	4%
9	Entire causeway	Standard	6000	$83.9	$1.00	0	1%
10	Entire causeway	Berm	6000	$97.9	$1.00	0	1%

The most effective solutions are the ones meant to protect the areas in front of the hot-spots directly. However, from an engineering point of view, it will be easier to construct a continuous revetment, including the hot-spots. Protecting the causeway score lower in terms of effectiveness buy it may provide interesting opportunities for long-term development of the island, including possible relocation of part of the population of Ebeye towards the island of Gugeegue. Our recommendation (provided that sufficient funding is available) would be the construction of a revetment protecting the entire ocean side of the island as well as the southern tip, in order to avoid possible side-effects induced by the revetment (i.e. local erosion at the end of the revetment).

The solution for coastal protection recommended in the study (i.e. revetment at the ocean side of the island) is however just one of the option for reducing risks. Other possible options are related to the reduction of the exposure and vulnerability components. The analysis proposed methodology could be used as a basis for a long-term adaptive planning of the island.

2 Introduction

2.1 Introduction

The Republic of the Marshall Islands (RMI) consists of an atoll archipelago located in the central Pacific, stretching approximately 1,130 km north to south and 1,300 km east to west. The archipelago consists of 29 atolls and 5 reef platforms arranged in a double chain of islands named Ratik and Ralik (Owen at al., 2016). The atolls and reef platforms are host to approximately 1,225 reef islands, which are characterised as low-lying with a mean elevation of 2 m above mean sea level. Many of the islands are inhabited, though over 74% of the 53,000 population (2011 census) is concentrated on the atolls of Majuro and Kwajalein.

The limited land size of these islands and the low-lying topographic elevation makes these islands prone to natural hazards. As generally observed, small islands have low adaptive capacity, and adaptation costs are high relative to gross domestic product (GDP). The likelihood that a hazardous event will have a significant impact on the Marshall Islands has risen with the increasing levels of population and assets in the urban areas of Majuro and Ebeye (Kwajalein atoll) (PCRAFI, 2015). In addition, climate change effects will also increase the likelihood of a hazard.

Risk assessments are objective useful tools to identify most vulnerable areas and for reducing those risks. Risk is, by definition, the product of hazard, exposure and vulnerability. Hazard is the probability that an event of a certain magnitude and with a negative impact (e.g. inundation) will occur. While hazard is related to the physical system aspects of risks, exposure and vulnerability encompass socio-economic characteristics. More specifically, exposure relates to exposed assets and people and, in the case of assets, refer to the total value of properties found in the inundated area. The last factor, vulnerability, refers to the damage inflicted upon exposed property in case of inundation (Kron, 2005).Therefore, a risk assessment generally involves the quantification of these three components. Once a risk analysis is carried out, possible different adaptation measures can be tested, in order to evaluate the effectiveness of each of them in achieving the predefined objective in terms of risk reduction.
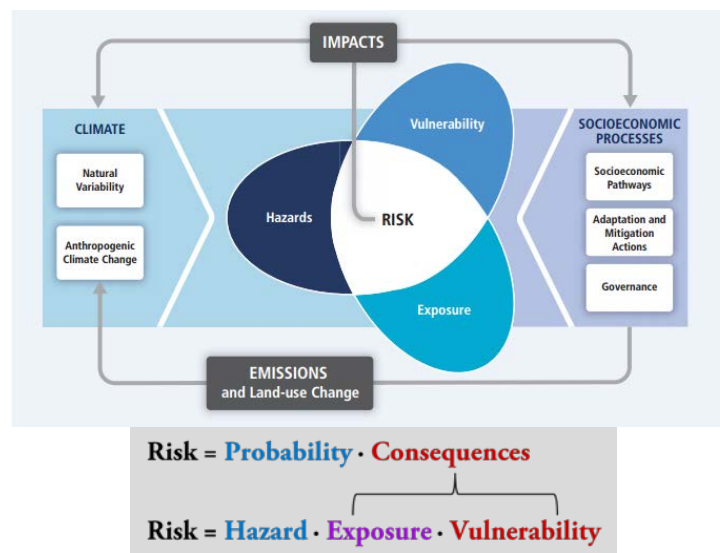
Figure 2.1   Definition of risk (IPCC, 2014; Kron, 2005).

According to the fourth assessment of the International Panel of Climate Change (IPCC), the potential impacts of climate change and variability on small islands were presented as follows:

- Sea-level rise is expected to exacerbate inundation, storm surge, erosion and other coastal hazards, thus reducing the island size, threatening vital infrastructure, settlements, and facilities that support the livelihood of island communities.
- Limited water resources in small islands are especially vulnerable to future changes, and distribution of rainfall is likely to be seriously compromised.
- Increasing sea surface temperature, rising sea level, and growing ocean acidity are very likely to affect the health of coral reefs and other near shore, marine and coastal ecosystems. These impacts exacerbate non-climate change-related stresses on the systems.
- Changes in the occurrence and intensity of El Niño-Southern Oscillation (ENSO) events are likely to have severe impacts on commercial and artisanal fisheries. Forests on many small islands can easily be decimated by violent cyclones or storms, while increases in extreme events affect the adaptation capacity of the slow-regenerating forests.
- Sea-level rise, inundation, seawater intrusion into freshwater lenses, soil salinization and decline in water supply are very likely to adversely impact coastal agriculture. Away from the coast, changes in extremes (e.g., flooding and drought) are likely to have a negative effect on agricultural production.
- Effects of climate change on tourism are likely to be direct and indirect, and largely negative. Sea-level rise and increased sea water temperature will cause accelerated beach erosion, degradation of coral reefs, and bleaching. In addition, a loss of cultural heritage from inundation and flooding reduces the amenity value for coastal users. Water shortages and increased incidence of vector-borne diseases may also deter tourists.

The World Bank has approached Deltares to carry out a hazard assessment for the two islands of Ebeye and Majuro and a relative coastal risk assessment for the island of Ebeye (Figure 2.2 and Figure 2.3). The coastal risk assessment will be the basis for identifying priorities areas of interventions. For those areas where risk will be higher, a conceptual design and an indicative cost estimate of suitable coastal protection solutions will be proposed.

2.2 Study site description

The area of interest is located in the Western Pacific Ocean and consists of a group of atolls that form the Republic of the Marshall Islands (Figure 2.2).

Ebeye is built on a small islet on the south eastern side of Kwajalein Atoll (8.78°N 167.74°E), see Figure 2.3. The part above sea level stretches about 2 km from north to south and is approximately 250 m wide bordering a large lagoon to the east and the open ocean to the west. The lagoon is shallow with an average depth (d) of approximately 40 m. On the eastern ocean side, the islet is fronted by a reef flat. This reef flat varies slightly in width between 100-130 m. From there on, the depth quickly increases, reaching depths of ~6000 m just a few kilometres out the coast. The islet is covered entirely with buildings and infrastructure and

hence densely populated. About 12,000 inhabitants live in an area of merely 0.36 km^2, i.e. 1 person per 30 m^2.

The main part of the capital lies on the eastern side of Majuro Atoll (7.09°N 171.38°E) and has a half-moon shape, following the islands geology, see Figure 2.3. The estimated total length of the city is about 20 km and varies in width between 100-550 m. Similar to Ebeye, the parts of the lagoon next to the city are mostly shallow with depths of 0.5 - 5 m, and reaching depths of about 35 m in the lagoon. The reef flat on the ocean side is typically 200 m wide in the east, whereas it is narrower in the south, being about 80 m wide. The total population of the capital Majuro is about 27.000 people.
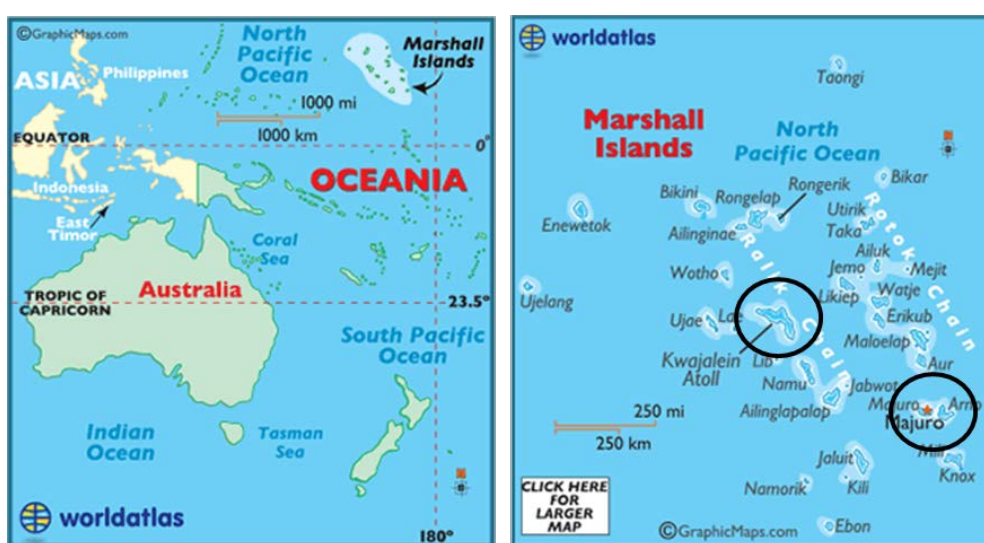
Figure 2.2 Geographical location of the Marshall islands (source: http://www.worldatlas.com/webimage/countrys/oceania/mh.htm). The two atolls of Kwajalein and Majuro are highlighted with the two circles.

Figure 2.3 Aerial view of the two islands of Ebeye (left figure) and of the DUD (Delap-Uliga-Djarrit) main population centre of the island of Majuro (right figure).

3 Objectives of the study

The present assignment is part of a larger "Climate Resilient Coastal Protection Project", with the objective of improving early warning systems, reducing risk to climate change effects and coastal hazards through investments in shoreline protection, mitigating the financial impact of protection of RMI. Communities exposed to storm surges, king tides, typhoons, erosion, and sea level rise, will benefit from the project through reduced risk of damage to infrastructure in the coastal zone. The project will also help improving capacity of national and local government agencies adapt to climate change, reduce disaster risk, and set priorities for resilient investments. By it the Marshall Islands population and general economy will also benefit from the project.

The main objective of this present study is to provide a quantification of coastal hazards for Ebeye and Majuro and a coastal risk assessment for the island of Ebeye, which will be used as an input to the final project design, particularly to quantify the scope, extent, and potential coastal investment works. In order to reach this objective, a number of intermediate steps are required and will be undertaken as part of this study:

1   Quantification of coastal hazards. In particular, the following contributors to coastal hazards will be included in the analysis:
•   Deep water wave conditions for extreme events of different return periods
•   Water levels (including the effects of tides, wind stress effect, inverse barometric effect and El Niño–Southern Oscillation (ENSO) effects)
•   Typhoons
•   Tsunamis
•   Climate change effects on waves climates, and sea level rise

The hazards will be quantified for both islands of Ebeye and Majuro.

2   Assessment of the impacts of coastal hazards, in order to quantify the impact of the coastal hazards (i.e. inundation extent and coastal erosion) on the island of Ebeye. This step will make large use of numerical modelling techniques in order to transform the offshore coastal hazards (see 1) to direct impacts on the island.

3   Identification of a relative coastal risk index, including information on the effects of hazards, and exposure.

4   Relative coastal risk assessment, to assess the difference in risks at different locations of the island, for different return periods and time horizons accounting for the effects of sea level rise and climate change.

5   Selection of priority areas of interventions, at locations which will be identified as high risk areas under point 4.

6   Conceptual design of adaptation options and cost-estimate of interventions which can be used an input for the final project design.

4 Methodology

4.1 Introduction

In order to achieve the objectives of the project as described in Chapter 2, the project was separated into five phases:

1   Data collection and numerical models
2   Quantification of coastal hazards,
3   Assessment of the impacts of coastal hazards
4   Coastal risk assessment and selection priority areas for intervention
5   Conceptual design of adaptation options and cost-estimate

The methodology for each phase will be described in this chapter.

4.2 Data collection and numerical models

Different sources are consulted to collect the data needed for the next four phases. Data is collected from open data sources, numerical models, scientific reports, information collected during the field visit and combined with expert judgement. In particular, the following data was used in the study:

- Bathymetry
- Topography
- Water levels
- Wind and waves
- Historical typhoons
- Historical tsunami's
- Climate change and sea level rise
- Exposure

The nature of this data is described in more detail in Chapter 5.1. In addition, this information will be complemented using numerical modelling techniques.

4.3 Quantification of coastal hazards

For the quantification of the coastal hazards at Ebeye and Majuro, the following hazards are assessed:

- Extreme wave conditions (deep water wave height, period and direction) for different return periods: T = 5, 10, 30 and 50 years.
- Water levels at the ocean side and lagoon of the islands. This includes tidal elevation, storm surge and ENSO effects.
- Typhoons. Historical data on typhoon tracks are collected and subsequently used to force a Delft3D model which calculates the typhoon induced surge and waves near Ebeye and Majuro.
- Tsunamis. The quantification of a potential hazard from a tsunami will be based on calculations with a Delft3D model.
- Climate change effects on waves and sea level rise. Local changes in waves and sea level rise will be based on Representative Concentration Pathway (RCP) 4.5 and RCP 8.5 scenarios for the 2030, 2050 and 2100 time horizons.

These coastal hazards are quantified and subsequently used as input for the assessment of the impacts of the coastal hazards on the island of Ebeye.

4.4 Assessment of the impacts of coastal hazards

The quantified coastal hazards will all have an impact on the island of Ebeye. The following impacts will be quantified within this project:

- Inundation extents and depths. The (deep water) hazards will be translated into nearshore impacts (inundation) using a two-dimensional XBeach model of Ebeye. The model will be applied for the different return periods and validated with information collected during the field visit from local stakeholders. The modelling study will result in two-dimensional maps of inundation depths on the island.
- Erosion; structural and due to extreme events. Structural erosion due to sea level rise will be estimated based on the widely known Bruun rule (Bruun, 1962). Coastal erosion during storm events of different return periods will be estimated by means of empirical formula available via the SimpleCoast project (http://www.simplecoast.com/).

The effects of climate change on waves and wind climates and sea level rise will be included in the numerical modelling and empirical calculations, in order to assess how risk may change for different time horizons.

These inundation depths and erosion extents for all hazards (including different return periods and time horizons) will be used as input for the coastal risk assessment.

4.5 Coastal risk assessment and selection priority areas for intervention

The information on the impacts of hazards, exposure and vulnerability will be combined and form a Coastal Index. This Coastal Index will quantify the spatial difference in risks on Ebeye for different return periods and time horizons, accounting for the effects of sea level rise and climate change. The assessment will be based on information from existing databases, satellite images, the field visit and modelling results.

The Coastal Index will be based on tangible and intangible damages, see Figure 4.1. These damages are expressed in a monetary value (USD) per return period, and reflect direct and indirect damages. For the direct damages a certain inundation depth (hazard) results in a certain percentage of damage (vulnerability) to a certain receptor (exposure). Since for multiple return periods the hazards have been determined, it is possible to calculate the Expected Annual Damage (EAD; in $/year) with Equation(4.1). EAD can be interpreted as the average damage over a very long period of time. The EAD is calculated by the integral of the damage times the frequency.

$$EAD = \int_0^1 D(\mathrm{p}) \cdot \mathrm{dP} \tag{4.1}$$

The EAD due to both erosion and inundation will be assessed. The indirect damages and intangible damages will be quantified in $/year, and assumed to be both 10% of the direct damage. Intangible damages are damages related to social and environmental effects (e.g. drowning and inconvenience of people). Indirect damages are related to disruption as a result of the flooding (e.g. removal of debris, loss of wages, etc.). The total EAD (direct and indirect) is calculated for each RCP scenario (4.5 and 8.5) and time horizon (current, 2030, 2050 and 2100). From this set a Coastal Index (CI) is obtained for each time horizon by averaging the

individual EAD's of the RCP scenarios. Selection of the priority areas for intervention will be based on the areas identified with high values of risk as defined in the Coastal Index.
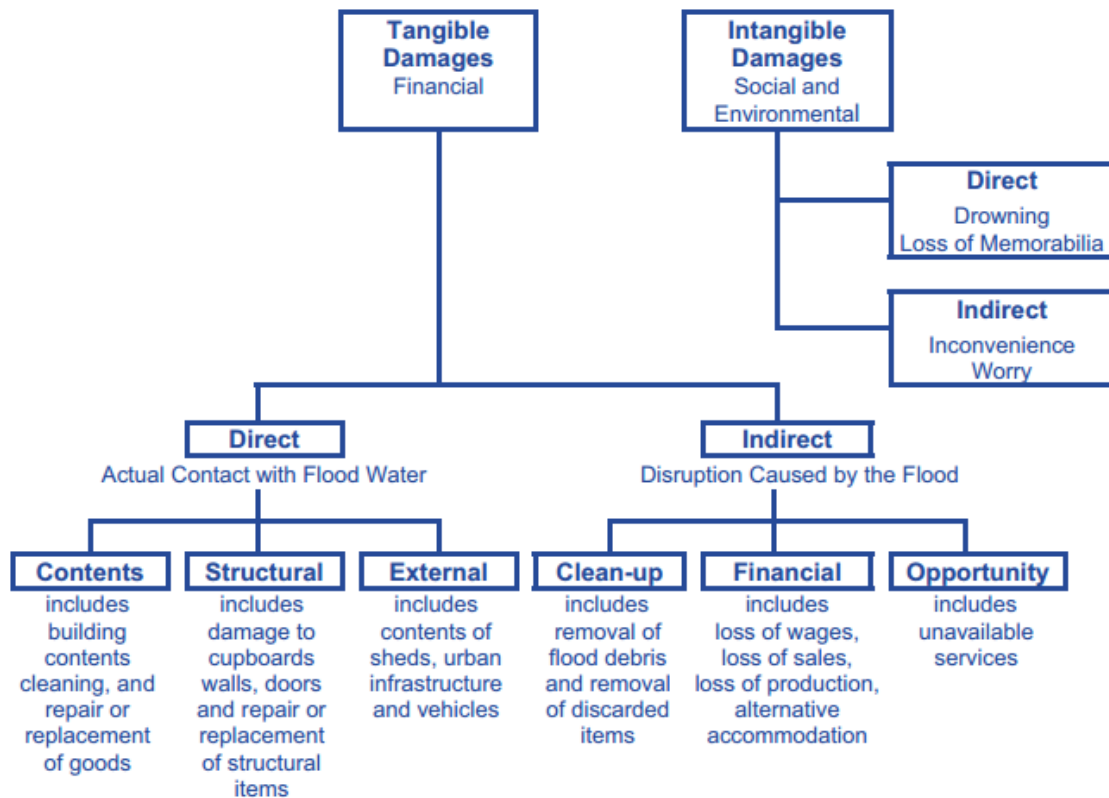
Figure 4.1   Types of damage. Source:
http://www.environment.nsw.gov.au/resources/floodplains/19_flood_manual.pdf

4.6   Conceptual design of adaptation options and cost-estimate

A conceptual design of possible suitable coastal protection solutions will be developed for various segments of the Ebeye coastline. The options will consider:

- Various types of hard or structural, ecosystem-based, and sediment-based solutions appropriate for the prevailing wave, sea, and land conditions;
- The quantified hazards using the numerical models (e.g. nearshore wave heights) and the basic design parameters will be derived based on formula available via the SimpleCoast project (http://www.simplecoast.com/).
- Estimates of constructions costs based on rough bill of quantities. Indicative examples of cost-estimates for similar projects on the islands have been collected before and during the field visit. Moreover, the report from Tonkin+Taylor (2016) has been used, which provides an overview of solutions and costing for coastal protection works in similar environment.
- The feedback on how these solutions may affect the coastal risk index.

Prioritization of investments will be done based on cost-effectiveness, starting with protecting the areas at higher risks in the current situation, and considering a certain available budget. More expensive solutions will also be suggested as part of the study in relation to a longer adaptive time-planning of the island.

5 Data and numerical models

5.1 Introduction

Different sources of data will be used and combined in order to achieve the objectives of the project, as described in Chapter 2. Data sources consist of existing data, which have been complemented with information and data derived during the field mission. In addition, different numerical models will be implemented using those data as input.

5.2 Data description

For the coastal hazards and risk assessment the following data types and information are collected: bathymetry, topography, wind-, wave-, and water level data, typhoon tracks and intensity, tsunamis from regional sources, climate change effects and exposure data.

5.2.1 Bathymetry

Subtidal (i.e. deepwater) bathymetry data will be derived as a combination between bathymetric data of the Republic of the Marshall Islands and Vicinity (Hein et al., 2007) and GEBCO's global bathymetric data sets. Hein et al. (2007) compiled the data set from surveys conducted by the USGS, Korean Ocean Research and Development Institute, and published gridded data (http://pubs.usgs.gov/mf/1999/2324/). The GEBCO's gridded bathymetric data sets are global terrain models for ocean and land and include the GEBCO_2014 Grid, which is a global 30 arc-second interval grid of 1 by 1 km. GEBCO's global elevation models are generated by the assimilation of heterogeneous data types, under the assumption that all data sets have a mean sea level reference.

For the quantification of the effects of coastal hazards on the island, detailed bathymetric measurements in the intertidal area are required since these areas are not included in the above datasets. These data were collected during the field mission by means of an echo sounder (Plastimo echotest: resolution 0.1 m – maximal measurable depth = 80 m) on a number of cross-shore transects from the shore down to a depth of 80 m (Figure 5.1).
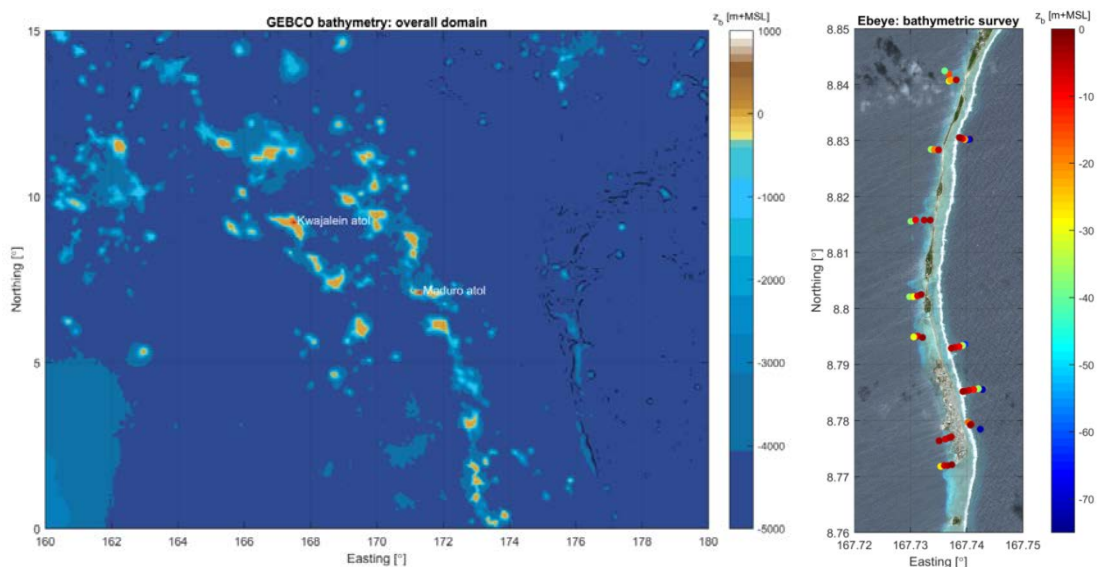
Figure 5.1   Offshore bathymetry data derived from the GEBCO dataset for the study area (left figure); and nearshore measured bathymetry data collected during the field mission (right figure).

5.2.2 Topography

Detailed topographic data are essential for carrying out a coastal hazard and risk assessment on low-lying atoll islands such as Ebeye. Unfortunately, no digital elevation data for the island was available at the start of the study. To overcome this data limitation, during the mission a quick topographic survey of the island of Ebeye and of all the coastal defences has been carried out. Measurements were collected by means of a Trimble CenterPoint-RTX with a maximum vertical accuracy of 10 cm (Figure 5.2). The data collected were first corrected based on field observations and then interpolated in order to create a digital elevation map of the island (Figure 5.3). An overview of the current coastal defences on the island is shown in Figure 5.4.

It has to be pointed out that the survey was carried out with a relatively simple instrument and with strict time/budget limitation for this task. It would be advisable, for more detailed follow-up studies, to carry out a more comprehensive topographic survey (e.g. using LIDAR, and/or drone techniques, complemented with dGPS measurements on the ground). The survey could be used to derive an accurate digital elevation terrain model of the island (and possibly of all inhabited islands in The Marshall Islands.

Figure 5.2   Topographic survey of the island.
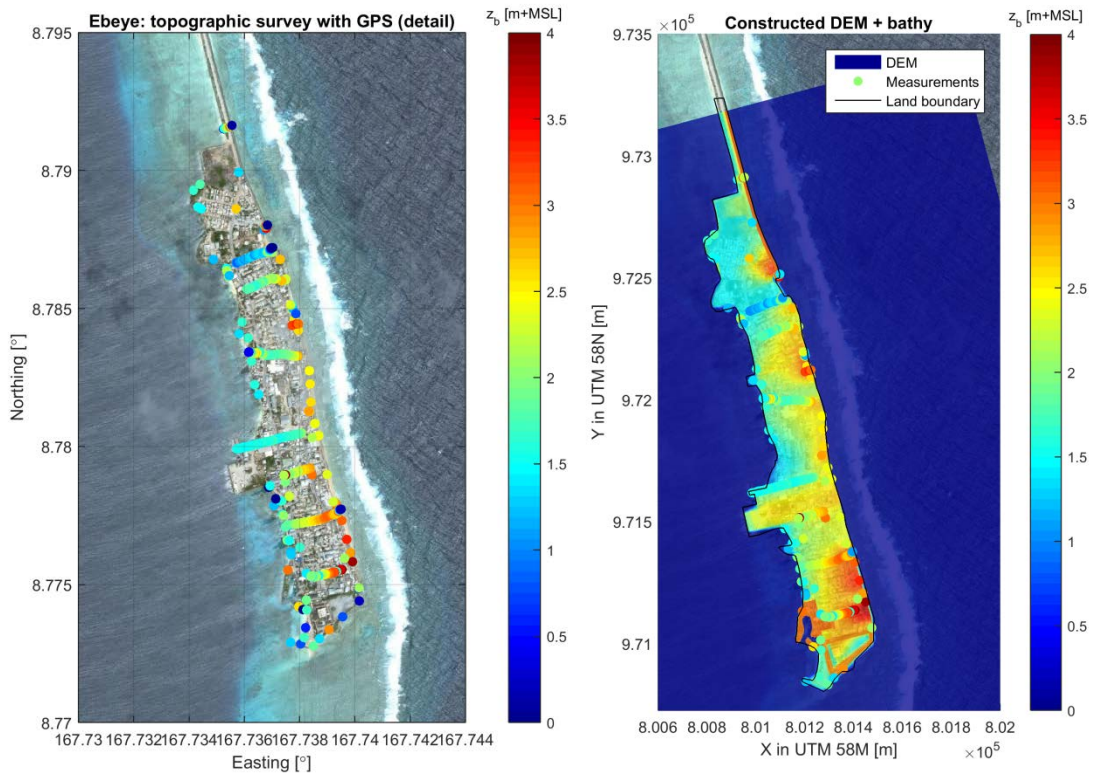
Figure 5.3   Measured topographic point (left figure) and interpolated digital elevation map (right figure).

Figure 5.4   Observations of the types of coastal defences and/or materials, collected during the site visit.

5.2.3   Water levels

Water levels are the result of the combination between a tidal level and a residual (i.e. non-tidal) level. The residual levels are again the result of number of oceanographic and/or meteorologically induced effects (e.g. wind, barometric pressure, temperature, El Nino / La Nina effects, etc.)

1   Tidal levels are derived from the global TOPEX/Poseidon dataset (i.e. TPXO 8.0; Egbert and Erofeeva, 2002) combined with information from the Kwajalein NOAA tidal gauge (http://tidesandcurrents.noaa.gov/stationhome.html?id=1820000) via a harmonic analysis based on the tidal constituents (amplitude and phases).

2   Residual effects are derived from the difference between water levels measured at the Kwajalein NOAA tidal gauge and the predicted tidal levels based on the tidal constituents.

5.2.4   Wind and waves

Long time series of wave and wind data were not available at Ebeye and Majuro. However, other sources of wave data are available, to be used as an alternative to historical buoy measurements. Most commonly, wave parameters can be extracted from a global reanalysis dataset called ERA-Interim (Dee et al., 2011). By means of remodelling global weather conditions of the past, this dataset can supply synthetic data at places where no wind or wave records exist. The data are 6 hourly, starting from 1979 and are available on a global grid with a resolution of 0.75° x 0.75°, which is about 80 x 80 km. The data contains information on wind speed at 10 meters above mean sea level (U_{10}), wind direction as well as on wave conditions (wave height, period and direction).

The wind climate at Ebeye is characterised by trade winds blowing from the east, also leading to wind-sea and swell waves from that direction (Figure 5.5). However, the highest winds and waves affecting the islands mainly result from typhoons that are generated around the central Pacific islands and proceed to the West, and by extra-tropical typhoons from the North Pacific (Mori et al.,2010; Storlazzi et al., 2015) (see section 5.2.5). These extremes are not recognizable in the windroses of Figure 5.5, because typhoons are too compact to be properly accounted for in the course grid of ERA-Interim. Wind and wave patterns show a seasonal variation (Figure 5.6). Typical monthly offshore wave heights and wind speeds range between 1.4 – 2.4 m and between 4 and 9 m/s (Figure 5.6 A,D). The wave and wind directions vary between 50 and 120 degrees (Figure 5.6 B,E). However, during boreal (northern hemisphere) winter, winds pick up and the wave heights and wave periods are accordingly larger with Hs ≈ 2.4 m and Tm ≈ 9 s respectively (Figure 5.6 A,C). Mean wave periods also increase because of larger trade-wind swells in the region.
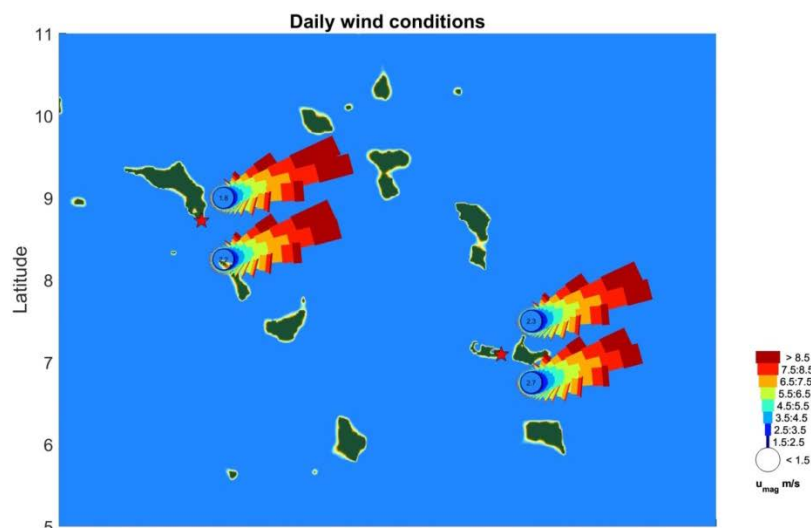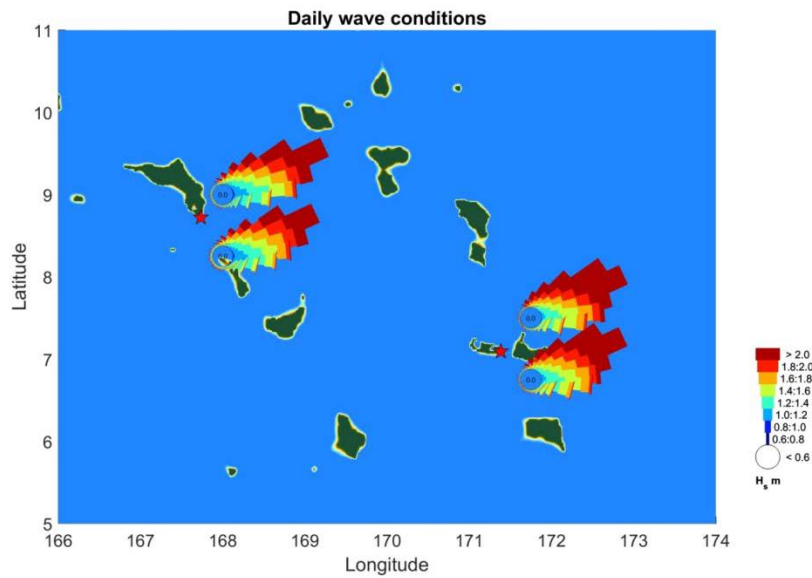
Figure 5.5   Wind (figure above) and wave (figure below) data at the islands of Ebeye and Majuro as derived from the ERA-Interim dataset.

Monthly variation wave height
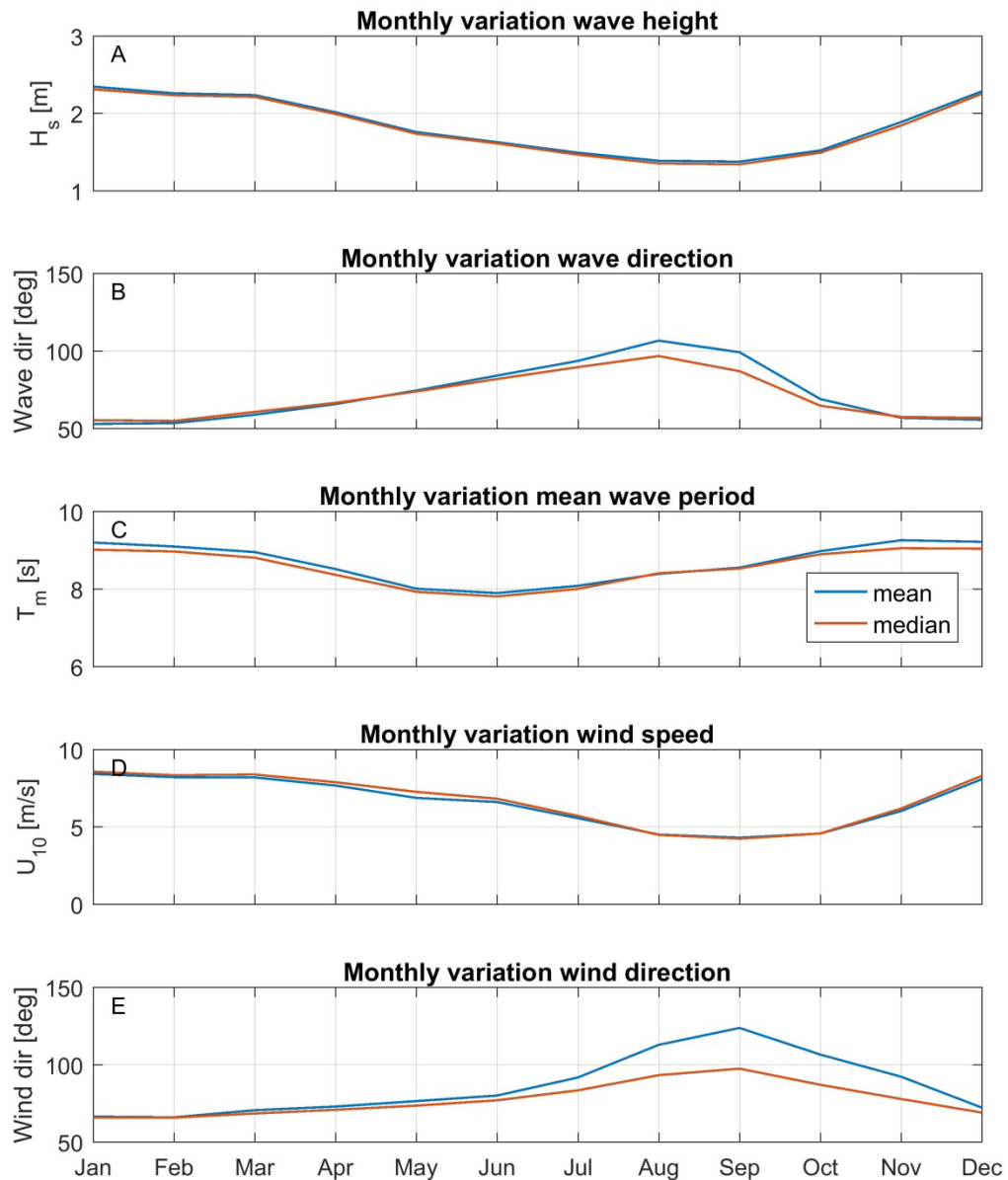
Figure 5.6   Monthly variation of wind and wave conditions at Ebeye.

5.2.5   Typhoons

Pacific typhoons generally develop around the Marshall Islands, with an occasional full hit on the islands (Figure 5.7). Generally, the northern atolls are more subject to typhoons than the southern atolls. The storms impact the atolls of Ebeye and Majuro occasionally, with a strong correlation between typhoons frequency and the ENSO effects (El Niño–Southern Oscillation) (Wright, 2004). In particular, years characterized by strong El Niño event have a larger probability of a typhoon.

Since wave measurements near the Marshall Islands are limited, Global Wave Models have been used as a data source (Section 5.2.4). However, in these models rapidly rotating storm systems (i.e. hurricanes / typhoons) are not resolved and therefore its effect on wave height

and storm surges underestimated. Therefore, the effects of typhoons is analysed based on historical typhoon tracks derived from the IBTrACS database (International Best Track Archive for Climate Stewardship; https://www.ncdc.noaa.gov/ibtracs/). The database contains the most complete global set of historical tropical cyclones available (Figure 5.7). In this study all tracks from the IBTrACKS with a categories of a tropical storm or higher (i.e. categories 1 until 5) will be modelled with a Delft3D-FLOW and WAVE model in order to determine the extreme wave heights and storm surges as result of typhoons (see section 6.4).

Based on the IBTrACKS it is concluded that typhoons around the RMI have a mean wind speed of 23 m/s with a mean pressure of 954 mbar. This is because the majority of rapidly rotating storm systems is lower than the hurricane category, as defined by the Saffir-Simpson scale (i.e. tropical depressions or tropical storms).
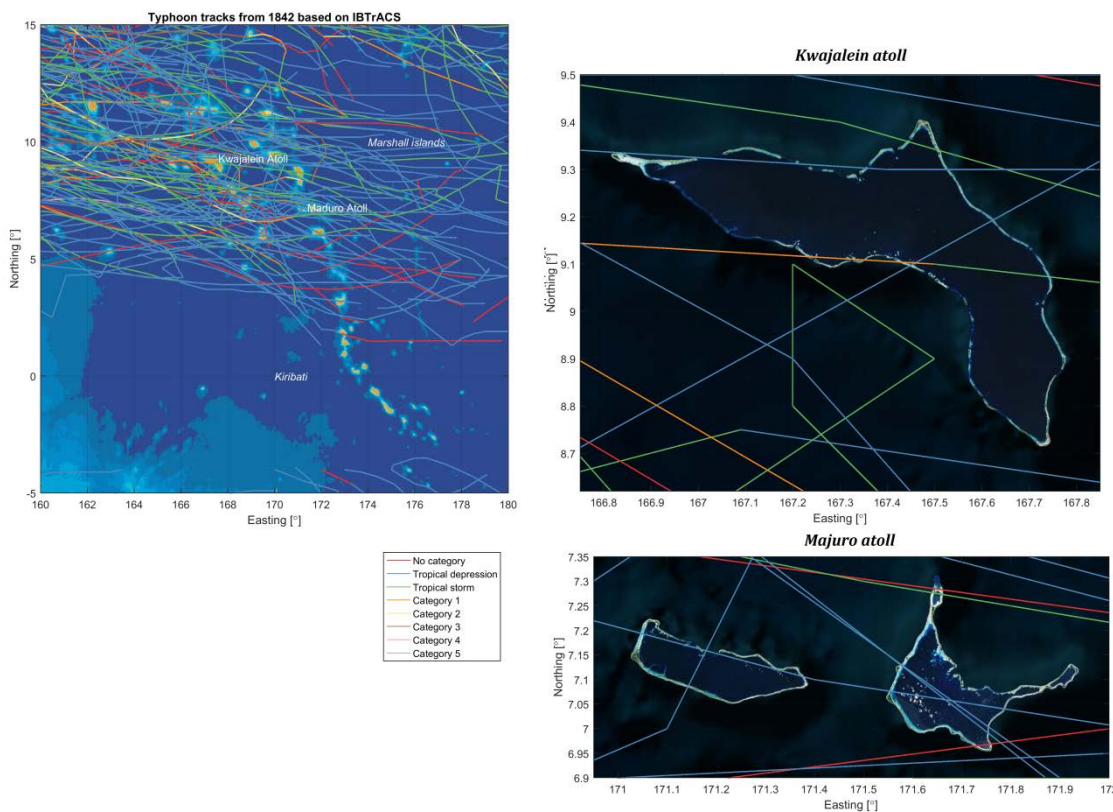
Figure 5.7 Typhoon tracks from 1945 across the study area per category based on IBTrACS database (https://www.ncdc.noaa.gov/ibtracs/. Left upper panel: area of interest around RMI. Right upper panel: zoom on Kwajalein atoll. Right lower panel: zoom on Majuro. Colours indicate Saffir-Simpson hurricane scale)

5.2.6 Tsunamis

Tsunamis are long period waves generated by disturbance in the water column and may be caused by tectonic movements, underwater landslides, volcanic eruptions or meteor impacts. Tectonic movements are the most frequent cause of tsunamis. However, the RMI is located rather far from the major regional tsunamis sources (Figure 5.8). Nevertheless, it is possible that a tsunami generated at Chili at the Nazca and South America plates reaches RMI. Based on available literature (Robertson and Hwang, 2005; Hess et al., 2015), there seems not to be examples of tsunamis events at the islands caused by local sources (i.e. landslides or nearby earthquakes).

Most of the tsunami waves that have been recorded from the past large events from mega thrust earthquakes (e.g. 2011 Tohoku tsunami) resulted in minor impact (i.e. inundation) at the RMI. Tsunamis waves generated by the Tokoku event in 2011 were estimated at less than 1 m in the RMI and occurred at low tide therefore not causing remarkable damages (Hess et al., 2015; Robertson and Hwang, 2015).

In this study, inundation depths due to tsunamis will be estimated based on numerical modelling from the Tokoku event in 2011 (i.e. most recent recorded past event). Sea level rise will increase the risk for inundation due to tsunami's, therefore present and future sea level rise scenarios will be taken into account.
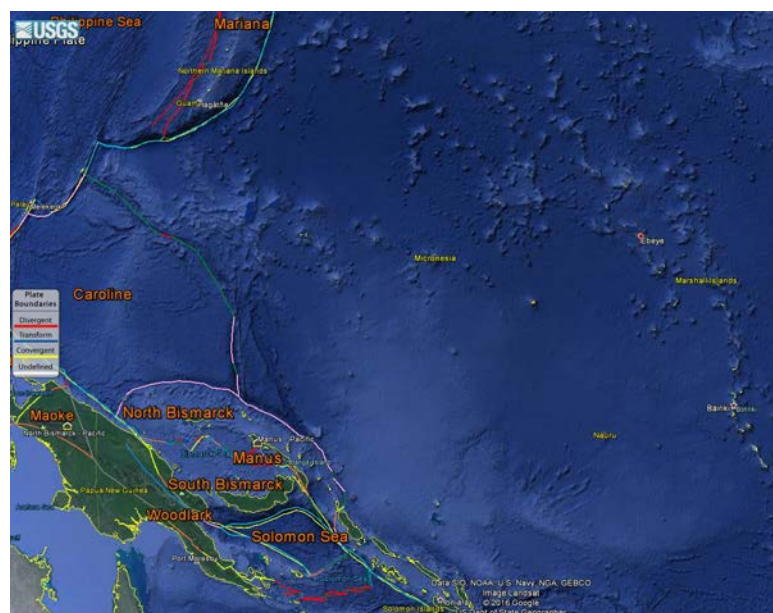
Figure 5.8   Plate boundaries around the Marshall islands. The red circle indicated the location of the Marshall islands.

5.2.7 Climate change and sea level rise

A detailed climate change analysis for the Pacific islands and, in particular for The Marshall Islands, is available for example through the Australian Bureau of Meteorology and Commonwealth Scientific and Industrial Research Organization (CSIRO, 2014). Among others, the analysis includes prediction for sea level rise scenarios based on downscaled RCP projections, see Figure 5.9. Changes in wave conditions due to future climate change scenarios have been derived from Hemer et al. (2013), see Figure 5.10.
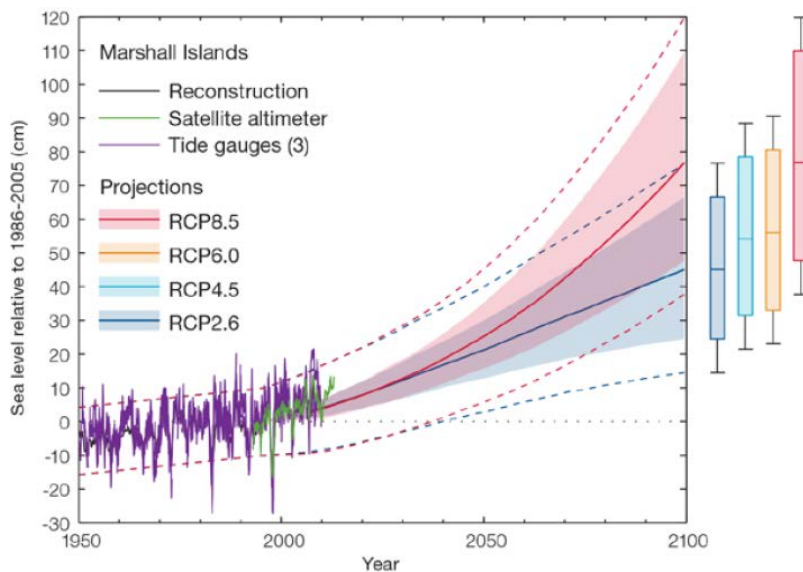
Figure 5.9   Observed and projected relative sea level change near the Marshall Islands. Multi-model mean projections from 1995–2100 are given for the RCP scenarios (CSIRO, 2014).
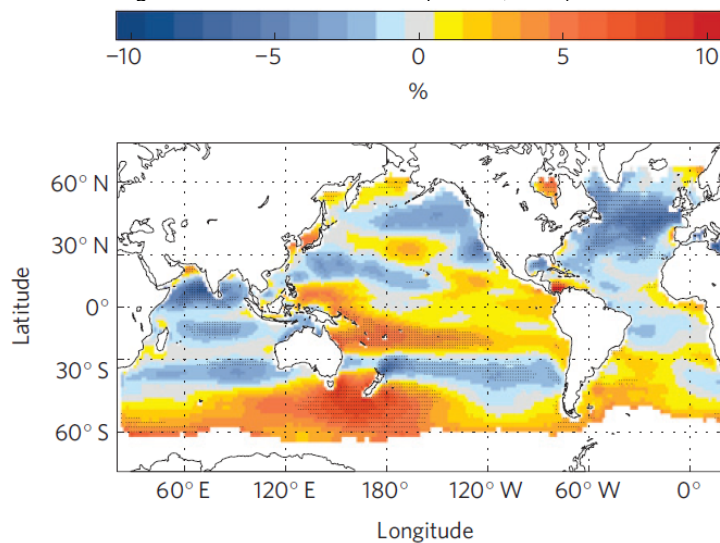
Figure 5.10   Averaged multi-model annual mean HS for the future time-slice (2070–2100) relative to the present climate time-slice (1979–2009) (% change). From Hemer et al. (2013).

5.2.8   Exposure and vulnerability

Exposure data are available through PCRAFI (2015). In particular, the dataset associated to the report from 2010 includes information for each structure on:

- Exact location and footprint of the structure (Figure 5.11)
- Main purpose (e.g. residential, public, commercial etc.) and occupation (e.g. single family, multiple families, general commercial etc.)
- Construction: masonry/concrete, timber frame etc.
- Number of stories
- Indication of the value in US$ (Figure 5.11)

The PCRAFI dataset is complemented with information on costs from additional infrastructures which were not included as part of this dataset. In particular:

- the power plant
- the water treatment plant

It is assumed that the value of the power plant and the water treatment plant are each 4 million USD. However, it is important to realize that these numbers are based on assumptions, as no more precise figures were available when the study was carried out. Nevertheless, these calculations can easily be adapted whenever new and more precise figures become available. Moreover, for the purpose of this study, we will mainly focus on the relative effect that the different solutions will have on the expected damages rather than on absolute values.
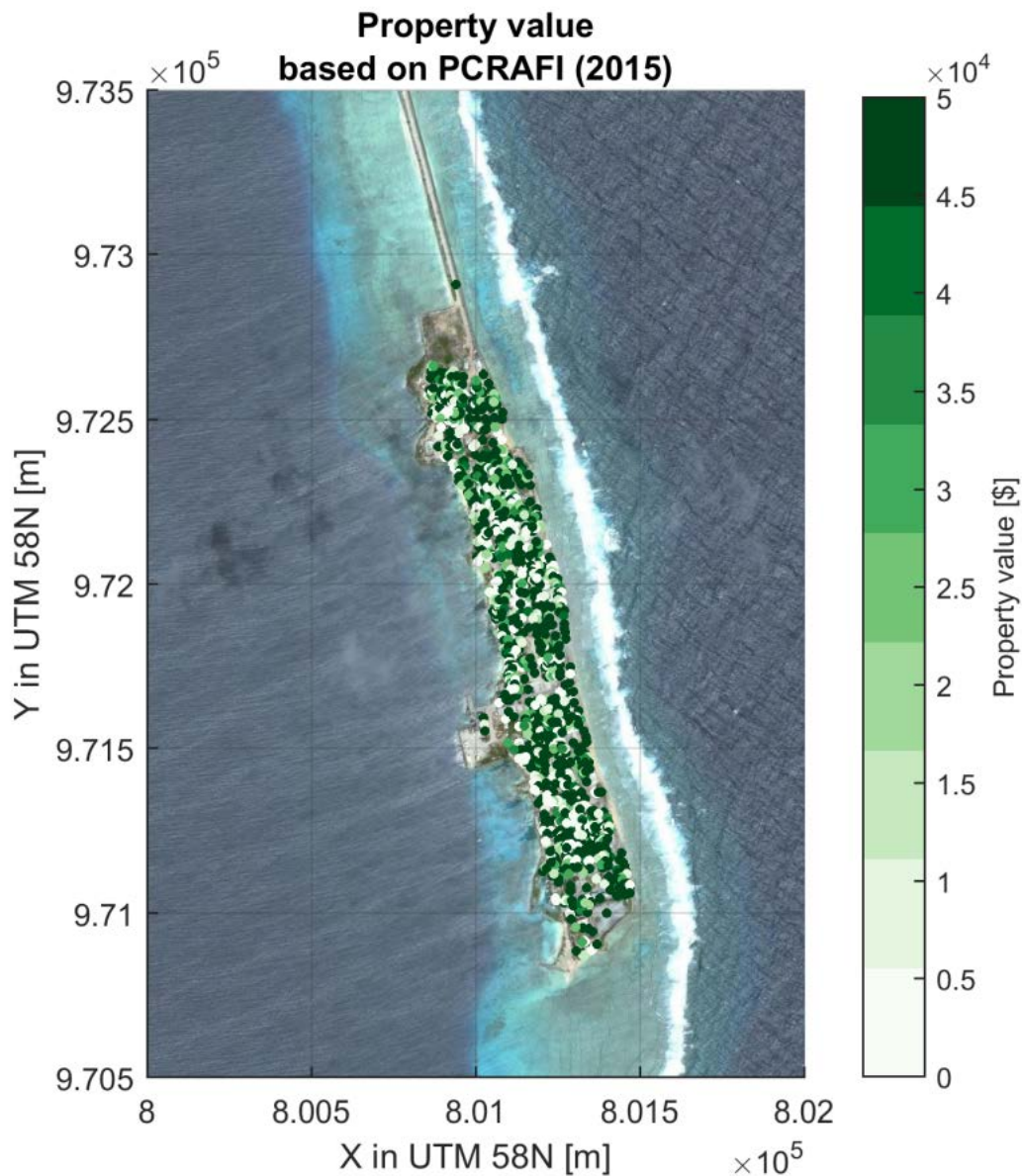
Figure 5.11 Exposure data (property values) for Ebeye island (PCRAFI, 2015).

Vulnerability refers to the damage inflicted upon the exposed property and it is generally assessed using depth-damage curves (i.e. vulnerability curves). A lot of different depth-

damage curves exist in literature, and which describe damages for different inundation depths (e.g. Budiyono et al. (2015), Pistrika et al. (2014), . The types of houses, infrastructures and construction materials can generally explain the differences between those curves. For this study the depth-damage curve for America Samoa (Paulik et al., 2015) is applied, since construction and building type is similar.
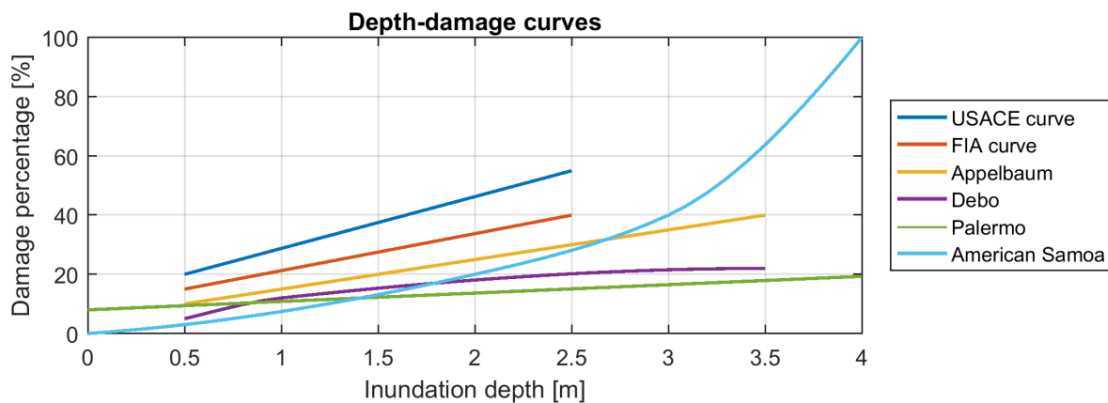
Figure 5.12   *Different depth-damage curves as found in literature. In this study, the curve from American Somoa has been uses (Paulik et al., 2015).*

5.3   Numerical models
With the collected data as input, numerical models are used to quantify the coastal hazards at Ebeye and Majuro. A Delft3D model (Lesser et al., 2004) is used to assess the effects of typhoons on the surge and waves near Ebeye and Majuro. Also, a more complete (but computationally more expensive) XBeach model (Roelvink et al., 2009) is setup to transform the collected deep water hydrodynamic data to nearshore hazards (i.e. inundation).

5.3.1   Delft3D
In order to determine the impacts of typhoons on the coastal hazards at Ebeye and Majuro, the collected information on historical typhoons need to be translated into (deep water) wave information and surge near the coast of Ebeye and Majuro. This is calculated using a Delft3D model system, in particular using the Delft3D-FLOW hydrodynamic model coupled with the Delft3D-WAVE wave model. Within Delft3D-FLOW, time-series for space varying wind velocity components and atmospheric pressure on a spider web grid can be used to simulate the impact of such an event (Deltares, 2014).

The collected information on typhoon tracks and corresponding wind speeds and pressure fields (section 5.2.5) are used to force the Delft3D-FLOW & WAVE model. The model then calculates the typhoon induced surge and waves near Ebeye and Majuro. The resulting wave characteristics and surge is subsequently used as input for the XBeach model, in order to calculate the nearshore coastal hazards (only for Ebeye island).

5.3.2   XBeach
To determine the coastal hazards at Ebeye, the collected deep water hydrodynamic data needs to be transformed into nearshore hydrodynamics. The propagation of the waves and water levels across the reef towards the shore will be carried out by means of the XBeach model (Roelvink et al., 2009). XBeach was originally derived for mild-sloping sandy beaches, but with some additional formulations, XBeach has been successfully applied in reef

environments (Pomeroy et al., 2012; Van Dongeren et al., 2013), including the nearby Roi-Namur island on Kwajalein Atoll (Quataert et al., 2015).

A two-dimensional XBeach model of the islands will quantify inundation extents and depths for different return periods. To determine the impacts of sea level rise on inundation of the island, the offshore water level at the boundary of the XBeach model will be increased according to the sea level rise scenarios.

In order to setup the XBeach model the following data will be used:
• deep water extreme wave conditions (wave height, direction and period);
• wind directions and velocities;
• tidal elevations;
• bathymetry and topography of Ebeye, down to depth of approximately -20 m below MSL at the ocean side of the island and in the lagoon;
• bed roughness, using the roughness coefficients of the Roi-Namur XBeach model by Quataert et al. (2015).

6 Quantification of coastal hazards

6.1 Introduction

In this chapter, the coastal hazards are quantified for both islands of Ebeye and Majuro. The effects of the hazards are translated to impacts and related risks in Chapter 7 (only for the island of Ebeye). The following contributors to coastal hazards will be analysed: water levels, wind and waves (originating from the ocean and lagoon), typhoons, tsunamis and climate change effects on wave climates and sea level rise.

6.2 Water levels

Tidal constituents are derived from the global TOPEX/Poseidon dataset combined with information from the Kwajalein NOAA tidal gauge (http://tidesandcurrents.noaa.gov/waterlevels.html?id=1820000). The constituents for Ebeye and Majuro are shown in Table 6.1.

Table 6.1   Amplitude in meters and phases (between brackets in degrees) of the largest tidal constituents at Ebeye and Majuro (source: TOPEX/Poseidon, NOAA).

	Ebeye	Majuro
M2	0,49 (127)	0,74 (128)
S2	0,27 (149)	0,38 (147)
N2	0,13 (127)	0,15 (127)
K2	0,10 (146)	0,11 (142)
K1	0.10 (66)	0.11 (71)
O1	0.07 (39)	0.06 (40)

Based on the information of the separate tidal constituents it is possible to compute the tidal levels since both the amplitude and phase information are known. A tidal prediction for every minute for the last 100 years has been carried out in order to determine statistics related to the tidal range (i.e. mean, min and max) and the highest and lowest astronomical tide (i.e. HAT and LAT). The HAT (i.e. worst-case scenario) will be used in the assessment of the impact of coastal hazards.

Table 6.2   Tidal statistics in meters at Ebeye and Majuro.

	Ebeye	Majuro
Tidal range: mean	1,73	2,50
Tidal range: min	0,48	0,57
Tidal range: max	1,86	2,77
HAT (+MSL)	+1,00	+1,39
LAT (+MSL)	-0.91	-1,37

Residual effects are derived from the difference between the measured water levels at Kwajalein and the computed water levels. The result is a time series of residual water levels between 1980 and 2016, when measurements were available. These values will be used in an extreme value analysis (peak-over threshold approach) to determine extreme residual water level for selected return periods as shown in Figure 6.1. The residual water level

includes effects due to a number of oceanographic and/or meteorologically processes (e.g. wind setup, wave setup, atmospheric pressure drop, ENSO effects).

Separate contributions of wind, atmospheric pressure and ENSO effects can be estimated based on empirical formulas and/or literature. For example during large wind events the wind setup in the lagoon is estimated based on McCartney (1976) to be 5-10 centimetres. During daily conditions a pressure drop of 10 mbar from 1010 to 1000 mbar can result in a surge of about 10 centimetres. This value can increase to 30 centimetres for larger pressure drops during typhoons. ENSO-effects are estimated to be able to increase the water level by 10-20 centimetres (NOAA, 2012). In this study, however, the total extreme residual water level will be used, which includes all these combined processes.

For the assessment of the impact of coastal hazards we need a total water level. Therefore, the extreme tidal water level (HAT) will be combined with the extreme residual water level. Tidal water levels do not vary for different return periods, since it is generated by gravitational pull of the moon and sun. Residual water levels do vary for different return periods, since these are the result of a number of oceanographic and/or meteorologically induced processes. During extreme events (i.e. high return periods) high residual water levels occur due to a combination of effects such as wind setup, pressure drop and ENSO-effects. By applying an extreme analysis on the residual water levels (separate from the tidal elevations) it is possible to determine the extreme water levels. The set of total water levels (i.e., tide and residual) for different return periods is summarized in Table 6.3.
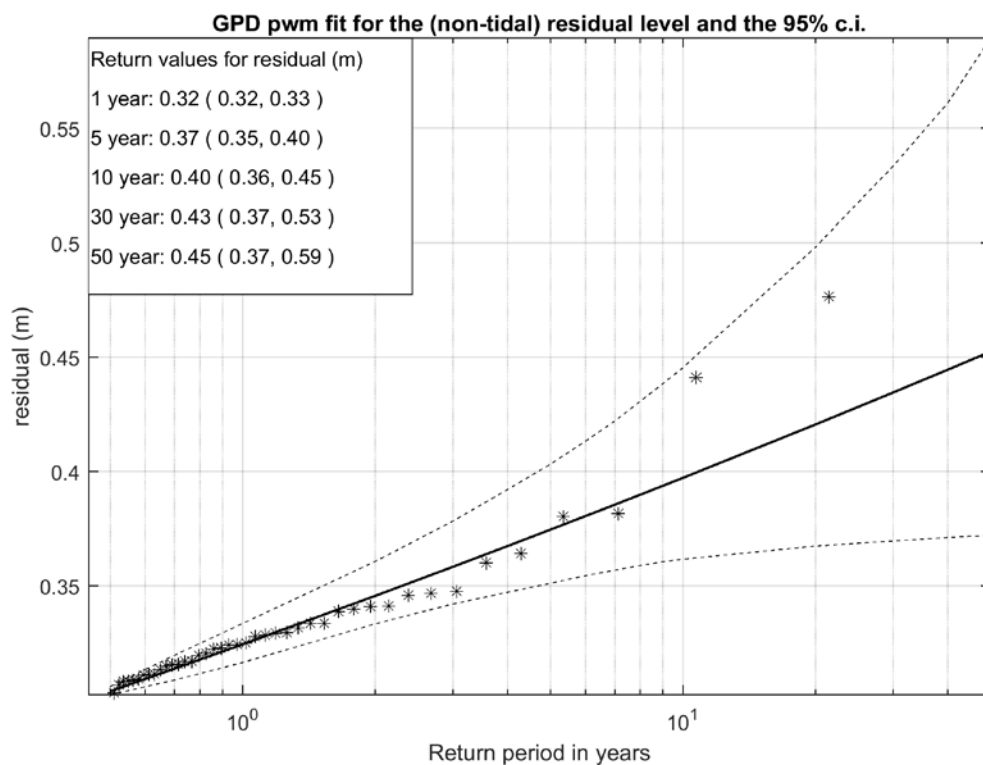
Figure 6.1   Extreme value analysis of the residual water level. The tables list the 1,5,10,30 and 50 year values and the 95 % confidence intervals (in brackets).

Table 6.3   Extreme total (tide and residual) water levels at Ebeye and Majuro for different return periods w.r.t. MSL.

R.P.	Ebeye (m)	Majuro (m)
5	1.37	1.76
10	1.40	1.79
30	1.43	1.82
50	1.45	1.84

6.3   Wind and waves

6.3.1   Hazards from the ocean

Extreme wave heights

For the determination of extreme wave height statistics ERA-Interim wave data have been used (section 5.2.4). As the resolution of these models may not be sufficient to resolve small scale features (e.g. other islands around Ebeye and Majuro) it is important to validate these data versus available local measured data. Measured data are available for example from NOAA at Kwajalein (wind: http://www.ndbc.noaa.gov/station_history.php?station=KWJP8) and Majuro (waves: http://www.ndbc.noaa.gov/station_history.php?station=52201).

Long-term wave records do not exist for Ebeye. To still be able to validate the accuracy of the ERA-Interim data in the Marshall island region, a comparison was made between ERA-Interim data near Majuro with buoy measurements off the coast of Majuro. The historical time-period of the ERA-Interim data spans from year 1979 until 2015. Buoy measurements of Majuro that were used for the validation encompass the years 2010-2015, but include some downtime, resulting in gaps in the wave records.

The estimation of extreme wave height values is based on a peak over threshold approach (PoT) (Figure 6.2).
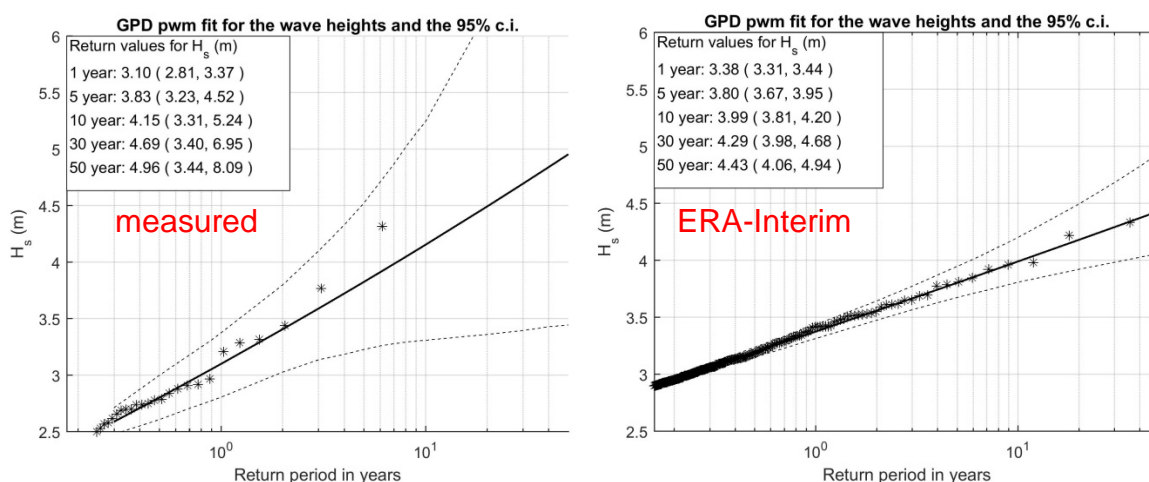
Figure 6.2   Results of the "peak over threshold" analyses for the buoy measurements at Majuro (left) and the ERA-Interim data (right). The graphs show the significant wave height for different return periods. The tables list the 1,5,10,30 and 50 year values and the 95 % confidence intervals (in brackets).

By means of a PoT analysis it is possible to determine the wave height, and associated return periods (RPs), for high wave events. In general, the highest RP which can be derived is limited by the time-span of the measured/modelled data. In this case, measured data have a quite limited duration (about 5 years), limiting the accuracy of the wave conditions derived for higher return periods. However, by following the general trend in the data, RPs beyond that limit can be derived, although the uncertainty of the estimate grows for increasingly higher RPs.

The set of wave heights and corresponding RP values derived from measurements and ERA-Interim data for Majuro are summarized in Table 6.4. The table shows that the two datasets are generally consistent. The ERA-Interim estimates are slightly lower, with the difference increasing with higher return periods. However, due to the very short duration of the measurements, uncertainties in the determination of wave height with higher return periods are quite large for the measured series (see the standard deviations σ as an indication of the uncertainty in Table 6.4). It can therefore not be concluded that the ERA-Interim data underestimate the wave height return periods. This is fostered by the fact that wind speeds in the region were rather overestimated by ERA-Interim than underestimated, as can be concluded from a comparison with weather station data on Kwajalein (Figure 6.3).

Table 6.4   The 5, 10, 30 and 50 return periods of extreme wave heights at Majuro (left and middle) and Ebeye (right) as determined by PoT analyses of buoy and ERA-Interim data. Uncertainties in the estimates are indicated by the standard deviation (σ).

RP [yr]	Hs Measured (m) *Majuro*	σ (m)	Hs ERA-Interim (m) *Majuro*	σ (m)	Hs ERA-Interim (m) *Ebeye*	σ (m)
5	3.83	0.35	3.80	0.08	3.56	0.07
10	4.15	0.55	3.99	0.11	3.74	0.11
30	4.69	1.13	4.29	0.20	4.04	0.22
50	4.96	1.57	4.43	0.26	4.17	0.29
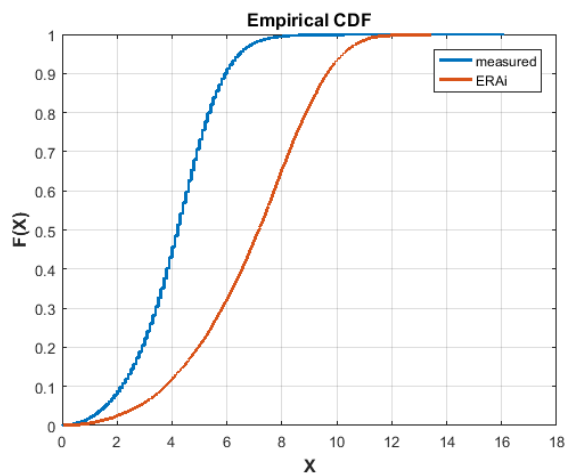
Figure 6.3   Cumulative distribution function of measured (blue) and ERA-Interim (brown) wind speeds at Kwajalein. The variable X represents the windspeed U10 (m/s). ERA-Interim data shows higher windspeeds than measured data.

Other data sources have also been checked (e.g. GCM-WaveWatch3 data vs. measurements) but finally not used in the analysis as they even resulted in a larger difference with respect to the measurements. Hence, ERA-Interim is chosen as the data source for further analyses in the report without corrections.

Similarly, and based on the same ERA-Interim dataset, RPs and associated wave heights have been derived for Ebeye and are together with their uncertainties listed in the two columns on the right hand side of Table 6.4. The table shows that these values are slightly lower than the values for Majuro.

Extreme wave periods
The Majuro buoy data reveal that wave peak periods are 50% of the time above 10 s, reaching up to 20 s. This is consistent with the frequent observation of swell conditions in the Marshall Island region (Storlazzi et al., 2015; Cheriton et al., 2016). Since wind-sea wave-height extremes due to typhoons are not captured by ERA-Interim, the wave-height presented in Table 6.4 are associated with swell-dominated wave conditions. Peak periods of 20 s occur about once every year, hence, for all RPs, wave periods of 20 s are assumed during peak hours in the swell-wave simulations of Ebeye island.

Wave directions
All data sources reveal that extreme waves in the area typically approach from North-Easterly direction. Based on ERA interim data, the 30-year averages of extreme wave directions and wave heights in the Marshall Island area are shown in Figure 6.4.

Based on the results of extreme wave directions and the slight North-Westerly orientation of Ebeye, it is reasonable to assume coast-normal incidence of large swell waves in the model simulations, as this will result in the largest impact (i.e. most conservative approach).
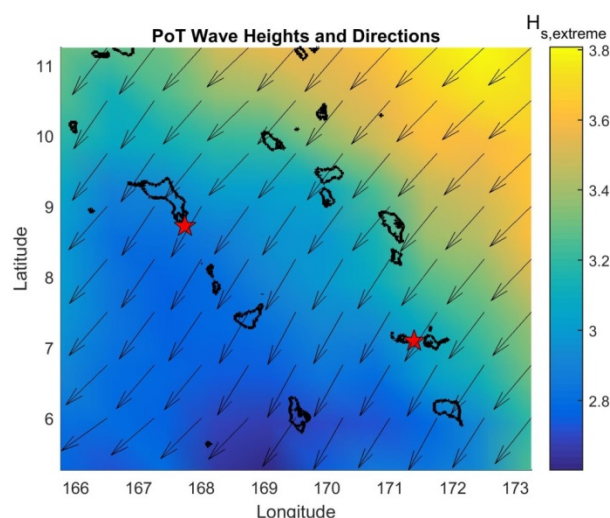
Figure 6.4   Map of extreme wave directions and wave heights in the Marshall island region based on ERA interim data. Red stars indicate the location of Ebeye (left) and Majuro (right).

6.3.2   Hazards from the lagoon
The hazards at the lagoon side of Ebeye are water levels and locally generated waves in the lagoon. Water levels are known and consist of tidal constituents (Table 6.1), residual water levels (Table 6.3) and sea level rise (Table 6.8). The locally generated (wind-induced) waves

in the lagoon are quantified using a Delft3D-WAVE model. It is assumed that the waves originating from the ocean all break at the (coral) reefs, and therefore do not affect the wave heights in the lagoon. The atoll is modelled as a closed lagoon with a uniform depth of 40 m below MSL (Figure 6.5) and forced with wind fields (i.e. speeds and directions). This is however an assumption, as no digital bathymetry of the entire atoll was available at the start of the study. In reality, some waves can penetrate through the opening in between the islands. For future, more detailed studies, it is advised to collect and generate a digital bathymetry dataset of the entire atoll, which could be used for different purposed (i.e. flooding studies, navigation, assessment on availability of sediment resources in the lagoon, etc.).
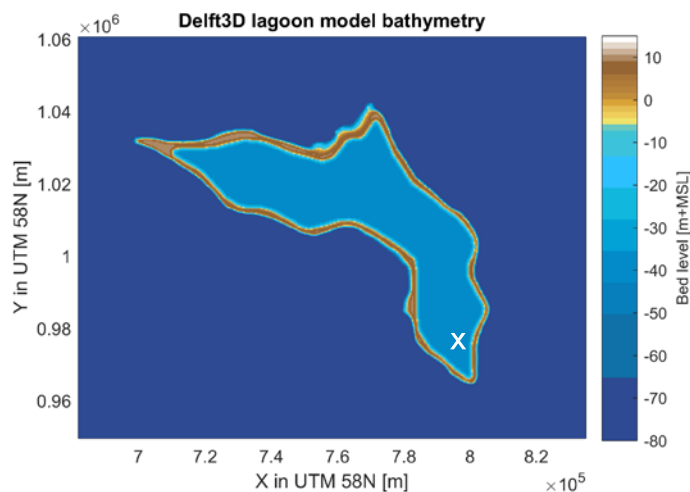
Figure 6.5   *Model setup: bathymetry for the delft3D-WAVE lagoon model.*

An observation point in the Delft3D model in the lagoon near Ebeye (marked 'x' in Figure 6.5) is used to assess the wave conditions and to determine the (maximum) wave height that occurred during wind conditions for each return period. This information forms the basis of the extreme analysis of the waves as a result of the locally generated waves in the lagoon. The results of the extreme value analysis for the waves in the lagoon are shown in Figure 6.6, with wave heights ranging from 0.67 m to 1.06 m for return periods of 5, 10, 30 and 50 years. These wave heights will be used as input for the assessment of the impacts of the hazards from the lagoon on the island of Ebeye in Chapter 7.
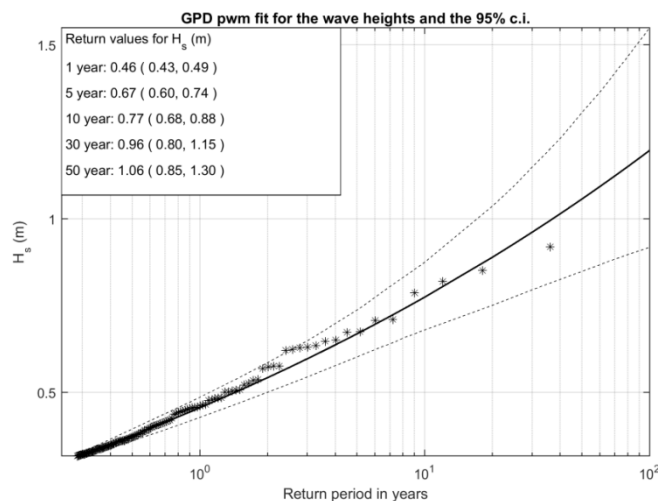
Figure 6.6   *Extreme value analysis for the wave heights in the lagoon near Ebeye based on the Delft3D-WAVE modelling results.*

6.4 Typhoons

In the area of interest (Northing: -5 till 15 degrees, Easting: 160 till 180 degrees), 60 typhoons are listed in the IBTrACS database between 1979 and 2015, of which 30 tracks have a wind speeds larger than 18 m/s (the threshold for storm with an intensity of tropical storm or higher). Smaller depressions are already resolved within the global ERA-Interim wave model and are therefore taken into account as part of the regular wave conditions. These 30 tracks are modelled with a Delft3D-FLOW and WAVE model in order to determine the extreme wave heights and storm surges as result of typhoons.

Measurements of the typhoons (i.e. generated winds and waves) are absent for the Marshall Islands. Therefore, measurements available for hurricane Iniki at Hawaii have been used to validate the parametric hurricane relations and to test the capability of the Delft3D model to reproduce wind speeds, pressure drops and resulting wave height at several measurement locations (Appendix A).The forcing for the Marshall Islands model is based on parametric surface fields (maximum wind v_{max} and pressure p_c) based on the validated relations in Appendix A, and information on the typhoon track.

6.4.1 Model setup

In order to determine the surge and significant wave height near Ebeye and Majuro, as a result of a rotating storm system, a Delft3D-FLOW and WAVE model of the area of interest (Northing: -5 till 15 degrees, Easting: 160 till 180 degrees) has been implemented. The model contains of 200 x 200 grid cells. These values represent deep water conditions and will be imposed to the XBeach model in order to propagate them to nearshore and determine the impact (i.e. inundation).
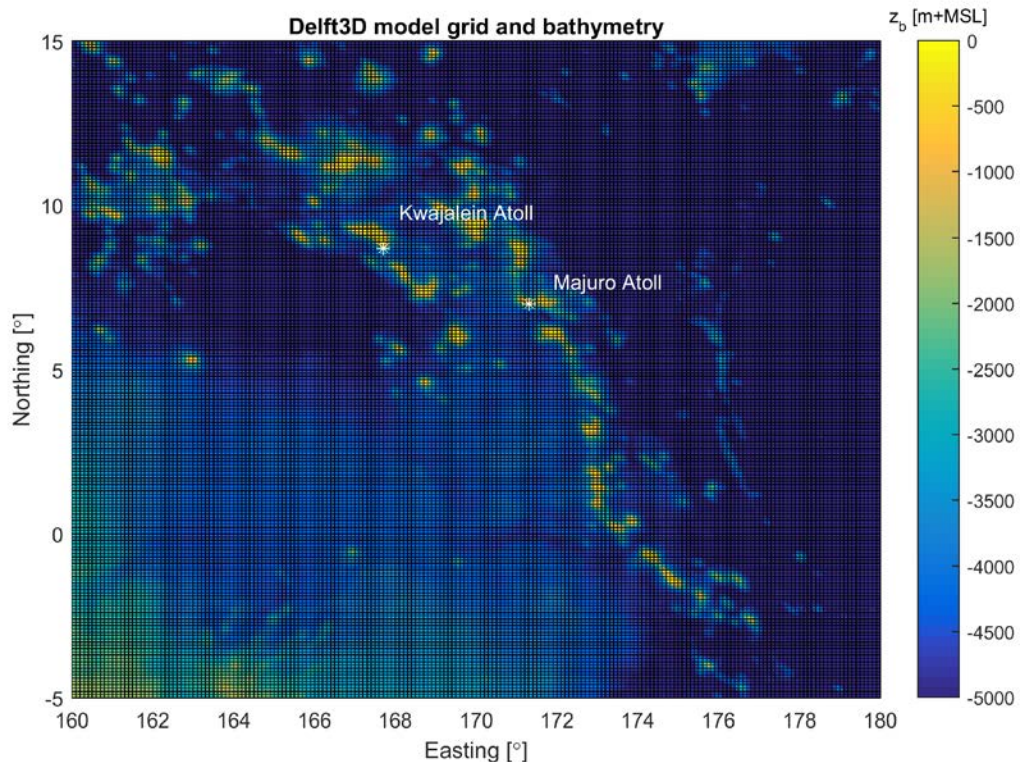
Figure 6.7   Model setup: applied grid and bathymetry for the typhoon modelling around the Marshall Islands. With the white stars the two observation points are presented. Majuro: 7.05, 171.35 degrees. Ebeye: 8.75, 167.75 degrees.

The only forcing in the model are the wind speeds and pressure drops from the selected 30 typhoons. This means that all waves are generated inside the model domain since no boundary conditions are imposed and that water level variations due to meteorological forcing are always the residual water level (i.e. surge), since no tidal water level variations from the boundaries or inside the model exist.

All the typhoon conditions simulated are summarized in see Table 6.5. The information presented only contains the maximum sustained wind speed and minimal pressure drop. However in the IBTRACKS database also information related to the track and matching wind speed or pressure drop is available. This information, in combination with the relationships for the generation of parametric hurricane surface fields (see Section A.1), are needed to create wind speeds and pressure drops for the entire time span of a storm and this for all the different storm conditions modelled with Delft3D.

Table 6.5   Storm conditions modelled with Delft3D showing the typhoon names, year of occurrence, maximum sustained winds and minimal pressures with a minimal intensity of a tropical storm (T.S.) sorted per year.

Year	Typhoon name	Maximum sustained wind (m/s)	Minimal atmospheric pressure (mbar)	Category
1978	ALICE	52,9	929	3
1980	CARMEN	28,5	985	T.S.
1981	FREDA	49,0	945	2
1982	PAMELA	48,5	940	2
1983	ELLEN	59,8	929	4
1985	SKIP	37,8	970	1
1986	GEORGETTE	32,7	970	T.S.
1987	WYNNE	61,3	921	4
1987	HOLLY	66,4	902	4
1988	ROY	51,6	940	3
1990	AKA	27,0	993	T.S.
1990	OWEN	56,8	930	3
1991	ZELDA	33,8	973	1
1992	AXEL	29,9	980	T.S.
1992	KENT	52,9	937	3
1992	DAN	48,4	942	2
1992	GAY	60,7	922	4
1994	LI	33,4	996	1
1994	PAT	39,6	965	1
1997	KELLY	18,5	997	T.S.
1997	OLIWA	64,8	918	4
1997	DAVID	44,6	948	2
1997	GINGER	56,2	930	3
1997	JOAN	58,7	922	3
1997	PAKA	68,4	932	4
2000	CHANCHU	18,6	996	T.S.
2002	FENGSHEN	59,4	916	4
2002	ELE	51,4	941	3
2004	SONGDA	52,9	925	3
2013	PEWA	31,8	989	T.S.

Deltares

Computational results for waves (i.e. wave height, period and direction) and water levels (i.e. surge) are monitored at two observation points in the model near Ebeye and Majuro. These time series are used to determine the (maximum) wave height (with matching peak wave period) that occurred during each typhoon and will form the basis of the extreme analysis of the waves as a result of typhoons. On top of that, the maximum surge is determined.

6.4.2   Model results
From each of the 30 typhoons simulations, the maxima have been stored, which will be used as input to the nearshore XBeach modelling. The result is an overview of the maximum observed significant wave height with matching peak wave period and maximum storm surge level during the different simulated typhoons as can be seen in Figure 6.8 and Figure 6.9. It is possible that the maximum surge does not occur at the same time as the maximum wave height. The presented wave period is the wave period that occurred during the maximum wave height (Table 6.6).

Based on these results one can see that a typhoon with higher sustained wind speeds do not necessarily have to result in higher wave heights at Majuro or Ebeye, because wave heights are also dependent on the track location with respect to the island. For example at Ebeye typhoon Zelda (1991), with a maximum wind speed of 34 m/s (category 1), resulted in the model in a wave heights of 4.9 meters. This is only slightly lower than typhoon Paka (1997) with a maximum wind speed of 68 m/s (category 4). For storm surges the atmospheric pressure drop is mainly relevant. Therefore the exact track in relation to the atoll is determining. The results in Table 6.6 is used as input to carry out an extreme value analysis and determining the wave height and storm surge levels for different return periods at Ebeye and Majuro (Figure 6.10 and Figure 6.11).

Table 6.6   Maximum significant wave height, peak wave period and storm surge level occurred during the simulation with Delft3D for Ebeye and Majuro.

Typhoons	Maximum significant wave height (m), peak wave period (s) and storm surge (m) at Ebeye			Maximum significant wave height (m), peak wave period (s) and storm surge (m) at Majuro		
1978_ALICE	4,0	7,5	0,19	1,6	7,7	0,08
1980_CARMEN	0,3	8,2	0,00	0,4	6,5	0,01
1981_FREDA	2,2	6,1	0,07	1,8	5,1	0,04
1982_PAMELA	7,9	10,6	0,22	4,6	6,7	0,21
1983_ELLEN	0,4	5,4	0,02	0,5	6,6	0,01
1985_SKIP	0,2	7,0	0,00	0,3	5,4	0,00
1986_GEORGETTE	0,2	5,4	0,02	0,4	6,6	0,01
1987_HOLLY	0,9	9,3	0,04	0,7	8,8	0,02
1987_WYNNE	1,5	5,6	0,06	1,3	6,0	0,04
1988_ROY	5,3	9,1	0,15	2,2	5,7	0,16
1990_AKA	0,0	1,8	0,01	0,1	1,8	0,00
1990_OWEN	1,6	5,1	0,09	1,3	4,8	0,06
1991_ZELDA	4,9	8,4	0,18	2,0	5,5	0,09
1992_AXEL	1,8	8,8	0,07	3,8	5,8	0,12
1992_DAN	0,6	9,0	0,02	0,6	7,5	0,02
1992_GAY	2,6	7,3	0,12	1,6	7,8	0,09
1992_KENT	1,0	4,4	0,09	0,8	3,9	0,06
1994_LI	0,5	10,0	0,00	0,5	7,8	0,01
1994_PAT	0,3	5,3	0,02	0,2	5,4	0,00
1997_DAVID	1,4	4,6	0,05	1,4	3,8	0,05
1997_GINGER	0,6	3,1	0,02	0,2	5,0	0,02
1997_JOAN	1,0	3,8	0,03	1,1	4,1	0,03
1997_KELLY	1,9	5,5	0,05	1,1	4,0	0,03
1997_OLIWA	0,4	8,0	0,03	0,4	6,3	0,02
1997_PAKA	5,3	10,2	0,07	7,3	9,1	0,19
2000_CHANCHU	0,2	5,7	0,00	0,5	4,4	0,02
2002_ELE	1,0	12,1	0,00	1,1	10,7	0,00
2002_FENGSHEN	1,6	10,8	0,06	1,3	10,6	0,05
2004_SONGDA	0,9	3,7	0,06	0,6	3,3	0,03
2013_PEWA	0,8	11,1	0,00	0,8	9,5	0,00

The result of the Extreme Value Analysis is shown in Table 6.7 in which the maximum wave height and storm surge for four return periods (RP = 5, 10, 30 and 50 years) are given. Higher wave heights can be seen for the same return period at Ebeye than Majuro which is a result of the way Pacific typhoons generally develop in this part of the Pacific, intensifying while moving towards the north-west. The same can be concluded when considering the storm surge level.

In the simulations no clear pattern for the peak wave periods was found. In general during larger impacts (i.e. large maximum wave heights) a peak wave period of 9 -11 seconds was observed in the model. Therefore we assume a peak wave period of 10 seconds during the peak of the storm for all simulations.

The residual water levels (i.e. storm surge levels due to atmospheric pressure drop from typhoons) do not exceed the found extreme residual water levels from Section 6.2. In the assessment of the impact of coastal hazards the worst-case scenario will be modelled. This means that the combined effect of wind setup, atmospheric pressure drop and El Nino / La Nina results in a higher residual water level compared to the storm surge level due to atmospheric pressure drop from typhoons. Therefore, for typhoons this means the combination of the extreme wave heights from Table 6.7 in combination with the water levels from Table 6.3.

Table 6.7   Maximum significant wave height (Hs) and storm surges (SSL) for Ebeye and Majuro as a result of typhoons.

Return period in years	Maximum Hs (m) at Ebeye	Maximum SSL (m) at Ebeye	Maximum Hs (m) at Majuro	Maximum SSL (m) at Majuro
5	3,16	0,08	2,27	0,10
10	4.61	0,10	3,34	0,12
30	7,21	0,15	5,42	0,19
50	8,57	0,16	6,58	0,24

6.4.3   Conclusion

For the assessment of the impact of coastal hazards a wave height and storm surge from rapidly rotating storm systems (i.e. typhoon) is required. In order to take this into account, thirty tracks from the IBTrACKS with intensities of tropical depressions or typhoons have been modelled with Delft3D. The result is a table of maximum modelled wave heights and storm surges. Based on this result, we applied an extreme value analysis to determine the significant wave height and storm surge for four return periods. The found values are however deep water conditions and need to be transformed to nearshore conditions and eventually impacts (i.e. inundation) with XBeach (Chapter 7).
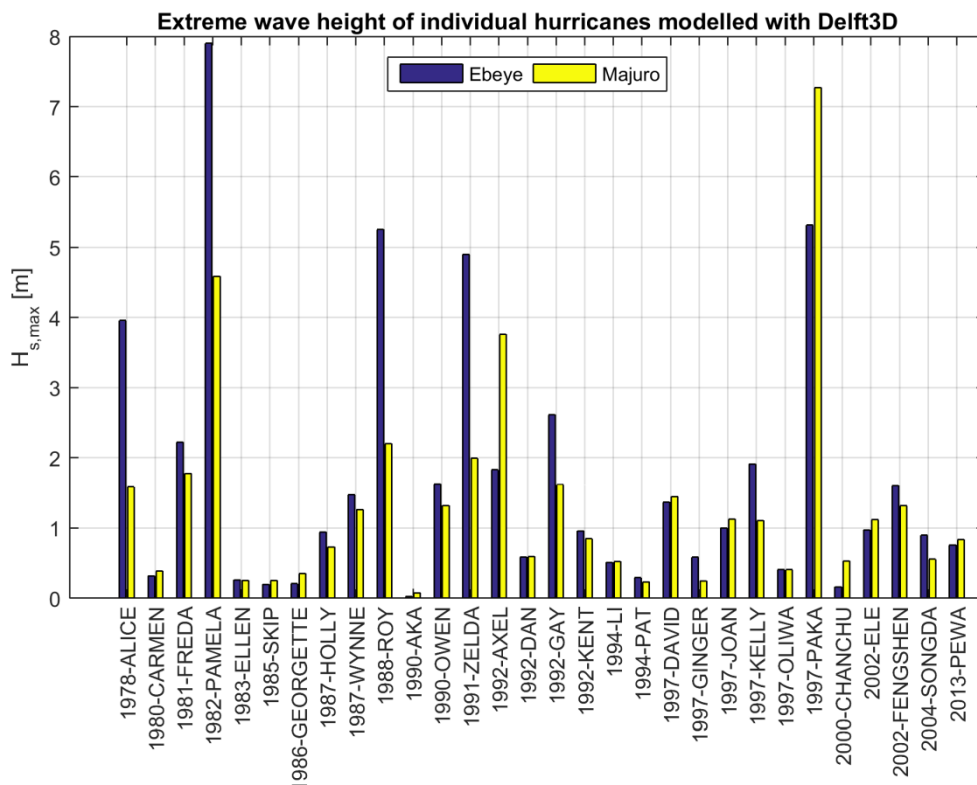
Figure 6.8   Maximum modelled significant wave height at Ebeye and Majuro for each simulated typhoon event.
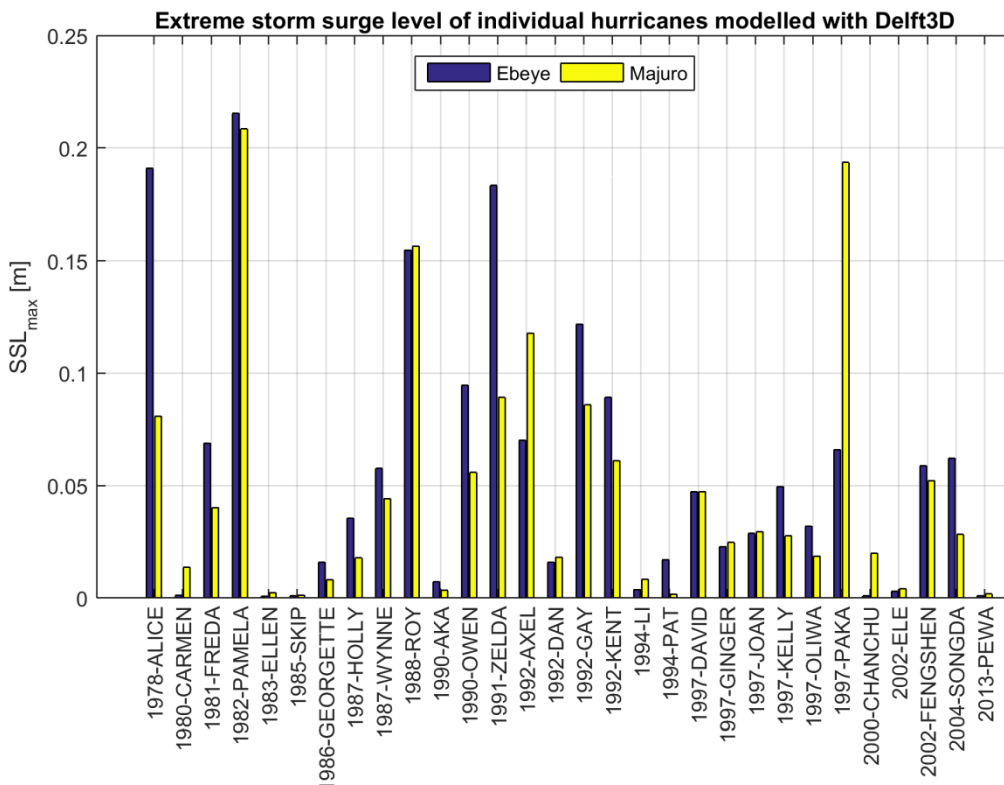
Figure 6.9   Maximum modelled storm surge level at Ebeye and Majuro for each simulated typhoon event.
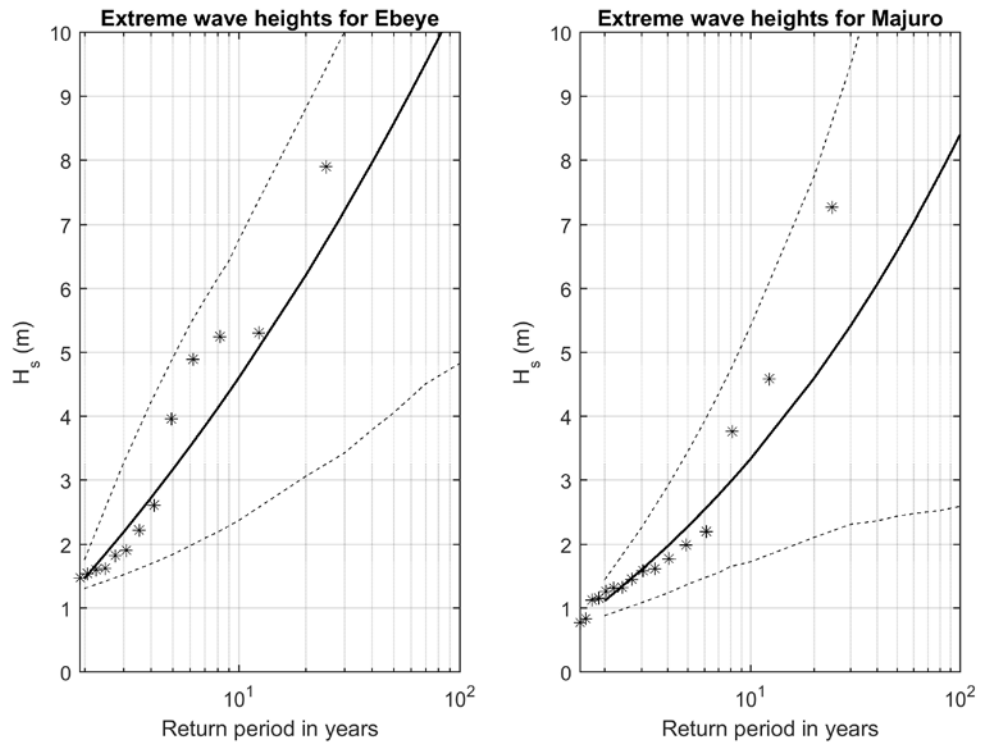
Figure 6.10 Extreme value analysis of the modelled wave heights at Ebeye (left) and Majuro (right) induced by the typhoons.
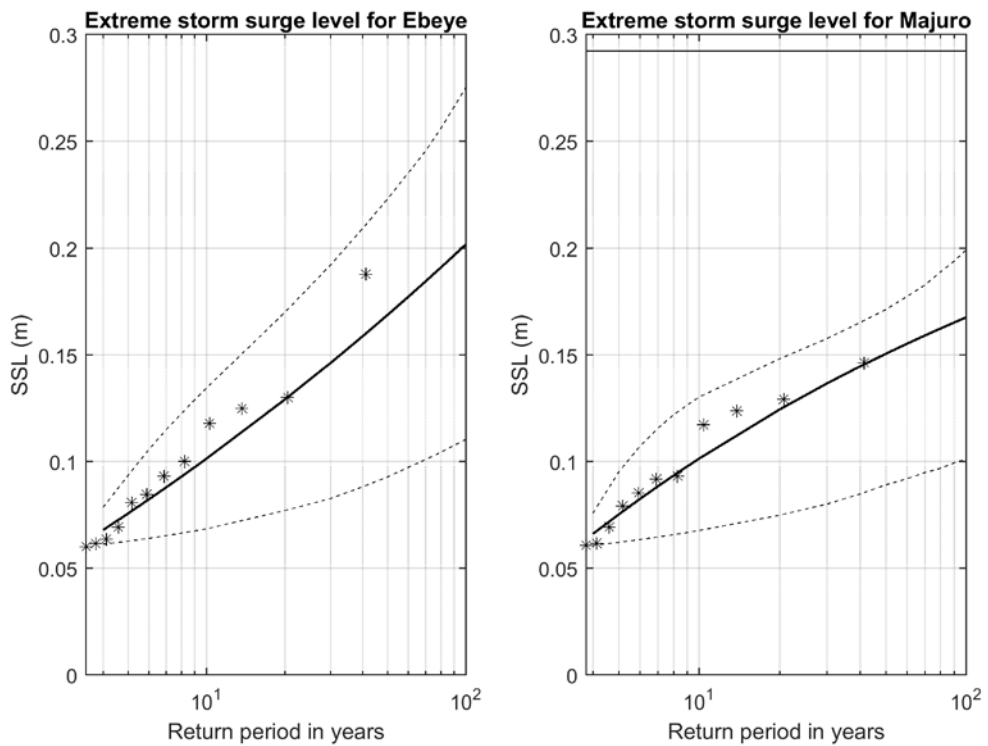
Figure 6.11   Extreme value analysis of the modelled storm surge levels at Ebeye (left) and Majuro (right) induced by the typhoons.

Deltares

6.5 Tsunamis

The impacts of natural disasters such as tsunamis, that do not occur that often at the RMI, (Section 5.2.6), have various generation mechanisms. It is therefore hard to apply a comprehensive risk analysis with return periods. On top of that, based on literature, tsunamis resulted in minor impact at the RMI, especially if compared with the impact of the major typhoon and swell events. Therefore, only the most recent event Tohoku Earthquake is analysed in more detail. The Tohoku Earthquake of March 11 2011, with epicentre off the coast of Japan, created a major tsunami that caused numerous deaths and enormous destruction, especially in Japan.

The impact of a tsunami wave (i.e. inundation) depends on the combination of the tsunami wave (i.e. amplitude) and the water level (i.e. tide). Based on measurements (buoy 52,401) and numerical modelling, it was estimated that at deep water the first tsunami wave, as result of the earthquake, had an amplitude of 0.3 – 0.4 meter with a period of 20 minutes near the RMI. A high resolution Delft3D model was applied to determine the inundation depth of Ebeye since the height of a tsunami wave increases as the water becomes more shallower (through wave shoaling). The eventual wave height at the shore determines the run-up and inundation at the island.

The Delft3D-FLOW model applied has rectangular non-equidistant grid with 2700x1638 grid cells (Figure 6.12). The resolution varies from 1000x1000 to 100x100 meter at the area of interest. The model is forced at one side (northwest of Ebeye) with the water level variation observed by the nearest DART buoy (http://nctr.pmel.noaa.gov/Dart/). The opposite boundary (southeast of Ebeye) is an open Riemann boundary in order to let the tsunami wave propagate out of the area with minimal reflections. The two sides of the model have closed boundaries. The result is an estimate of the tsunami amplitude near the shoreline.

The maximum amplitude modelled, see Figure 6.12 increases around Kwajalein Atoll due to shoaling. Due to the wave propagation and bed level variations, the maximum tsunami amplitude varies substantially around the atoll. At deeper water the maximum amplitude is similar to the amplitude at the northwest boundary. For Ebeye the maximum amplitude modelled is 100 centimetres, which is consistent with literature values (Robertson and Hwang, 2015, Section 5.2.6). This value should be added up to the tidal water level at that moment in order to determine the actual inundation.

In this study, the maximum modelled amplitude was combined with the water level during high water (i.e. worst-case scenario). For future sea level rise scenarios the tidal water level will vary (i.e. increase depending on the RCP scenario and time horizon).
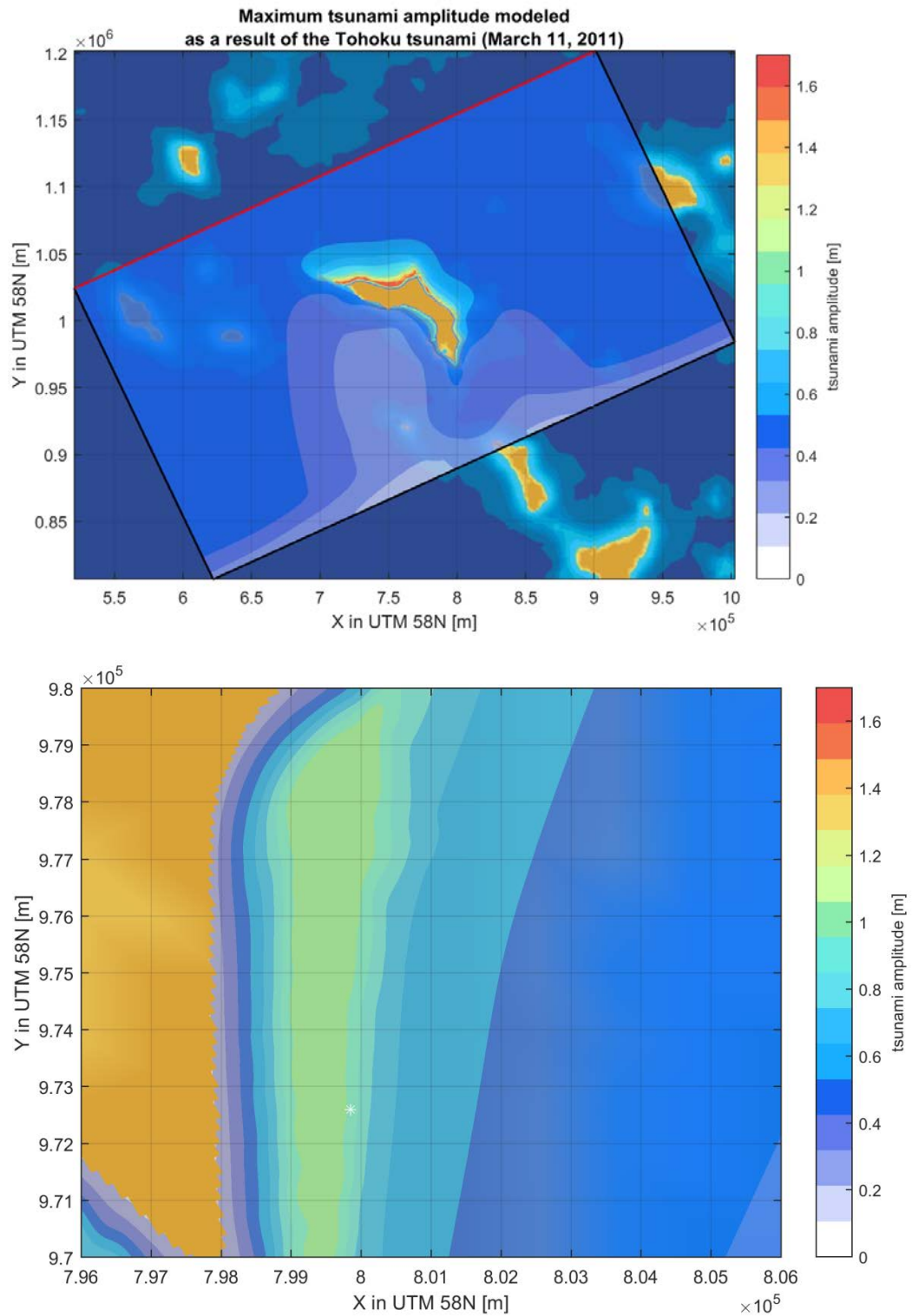
Figure 6.12   Maximum tsunami amplitude around Kwajalein atoll (upper panel) and Ebeye (lower panel). White star illustrate the location of Ebeye.

6.6 Climate change and sea level rise

Based on the collected information on the projections for Kwajalein Atoll area (Section 5.2.7), the expected scenarios for sea level rise and wave height changes are determined for 2030, 2050 and 2100, see Table 6.8.

Table 6.8   Climate change scenarios used in the study

		Time horizon		
		2030	**2050**	**2100**
RCP 4.5	Sea level rise [m]	0,12	0,23	0,53
RCP 8.5	Sea level rise [m]	0,13	0,26	0,78
Hemer et al. (2013)	Wave height change [%]	+1.00	1,50	+ 2.00

Based on the available information, it is assumed that climate change effects on the hazards from the lagoon, typhoons and tsunamis are only affected by sea level rise as wave height changes are projected to be very small. These sea level rise rates are also based on the information in Table 6.8.

7 Assessment of the impacts of coastal hazards

7.1 Inundation of the island of Ebeye

7.1.1 Introduction

Coastal hazards offshore have been quantified in Chapter 6. In this chapter, offshore conditions have been translated to inundation extent and depths by using a two-dimensional XBeach model of Ebeye (Section 5.3.2). The model has been applied for different return periods and time horizons (i.e. including the effect of sea level rise) and validated with information collected during the field visit from local stakeholders.

Inundation extents have been computed separately by considering different contributions from different physical processes, for different time horizons and sea level rise scenarios, and then combined in Section 7.1.7:

- Swell waves from the ocean (Section 7.1.3)
- Wind-wave from the lagoon (Section 7.1.4)
- Waves generated due to typhoons (Section 7.1.5)
- Tsunami's wave (Section 7.1.6)

The topography and grid resolution of the XBeach model are shown in Figure 7.1, more information on the island topography and bathymetry can also be found in Section 5.2.1 and 5.2.2. The XBeach grid consists of 519x138 (cross-shore x longshore) grid cells. In longshore direction the grid is equally spaced with a resolution of 20 m, it decreases from 20 m (offshore) to 1 m (nearshore) in cross-shore direction. Only the central part of Ebeye is modelled with XBeach, while flooding of the causeway is computed by using overtopping formula in Section 7.2. The model is somewhat extended in longshore direction in order to overcome any lateral boundary effects.
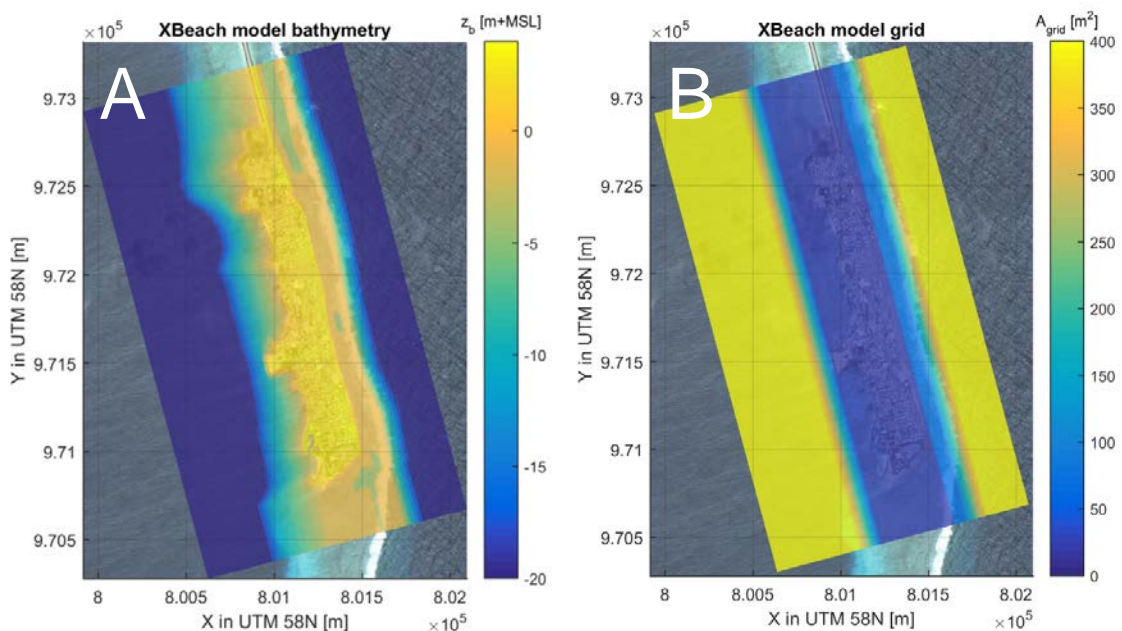
Figure 7.1   XBeach model set-up. Subfigure A) depicts the topography as implemented in the model. Subfigure B) shows the cell sizes in m^2.

Wave conditions from the ocean attack the coastline from the east in shore-normal direction (see also Section 6.3.1 and Section 6.4). Waves from the lagoon enter the model domain from the west. On the lateral boundaries, Neumann conditions are imposed. Swell wave and typhoon scenarios are simulated assuming a design storm with a duration of 30 hours, see Figure 7.2, with a time series of water levels and waves. This design storm includes approximately three tidal cycles with a spring-high tide during the peak of the storm, i.e. 15 hr after the start of the simulation, see Figure 7.2. Besides the periodical water level modulation by the tide, also a stationary storm surge and sea level rise are included, which vary for different return periods and time horizons (for information on water levels see Section 6.2). Given the small size of the domain, all water level changes that are imposed occur simultaneously across the entire model domain.

Prescribed deep water waves increase from initially an arbitrary 2 m linearly towards their maximum value during the peak of the storm (after 15 hours), after which wave heights decrease again to 2 m towards the end of the simulation. The maximum wave height also depends on the return period and time horizon and hence varies between simulations.

The bed roughness is non-uniform with Chezy values ranging between 30 to 60 $m^{1/2}$ s^{-1}. Offshore and on the reef flat, the bathymetry is assumed to be relatively smooth. The fore reef on the other hand is quite rough as large coral canopies are known to create a course relief in these parts. Furthermore the island itself represents a rough surface for overtopping waves. At areas with higher bed roughness a lower Chezy coefficient is applied, see also Figure 7.3.

The upcoming sections present the impact (inundation) of the different hazards in the following order: swell waves (Section 7.1.3), waves from the lagoon (Section 7.1.4), typhoons (Section 7.1.5) and finally tsunamis (Section 7.1.6). First, a model validation will be carried out in Section 7.1.2.
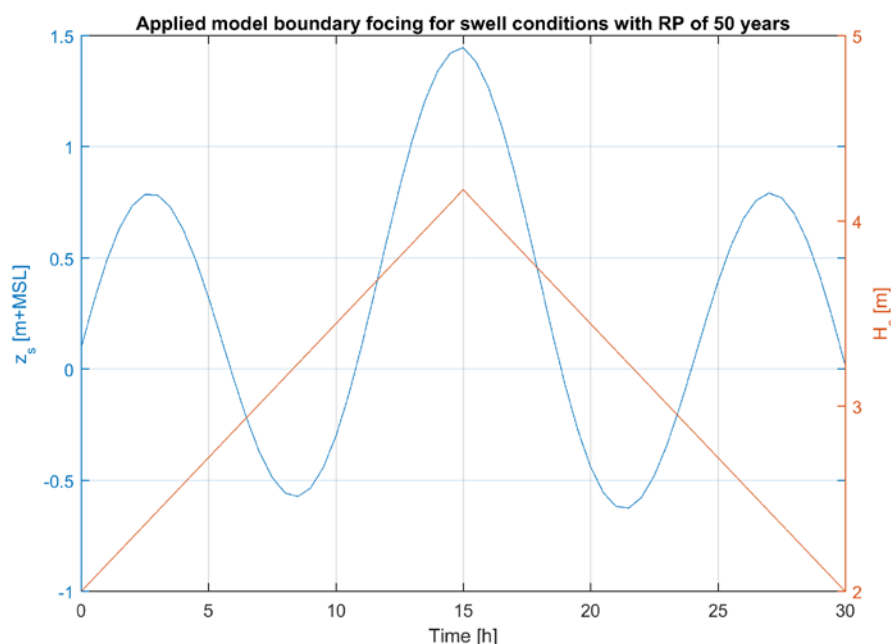
Figure 7.2   Applied time series of water levels and wave heights in XBeach for swell conditions with a return period of 1/50 years.
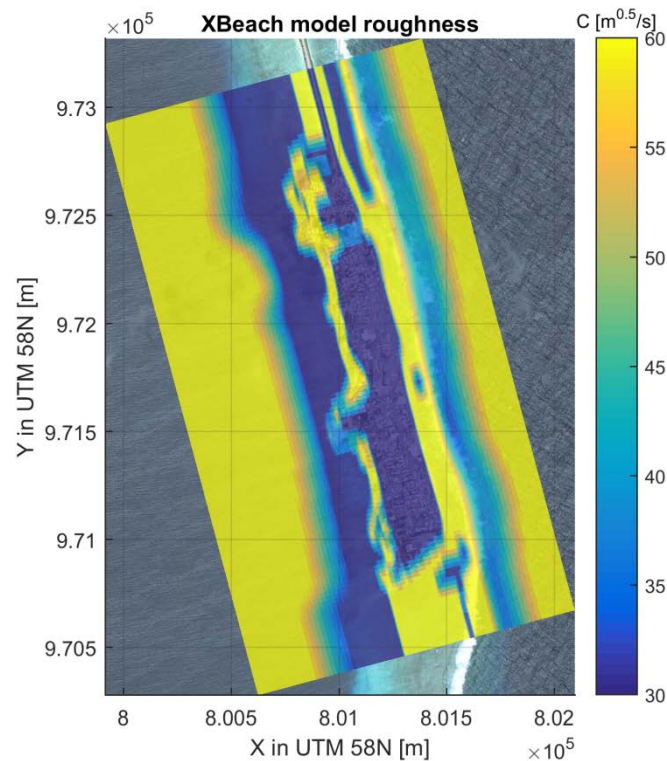
Figure 7.3 XBeach bed roughness in Chezy [m½/s].

7.1.2 Model validation

Most of the available literature on waves and hydrodynamics has been developed for sandy beaches. However, hydrodynamics on coral reefs are general quite different than from sandy environment (Quataert et al., 2015). Unfortunately, no measurements were available at the island of Ebeye. Therefore, in order to verify model performances, calculated wave heights and water levels on the reef are compared with measured values during a large swell event that occurred in March 2014 at Roi-Namur, located at the northern tip of Kwajalein Atoll (Quataert et al., 2015; Cheriton et al., 2016). The event was characterized by offshore significant wave heights (H_s) ranging between 3 and 4 m and peak periods (T_p) above the 18 s (Cheriton et al., 2016), therefore similar to the conditions simulated.

Wave heights

Offshore swell waves with a return period of 5 years (i.e. H_s = 3.6 m, see Table 6.4) and therefore very similar to the conditions which occurred during the 2014 event, were used to force the model.

Waves are predicted to break at the outer reef edge and decrease further in wave height as they progress over the reef flat towards the coastline, as can be seen from Figure 7.4. The modelled short and long wave height at Ebeye at the reef were respectively $H_{s,hf,Ebeye}$ ≈ 1 m $H_{s,lf,Ebeye}$ ≈ 1.3 m. Considering that the reef flat at Roi-Namur is wider than at Ebeye (respectively 250-300 compared to 100-150 meter), these values are in line with the observed values during the March 2014 event, which resulted in short and long wave height at the reef, respectively of $H_{s,hf,RoiNamur}$ ≈ 0.9 m and $H_{s,lf,RoiNamur}$ ≈ 1.2 m (Gawehn, 2015).

Note that after breaking, short wave heights generally decrease over the reef flat, whereas the long wave height tends to increase. The reason for this is a steady transfer of momentum from higher to lower frequencies (Gawehn et al., 2016). The hydrodynamics may be affected by the local mining pits in the reef flat. However, little is known about the impacts of these pits on the reef hydrodynamics. A short analysis is conducted within this study based on the modelling results in Appendix B.

<u>Wave-induced setup</u>

It is a known fact that breaking waves can induce a large water level setup on coral reef flats, reaching up to 1.3 m over the concurrent sea level offshore (Vetter et al., 2010), as also shown by Figure 7.5.
 A. This mechanism is also crucial to explain high water levels in the nearshore and even inundation of island areas during periods of low tide (Cheriton et al., 2016; Gawehn et al., 2016). Again comparing the wave induced setup with measurements found during the storm-swell event at Roi-Namur, values are very similar. While the model results of Ebeye reveal a setup of approximately 0.8 m above the offshore water level (1 m) (see Figure 7.5), Roi-Namur experienced wave setup of approximately 0.7-0.9 m (Cheriton et al., 2016). Numerical boundary effects can be visible close to the open boundaries of the domain. For example, in Figure 7.5 the mean water level during the peak of the storm decreases at around 2500 meter distance. These boundary effects will, however, have a negligible effect on the calculated impacts since they are located far enough from the actual area of interest.

To conclude, this simulation provides confidence on the reliability of the model results, both in terms of wave transformation over the reef as well as wave setup induced by breaking waves. Therefore, this model setup will be the used to simulate the different scenarios as described in Section 7.1.1.
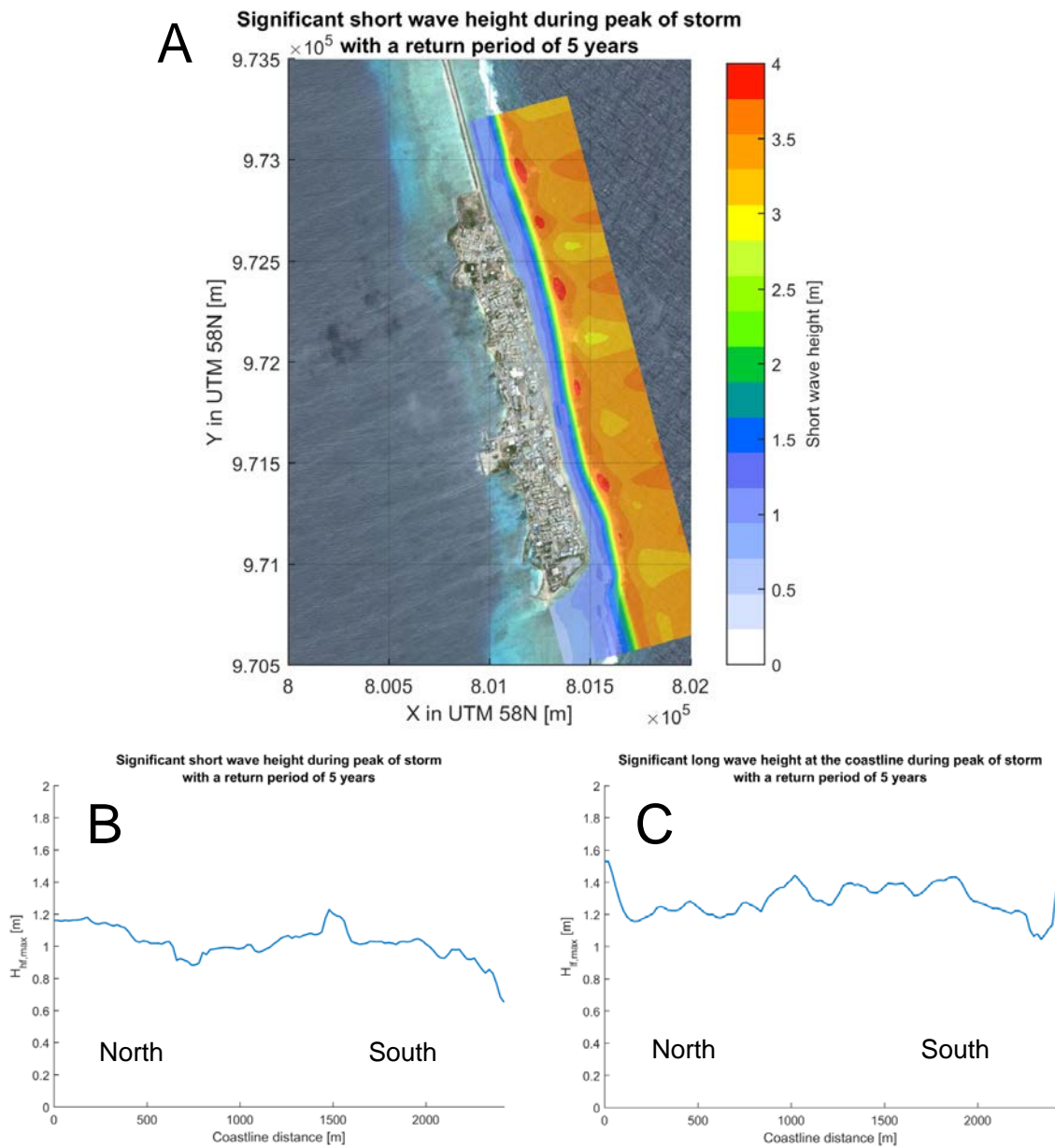
Figure 7.4   Simulated significant short and long wave heights during the peak of a storm-swell event with a return period of 5 years. Subfigure A) presents a map of the significant short wave heights over the entire domain. The lower subfigures depict the short (B) and long (C) wave heights at the coastline. The coastline distance is defined as the alongshore distance relative to its Northern end.
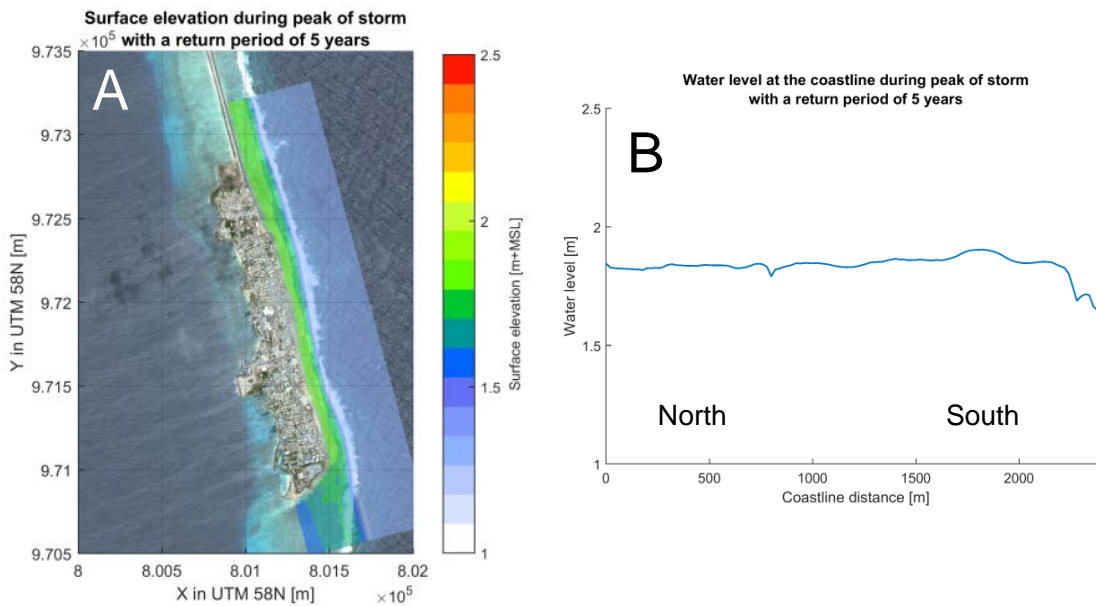
Figure 7.5   Simulated water levels during the peak of a storm-swell event with a return period of 5 years. Subfigure A) presents a map of water levels over the entire model domain. Subfigure B) shows the water levels at the coastline. The coastline distance is defined as the alongshore distance relative to its Northern end. In B some numerical boundary effects are visible.

7.1.3   Inundation due to swell waves

The inundation caused by swell waves with a 10 year return period (H_s = 3.74 meter) is shown as an example to illustrate which parts of the islands are mostly affected in the present situation (Figure 7.6). The impact of swell waves with other return periods is expressed as % of inundated island area. This percentage depends on the definition of inundation and is hence given for both a minimum inundation depth of 20 cm and a minimum inundation depth of 50 cm (see Table 7.1).

As may be expected, the lower parts of the island are the most affected. These are located in the northern part of Ebeye and closer to the lagoon (see also Figure 5.3). Higher parts of the islands or areas protected by seawalls (e.g. power plant in the south of the island; container park near the harbour) are more protected. However, for example, the wall surrounding the power station is sufficient to withstand regular storm conditions but becomes insufficient to withstand swell waves with a return period of 5 years or higher.

Generally, the patterns in the inundation map presented in Figure 7.6 do not change much as the wave height return periods increase, i.e. the vulnerable parts stay the same. Yet, the inundated area increases. A difference in wave height of 0.6 m between the 5 and 50 year wave height return period (i.e. H_s = 3.56 m and H_s = 4.17 m) leads to more than 25 % additional inundation with at least 20 cm of water, as shown in Table 7.1. However, small return periods waves are already sufficient in the present situation to inundate large part of the island with a minimum inundation depth of 20 cm, whereas higher return periods cause a substantial inundation, with a larger inundation depth of more than 50 cm (Table 7.1).

Table 7.1 Percentage of island inundation induced by swell-wave with return periods 5, 10, 30 and 50 years. The % relative to the island area is given for a minimum inundation depth of 20 cm and 50 cm.

RP [yr]	Hs [m]	[%] of island inundation	
		Inundation depth > 20 cm	**Inundation depth > 50 cm**
5	3.56	21.6	4.4
10	3.74	30.0	5.5
30	4.04	43.8	8.5
50	4.17	48.6	10.2

As expected, the already critical present situation is expected to worsen in the future. The same information for the present situation is shown for different time horizons (2030; 2050 and 2100) and two RCP scenarios (RCP 4.5 and RCP 8.5) in Table 7.2 and Figure 7.7. It is clear that for different time horizons and two RCP scenarios the inundation extent increases. In particular, inundation events with a smaller return period will increase relatively the most (e.g. 1/5 years: 22% versus 60-74% inundated, factor 3). For larger events the increase in inundation area is relatively smaller (e.g. 1/50 years 48% versus 75-85%, factor 2).

Table 7.2 Percentage of island inundation induced by swell-wave with return periods of 5, 10, 30 and 50 years. The % relative to the island area is given for a minimum inundation depth of 20 cm.

[%] of island inundation (>20 cm)					
RP [yr]	**Hs [m]**	**Current SLR = 0 m**	**RCP 4.5: 2030 SLR = 0.12 m**	**RCP 4.5: 2050 SLR = 0.23 m**	**RCP 4.5: 2100 SLR = 0.53 m**
5	3.56	21.6	29.8	39.9	60.1
10	3.74	30.0	40.1	47.1	65.2
30	4.04	43.8	51.2	57.2	72.1
50	4.17	48.6	55.6	61.5	75.3
RP [yr]	**Hs [m]**	**Current SLR = 0 m**	**RCP 8.5: 2030 SLR = 0.13 m**	**RCP 8.5: 2050 SLR = 0.26 m**	**RCP 8.5: 2100 SLR = 0.78 m**
5	3.56	21.6	30.6	41.9	73.5
10	3.74	30.0	40.9	49.4	77.7
30	4.04	43.8	51.7	58.8	83.3
50	4.17	48.6	56.1	63.0	85.3
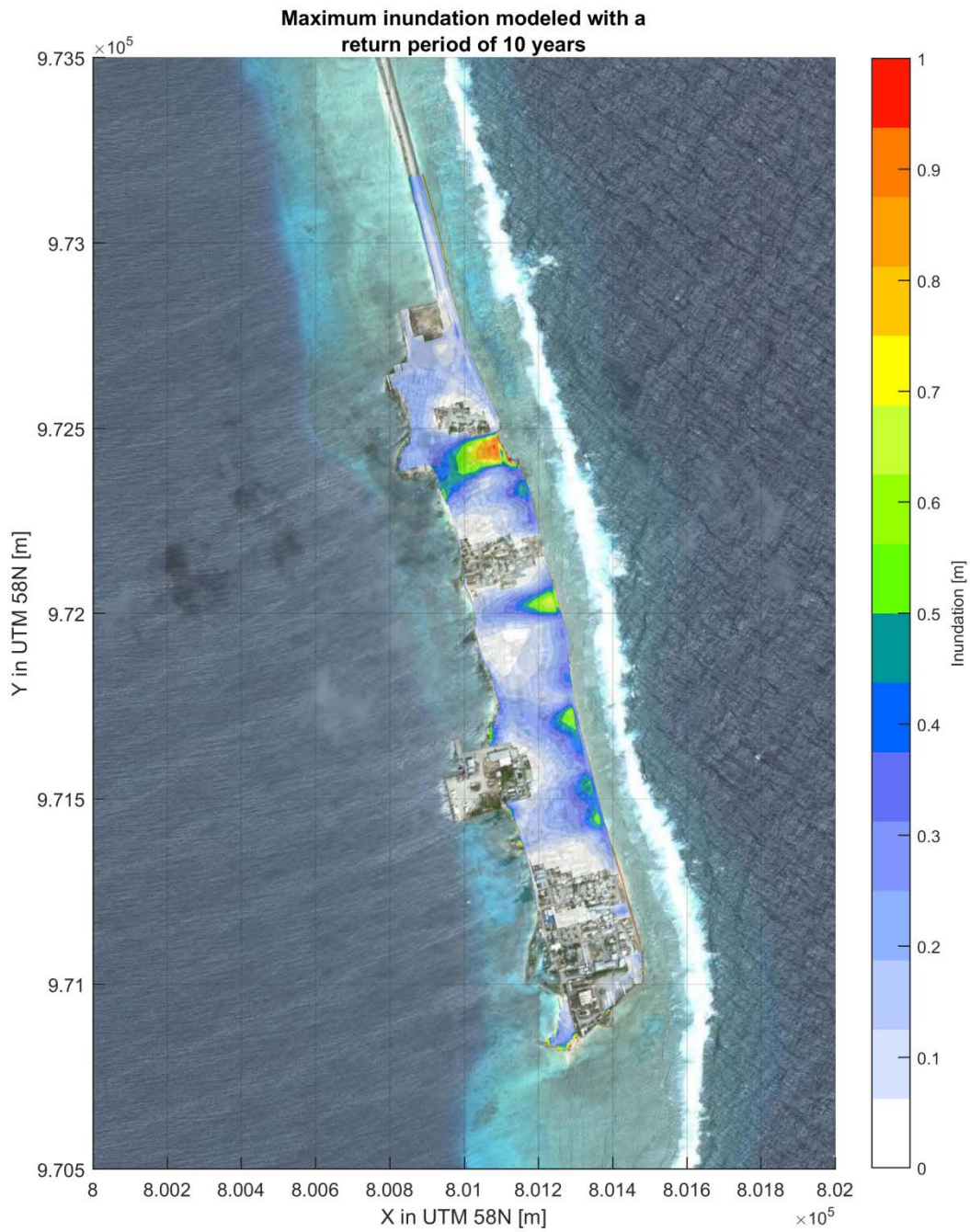
Figure 7.6   Inundation map showing the impact of swell waves for the current situation with an offshore wave height of Hs = 3.7 m (return period of 10 years).

Figure 7.7   Inundation map showing the impact of swell waves for sea level rise scenario RCP 8.5 2100, with an offshore wave height of Hs = 3.7 m (return period of 10 years).

7.1.4   Inundation from the lagoon
Locally generated waves in the lagoon are limited in height (0.5 - 1.0 meter), but can, during high water and in combination with surge, reach some of the houses at the backshore of Ebeye. This is especially the case for some parts in the north and middle of Ebeye where the bed level is only a few decimetres above the water level during high water.

Figure 7.8   Inundation of the area near the harbour due to westerly waves from the lagoon.

During conditions with return periods of 1/5 years (H_s = 0.46 meter) about 2% of the backshore will get inundated (water depth > 0.2 meter), with increasing surface for higher return periods (Table 7.3). Nevertheless, for all the simulated scenarios the impacted area is relatively small. From this we can assume that the hazards from the open ocean are generally more threatening than the ones from the lagoon, when we consider the effects over the entire island. Also, there is hardly any area which gets inundated by more than 50 centimetres of water, regardless of the return period.

The inundation map for a return period of 1/10 is shown in Figure 7.9. One can see inundation of around 30 centimetres in the northern area (i.e. North Camp) which had been reclaimed in the past. On top of that, the model predicts severe inundation ($\approx$ 40 cm) in the central part, north of the harbour.

Table 7.3   Percentage of island inundation induced by waves from the lagoon with return periods 5, 10, 30 and 50 years. The % relative to the island area is given for a minimum inundation depth of 20 cm and 50 cm.

RP [yr]	Hs [m]	[%] of island inundation	
		Inundation depth > 20 cm	Inundation depth > 50 cm
5	0.67	1.6	0.0
10	0.77	1.9	0.0
30	0.96	2.5	0.1
50	1.06	5.3	0.4

The inundation extent is expected to increase for different time horizons, under the two RCP scenarios, (Table 7.4). For example under RCP 8.5 in 2100 and for wave conditions with a return period of 1/10 years more than 40% of Ebeye is expected to get inundated versus 2% under the current sea level. Figure 7.10 shows the inundated area, according to model simulations, for RCP 8.5 in 2100. Large part of the coastal area at the lagoon side of Ebeye is supposed to get inundated, except for the higher parts (i.e. container park near the harbour and house of the king).

Table 7.4   Percentage of island inundation induced by waves from the lagoon with return periods 5, 10, 30 and 50 years. The % relative to the island area is given for a minimum inundation depth of 20 cm.

| [%] of island inundation (>20 cm)					
RP [yr]	**Hs [m]**	**Current SLR = 0 m**	**RCP 4.5: 2030 SLR = 0.12 m**	**RCP 4.5: 2050 SLR = 0.23 m**	**RCP 4.5: 2100 SLR = 0.53 m**
5	0.67	1.6	6.5	15.2	28.2
10	0.77	1.9	11.5	16.3	29.6
30	0.96	2.5	13.2	17.7	31.7
50	1.06	5.3	15.3	19.7	34.1
RP [yr]	**Hs [m]**	**Current SLR = 0 m**	**RCP 8.5: 2030 SLR = 0.13 m**	**RCP 8.5: 2050 SLR = 0.26 m**	**RCP 8.5: 2100 SLR = 0.78 m**
5	0.67	1.6	10.2	16.4	41.2
10	0.77	1.9	11.9	17.5	42.8
30	0.96	2.5	13.7	19.2	44.8
50	1.06	5.3	15.6	21.2	47.1

Figure 7.9   Inundation map showing the impact of waves from the lagoon for the current situation with an offshore wave height of Hs = 0.7 m (return period of 10 years).
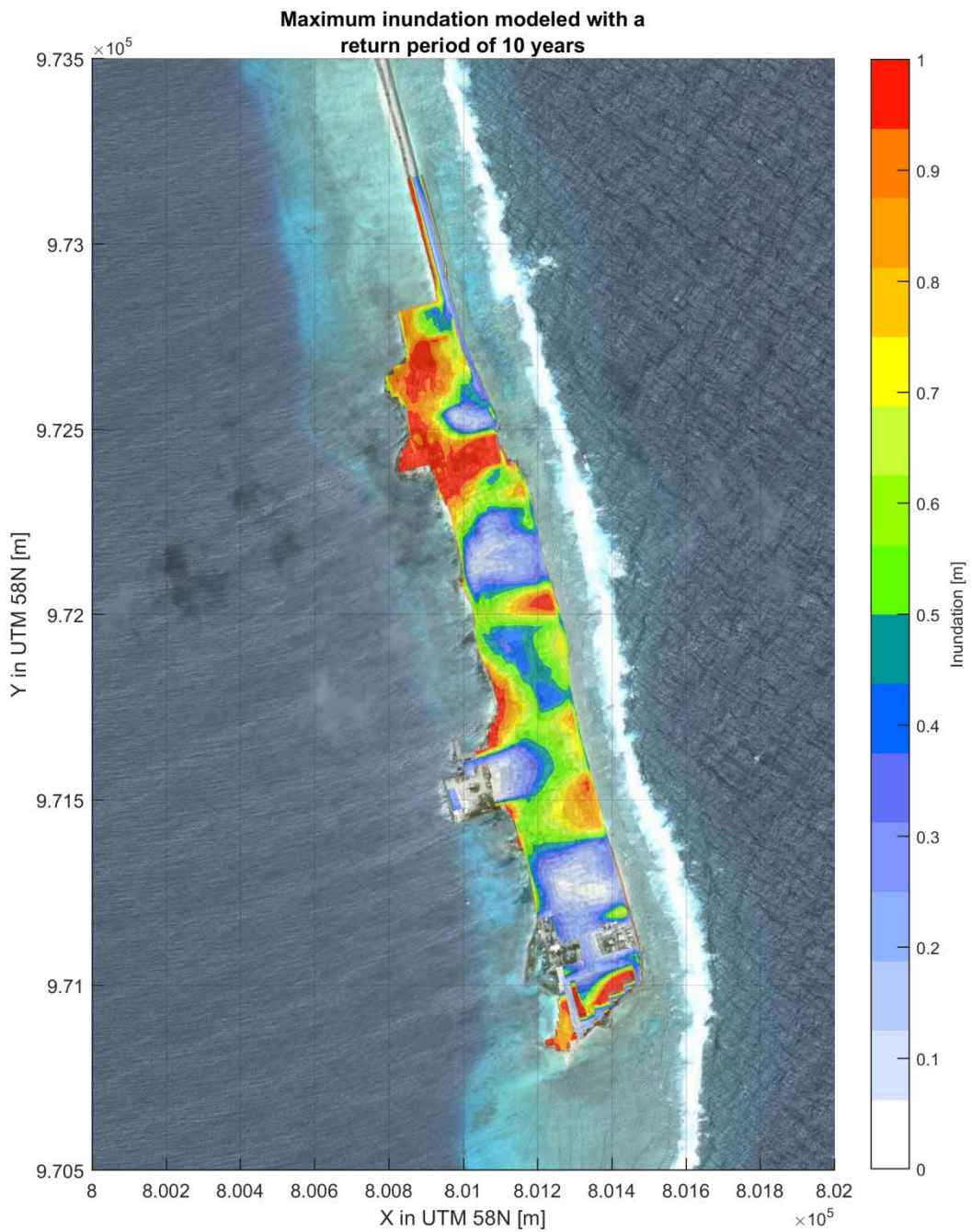
Figure 7.10   Inundation map showing the impact of waves from the lagoon for sea level rise scenario RCP 8.5 2100 with an offshore wave height of Hs = 0.7 m (return period of 10 years).

7.1.5   Inundation due to typhoons

Wave conditions generated during typhoons have lower wave periods than swell conditions (10 s compared to 20 s). Therefore, it is expected that swell conditions with a similar wave heights will result in more impact (i.e. inundation) than wave conditions generated by typhoons. Compared to the extreme swell conditions derived from ERA-Interim (see Section 6.3.1), the wave heights for typhoons are lower compared to the swell events for return periods of 1/5 and 1/10 years. For larger return periods the wave heights generated by typhoons exceed the swell conditions.

The result in terms of inundation during typhoon conditions with a return periods of 1/5 years is indeed smaller compared to the swell conditions (5% versus 44% for swell conditions, assuming a threshold for inundation depth of 20 cm; see Table 7.5 versus Table 7.1). Also for a return period of 1/10 years the amount of inundation due to typhoons is still lower (12% inundation compared to 53% for swell conditions). For larger return periods the wave height for typhoons starts to increase very rapidly, exceeding the inundation due to swell conditions.

For a return period of 1/10 the inundation map is shown in Figure 7.11. The result is somewhat similar to the impact as a result of swell conditions (Section 7.1.3). Lower parts of Ebeye will get inundated with no inundation exceeding the value of 1 m. This does, however, happen for wave heights generated by typhoons with higher return periods.

Table 7.5 Percentage of island inundation induced by typhoon waves with return periods 5, 10, 30 and 50 years. The % relative to the island area is given for a minimum inundation depth of 20 cm and 50 cm.

RP [yr]	Hs [m]	[%] of island inundation	
		Inundation depth > 20 cm	Inundation depth > 50 cm
5	3,16	5.2	1.7
10	4,61	11.7	3.2
30	7,21	69.2	36.1
50	8,57	90.0	79.5

For different time horizons and two RCP scenarios the inundation extent increases. This can be seen visually for a return period of 1/10 years by 2100 in Figure 7.12, assuming a sea level rise scenario RCP 8.5. Especially the increase in the amount of inundation for relatively frequent events (return period 1/5 years) by 2100 and considering scenario RCP 8.5 is worrying (e.g. an event with a return period of 1/5 years will lead to an increase in inundated area from 5% (in the current situation) to 36% (by 2100) (increase of a factor 7), see Table 7.6.

Table 7.6 *Percentage of island inundation induced by typhoon waves with return periods 5, 10, 30 and 50 years. The % relative to the island area is given for a minimum inundation depth of 20 cm.*

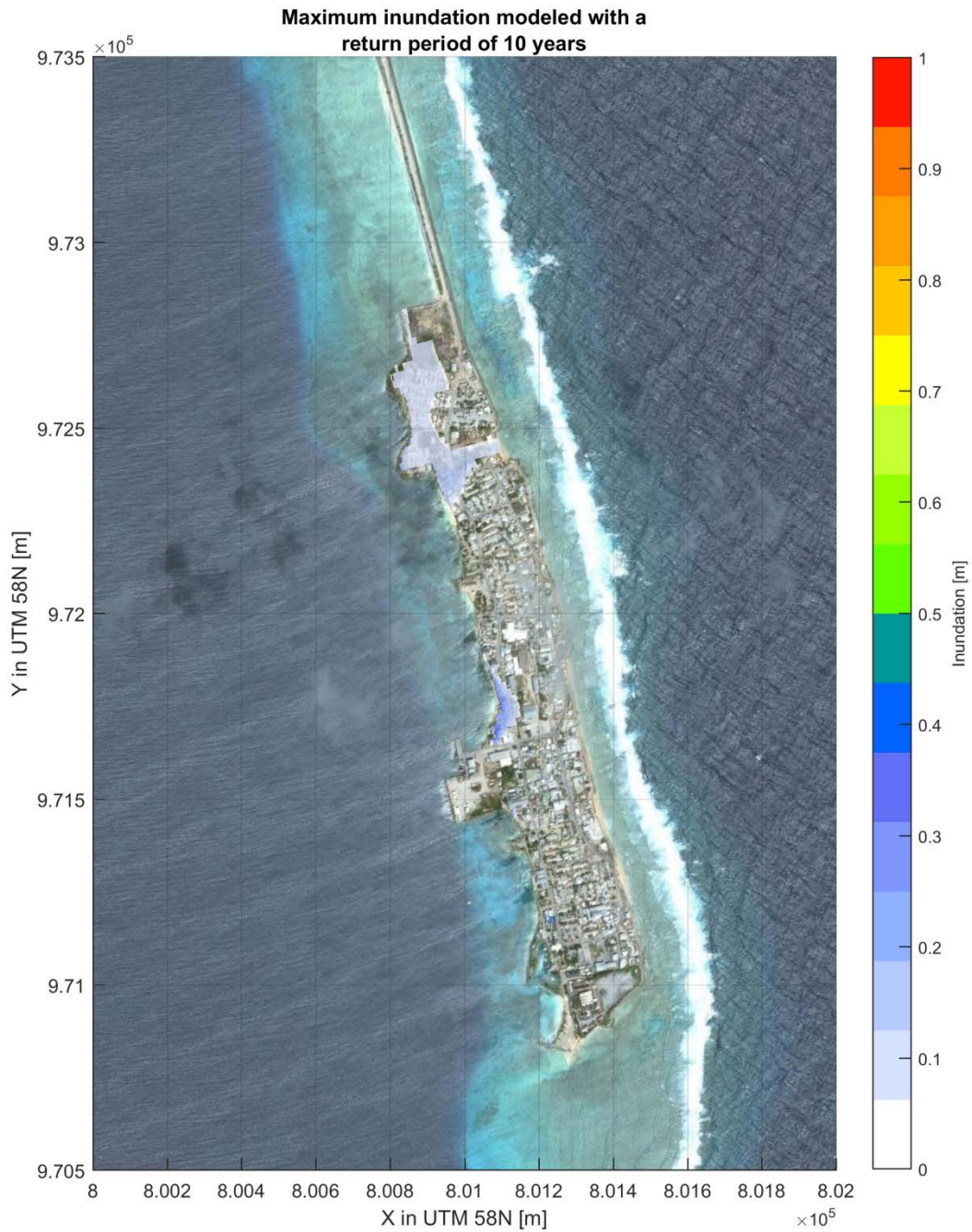| [%] of island inundation (>20 cm)					
RP [yr]	**Hs [m]**	**Current** SLR = 0 m	**RCP 4.5: 2030** SLR = 0.12 m	**RCP 4.5: 2050** SLR = 0.23 m	**RCP 4.5: 2100** SLR = 0.53 m
5	3,16	5.2	6.1	7.1	15.2
10	4,61	11.7	17.9	22.1	44.4
30	7,21	69.2	76.2	80.6	86.8
50	8,57	90.0	93.4	93.3	94.0
RP [yr]	**Hs [m]**	**Current** SLR = 0 m	**RCP 8.5: 2030** SLR = 0.13 m	**RCP 8.5: 2050** SLR = 0.26 m	**RCP 8.5: 2100** SLR = 0.78 m
5	3,16	5.2	6.2	7.5	35.8
10	4,61	11.7	18.4	26.5	68.6
30	7,21	69.2	76.6	82.1	91.8
50	8,57	90.0	93.4	93.4	94.1

Figure 7.11   Inundation map showing the impact of typhoon waves for the current situation with an offshore wave height of Hs = 4.6 m (return period of 10 years).

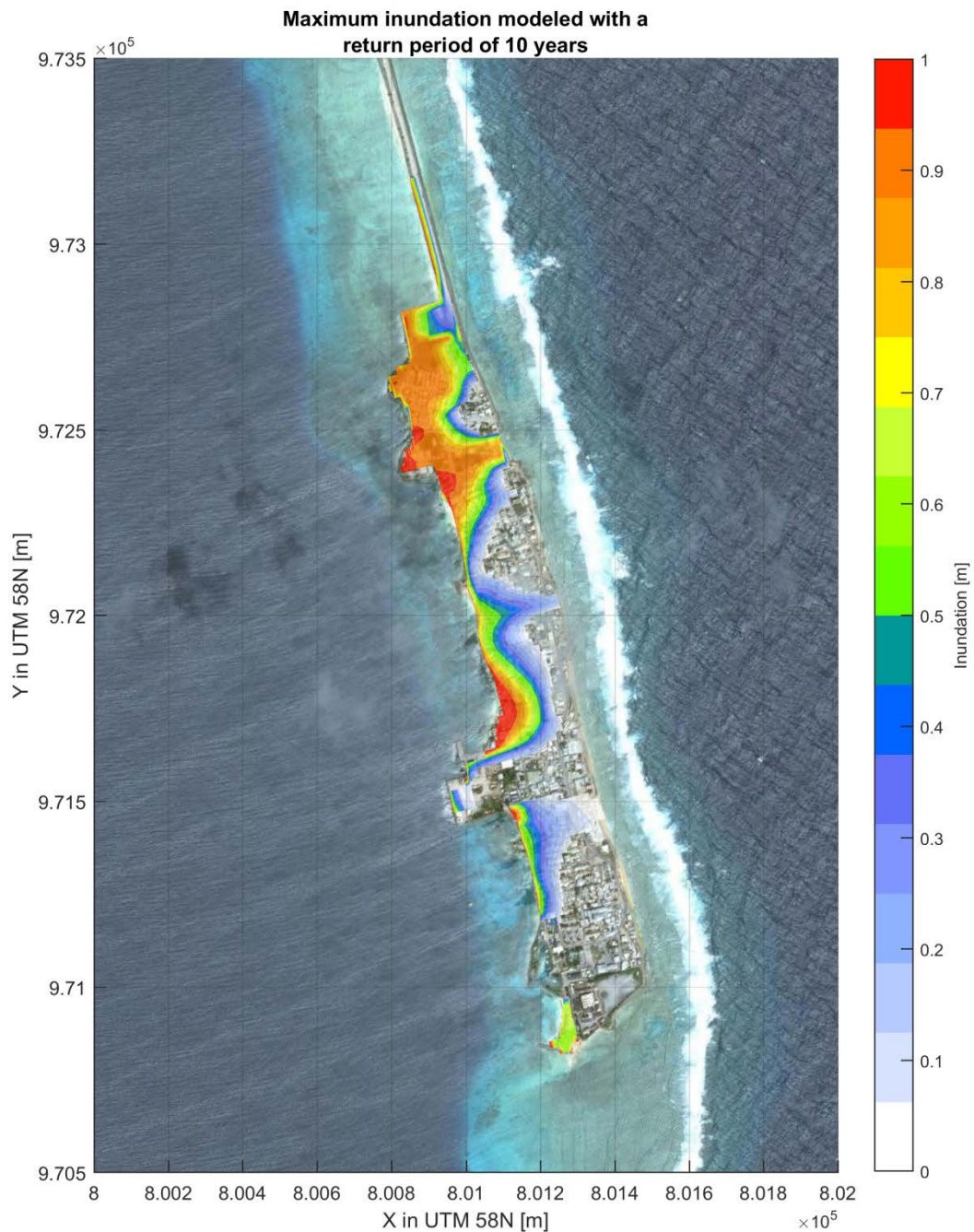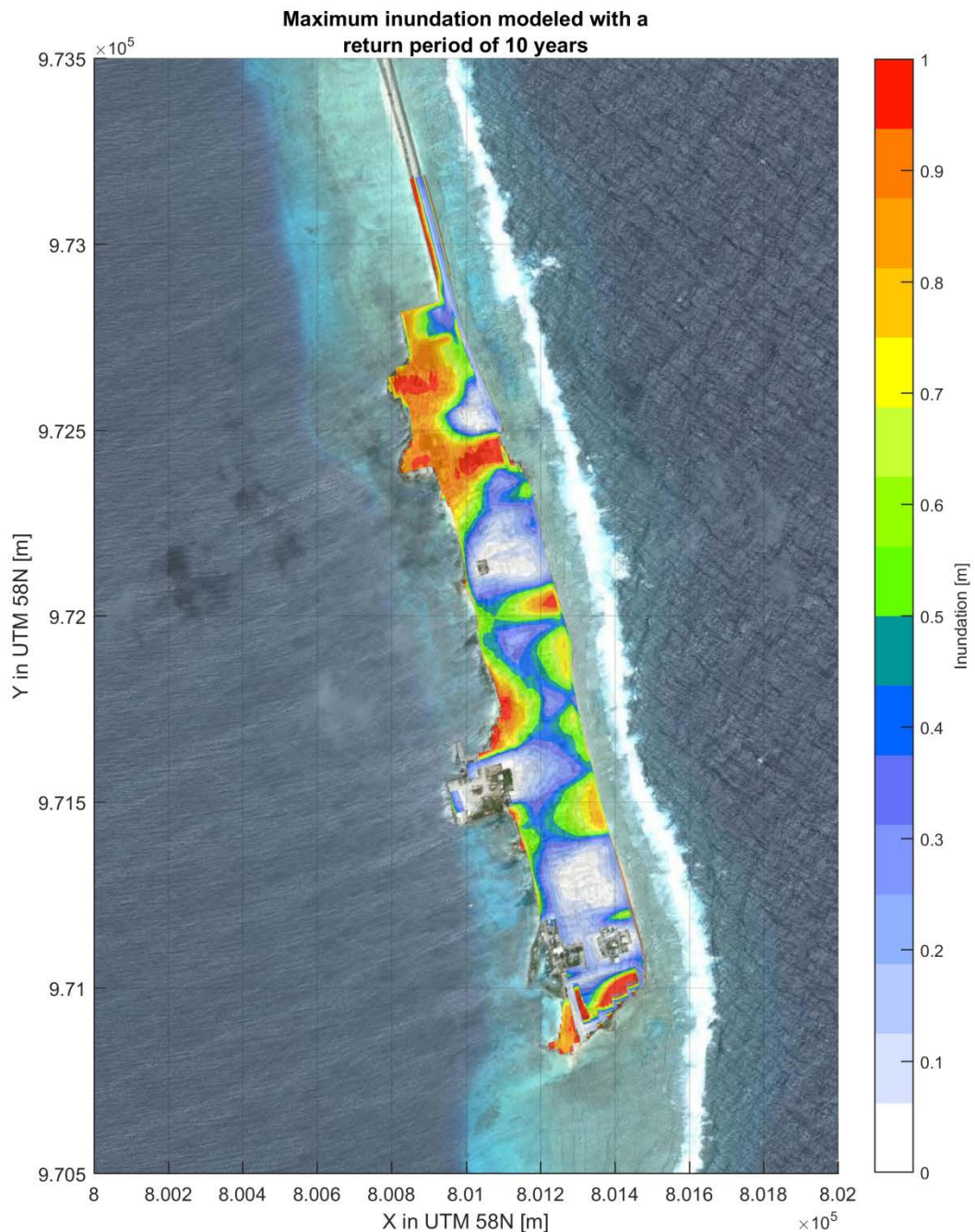*Figure 7.12   Inundation map showing the impact of typhoon waves for sea level rise scenario RCP 8.5 2100 with an offshore wave height of Hs = 4.6 m (return period of 10 years).*

7.1.6   Inundation due to tsunamis

At Ebeye, a maximum tsunami amplitude at the coastline of 100 centimetres was computed for the Tokoku event (Section 6.5). This value, based on a numerical simulations, is also consistent with literature values (Robertson and Hwang, 2015, Section 5.2.6). However this value should be added to the tidal water level of that specific moment. On top of that, for future sea level rise, the tidal water level will increase depending on the RCP scenario and time horizon. In this section, we will show the impact (i.e. inundation) of the Tokoku tsunami

during high water (i.e. worst-case scenario) for the current situation and for different time horizons and sea level rise scenarios.

For the current situation, see the left panel of Figure 7.13, the amount of inundation is relatively limited. Especially if one compares this to large swell (Chapter 7.1.3) or typhoon events (Chapter 7.1.5). There is limited inundation (< 0.3 meter) around the relatively low part in the north, which also results in about 10 centimetres of inundation at the backshore, but overall the impact of a tsunami such as the Tokoku event is limited. These results of the current situation are in agreement with observations in the field, since Tokoku resulted in hardly any damage at Ebeye.

For the most severe future scenario (i.e. RCP 8.5 during 2100: sea level rise of 0.78 meter) the amount of inundation increases, see the right panel of Figure 7.13. Especially in the lower northern part of Ebeye large inundation depth (> 0.75 meter) are observed; the tsunami also results in more inundation at the backshore. However, compared to other coastal hazards, the impact of a tsunami is minor.
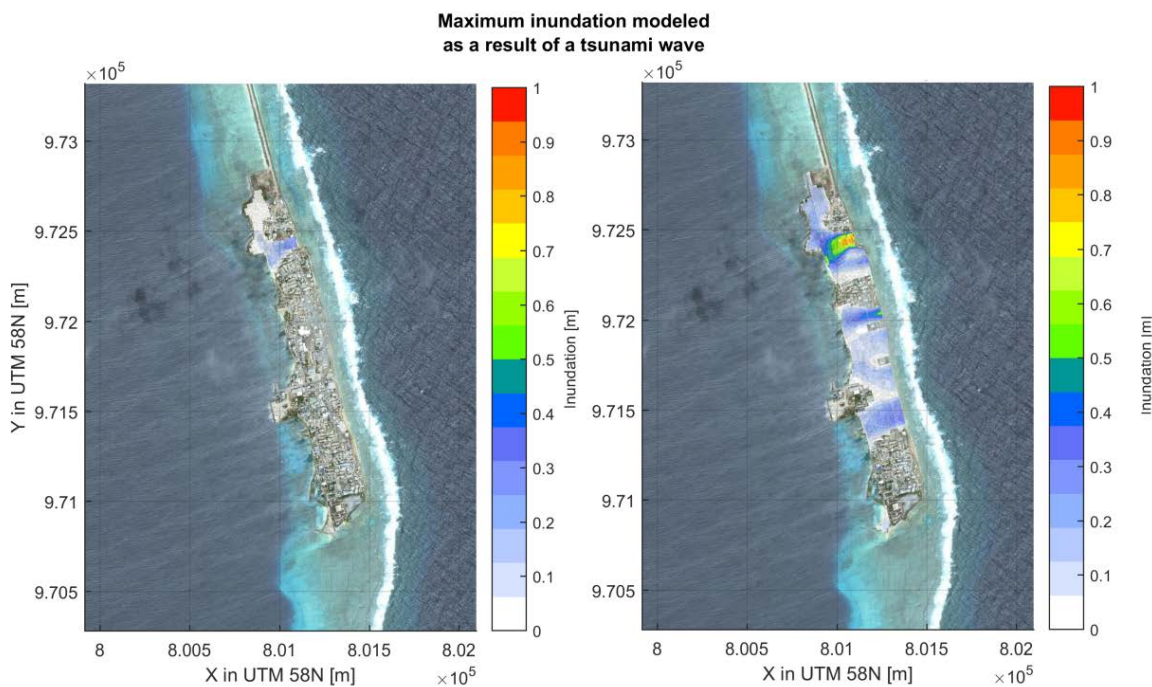
Figure 7.13   Maximum inundation modelled as a result of a tsunami wave. Left panel: current situation. Right panel: for sea level rise scenario RCP 8.5 2100

7.1.7 Combination of the inundation effects

For the risk assessment the maximum inundation depth per return period is determined. This is done by taking the maximum inundation water level per contribution. The result is the maximum inundation depth per grid cell. The inundation can either occur during extreme swell conditions, locally-generated waves from the lagoon, due to typhoons or tsunami's. Inundation at the causeway is determined via an overtopping formula; see Section 7.2, more suitable to assess the overtopping of a revetment, accounting for the contribution of both short and long waves.

For low return periods, swell conditions are the dominant flooding factor. For higher return periods, the typhoon conditions become more dominant. Inundation from the lagoon is never the most threatening factor for inundation. In fact, the lower parts of Ebeye at the lagoon side also gets inundated during larger swell conditions by water coming from the ocean side, which crosses the island.

The maximum inundated area for a return period of 10 years for the present situation and in 2100 (under sea level rise scenario RCP 8.5), is shown respectively in Figure 7.14 and Figure 7.15. The figure shows that by 2100 nearly the entire island may get inundated by an event with a return period of 10 years. This is directly related to the rise in sea level, as waves will be able to reach the atoll easier resulting in more inundation. Table 7.7 shows the complete matrix of inundation areas for different future scenarios. For future situations (under two RCP scenarios and for 3 time horizons) the inundation area increases.

Table 7.7   Percentage of maximum island inundation with return periods 5, 10, 30 and 50. The % relative to the island area is given for a minimum inundation depth of 20 cm.

[%] of island inundation (>20 cm)				
RP [yr]	**Current** SLR = 0 m	**RCP 4.5: 2030** SLR = 0.12 m	**RCP 4.5: 2050** SLR = 0.23 m	**RCP 4.5: 2100** SLR = 0.53 m
5	21.7	30.1	41.0	61.1
10	30.2	40.7	47.9	66.2
30	69.9	76.4	80.7	87.0
50	90.0	93.4	93.3	94.0
RP [yr]	**Current** SLR = 0 m	**RCP 8.5: 2030** SLR = 0.13 m	**RCP 8.5: 2050** SLR = 0.26 m	**RCP 8.5: 2100** SLR = 0.78 m
5	21.7	33.0	43.1	74.0
10	30.2	41.4	50.3	78.2
30	69.9	76.7	82.2	91.8
50	90.0	93.4	93.4	94.1

Maximum inundation modeled with a return period of 10 years

Figure 7.14   Inundation map showing the maximum impact of coastal hazards for the current situation, and considering a return period of 10 years.

Deltares
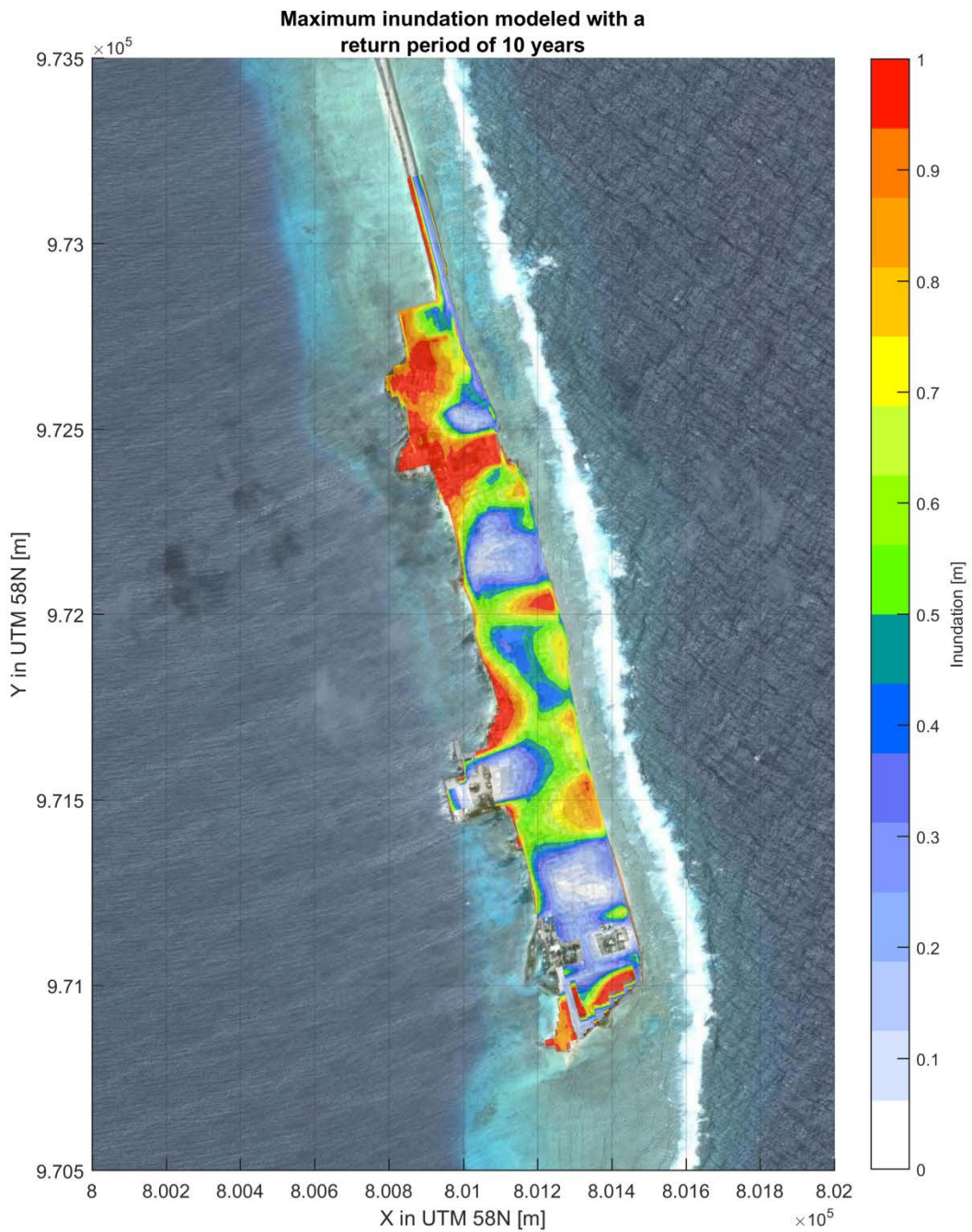
Figure 7.15 Inundation map showing the maximum impact of coastal hazards for sea level rise scenario RCP 8.5 2100, and considering a return period of 10 years.

7.2 Overtopping of the causeway from Ebeye to Gugeegue

Wave overtopping is often a primary concern for coastal structures constructed to defend against inundation. In the case of Ebeye, the causeway towards Gugeegue is protected by a structure (i.e. revetment) which during extreme conditions can be overtopped. The result of such an overtopping event is debris covering the causeway and inundation of the road (Figure 7.15). The causeway towards Gugeegue can be separated in two main parts: one part protected by a "well-constructed" revetment, starting in the northern part of the island (height of 3.1 m +MSL) with a total length of approximately 1.4 km, and a lower more "poorly-constructed" revetment (maximum height of 2.2 m +MSL or lower) with a total length of about 5.6 km northward toward Gugeegue (see Figure 5.4 for the locations of the two types of revetments (well-constructed and poorly-constructed). Figure 7.17 shows two pictures at two representative sections of the revetment. The main reason that the revetment decreases in height and quality moving towards the north is that construction funding's were not sufficient to complete the construction works of the new, well-constructed, revetment. Although wave overtopping is observed along the entire causeway, serious and regular damages to the road behind the revetments are observed especially at the poorly constructed revetment.

Wave overtopping of single short-waves is not explicitly taken into account by the XBeach simulations, as shown in Section 7.1. Therefore an additional calculation is applied to simulate accurately the wave overtopping over the revetment. Overtopping at the causeway is computed at two representative transects. One transect at the well-constructed revetment, and one transect at the poorly constructed revetment.

Figure 7.16 Picture of the causeway after a mild storm events on the 19th of August 2016. Debris was brought by the waves on the causeway.

Figure 7.17 Left picture: well-constructed revetment. Right-picture: poorly constructed revetment.

The approach follows the formulation of the EurOtop Overtopping Manual (2007) for wave overtopping rates for smooth and rough impermeable slopes as provided via the SimpleCoast website (www.simplecoast.com). The default formulation without a variation on the standard coefficient is applied. Only a roughness coefficients for rocks (one layer, impermeable core; y_f: 0.60) is used. The significant short wave height, wave period and water level (i.e. water level offshore + local wave setup) at the toe of structure derived from the XBeach simulation are used as input to the calculations. To take into account water level variations due to long waves the setup is enhanced with half of the significant long wave height.

Figure 7.18 shows overtopping rates at the well constructed and poorly constructed sections of the revetment. Already for a return period of 1 year, overtopping occurs. For the well-constructed revetment this is about 100 l/m/s but it increases up to 1000 l/m/s for the poorly constructed revetment. The overtopping increases when the return period increases. For lower return periods (i.e. 1/5 and 1/10 years) swell conditions are more critical to wave overtopping, while for higher wave period (i.e. 1/30 and 1/50 years) typhoon conditions are the most critical factors leading to overtopping. Considering future sea level rise scenarios, the amount of wave overtopping will increases, as shown at one example for the good constructed revetment for RCP 8.5 (Figure 7.19). Note that maximum overtopping rates have been cut in the figures to a maximum value of 1000 l/s/m as, values above this threshold, are so high that it is not even possible to talk about overtopping rates; the revetment in fact is behaving more as a weir rather than a real revetment.

Different limits are provided in relation to wave overtopping; for example, the serviceability Limit State (SLS) and Ultimate Limit State (ULS). In particular, in order to satisfy the ultimate limit state, the structure must not collapse when subjected to the peak design load for which it was designed. Allsop et al. (2009) suggests that damages occur to paved or armoured promenade behind a seawall when a mean discharge exceeds 50 l/s/m. The limit of 50 l/s/m has been added as horizontal dashed line to Figure 7.16 and Figure 7.17, indicating how this limit is largely over exceeded at the two types of the revetment, especially for the higher return periods.

Figure 7.18 *Development of the mean overtopping discharge based on the EurOtop Overtopping Manual (2007) forced with nearshore XBeach values for different return periods and contributions. Upper panel for the well-constructed revetment. Lower panel for the poorly constructed revetment. The horizontal red dashed line indicates the serviceability limit state of 50 l/s/m.*
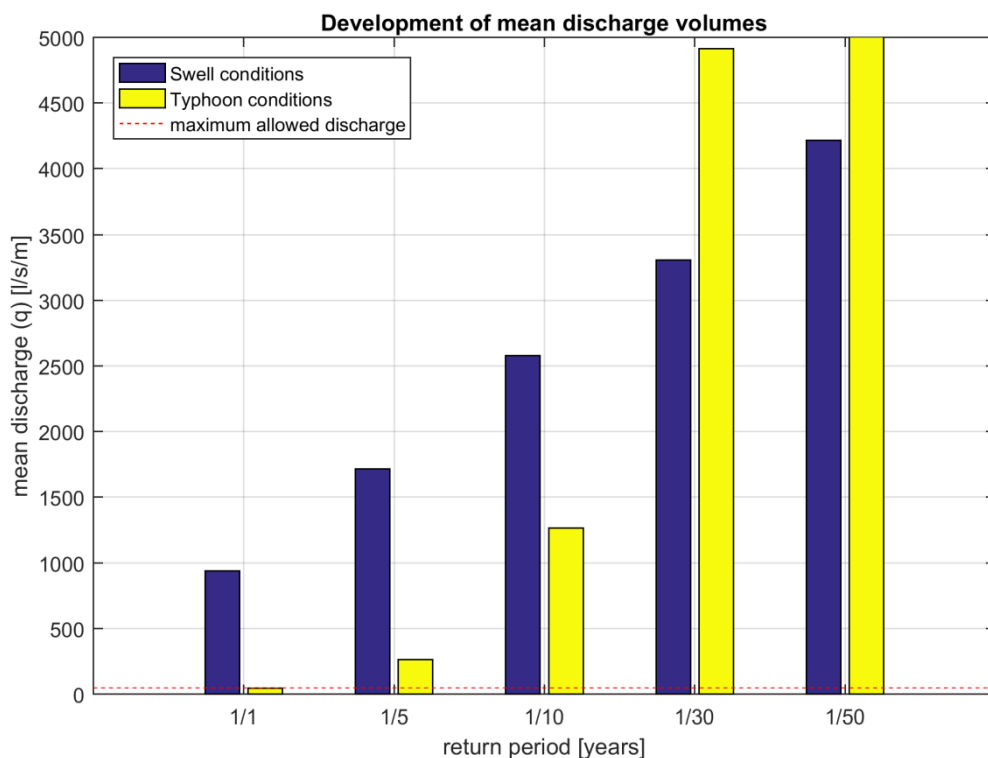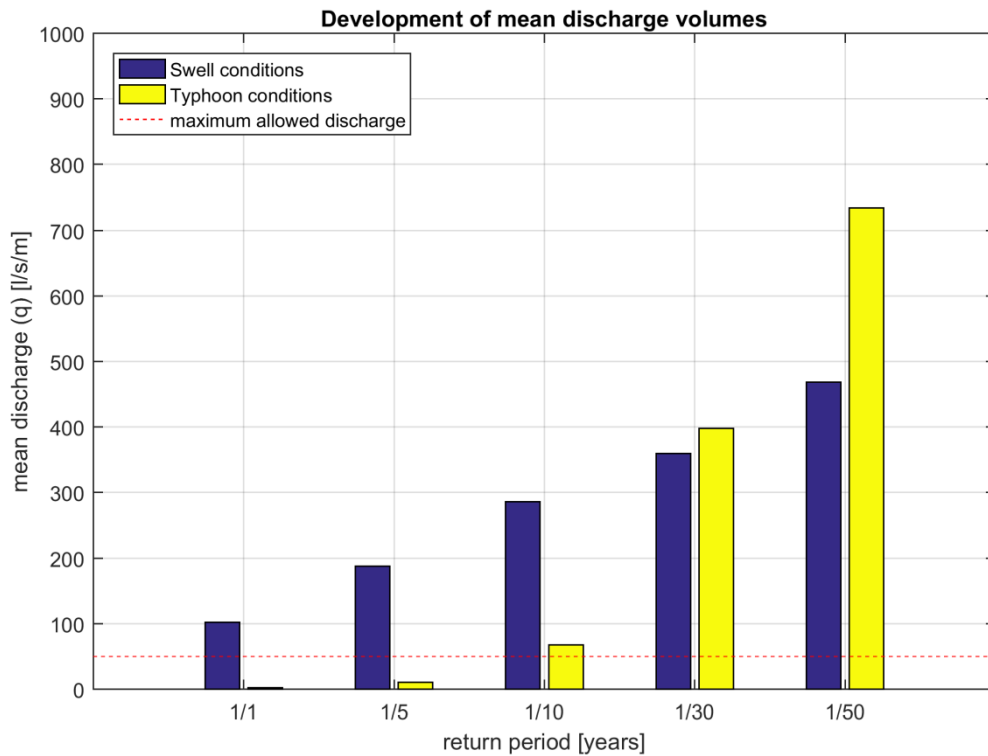
Deltares
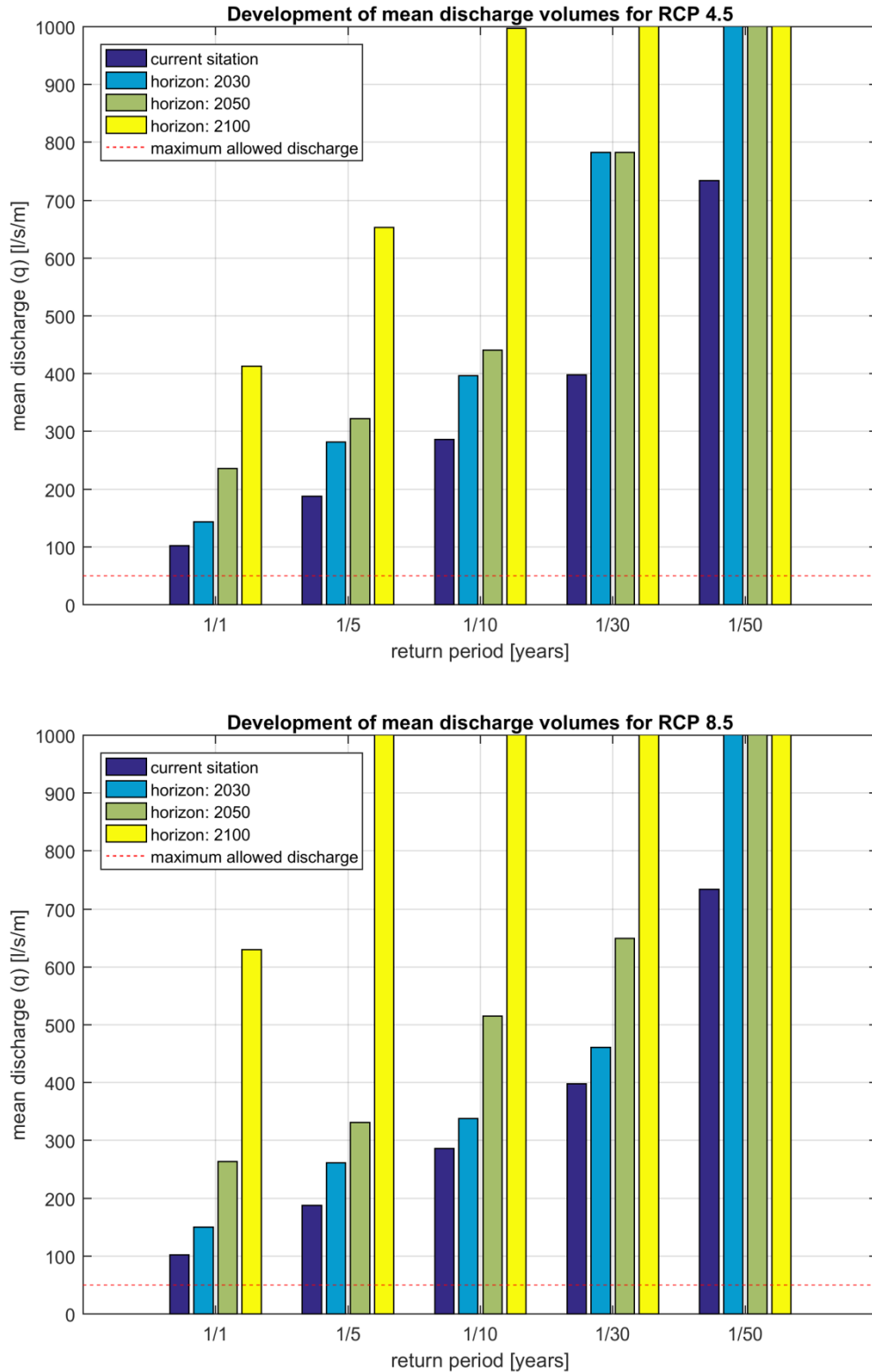
Figure 7.19 *Development of the mean overtopping discharge based on the EurOtop Overtopping Manual (2007) forced with nearshore XBeach values for the well-constructed revetment for different time horizons and RCP scenarios.*

7.3 Coastal Erosion

7.3.1 Introduction

Coastal erosion is in general a complex phenomenon which can be the result of many different causes, some of them natural and some of them anthropogenic, acting at different temporal and spatial scales.

Among the <u>natural causes</u>:

1) Storm erosion driven by gradients in cross-shore sediment transport.
2) Seasonality in wave regime and alongshore sediment transport pattern which may lead to periods with narrower beaches and others with wider beaches.
3) Natural gradients in alongshore sediment transport, leading to long-term erosion/deposition trends.
4) Sea level rise and climate change can contribute to exacerbate those effects.

Among the <u>anthropogenic causes</u>:

5) Changes to the local hydrodynamics and sediment transport patterns. This effect, for example, can be related to the construction of the causeway which has closed off completely part of the lagoon.

6) Changes in sediment redistribution along the coastline due to local man-made constructions such as: revetments, sea walls and small land reclamation, which may have affected the local sediment transport patterns.

7) Construction of minining pits on the reef in front of the coastline. Mining pits may generate local gradients in alongshore transport and return currents, therefore leading to local erosion.

In order to address the full spectrum of the problems, several different models would be required, that can tackles these issues at the different spatial and temporal scales. Also very detailed data (e.g. in terms of bathymetry, grain size characteristics, historical overview of man-made interventions, etc.) would be required, which were not available for the present study.

Due to this limitation, coastal erosion in this section only address the effect of the potential erosion after a storm (1), and coastal retreat due to sea level rise (4).

Parts of the Ebeye coastline are currently experiencing coastal erosion, as can be seen in Figure 7.20. Some of the storm water outfalls in the south-east of the islands, are now completely exposed, indicating that coastline erosion at some locations might have exceeded the 15-20 m.

Visual observations of coastal types and defences at Ebeye (Figure 5.4) show that there are two types of beaches, i.e. a mixed (gravel-rocks-sand) and sandy beach. In this section, the direct consequences in terms of coastal erosion are evaluated for different return periods and time horizons, looking at the effect of expected climate change scenarios and sea level rise.

Figure 7.20   Coastal erosion at the ocean side of Ebeye.

7.3.2   Method

In this study, it is assumed that the coastal erosion may occur due to both storms and structural processes (i.e. sea level rise). Both processes are quantified using empirical relations available via the SimpleCoast project (http://www.simplecoast.com/). The empirical formulas for both structural and storm-induced erosion are originally derived for sandy coasts and therefore not directly applicable on the beaches fronted by (coral) reefs at Ebeye. Unfortunately, empirical relations on erosion for (coral) reef-lined coasts are not directly available. The Bruun rule (Bruun 1962) and the Van Rijn (2009) method will give an approximation of the expected erosion values and will provide the relative impacts of climate change and sea level rise on the coastal erosion at Ebeye. The validity of the Bruun rule has been questioned in literature (e.g. Cooper et al., 2004; Ranasinghe et al., 2012), however no practical alternative exist within the scope of this study and for this type of environments to quantify the effects of sea level rise on structural erosion.

For six transects along the coastline of Ebeye, the storm-induced and structural erosion are calculated (Figure 7.21). For three transects along the lagoon-side of the island only the structural erosion is calculated, since the wave-impact from the lagoon due to storms is limited. Inputs for these calculations are the characteristics of the beach (e.g. beach slope, beach height and grain size) and nearshore hazards (e.g. wave height, wave period and storm surge level). The nearshore hazards are taken from the XBeach results (Section 6).

Figure 7.21 Selected transect for erosion calculations (black line).

Structural erosion due to sea level rise will be estimated based on the Bruun rule (Bruun, 1962). The Bruun rule assumes that with a rise in sea level, the equilibrium profile of the beach and shallow offshore moves upward and landward. This simple model calculates the retreat (R) by including an increase in sea level, (S), cross shore distance (L) to the water depth (h) taken by Bruun as the depth to which nearshore sediments exist (depth of closure), and B is the height of the dune:

$$R = S \cdot \frac{L}{h+B} \tag{7.1}$$

For the application of the Bruun rule to the transects of Ebeye:
- the sea level change (S) will be based on Table 6.8;
- the dune height (B) will be derived from the topography (Section 5.2.2);
- the toe of the beach will be taken as the depth of closure, since the reef is non-erodible. Therefore, the water depth (h) will be determined at the toe of the beach and the cross-shore distance (L) will be the distance between the toe and top of the beach.

Coastal erosion during storm events will be estimated using the method of Van Rijn (Figure 7.22). Van Rijn (2009) has used a detailed cross-shore model (CROSMOR) to simulate the dune erosion process. The CROSMOR-model has also been used to study the effect of various key parameters on the computed dune erosion after 5 hours (duration of standard storm). Basically, the proposed method produces dune erosion values with respect to a defined reference storm (storm with a constant storm surge level, wave height and duration of 5 hours). This resulted in a simplified dune erosion rule (DUNERULE-model), as follows:

$$A_{d,t=5} =$$

$$A_{d,ref}\left(d_{50,ref}/d_{50}\right)^{a1}\left(S/S_{ref}\right)^{a2}\left(H_{s,o}/H_{s,o,ref}\right)^{a3}\left(T_p/T_{p,ref}\right)^{a4}\left(tan\beta/tan\beta_{ref}\right)^{a5}\left(1+\theta_o/100\right)^{a6}$$

$$(7.2)$$

with:

$A_{d,t=5}$ = dune erosion area above storm surge level after 5 hours (m3/m),

$A_{d,ref}$ = dune erosion area above S storm surge level after 5 hours of the Reference storm
= 170 (m3/m),

S = storm surge level above mean sea level (m),

S_{ref} = storm surge level above mean sea level of Reference storm= 5 (m),

$H_{s,o}$ = offshore significant wave height (m),

$H_{s,o,ref}$ = offshore significant wave height of Reference storm= 7.6 (m),

T_p = peak wave period (s),

$T_{p,ref}$ = peak wave period (s) of Reference storm= 12 (s),

d_{50} = median bed material diameter (m),

$d_{50,ref}$ = median bed material diameter of Reference profile= 0.000225 (m),

$tan\beta$ = coastal slope gradient defined as the slope between the -3 m depth contour (below mean sea level) and the dune toe (+3 m),

$tan\beta_{ref}$ = coastal slope gradient defined as the slope between the -3 m depth contour and the dune toe (+3 m) of the Reference storm = 0.0222 (1 to 45),

α_o = offshore wave incidence angle to coast normal (degrees),

α_1 = exponent=1.3,

α_2 = exponent=1.3 for S<S_{ref} and α_2=0.5 for S>S_{ref},

α_3 = α_4 = α_6 = 0.5 (exponents),

α_5 = exponent= 0.3.
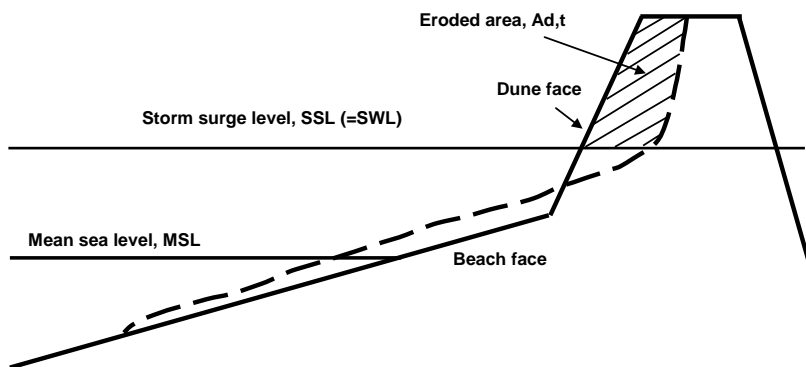
Figure 7.22 Coastal erosion during storm events according to the method of Van Rijn.

The average horizontal dune recession (R_d) can be estimated from:

$$R_d = A_d / (h_d - S)$$

$$(7.3)$$

For the application of the method of Van Rijn to the transects of Ebeye:

- The (coral) reef strongly affects the nearshore hydrodynamics by dissipating short wave energy, generating long waves and increasing water levels due to wave-induced setup.

These long wave effects are not included in the dune erosion rule by Van Rijn. To exclude the effect of the (coral) reef on the nearshore hydrodynamics, the storm surge level (S), short wave height (H_s) and period (T_p) at the toe of the beach are used as input for the erosion calculations for Ebeye. Since the long wave height is not included in the method of Van Rijn, but an important part of the reef hydrodynamics, it is added to the storm surge level. Because of its long wave period it is included as an increase in water level during the storm.

- Across the coastline of Ebeye two types of beaches are found. The median grain size (D_{50}) of both types of beaches are based on the observations during the field visit, resulting in a D_{50} of approximately 0.00035 m (350 µm) for the sandy beach and a D_{50} of 0.05 m (5 cm) for the mixed beach. The formula has been originally developed for sandy dunes and therefore should be used with care for coarser fractions, possibly leading to inaccuracies in results.
- The coastal slope gradient (tanβ) will be equal to the slope of the beach.

The calculated retreat values for both structural and storm-induced erosion are presented in the next sections. The values will be used as input for the Coastal Index in Chapter 8, where the erosion values will determine relative risk of erosion along the coastline of Ebeye.

7.3.3 Results on storm-induced erosion

In Figure 7.23 the results of the storm-induced erosion calculations using the Van Rijn method are shown for transect 3. Transect 3 consists of a beach with fine sediment, with a D50 of approximately 0.00035 m. The results show the coastline retreat values after a storm for different time horizons (horizontal axis) and return periods (coloured bars). For some of the higher return periods and time horizons retreat values are missing in the plots. In these cases the storm surge level (SSL) was higher than the dune height, resulting in inundation of the island, and no retreat values can be calculated.

The retreat values for the swell events (top panels) are higher than the retreat values for the typhoon events (bottom panels), which is mainly caused by the difference in wave period for both hazards, i.e. for swell events 20 s and for typhoons 10 s.

Generally, retreat values increase as the return period increases, which is the result of the increasing wave height. Additionally, retreat values become higher as the time horizon increases, due to the rise in sea level. However, differences between scenarios RCP 4.5 and 8.5 are small, which can be explained by the small differences in sea level rise values for time horizons 2030 and 2050 (see Table 6.8). The water levels and wave heights at the toe of the beach increase only slightly for the higher time horizons and RCP scenario (not shown), and therefore have a limited effect on the retreat values, see Equation (7.2).

Figure 7.23   Coastal erosion for transect 3 (D50 = 0.00035 m) due to swell events (top panels) and typhoons (bottom panels) for climate change scenarios RCP 4.5 (left panels) and RCP 8.5 (right panels). Retreat values are shown for each time horizon and for the return periods of 5 (dark blue), 10 (light blue), 30 (green) and 50 (yellow) years.

In Figure 7.24 the results of the storm-induced erosion calculations using the Van Rijn method are shown for transect 2. Transect 2 consists of a beach with coarse sediment, with a D_{50} of approximately 0.05 m.

The retreat values for transect 2 are representative for all the mixed beaches (see Figure 7.21)
) with a D_{50} of 0.05 m. The results show significantly lower retreat values after a storm with respect to the results in Figure 7.23 due to the higher grain size.

The results for the higher grain size show similar trends in retreat values as the fine grain size (Figure 7.23). Again, retreat values for the swell events (top panels) are higher than the retreat values for the typhoon events (bottom panels), retreat values increase as the return period increases, and differences between scenarios RCP 4.5 and 8.5 are small.

These two values provide a rough range of possible expected erosion values after a storm, as a function of the grain size. Despite these formula may not be applicable to the coarser

sediment fraction, they provide an upper value to the erosion than one can expect during a storm, which can over exceed the 10 m for the finer sediment fraction and the largest events. Also, it is important to realize that storm-erosion is not a permanent process and that under equilibrium conditions, beaches tend to rebuild themselves naturally during periods of milder wave conditions. This has also been confirmed by local inhabitants during the field visit. Therefore, it is important that some dynamics of the beach will be maintained, in order to allow the beach to adjust to these different profiles (i.e. storm profile and profile under mild waves conditions). This implies no houses should be built within this area.

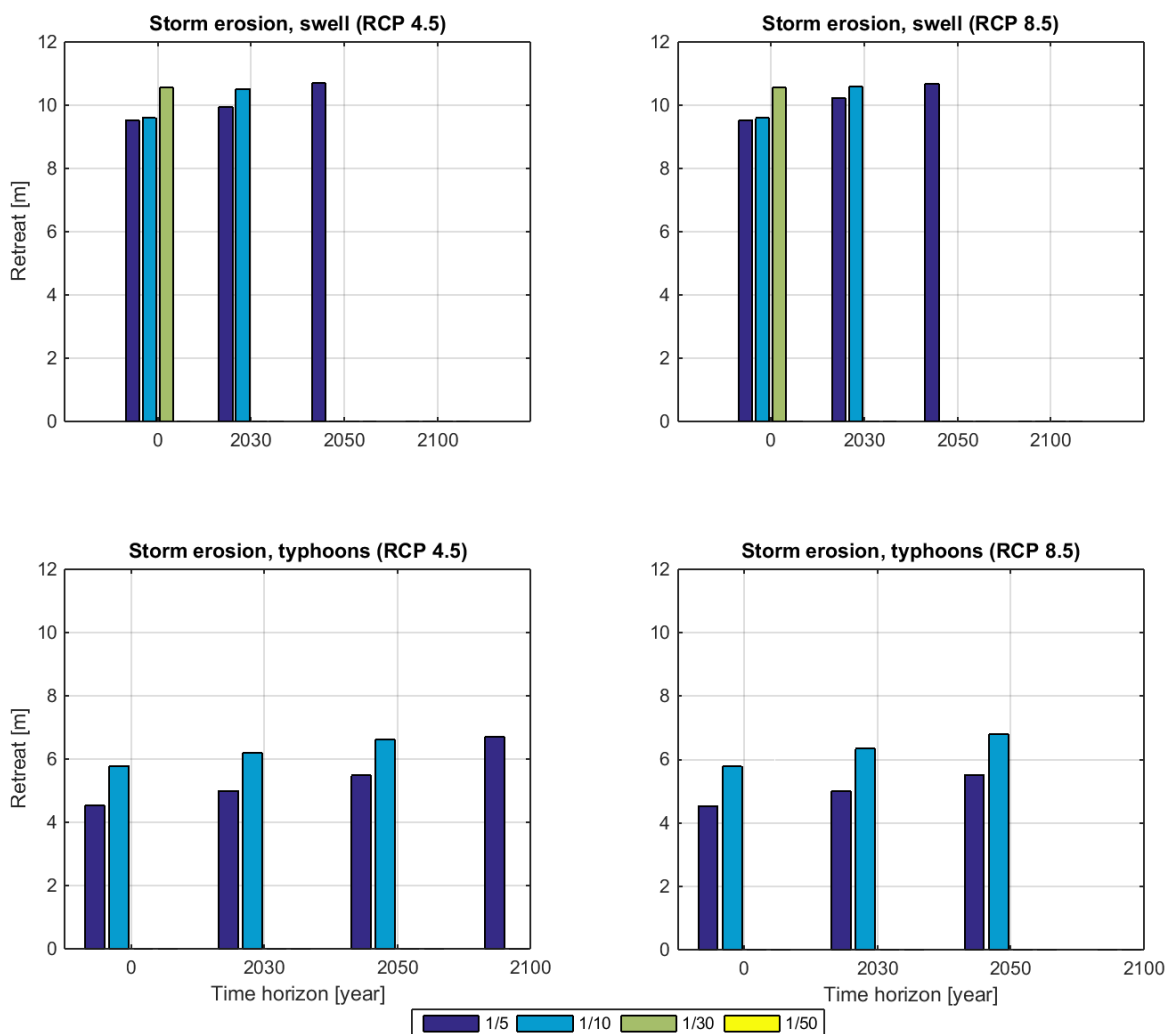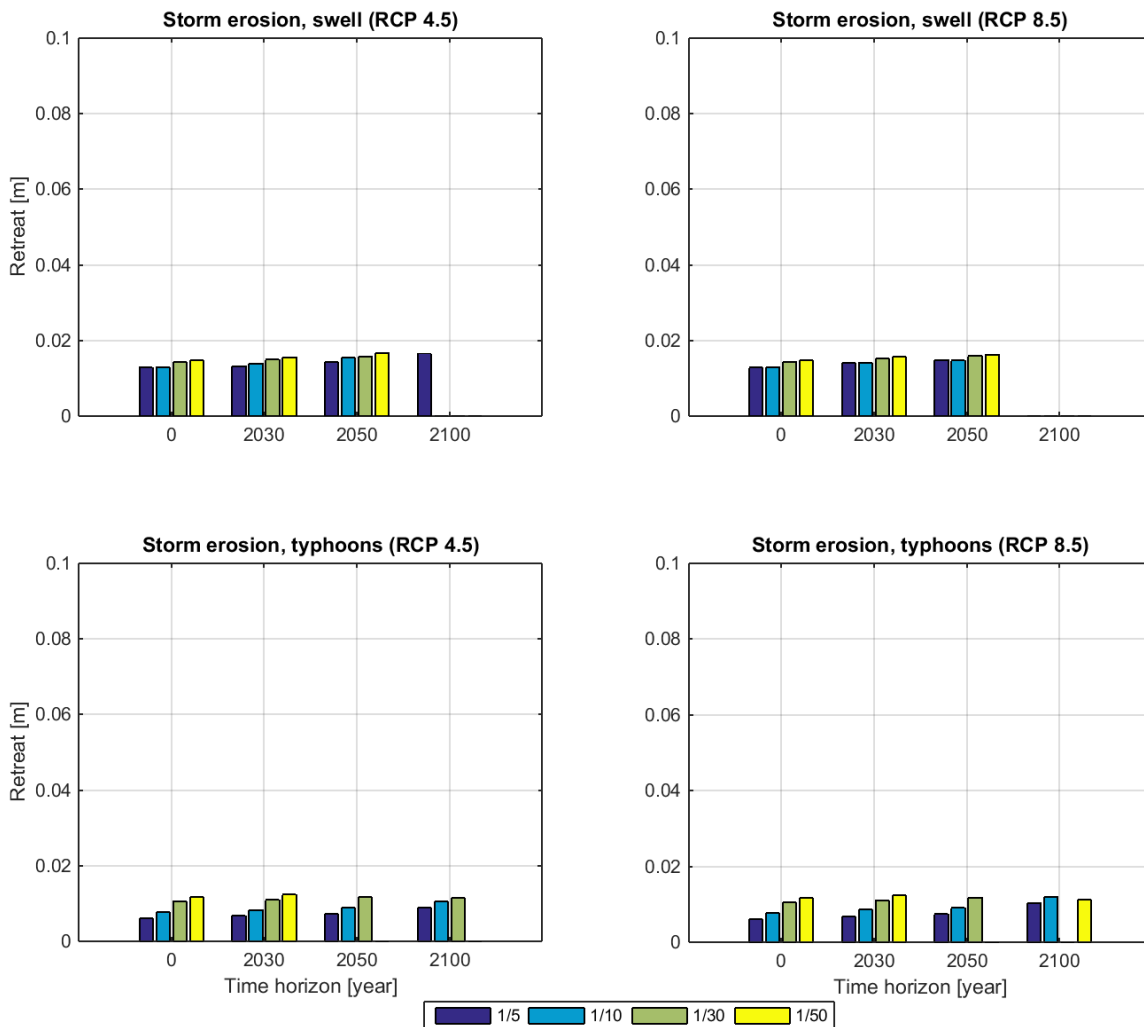*Figure 7.24   Coastal erosion for transect 2   (D50 = 0.05 m) due to swell events (top panels) and typhoons (bottom panels) for climate change scenarios RCP 4.5 (left panels) and RCP 8.5 (right panels). Retreat values are shown for each time horizon and for the return periods of 5 (dark blue), 10 (light blue), 30 (green) and 50 (yellow) years.*

7.3.4 Results on structural erosion

In Figure 7.25 the results of the structural erosion due to sea level rise calculations using the Bruun rule are shown for both ocean (transect 3) and lagoon (transect 6) side of the island. The results show the coastline retreat values due to sea level rise for different time horizons (horizontal axis) and RCP scenarios (coloured bars). The retreat values for these transects are representative for all transects at the lagoon and ocean side of the island (see Figure 7.21).

The results show lower retreat values for the lagoon side with respect to the ocean side of the island. This is caused by the lower dune height values at the lagoon side of the island. Furthermore, higher time horizons and higher RCP scenarios result in higher retreat values due to the increase in sea level rise.
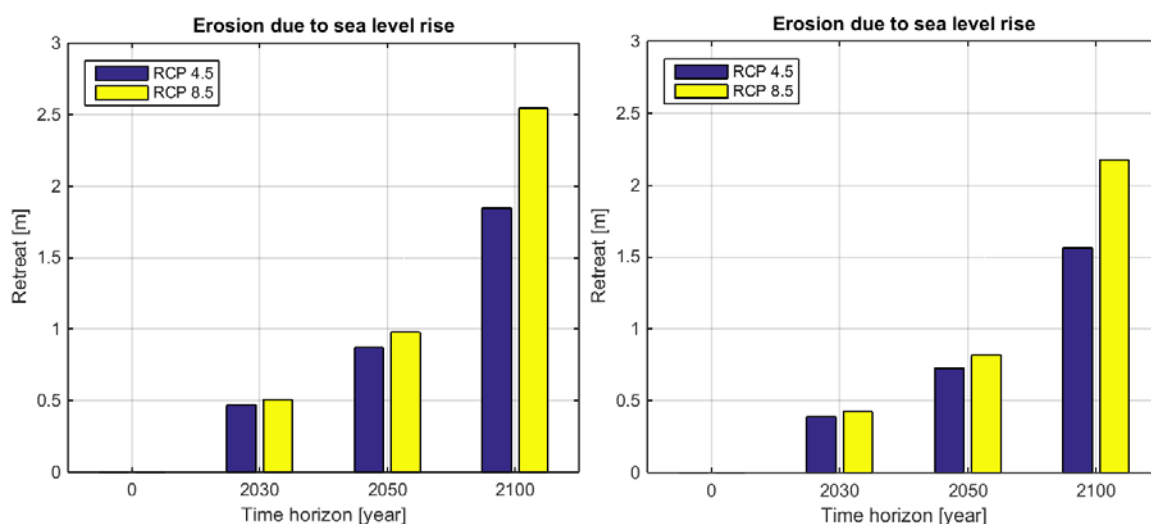
Figure 7.25   Coastal erosion due to sea level rise for transect 3 (left panel) and transect 6 (right panel). Retreat values are shown for each time horizon and climate change scenarios RCP 4.5 (blue bars) and RCP 8.5 (yellow bars).

7.3.5 Combining of the erosion effects

In the risk assessment in Chapter 8 the retreat values are needed for the current situation and future scenarios (two RCP scenarios and three time horizons). These retreat values are determined for each type of coastline (sandy and mixed beach) and for storm- and sea level rise-induced erosion. For future scenarios the retreat values increase, which is directly related to the rise in sea level, since wave and water level impact on the beach increases and therefore result in more erosion.

In order to capture erosion due to both event-driven and structural processes in the risk assessment, both retreat values are combined for the ocean side erosion.

7.4 Conclusions

In this section, the impacts of coastal hazards due to inundation (i.e. swell waves form the ocean, wind-waves from the lagoon, typhoons, and tsunamis) and coastal erosion has been computed for different return periods and time horizons.

This information will be used to derive a coastal risk assessment as part of Chapter 8, and to support the choice of suitable design of solutions and locations for adaptation (Chapter 9).

The results from the combined inundation maps clearly show that, if inundation during extreme events is already a serious threat in the present situation, by the end of the century this may lead to dramatic consequences when no action is taken. Most of the island will be subject to inundation with water depths reaching 1 m, for events with a return period of 10 years (or larger). Inundation due to swell and typhoons events are the biggest hazards to the island.

The effect of coastal erosion due to storm and long-term coastal retreat due to sea level rise was also estimated. Potential erosion up to about 10 m may results from an extreme storm event. Potential long-term structural erosion due to sea level rise is estimated to be 1.5 till 2.5 m by the end of the century. This, of course, assuming sufficient accommodation space, allowing for this retreat. However, at some location, this accommodation space is very limited, with houses already built very close to the shoreline, increasing the risk resulting from coastal erosion. However, coastal erosion is in general a very complex problem, which may have different causes, operating at different spatial and temporal scales. In order to address all these processes in details, detailed morphodynamic models would be required, based on accurate bathymetric, topographic and sediment characteristics information.

8 Coastal risk assessment and selection priority areas for intervention

8.1 Introduction
In this chapter, the methodology for risk assessment, as introduced in Chapter 4.5, will be applied to identify different areas at risk, due to the combined effect of flooding and coastal erosion. At areas with higher risks, solutions will be identified and tested with the same modelling framework (Chapter 9). Possible changes/improvements resulting from the implementation of the measures (i.e. reduction in flooding and/or coastal erosion) will be assessed based on the same risk index.

8.2 Method
In this study, risk is defined as hazard x exposure x vulnerability (Kron, 2005):
- Hazard is represented by the inundation depth in meter for a given return period. The XBeach model is used to derive these data (Chapter 7).
- Exposure relates to the exposed assets (i.e. receptors) and people. The data available through PCRAFI (2015) is adapted as described in Section 5.2.8 and is used to derive this information.
- Vulnerability refers to the damage inflicted upon the exposed assets. Flood-damage curves (i.e. vulnerability curves) will be used in order to access the direct damage to each asset (Figure 5.12) for calculated flood events.

The resulting direct damages (in $) are calculated for each asset and subsequently summed up to get the total direct damage for the island. It is assumed that the used dataset (i.e. the PCRAFI dataset complemented with the power plant and water treatment plant; see also Section 5.2.8) includes all the assets and therefore all the direct damages currently on the island. Nevertheless, damages may change in the future due to new houses and infrastructures built on the island and/or possibly different construction methods. However, the methodology is generic and flexible, and it allows including changes to the asset values.

The direct damages to the causeway are also taken into account. It is assumed that every storm results in a damage to the shoreline protection of $1.0 million (i.e. there is no variation based on the return period). This value is based on the damages to the shoreline protection as communicated by the PMU Office in Ebeye after tropical storm Nangka.

For the quantification of indirect damages and intangible damages (see Figure 4.1) additional data and analyses are needed, which were not available for Ebeye. Therefore, it is assumed that the indirect damages and intangible damages are each 10% of the direct damage to the assets (i.e. damage to buildings in the PCRAFI dataset; this is not related to the causeway). The result is a vertical increasing risk curve in of 20%. In any case, the method used for the damage calculation is flexible and can be easily adapted and updated whenever new data will become available. Also, flood damages are only used to set priority for interventions and distinguish effects of different types of measures on different types of assets.

Additionally, as part of the indirect damages, the effect of not being able to use the causeway towards Gugeegue after damages/flooding due to extreme events has been explicitly added as a separate item. This separate damage curve has been derived as follows: during yearly conditions the poorly constructed revetment gets overtopped with about 1000 l/m/s, see Section 7.2. It is estimated that the indirect damage, as a result of debris covering the

causeway, is not using the causeway for two weeks. The monetary value of not using the causeway for that period is estimated to be $140.000,-. This value is based on the GDP per capita per day ($10, http://data.worldbank.org/country/marshall-islands) multiplied with the number of days that the causeway can not be used, multiplied with the number of people using the causeway on a daily base ($10 x 14 days x 100 people = $14.000,-.). Not using the causeway results that people cannot reach their home of work, and thus GDP/capita is used as a proxy of added value lost. A linear relationship is assumed between 50 and 1000 l/s/s and the indirect damage.

The risk curve is obtained by calculating all the damages for all the return periods, as shown in Figure 8.1. The Expected Annual Damage (EAD; in $/year) is then calculated as the area under the risk curve:

$$EAD = \int_0^1 D(\mathrm{p}) \cdot \mathrm{dP}$$

(8.1)
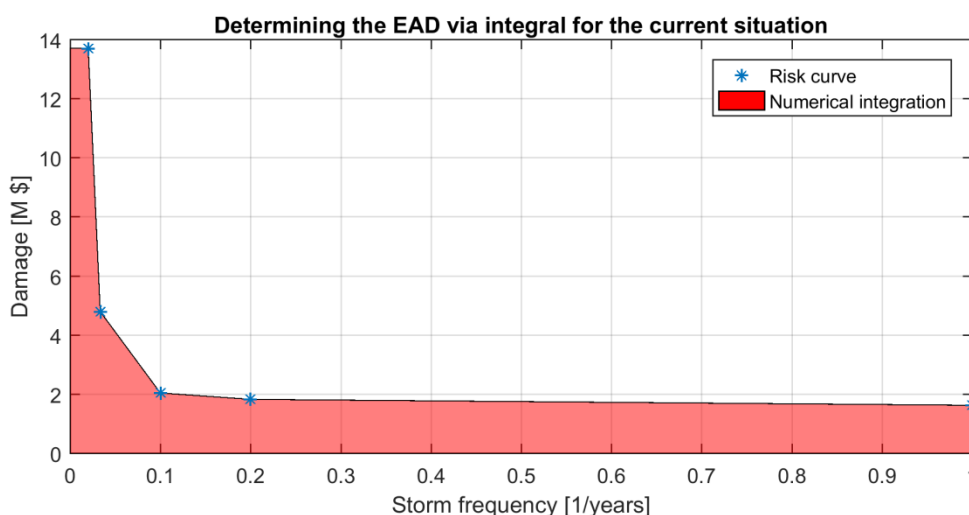
Figure 8.1   Determine the expected annual damage (EAD) by calculating the red area under the risk curve. The risk curve is defined by the (area averaged) damages per return period.

As described in Section 4.5, in order to obtain a Coastal Index (CI) the individual EAD's for each RCP scenario (4.5 and 8.5) and time horizon (current, 2030, 2050 and 2100), thus 2*4= 8 EAD's, are averaged. This means that all types of damages are integrated for every scenario (resulting in a EAD) and averaged.

8.3   Total damages and risk from inundation

First, the direct damages as a result of an inundation event are calculated from the hazards (i.e. inundation), exposure data (i.e. receptor value) and vulnerability (i.e. flood-damage curves). As an example, in Figure 8.2 the direct damages resulting from an event with a return period of 1/10 years are presented. The figure shows that there are two main areas where the direct damage resulting from the inundation are the largest. The first one is in the north where the topography of the island is lower (i.e. high hazard). The second one is in the middle part of Ebeye where a lot of assets are located (i.e. high exposure).

All the individual damages to receptors are summed up resulting in one value for the total direct damage for each inundation event. The damages for the entire island, for different return periods, are shown in Table 8.1. For example, the total damages range between $1.5 and $13.9 million for events respectively with a return period of 1/1 and 1/50 years.

These values are in the same order of magnitude as the values of damages compared to actual damages reported after a recent event ($\approx$ $ 1.308,000 after tropical storm Nangka, as communicated by the PMU Office in Ebeye). This verification gives confidence in the order of magnitude of the calculated damages. The values of computed damages have also been verified during a meeting at the Ministry of Public Works during the field visit.
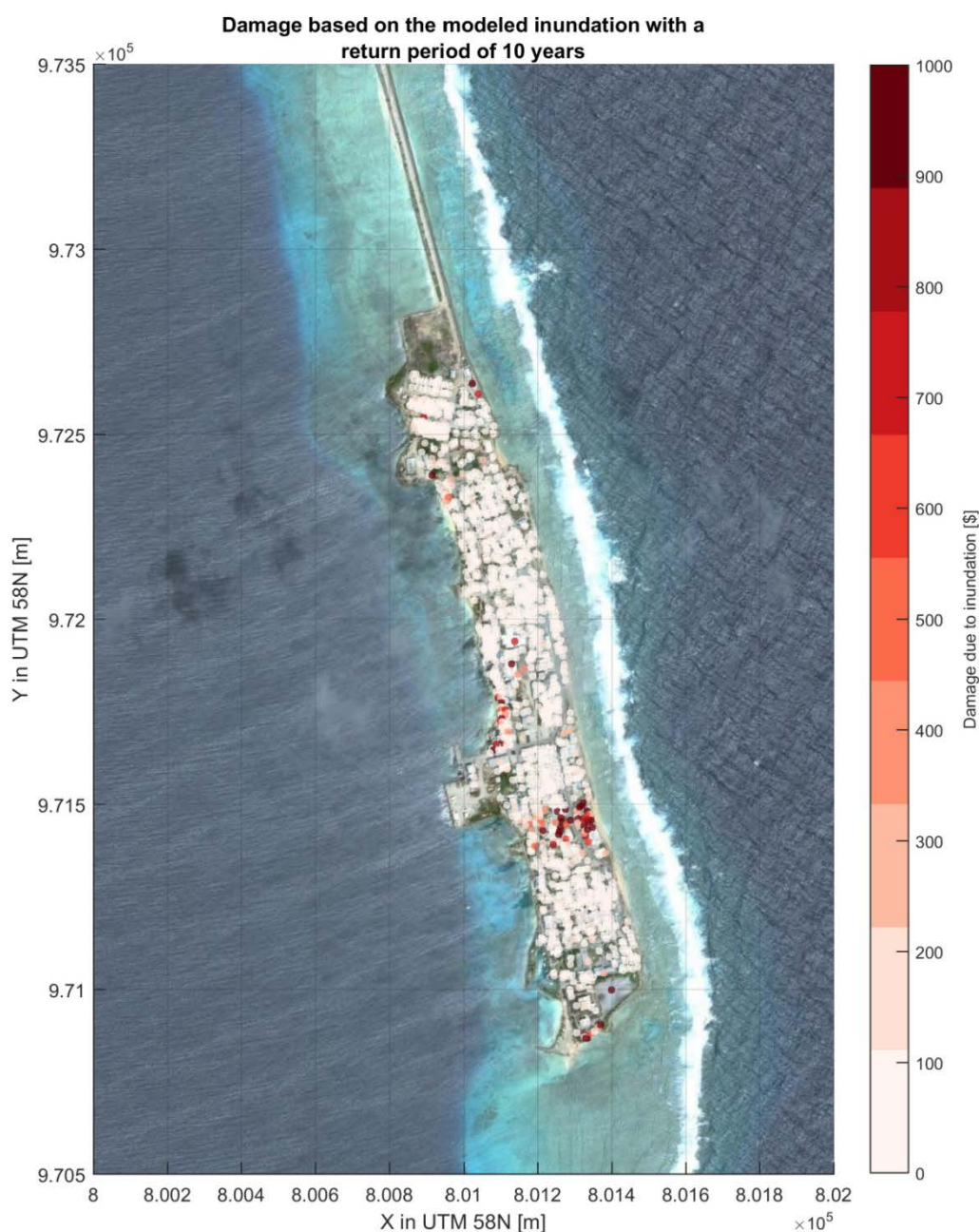
Figure 8.2   Damage in USD per receptor as a result of an inundation event with a return period of 1/10 years.

During extreme conditions the causeway can also get damaged. The resulting direct & indirect damages are also taken into account and combined with the direct damages to calculate the total damages in Table 8.1.

The table shows how the main contribution to the total damages are the direct damages. In order to put these values into perspective one can compare them with the total property value or the GDP of Ebeye. The total values of all assets of Ebeye are $119.0 million and the yearly GDP is estimated to $52.8 million (source: http://data.worldbank.org/country/marshall-islands).

The breakdown of the total damages for different categories is also shown in Figure 8.3, for an inundation event with a return period of 10 years. The different categories correspond to the ones defines in the PCRAFI exposure dataset (Section 5.2.8), updated to consider the damages to the water treatment plant, the power plant (under category "Public") the direct damages to the shoreline protection of the causeway, and the indirect damages related to the fact that the causeway cannot be used for a certain period after being damaged. The figure shows how the largest contribution to the damages is due to inundation of public properties and damages to the causeway.

Table 8.1   Direct and indirect damages as a result of inundation at Ebeye.

Return period [years]	Direct damage [million USD]	Indirect damage [million USD]	Intangible damage [million USD]	Total damage [million USD]
1	1.4	0.1	0.0	1.5
5	1.7	0.1	0.1	1.8
10	1.9	0.1	0.1	2.1
30	4.2	0.4	0.3	4.9
50	11.7	1.2	1.1	13.9
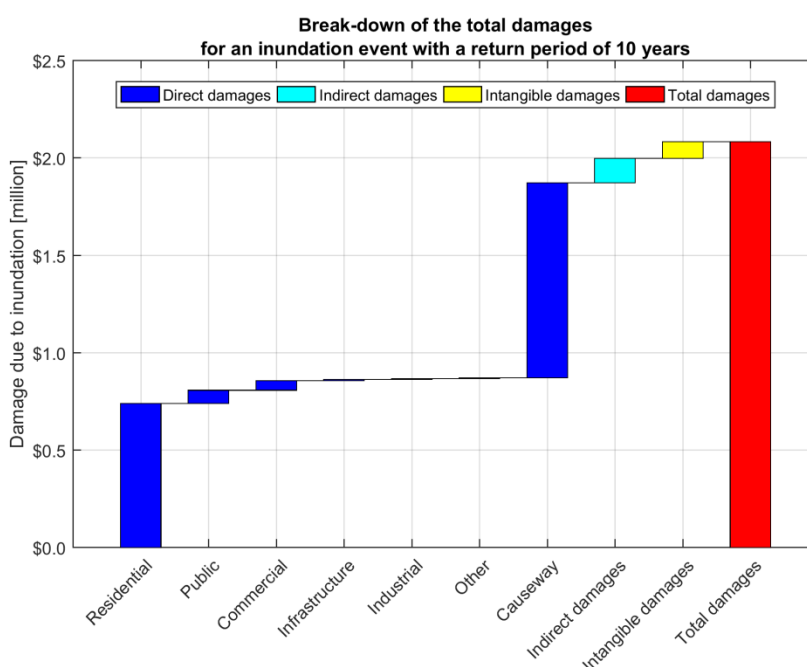
Figure 8.3   Breakdown of the total damages per category for an inundation event with a return period of 10 years.

The integrated damage values for different return period were then computed, providing the EAD values for a given scenario (RCP scenario in combination with a time horizon; i.e. SLR). This results in Figure 8.4. In the current situation (with the current mean sea level) the EAD is around $2.2 million. The risk due to flooding, as a result of sea level rise, will increase in 2100 up to $4.6 and $6.8 million, depending on the sea level rise scenario considered. The main increase occurs for a sea level rise of more than 0.5 meter (time horizon: 2100 under RCP 4.5 or 8.5). The presented risk does not take into account any economic development.

In this study indirect and intangible damages are assumed to be 20% of the direct damage to the assets. However, a proxy for these damages is the amount of people affected by inundation. We assume a person is affected by inundation when an inundation level of more than 20 centimetres is predicted by the model at his house. This calculation leads to Table 8.2. The amount of people affected per return period can, similarly to damages, also be integrated over the frequency leading to a new index defined as expected annual affected people (EAAP). The EAAP will, under sea level rise, double in the coming year since people will be affected regularly (i.e. during storms with lower return periods).
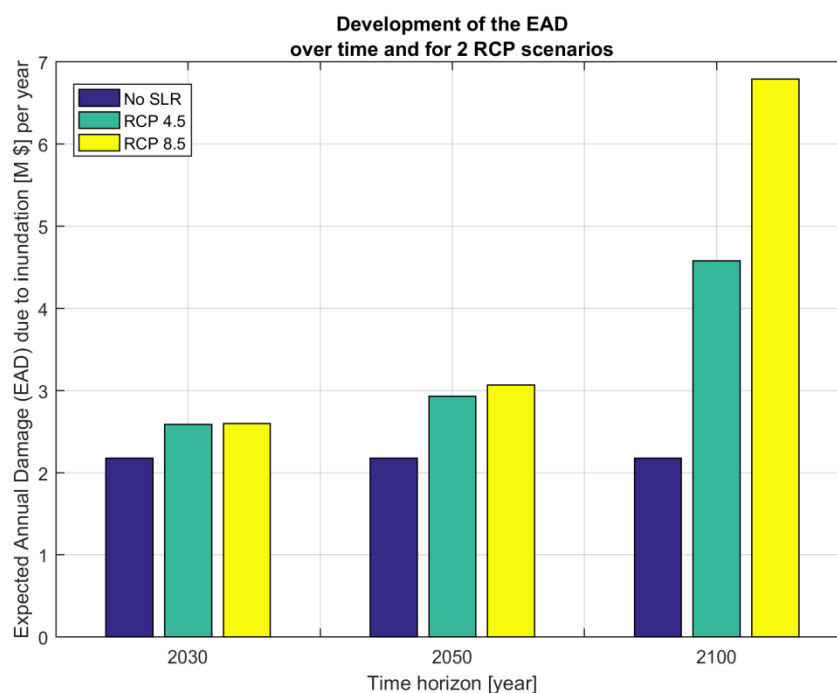
Figure 8.4   Expected Annual Damage (EAD) in $ per year for different time horizons and RCP scenarios for damages due to inundation.

Table 8.2   Amount of affected people for different return periods and integrated over storm frequency (EAAP) for the current sea level and for 2100 under two RCP scenarios

Return period [years]	Current situation	2100 under RCP 4.5	2100 under RCP 8.5
1	3,610	8,570	10,100
5	5,150	9,380	10,860
10	6,440	10,800	11,280
30	10,240	11,980	12,000
50	12,000	12,000	12,000
EAAP	5,030	9,292	10,673

8.4   Total damages and risk from erosion

Erosion due to both event-driven and structural processes will result in a retreat of the coastline. The risk or damage resulting from this retreat is estimated by calculating the total area of land lost due to erosion multiplied with the value of a square meter of land. Land in Ebeye at present can not be privately owned, since it is property of a single landowner. However, in this risk assessment, it is estimated that the price per m^2 of land is US$ 400,-. This is based on an estimate of costs of possible land reclamation (US$ 100,- per m^3 sand multiplied with an active height of 4 m) Losing a square meter of land results therefore in a damage of US$ 400,-.

For the current situation (i.e. without sea level rise) the erosion is only related to event-driven processes. Structural loss of land is therefore not taken into account. Figure 8.5 shows the damages as a result of storm erosion at 9 transects at Ebeye. The transect numbers are shown in Figure 7.21.

Transects 1 to 6 are located at the ocean side and can therefore be eroded due to storms from the ocean. It was assumed in Chapter 7.3 that storm-induced erosion does not occur for transects at the lagoon-side (i.e. transects 7 to 9). From Figure 8.5 one can conclude that only at transect 3 noticeable damages occur. This is related to the smaller grain size which characterize this transect. Transect 3 consists of a beach with fine sediment while the grain size at the other transects is much higher. Finer sediments will result in larger erosion during storm events, which may recover after the storm, in an equilibrium situation. However, in the area subject to erosion and accretion, development of houses and infrastructures should not be allowed. For this reason, we include this type of erosion in the risk assessment.

The total damage per event from all transects combined, increases from $0.24 million to $0.33 million for respectively return periods of 1/1 to 1/50 years, see Figure 8.5 for the damages per transect. The total damage is the summation of all the individual transects.

Similarly to Section 8.3, the EAD is calculated, giving one value of the damages due to erosion for a given scenario (RCP scenario in combination with a time horizon; i.e. SLR). This results in Figure 8.6. In the current situation (with the current mean sea level) the EAD due to erosion is around $0.26 million. The risk will, as a result of sea level rise, increase in 2100 between $1.7 million and $2.3 million. Sea level rise increases both the damages as a result of storm-induced erosion and the damages as a result of structural erosion.
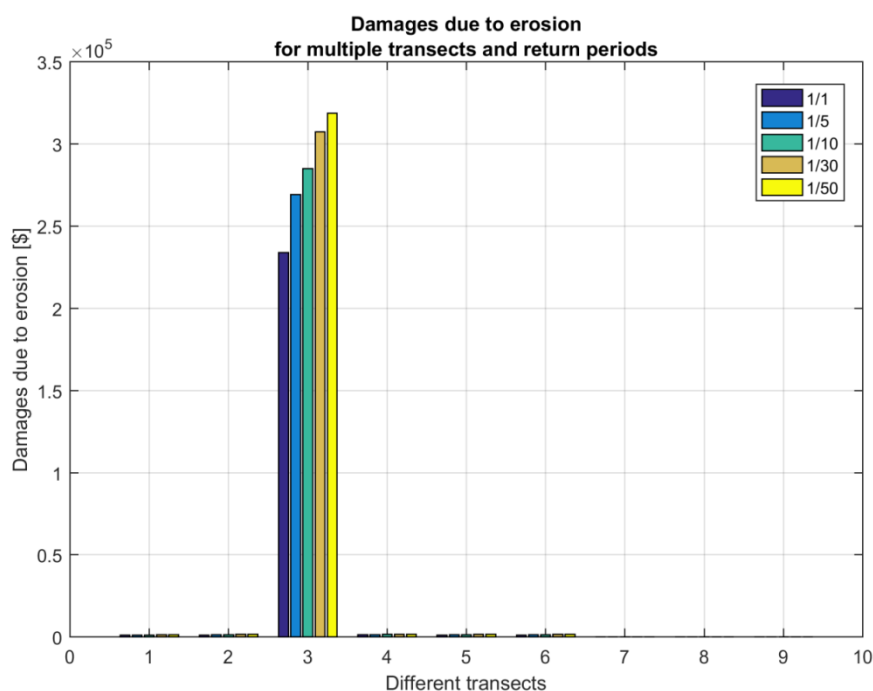
Figure 8.5   Damage in USD per transect as a result of an storm-induced erosion for different events.
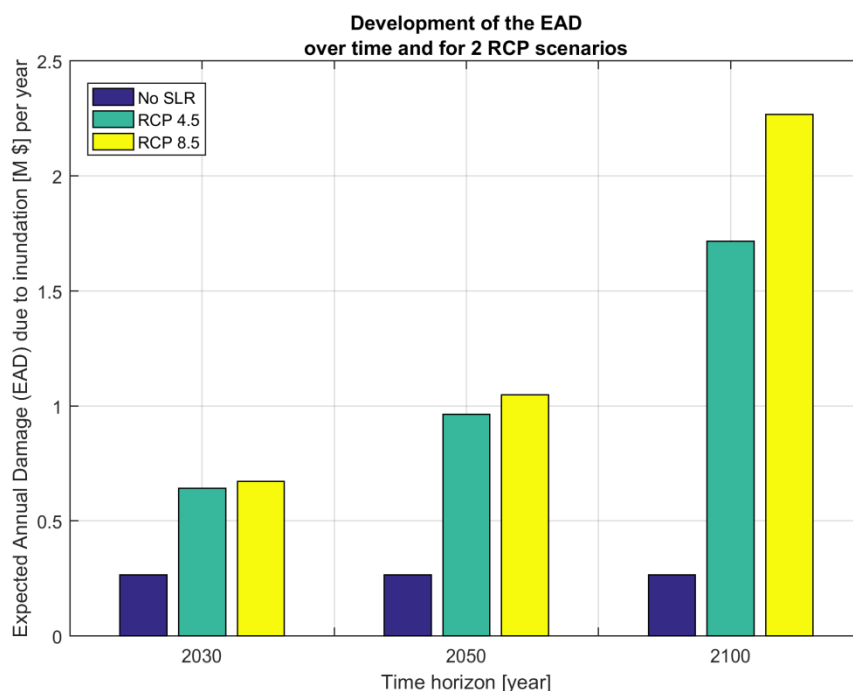
Figure 8.6   Expected Annual Damage (EAD) in $ per year for different time horizons and RCP scenarios for damages due to erosion.

8.5   Selection of hotspots for intervention

The combination of the total damages due to inundation (Section 8.3) and erosion (Section 8.4) result in the total damage for each return period, as shown in Table 8.3. The contribution of erosion to the total damage is significantly smaller with respect to the contribution from inundation.

Table 8.3   Direct and indirect damages as a result of inundation and erosion at Ebeye.

Return period [years]	Total damage due to inundation and overtopping [million USD]	Total damage due to erosion [million USD]	Total damage [million USD]
1	1.5	0.2	1.8
5	1.8	0.3	2.1
10	2.1	0.3	2.4
30	4.9	0.3	5.3
50	13.9	0.3	14.2

In order to select hotspots of interventions, the island of Ebeye has been divided into sectors. These sectors are based on existing coastal defences and coastal types (Figure 5.4) (e.g. an area protected by a vertical seawall is clustered into one area). The spatially varying damages have been clustered in each sector and an area-averaged damage (in $/m^2$ per year) is calculated for each return period, see Figure 8.7. There is a significant increase in damages for increasing return periods. Also, the two areas with higher average damages which were already visible in Figure 8.2 are again visible in this figure: one in the northern part of the island, and one in the middle.

Next, the area-averaged EAD (in $/m^2$ per year) is calculated for each time horizon. In Figure 8.8 the results of the area-averaged EAD are shown for the RCP 8.5 scenario. There is a significant increase in area-averaged EAD for increasing time horizons.

The eventual Coastal Index (CI) is obtained by averaging the EAD per m^2 for all the scenarios. The results are presented in Figure 8.9. The areas with a scenario-averaged and area-averaged EAD of more than $2.5 per m^2 are marked as 'highest' risk. The areas at highest risk will be selected for intervention and possible solutions will be presented in Chapter 9.

8.6   Conclusions

In this chapter, a procedure for coastal risk assessment has been implemented and carried out at the island of Ebeye. In particular, risks derived from flooding and coastal erosion have been combined in one index, integrating the information on events with different return periods and time horizons.

A number of assumptions have been made to construct flood-damage curves which could be representative of the situation in Ebeye, accounting for direct, indirect and intangible damages, based on the available information. The methodology which has been applied is flexible and can be easily updated whenever new data and information will become available

Deltares
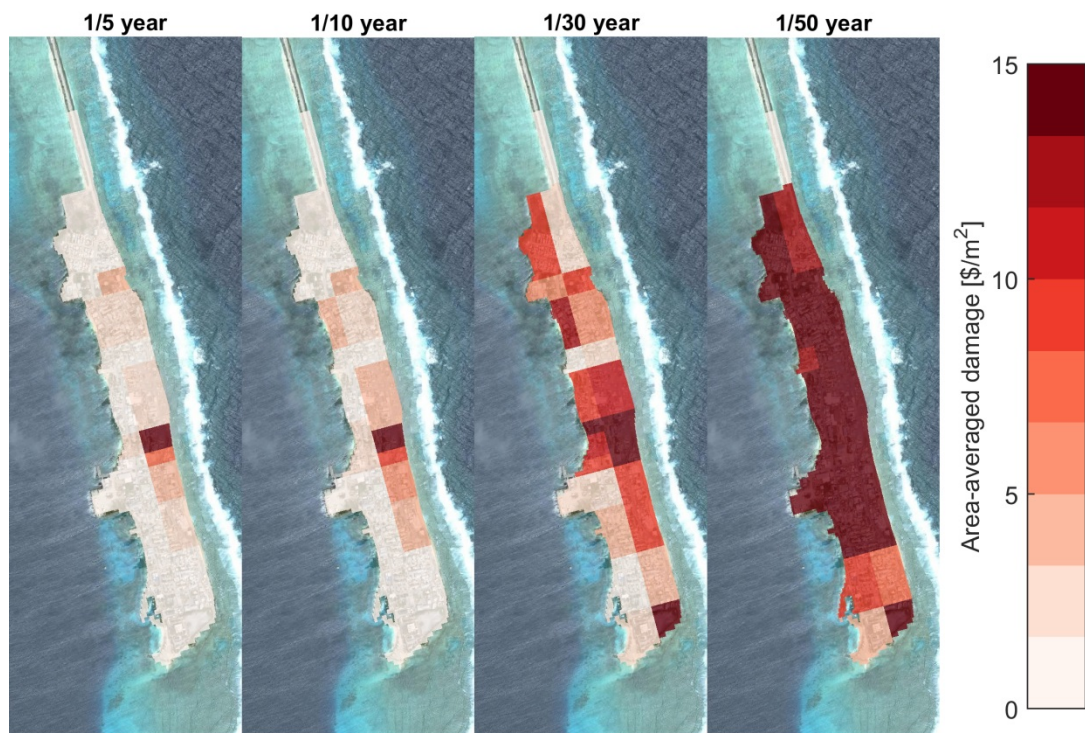
Figure 8.7   Average damage in USD/㎡ per areal unit in the current situation for all return periods.
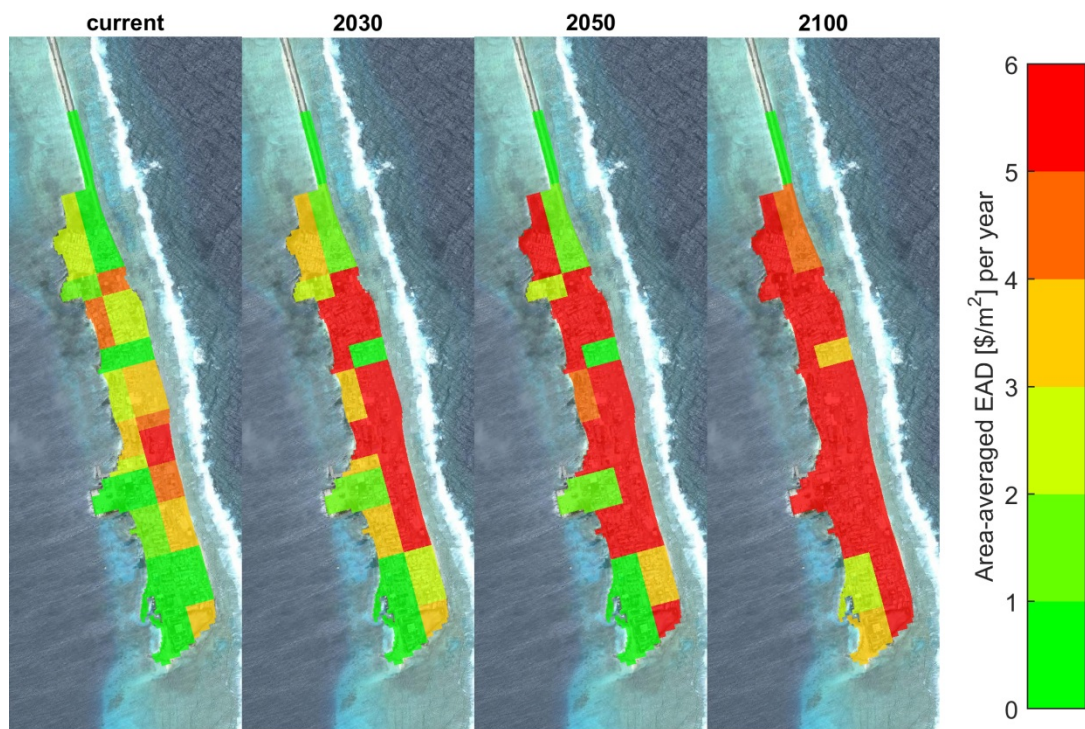
Figure 8.8   Expected annual damages per areal unit (USD/㎡) under sea level rise scenario RCP 8.5, for all time horizons.
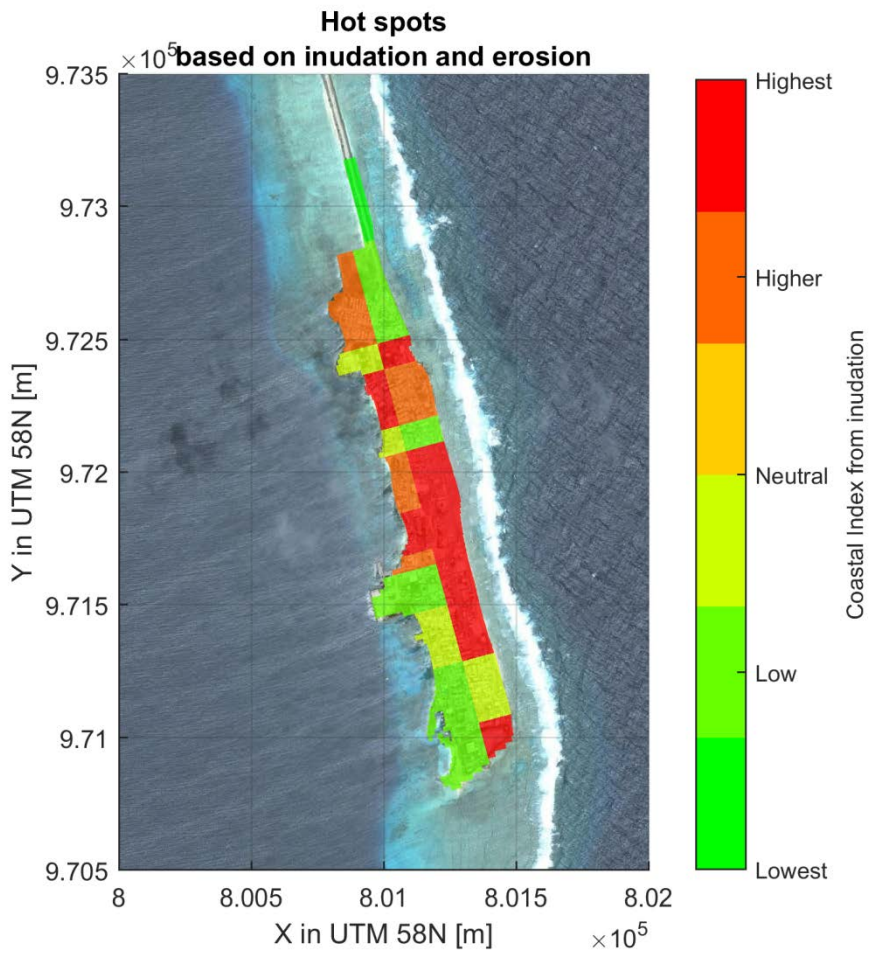
Figure 8.9   Definition of hotspots based on the Coastal Index, ranging from lowest (green) to highest (red) risk.

9 Conceptual designs of adaptation options and cost-estimate

9.1 Introduction

In this Chapter, conceptual designs of solutions are proposed at locations where higher risks have been identified in Chapter 8. Cost-estimates for the different solution schemes are also provided. The same risk analysis as presented in Chapter 8, is then repeated in this Chapter, to describe how different solutions may reduce the risks at different locations of the island.

9.2 Adaptation options

9.2.1 General settings

The analysis of possible adaptation solutions is based on wave conditions that are computed for 9 different representative transects as shown in Figure 9.1. Offshore-nearshore transformation of wave heights generated by either cyclones or swell have been computed for several return periods. The results with respect to wave conditions are taken on top of the reef flat, where the waves break due to the depth limitation.

Figure 9.1   Plan view with representative transects as used in the analysis presented in this chapter.

9.2.2 Wave conditions and water levels

Wave conditions for different return periods have been calculated by means of the XBeach model (Chapter 6). Wave heights on top of the reef have been computed. The mean value of the 9 wave heights as well as the minimum and maximum values of these 9 wave heights are listed in Table 9.1. Distinction has been made between cyclone-induced waves with relatively short wave periods of 10 s accompanied by low frequency waves of typically 1 to 2 minutes and swell waves with wave periods of around 20 s also accompanied by low frequency waves of 1 to 2 minutes wave periods. The cyclone-induced conditions ($H_{s,cyclone}$) are listed in the left columns of Table 9.1 and the swell conditions ($H_{s,swell}$) are listed in the rights columns of Table 9.1.

The low frequency waves ($H_{s,lf}$) are that long that they are only visible by a change in water level at the shore. They are generated due to the wave breaking on the outer reef. Therefore it assumed that the water level changes between about the mean water level $z_s \pm 0.5$ times $H_{s,lf}$. For example, for a 1:10 year cyclone wave condition this means that on average the water level varies between $z_{s,q}(\mu_{min})$=1.33m (1.86m − 0.5*1.07m) and $z_{s,q}(\mu_{max})$=2.40m (1.86m + 0.5*1.07m) with, on top, a design wave condition with H_s =1.4m and T_p=10s.

Table 9.1   Wave and water level conditions (Left: cyclone-induced conditions, Right: swell conditions). Distinction has been made between short wave height (Hs) and low frequency wave height (Hs, lf).

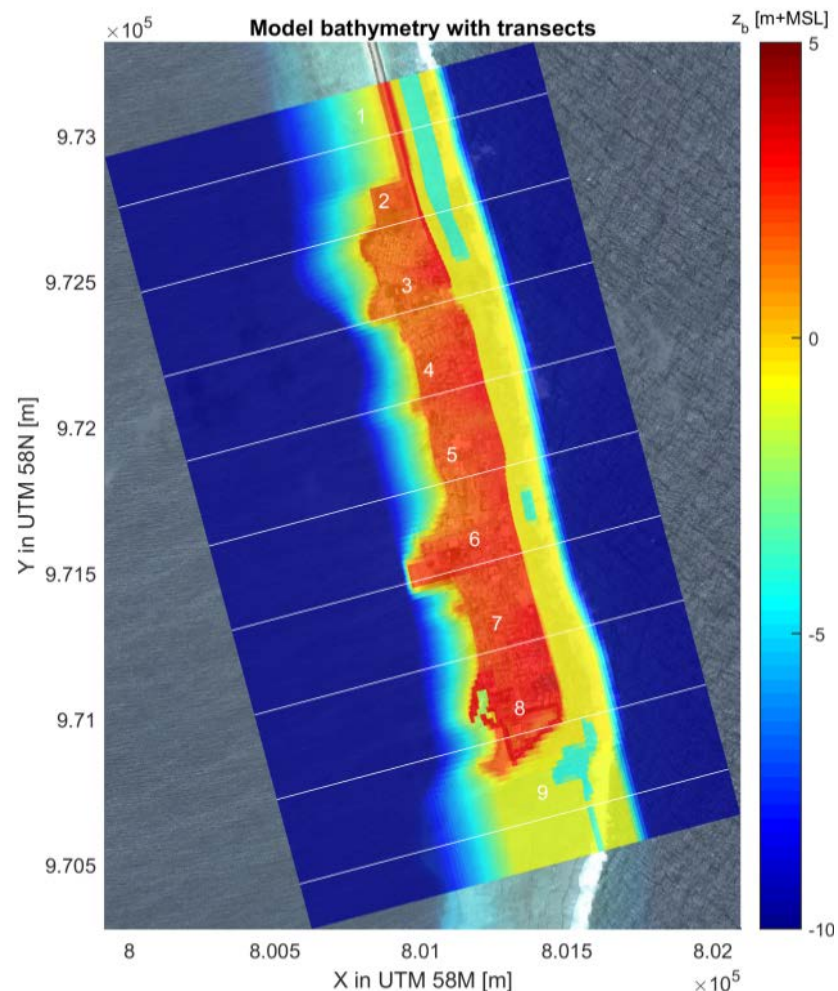|		Return Period							Return Period				
		1:1	1:5	1:10	1:30	1:50			1:1	1:5	1:10	1:30	1:50
H_s, cyclone	min	0.86	1.08	1.29	1.58	1.70	H_s, swell	min	1.37	1.51	1.58	1.62	1.64
T_p≈10s	mean	0.92	1.16	1.40	1.70	1.84	T_p≈20s	mean	1.54	1.68	1.74	1.82	1.86
	max	0.99	1.26	1.51	1.83	1.98		max	1.67	1.78	1.85	1.97	1.99
H_s, lf	min	0.65	0.84	1.02	1.16	1.18	H_s, lf	min	1.43	1.54	1.57	1.60	1.69
T_p>60s	mean	0.69	0.88	1.07	1.21	1.29	T_p>60s	mean	1.50	1.64	1.64	1.69	1.77
	max	0.71	0.92	1.12	1.25	1.41		max	1.62	1.76	1.73	1.80	1.88
z_s	min	1.37	1.63	1.87	2.23	2.40	z_s	min	1.73	1.85	1.92	2.01	2.05
	mean	1.36	1.62	1.86	2.23	2.40		mean	1.72	1.86	1.92	2.01	2.04
	max	1.38	1.65	1.90	2.26	2.43		max	1.76	1.90	1.96	2.04	2.08
z_{s-q}	μ_{min}	1.02	1.18	1.33	1.62	1.75	z_{s-q}	μ_{min}	0.97	1.03	1.10	1.16	1.16
	μ_{max}	1.71	2.06	2.40	2.83	3.05		μ_{max}	2.47	2.68	2.74	2.86	2.93

9.2.3 Overview of possible solutions for coastal defences

In Thomas and Hall (1992) an overview is given of different designs of sea defences that have the function of 1) protecting the shoreline from the effects of erosion, 2) protecting land and property from damage by wave attack and/or 3) preventing or alleviating flooding of low-lying land. The typical design life of a majority of these coastal protection defences is 30-70 years and the corresponding level of protection has usually a return period of 50-100 years.

This means for instance that for a sea defence with a design life of 30 years and a corresponding level of protection RP=1:50 yrs, that by the time the structure reaches the end of its design life there is a 45% chance that design conditions will have been exceeded. This increases for instance to 95% for a return period of 1:10 years. Equation (9.1) shows the calculation method in case other values are selected.

$$P := 1 - \left(1 - \frac{1}{RP \cdot n}\right)^{Life \cdot n}$$

In which:

    P   = probability of exceedence
    Life   = Design life of structure
    RP   = Return Period
    n   = maximum number of storms in a year of 3 hours (365*24/3)=2920

The cross-sections of existing sea walls vary a lot from location to location around the world. They can be classified as sloping or vertical structures, permeable and impermeable. In Table 9.2 to Table 9.5 the functional characteristics of different categories of sea walls are described as according to Thomas and Hall (1992). Key-items of a structure like 'hydraulic performance', 'maintenance', 'flexibility' and 'durability' are qualitive described per type of solution within a certain wave climate. The wave climate is characterised as 'mild' in case wave heights range between 0 and 1.5/2.0m; as 'moderate' in case wave heights range between 1.5/2.0m and 4m and 'severe' in case wave heights are greater than 4m.

The wave climate for Ebeye Island coastal defence is mild to moderate due to the wave breaking on top of the flat reef. Offshore the wave conditions can become severe but, as shown by Table 9.1, wave heights are limited up to about 2m maximum.
It is recommended to develop a cross-section that has a good hydraulic performance for this specific wave climate. Moreover, it should be durable, easily repairable, and also installation should not be too complex. Finally, in case the wave climate will change (i.e. due to climate change) or the functional requirements will modify over time, the structure should be (easily) upgradable. Rock armour and concrete units score in this respect high, see Table 9.2.

Solutions with geotubes are for instance not durable and difficult to be replaced once damaged. Solutions with sheet piles require drilling which is very costly in hard rock; steel solutions suffer from corrosion which results in either high maintenance or low durability. Pitched block revetments, a solution typically applied in The Netherlands, require strict installation specifications with very strict gravel specifications and are therefore also not recommended for Ebeye Island. Vertical block works are also difficult to install and are not flexible to adapt to updated wave climates of higher standards.

In Tonkin & Taylor (2016) a study is presented where possible solutions are put forward, and in which the use of local materials and labour is maximised. Different solutions are discussed; in particular: ecological-based approaches and low cost-solutions, vertical structures and revetments. It is concluded a.o. that revetments constructed of convential materials are the most effective at protecting land and with typically long design lives, whereas for instance low cost-solutions have often a low durability and poor environmental effects as these solutions deteriorate and fail and its material is then released into the marine environment.

To deal with the coastal flooding and erosion problems at Ebeye (Chapter 7), it is also our advice to develop a solution with a sloping permeable structure either made of rock or concrete in combination with rip-rap as foundation.

Table 9.2   Functional characteristics of sloping porous walls.

Type of slope protection	Range of wave climate	Hydraulic performance	Ease of access to shore	Maintenance	Flexibility	Durability (assuming good materials)
Rock Armour	All	Good (depending on underlayer)	Difficult (steps or ramps can give local weakness)	Requires crane	High	High
Rip-rap	Mils and moderate	Good	Difficult (steps or ramps can give local weakness)	Vehicle access (flatter than 1:4 may 'self-heal')	High	High
Random and Pattern placed concrete armour units	All	Medium to good (depending on underlayer)	Difficult (steps or ramps can give local weakness)	Can be a problem if units break	High	Medium to high, but less so with slender units
(i) Small blocks	Mils	Medium	Good	Relatively easy	Medium, will accommodate differential settlement to a degree	High in wave cliamte
(ii) Larger blocks	Moderate to severe	Medium to good, depending on unit	Difficult	Can be a problem if units break	Medium, will accommodate differential settlement to a degree	Medium, depending on slenderness of unit
Flexible armoured revetment systems	Normally mild	Medium (refer to manufacturer)	Fair to good	Well designed, will be low maintenance. Can be difficult to replace individual components	Medium, will accept differential settlement to a degree	Medium
Stone-filled gabion mattresses	Mild	Medium to good	Easy (but leads to problems of durability)	High	Good, will accept differential settlement	Very poor
Open stone asphalt	Mild to moderate	Medium	Easy for pedestrians depending on slope	Limited, but requires regular inspection	Limited	Fair

Table 9.3   Functional characteristics of sloping non-porous walls.

Type of slope protection	Range of wave climate	Hydraulic performance	Ease of access to shore	Maintenance	Flexibility	Durability (assuming good materials)
Stepped concrete slopes	All	Poor to medium	Good	Low, subject to joints	Inflexible, require good toe and foundations	High
Smooth concrete slopes	All	Poor	Relatively easy to include steps	Low, subject to joints	Inflexible, require good toe and foundations	High
Interlocking concrete slabs and blocks	Mild to moderate	Poor	Relatively easy	Low, requires regular inspection and rapid response in the event of damage	Medium, will accommodate differential settlement to a degree	High
Groud mattresses	Mild	Poor	Fair	Low	Inflexible	Medium
Grassed slopes	Occasional mild wave action	Poor	Good	May require mowing of grazing	Flexible	Not to be used in areas regularly subject to wave action
Asphaltic concrete	Mild to moderate	Poor	Good	Low, requires regular inspection and rapid response in the event of damage	Limited-medium	Medium
Asphalt grouted stone	Normally mild to moderate. Occasionally has been used in severe wave climate	Poor	Fair	Low	Limited	Medium to good

Table 9.4   Functional characteristics of vertical non-porous walls.

Type of slope protection	Range of wave climate	Hydraulic performance	Ease of access to shore	Maintenance	Flexibility	Durability (assuming good materials)
Mass concrete gravilty wall	All	Poor	Steps/ramps required	Low	Inflexible	High
Masonry gravity walls	All	Poor	Steps/ramps required	Low	Very limited	High
Brickwork	Mild to moderate	Poor	Steps/ramps required	Low	Very limited	Medium to poor
Timber sheet piles	Mild	Poor	Steps/ramps required over high walls	Low	Limited flexibility but piling tends to penetrate to firm soil, so little differential settlement	Medium
Steel sheet piles	Mild to severe	Poor	Steps/ramps	Difficult to maintain	Limited flexibility but	Medium to poor

			required over high walls	once damaged	piling tends to penetrate to firm soil, so little differential settlement	
Reinforced concrete cantilever	All	Poor	Steps/ramps required	Low	Inflexible, can suffer from differential settlement	Good
Reinforced soil	Novel technique but likely to be satisfactory up to moderate climate	Poor	Steps/ramps required	Low	Inflexible, could suffer badly from differential settlement	Potentially good

Table 9.5   Functional characteristics of vertical porous walls.

Type of slope protection	Range of wave climate	Hydraulic performance	Ease of access to shore	Maintenance	Flexibility	Durability (assuming good materials)
Gabion gravity wall	Mild	Fairly absorptive	Steps/ramps required – difficult to make durable	High maintenance	Fairly flexible	Very poor
Cribwork/ breastwork	Mild to moderate	Good if single-sized rock and sufficient width of section	Steps/ ramps required	Moderate	Fairly flexible	Medium, depending on whether crib is steel or timber hardwood or softwood

9.2.4   Conceptual design of a coastal defence

9.2.4.1   Crest level

The minimum crest level of a coastal defense depends on the allowable wave overtopping discharge during a storm. Often the allowable discharge is lower for a more frequently occurring condition than for a more rare condition.

In order to sketch some possible solutions, the crest level will be first set at +5m. Overtopping quantities are calculated for this level for both the cyclone-induced wave conditions as well as the swell wave conditions. The mean values of H_s as listed in Table 9.1 have been used in combination with the minimum and maximum $z_{s,q}$ water level values. These values have been cross-validated with the SimpleCoast toolkit which is freely available via the website www.simplecoast.com.

Table 9.6   Computed mean overtopping discharge for cyclone-induced and swell conditions.

RP	1:1	1:5	1:10	1:30	1:50
q-mean cyclones [l/s/m]	<0.01	0.05-0.5	0.5-3	2-20	5-50
q-mean swell [l/s/m]	1-5	3-15	4-20	5-35	5-50

The results as listed in Table 9.6 show that the overtopping quantities are very sensitive to the input conditions for cyclone-induced wave conditions. The governing conditions are however the swell conditions due to their larger wave period and larger low frequency wave heights and thus higher water levels.

The calculated mean overtopping discharge values can be verified against Table 9.7 that is taken from Geeraerts et al (2007). This table shows suggested mean discharge limits for different overtopping rates. The figure shows that with the crest level at +5m trained staff is probably safe up to a once in 5 year condition. Also vehicles are able to drive at low speed. For conditions that occur once in 50 years the overtopping conditions become so large that also vehicles driving at low speed should be prohibited to come near the coastal defense.

Table 9.7   Suggested limits for overtopping mean discharges according Geeraerts et al (2007).

Hazard type/reason	Mean discharge, q (l/s per m)
Pedestrians	
Unaware pedestrian, no clear view of the sea, relatively easily upset or frightened, narrow walkway or close proximity to edge	0.03
Aware pedestrian, clear view of the sea, not easily upset or frightened, able to tolerate getting wet, wider walkway	0.1
Trained staff, well shod and protected, expecting to get wet, overtopping flows at lower levels only, no falling jet, low danger of fall from walkway	1-10
Vehicles	
Driving at moderate or high speed, impulsive overtopping giving falling or high velocity jet	0.01-0.05
Driving at low speed, overtopping by pulsating flows at low levels only, no falling jets	10-50

The crest level of +5m is however about 2m or more above the current land level that is most often at a level between 2 and 3m. Therefore, it will require a large quantity of rocks within a cross-section, as visualised in below cross-sectional sketch (Figure 9.2). Also the retaining wall that protrudes 2-3 m above the level of the land of the island will create an obstacle to the sea sea and will result in difficult access to the reef.
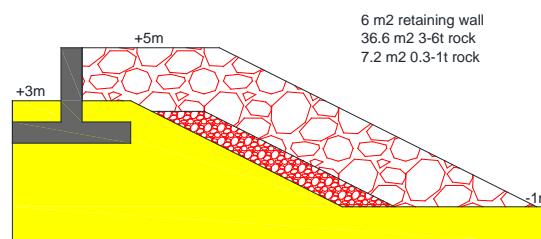
Figure 9.2   Typical Rock cross-section with high crest level.

Lowering the crest level, in order to get a more cost-effective solution and with less visual restrictions, is therefore recommended. This will however result in more overtopping than what is usually acceptable. However, compared to the current situation, it will already result in a very considerable improvement.

Figure 9.3 and Figure 9.4 provide an overview of mean overtopping discharges for different return periods and crest levels of the revetment, under cyclone and swell wave conditions, and assuming a 1:2 rock slope. As shown already in Table 9.6, the figures indicate that the overtopping rates for swell conditions are governing with respect to cyclone-induced wave conditions.

Based on the wave and water level conditions for swell type waves, we can calculate for both the lower and upper extremes, i.e. the combination of the minimum wave height and minimum water level and the combination of the maximum wave height and water level, that the mean overtopping discharge may vary between 10 and 50 l/s/m for a 1:1 yr RP when setting the crest level at +4.3m.

By knowing the constraints of available budget, this is therefore our recommended crest level which will be used as a basis to develop a conceptual design and cost-estimate of the solution.
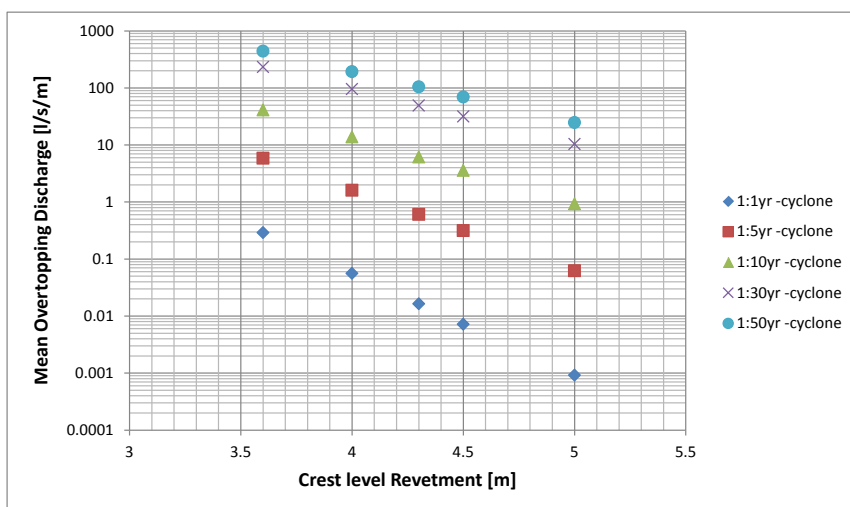
Figure 9.3   Mean overtopping discharge for different crest levels and return periods (cyclones).

Figure 9.4   Mean overtopping discharge for different crest levels and return periods (swell).

9.2.4.2   Hydraulic Stability

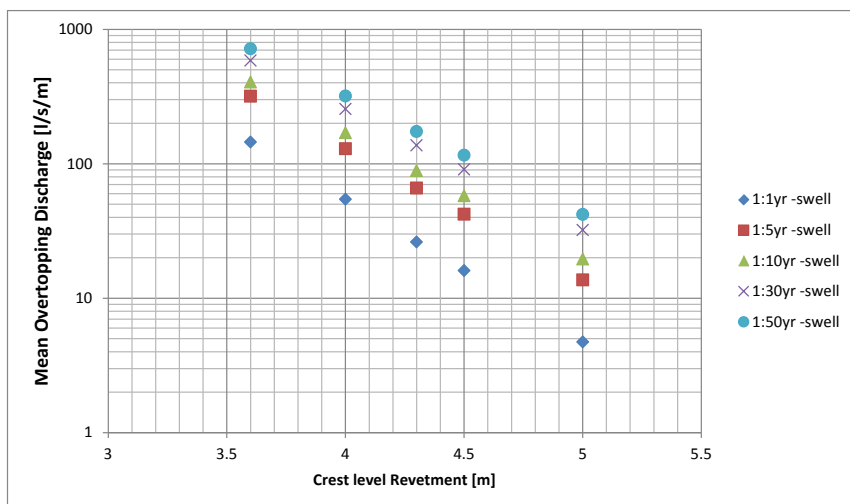In this section the hydraulic stability of the primary armour will be calculated. This means that the mass of a rock grading or concrete cube is determined while accepting a limited amount of damage during the design storm with a selected return period.

In the previous section, a crest level of 4.3m was suggested based on consideration on overtopping rates for a return period of 1:1 year. For more extreme events, the overtopping will increase considerably (by almost a factor 10 during a 1:50 yr condition). For the hydraulic stability we recommend to apply the 1:50 yr conditions since already for a design life of 30 years the chance of exceeding this condition within its design life is 45%. Below calculations are therefore based on this design return period.

<u>Rock</u>
Calculations assuming to use rock as primary armour layer are performed. The mass density of the rock is larger than 2,600 kg/m^3. Cyclone-induced waves, due to their smaller wave period, lead to the largest required rock size. Below two graphs are shown, one with the nominal diameter of rock versus the significant wave height (Figure 9.5) and one with the median mass of the rock grading versus the significant wave height (Figure 9.6).
This has been done for six slope gradients, i.e. 1:1.5 up to 1:4. The start of damage criterion has been used as acceptable damage level. This stability number is about equal to the slope gradient, thus for instance for a slope of 1:2 the start of damage criterion is S=2 and for a slope 1:3 the start of damage criterion is S=3. On the vertical axis, the nominal diameter of the rock (Figure 9.5) as function of the significant wave height [H$_s$], the cotangent of the slope [cotα] and the start of damage criterion [S-value] is set out, Thus D$_{n50}$(H$_s$, cotα, S-value). On the horizontal axis the significant wave height is set-out. In Figure 9.6, the same but then for the median rock grading mass M$_{50}$ has been used on the vertical axis. The median mass M$_{50}$ is calculated by using a mass density of rock of 2650 kg/m^3 times the nominal diameter to the power 3.
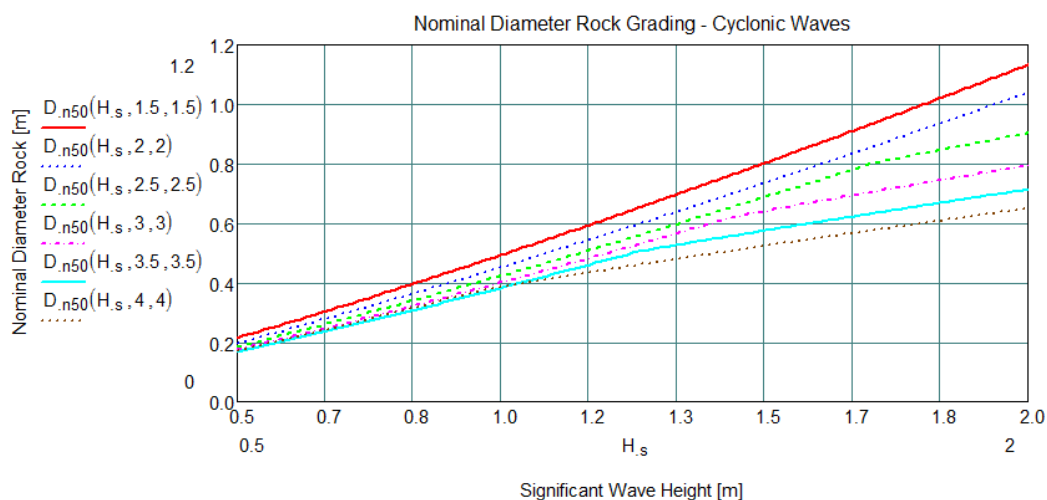
Figure 9.5 Nominal Diameter of rock grading under cyclone-induced waves for different slopes.
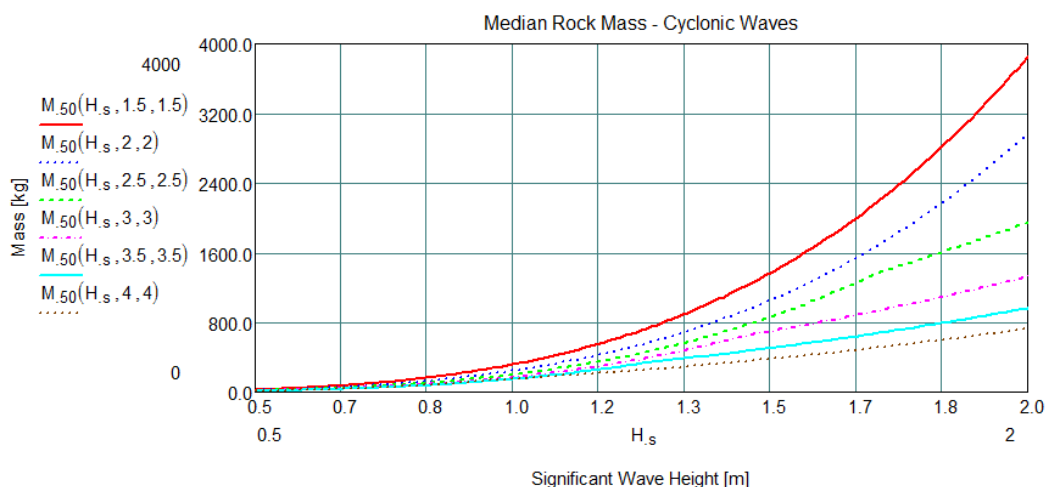
Figure 9.6   Median Rock mass under cyclone-induces waves for different slopes.

Figure 9.5 and Figure 9.6 show that, for a return period of 1:50 year (with $H_{s,max}$ =1.98m) and a slope gradient of 1:1.5, the minimum rock grade has to have a median mass of 3,850kg. A standard rock grading of 3-6t rock would be more than stable enough for this situation. For a slope gradient of 1:2.5 the median mass M_{50} is 1950 kg. The minimum rock grade has then to be 1-3t, see also Rock Manual, 2007. These two structures are also sketched in Figure 9.7.
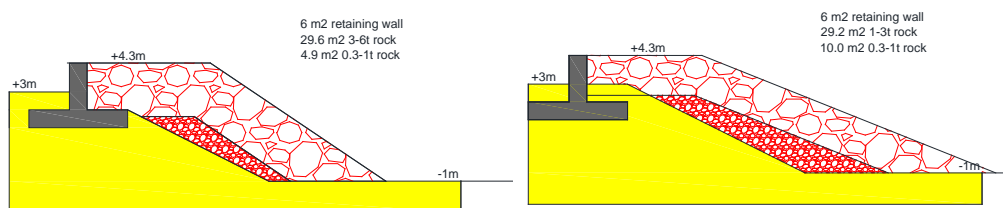
Figure 9.7   Typical Rock cross-sections with crest level for a 1:1 RP and allowing 10-50 l/s/m overtopping rates.
Left figure: slope gradient 1:1.5, right figure: slope gradient: 1:2.5.

Concrete cubes

The large rock (3-6t and 1-3t) will probably have to be imported. As this will result in large costs, it is likely that concrete, although it also has to be imported, will eventually become cheaper than a solution in which large rock gradings are needed.

For a design wave condition with a return period of 1:50 year the cube size has to be 1.0x1.0x1.0m. This is calculated by using a stability number N_{od} of 0.2. This value means the allowable number of displaced units in a strip of 1 unit size, see also Rock Manual, 2007. This cube size can be applied in either a double layer randomly placed armour or a single layer pattern (safety factor of 1.8) placed with 25% porosity, as shown in Figure 9.8 . The latter is the preferred solution as it is cheaper and easier to construct.

Figure 9.8   Stable, easy-to-construct solution with single layer cubes.

A typical cross-sectional design is shown in Figure 9.9.

6 m2 retaining wall
7.5 m2 cubes (25% porosity)
7.6 m2 1-3t rock
9.9 m2 0.3-1t rock/ selected QR

+4.3m
+3m
-1m
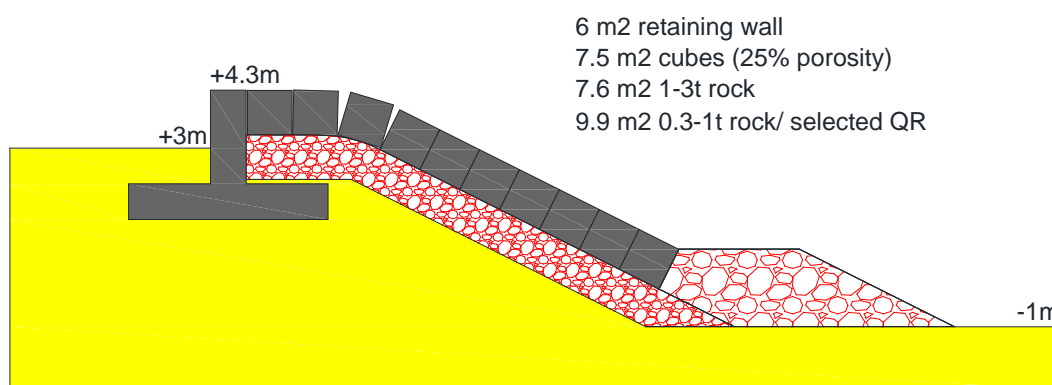
Figure 9.9   Typical single layer cube cross-sections with crest level for a 1:1 RP, allowing for 10-50 l/s/m overtopping rates.

9.2.5   Revetment with berm

An improved and climate-change resilient version of the previous design has been developed by using a berm on the reef that will promote wave breaking of the waves. The energy dissipation will result here in a solution with a lower crest level than for a standard revetment alternative. The reduction in overtopping discharge can be up to a factor of 10 as physical model tests have shown (Delft Hydraulics (current Deltares), 2007). Also smaller material for both rock and concrete cubes can be used by applying a berm on the seaward side of the structure.

Moreover, it is to be expected that sea level rise will result in higher water levels on the reef and therefore in higher wave conditions. This improved design, even when these more critical conditions will occur, will still promote wave breaking. Therefore, the solution can be considered flexible and easily adaptable, with minimal effort, to these more severe conditions.

In Figure 9.10, three options are drawn. The top cross-section consists of a base layer of 0.3-1t on top of a heavy grading of 1-3t rock. In the middle cross-section these two layers have been mixed which is likely to be easier for contractors to install, but some more reshaping will occur for the sloping part near the retaining wall. In the lower cross-section the 1-3t rock has been replaced by cubes with a rib size of 0.7m. The size of the cube is here smaller than in the standard revetment since the cubes will be submerged during the design conditions. At lower water levels the wave height will be lower and therefore the cube size is still stable. Optimizing the length of the berm is likely to be possible by using physical modeling.
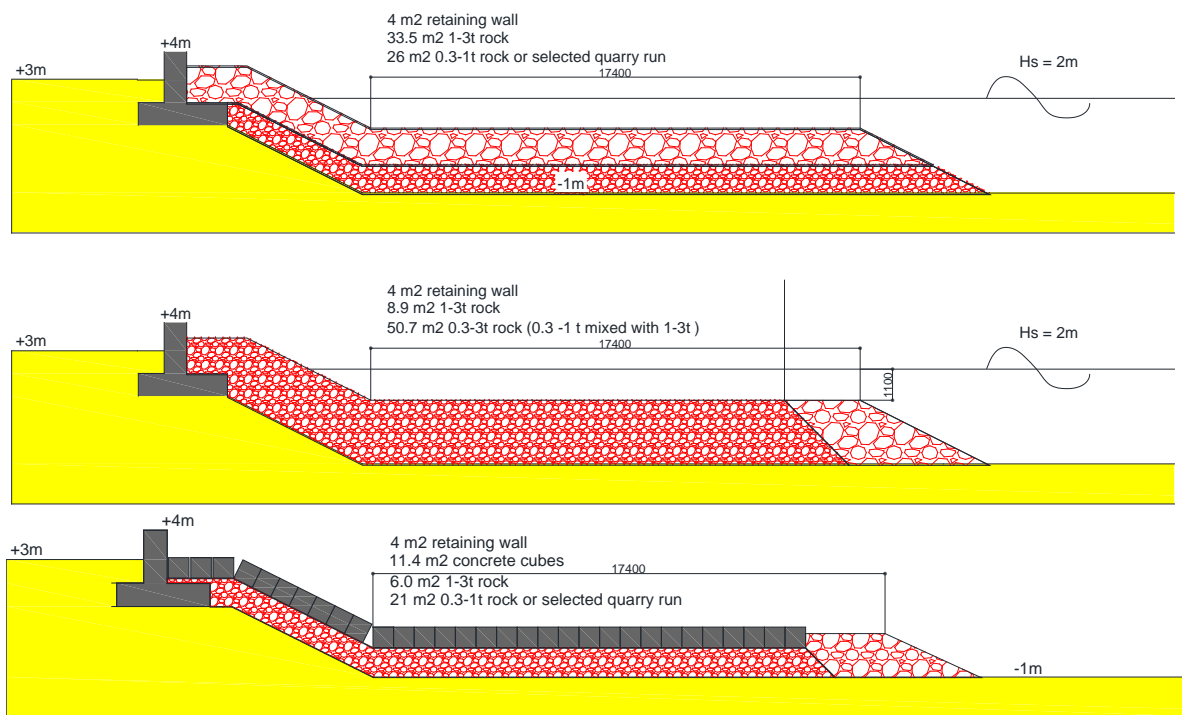
Figure 9.10 Durable berm type solutions, adaptable to conditions in case of sea level rise.

At sections where mining pits are present, it might not be possible to construct a berm since the pit has then to be filled up again. For these locations, a breakwater, constructed between the edge of the reef and the mining pit, is the preferred solution, see Figure 9.11.

During a design condition with a return period of 1:50 year the waves break on the breakwater and the transmitted significant wave height reduced to only around 0.5m. Therefore, at the island, only minor construction works are needed, for instance installing a wall of 0.6m high (crest level at +3.6m) in order to prevent the flooding from the high water level of around 3.0m, see $z_{s,q}$ of 1:50 year RP in Table 9.1 in combination with a low wave height.
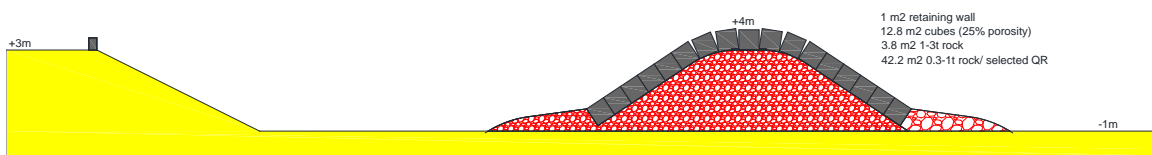
Figure 9.11 Parallel breakwater type solution in case mining pits are located within the preferred berm zone.

All solutions that are drawn here are within the inner reef (reef flat) of the coast. The available formulae from literature that are provided, for instance, in the Coastal Engineering Manual or the Rock Manual are not developed for situations where constantly wave breaking occurs. Also in case of very shallow water depths on the reef, the incoming waves will break and eventually may result into a bore. No design guidelines are available for these situations. Therefore, physical modeling is highly recommended to verify the hydraulic stability of the solutions and to verify the overtopping discharge. Moreover, physical modeling, usually also leads to reduced volumes of material by, for instance, optimizing the berm length. By doing a physical model study the available budget for the coastal protection works may be used to protect a longer stretch along the coastline. The designs of the different options are also only

developed for a storm condition with a return period of 1:50 years. As the chance of having a larger wave condition than the design condition of 1:50 years is large (45%), it is recommended to test the redundancy of the structure for overload conditions in the physical model as well. The outcome of such test should result in damages which can be easily repaired.

9.3   Cost-estimate of solutions
In Tonkin + Taylor (2016) unit price of different type of materials have been provided (in AUD) in Table 9.8 the same values have been reported and converted to USD. These rates have been used to assess the costs of the different options.

Transport costs are a major component of the total costs per meter cross-section. Tonkin + Taylor (2016) distinguish 4 ways of transport i.e. base, local transport, primary port and remote location. The following description is given to these ways of transport.

Base:
"Material is produced locally and transported by road within 30km." Assume AUD 20/m^3.

Local transport:
"Local transport within 200 km by road or barge including one handling. Assume AUD 150/m^3."

Primary port:
"Loaded at a primary port, transported up to 3000 km, unloaded and transported locally to site. Based on typical freight costs assume cost of AUD 500/m^3, although likely to fluctuate with location and local import taxes and duty. "

Remote location:
"Load barge at primary port, transport up to 2000 km and unloaded at wharf, jetty or directly onto land using a ramp. Mechanical plant is typically required to facilitate the offload. Assume AUD 1000/m^3 based on typical barge hire rates."

In the budget estimates provided as part of this report, only the rates of local transport and primary port transport are included. The heavy armour of 1-3t and 3-6t are expected to have rates of around 400 USD / m^3, only accounting for primary port transportation. Transport costs for aggregate/underlayer and ingredients for concrete are based on local transport rate of around 120 USD / m^3. However, it is important to mention that the cost estimates as summarized in Table 9.8 may be subject to large variation (e.g. depending on the origin of material used for construction, construction methods, costs for mobilization and demobilisation etc.). Therefore, the budget estimates as provided below for the different options should be primarily used for relative cost-comparison between different options, rather than absolute values.

Table 9.8   Unit price of materials as provided by Tonkin + Taylor (2016).

	AUD rate per m^3	USD (2016) rate per m^3
Armour rock 3-6t m^3 (>2600 kg/m^3)	180	145.1
Armour rock 1-3t m^3 (>2600 kg/m^3)	150	120.9
Aggregate/Underlayer 0.3-1t or selected QR m^3	80	64.5
Sand m^3	50	40.3
Mass Concrete (Standard 30Mpa) including	600	483.8

formwork m³		
Mass Concrete (Standard 30Mpa) including formwork m³	600	483.8
Local transport	150	120.9
Primary port transport	500	403.1
Remote location transport	1000	806.3

The revetments with rock armour with a slope 1:1.5 or 1:2.5 costs based on the above prices will have a linear price of about 20,000 USD per running meter (Table 9.9). When the primary armour rock is exchanged with concrete cubes of 1x1x1 m, the costs reduce to around 14,000 USD per running meter.

Table 9.9   Costs for standard revetment per linear meter.

	revetment 1:1.5 rock armour (left panel Figure 9.7)		revetment 1:2.5 rock armour (right panel Figure 9.7)		revetment 1:2 cube armour (Figure 9.9)	
	Volume m³	Costs USD	Volume m³	Costs USD	Volume m³	Costs USD
Armour rock 3-6t m³	29.3	4,252				
Armour rock 1-3t m³			29.2	3,532	7.6	919
Aggregate/Underlayer 0.3-1t or selected QR m³	4.9	316	10	645	9.9	639
Mass Concrete (Standard 30Mpa) including formwork m³	6	2,903	6	2,903	6	2,903
Mass Concrete (Standard 30Mpa) including formwork m³					7.5	3,628
Local transport	10.9	1,318	16	1,935	23.4	2,830
Primary port transport	29.3	11,812	29.2	11,772	7.6	3,064
Costs per running meter USD		**20,601**		**20,786**		**13,983**

The costs for the improved design, i.e. the berm type structures, which is our recommended solution, is 25,000 USD per running meter in case of 1-3t rock as top layer, and reduces to about 16,000 USD per running meter in case some more reshaping is allowed for the mixed layers of 0.3-1t and 1-3t (Table 9.10). The same costs of 16,000 USD per running meter is estimated when concrete cubes are used for the berm and slope.

Table 9.10   Costs for berm type revetment per linear meter.

	Berm breakwater rock armour 1 (top panel Figure 9.10)		Berm breakwater rock armour 2 (middle panel Figure 9.10)		Berm breakwater cube armour (lower panel Figure 9.10)	
	Volume m³/m	Costs USD	Volume m³/m	Costs USD	Volume m³/m	Costs USD
Armour rock 3-6t m³		-		-		-
Armour rock 1-3t m³	33.5	4,052	8.9	1,076	6	726
Aggregate/Underlayer 0.3-1t or selected QR m³	26	1,677	50.7	3,270	20.8	1,342
Mass Concrete (Standard 30Mpa) including formwork m³	4	1,935	4	1,935	4	1,935
Mass Concrete (Standard 30Mpa) including formwork m³		-		-	11.4	5,515
Local transport	30	3,628	54.7	6,616	36.2	4,378
Primary port transport	33.5	13,505	8.9	3,588	6	2,419
Costs per running meter USD		**24,797**		**16,485**		**16,314**

The costs for the parallel breakwater (to be used at location where mining pits are present) is around 18.000 USD per running meter (Table 9.11).

Table 9.11 Costs for parallel breakwater per linear meter.

	Parallel breakwater cube armour (Figure 9.11)	
	Volume m^3	Costs USD
Armour rock 3-6t m^3		-
Armour rock 1-3t m^3	3.8	460
Aggregate/Underlayer 0.3-1t or selected QR m^3	42.2	2,722
Mass Concrete (Standard 30Mpa) including formwork m^3	1	484
Mass Concrete (Standard 30Mpa) including formwork m^3	12.8	6,192
Local transport	56	6,773
Primary port transport	3.8	1,532
Costs per running meter USD		**18,162**

The cost for rock, especially the lower gradings that serve as aggregate/ underlayer, may be reduced in case use can be made of material provide by neighbouring islands.

9.4 Location of the solutions

In Section 9.2 and 9.3, different types of solutions have been proposed. The efficiency of the two cheapest revetment types is investigated by means of the XBeach model in Section 9.5. In particular: the standard revetment type with cube armours (Table 9.9) and the berm revetment type with cube armours (Table 9.10). In this section, different locations are described where the solutions may be applied, based on the results from the risk assessment as presented in Section 8.5. In particular, the two revetment types are tested for all different locations. Figure 9.12 shows an overview of all different locations where solutions have been implemented in the model and tested. All alternatives refer to designs aiming at protecting the island from the ocean side, as the hazards from the lagoon side are generally of lower intensity (Chapter 7). Table 9.12 summarizes the different options, with indication on lengths, costs and cost-effectiveness. In particular:

- Alternative 1 and 2 describe an extreme-case solution, where all the island is protected from the ocean side. These alternatives are representative of an upper boundary situation assuming that there is no direct limit in available budget for coastal protection works. The estimated total cost for this alternative ranges between $28.0 and $32.6 million.
- Alternative 3, 4, 5, and 6 aim at protecting the coastline at the two hot spots identified in Chapter 8.5. The first hotspot is located in the north of Ebeye (alternative 3 and 4) and hotspot 2 is in the middle of Ebeye (alternative 5 and 6). The costs for protecting one hot spot range between $3.6 to $4.2 million.
- Alternative 7 and 8 aim at extending the existing seawall towards the south resulting in a total cost ranging between $14.8 and $17.3 million. This is roughly the budget that may be available in the project as communicated by the client.
- Alternative 9 and 10 aim at extending the existing revetment next to the causeway, all the way towards Gugeegue. The cost for these alternative ranges between $83.9 and 97.9 million. This will decrease the direct damages of the shoreline protection of the causeway which is estimated to be $1.0 million per year. In this alternative it is still

possible that debris from the lagoon covers the road, since no protection is constructed at the lagoon side.
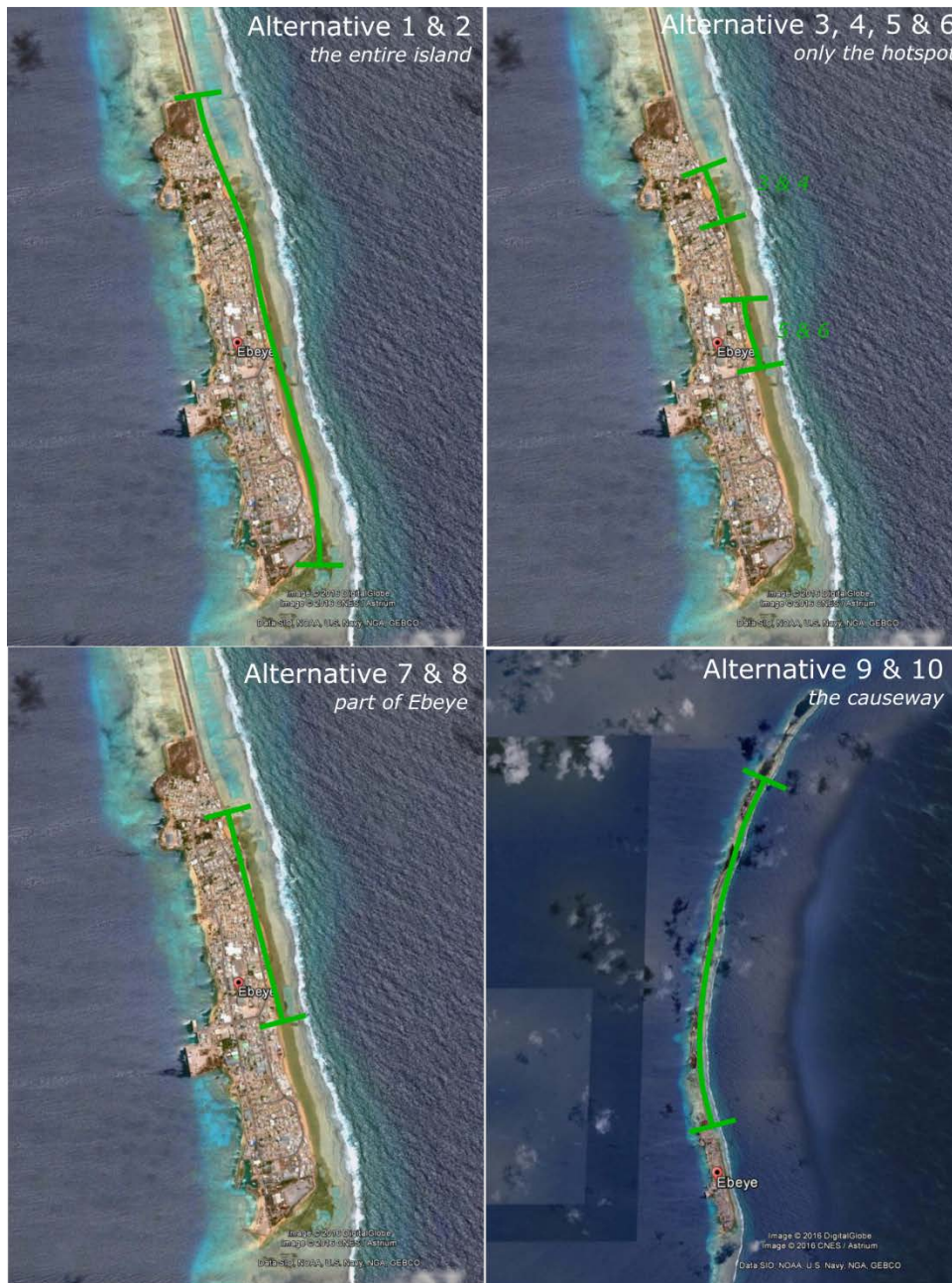
Figure 9.12 Different proposed locations for the adaptation options

9.5 Effectiveness of the solutions

In order to test the effectiveness of the different solutions, the same set of simulations, as presented in Chapter 8, is repeated but including the different coastal defence schemes. Finally, the cost-effectiveness of different alternatives is assessed by comparing the ratio between benefits derived from the reduction in Expected Annual Damages (EAD) and the construction costs.

The higher this ratio, the more cost-effective the adaptation option is. It is important to realize that this relative comparison is used in this study to compare cost-effectiveness of different solution; however, this comparison should be supported by a full cost-benefit analysis in later phase (not part of this study, see Section 11.3).

From Table 9.12 one can conclude that constructing a revetment for the entire island of Ebeye results in the largest reduction of the EAD of about $ 0.77 million. This is a decrease of 31% with respect to the current EAD (which is $ 2.44 million, Section 8.5).

As an example, Figure 9.13 shows the computed flooding maps for a 10 year return period event, both in the current situation and after the construction of the revetment along the entire island. During extreme conditions the proposed solution will still get overtopped, but it will protect the majority of Ebeye from large-scale inundation for storms with a return period of 30 years (and smaller). For storms with a return period of 50 years large-scale inundation will still occur. Moreover, flooding from the lagoon will also still occur as the revetment only protects the island from the ocean side.

Constructing only a revetment at the hotspot location in the north of Ebeye (alternative 3 and 4) is more cost-effective than constructing a revetment at the hotspot location in the central part of the island (alternative 5 and 6) (effectiveness percentile of 12-13% versus 6-7%). This is because construction a revetment in the north will reduce the damages as a result of storm-erosion. A possible downside of constructing a local revetment is that the water level in front and next to the revetment increases. This could result in locally more inundation (i.e. hazard). However, from Figure 9.14, one can conclude that this is not the case. These alternatives are also the most cost-effective solutions of all the options considered, as solutions are placed exactly at the position where the risk is the highest. However, from an engineering point of view, it may not be possible to construct the revetment exactly (and only) at these locations. Moreover, this may lead to side effects (i.e. local erosion at the side of the revetment; see also Section 9.6). As an example, a flooding map before and after construction of alternative 5 is shown in Figure 9.14.

Constructing a revetment to protect the entire causeway from shoreline damage is from an economic reasoning the least interesting. The cost-effectiveness is 10-13 times less effective than alternative 4. This is related to the long length of the causeway (6 km) and therefore high cost ($84 and 97 million). The reduction in EAD is however the largest of all the alternatives ($1.0 million). This is related to costs of the damage to the shoreline protection in the current situation. Moreover, the construction of the revetment towards Gugeegue will also lead to additional long-term benefits, as the possibilities for people to relocate from Ebeye towards this island (Section 10.2).

Finally, for each location, two revetment options are proposed (standard type and berm type, Section 9.2). Table 9.12 shows that the berm option performs slightly better, but costs are also higher. The result is a less cost-efficient solution. However, it is expected that the effect of the berm type of solution on the hazards is partly underestimated by the XBeach model due to model resolution, as it is also confirmed by physical modelling tests (Delft Hydraulics, 2008). Also, given the fact that berm type revetments have more flexibility to adapt to future sea level rise scenarios, this is our recommended solution.

For alternatives 1, 2, 7 and 8 (which are the most likely to be implemented) also the cost-effectiveness over time is considered (i.e. with sea level rise under two RCP scenarios). For the reference situation (without a solution) the EAD increases from $2.4 million dollar for the current sea level up to $6.29 – 9.05 million dollar, respectively for time horizon 2100 under RCP 4.5 and 8.5. On average the EAD increases $63,000 per year as a result of sea level rise. A similar calculation can be carried out for the proposed alternatives. For alternative 1

and 2 the EAD increases on average $36,000 per year and for alternative 7 and 8 the EAD increases $40,000 – 48,000 per year. This means that besides an initially decrease of the EAD (i.e. effectiveness) the proposed solutions get more effective over time since the EAD increases slower than without revetment. This means that each alternative has a double effect: first an initial reduction of EAD, and second a long-term reducing effect if sea level rises. For example, alternative 1 resulted in a decrease of the EAD of $0.77 million for the current sea level. This will increase up to $2.53-3.47 million in 2100, depending on the sea level rise considered, see also Table 9.13 and Figure 9.16. The reason for the 'double' effect can be found in the applied depth-damage curve which has a quadratic slope and therefore damages grow more than linearly.

The same calculation can be carried out for the EAAP (Expected Annual Affected People) (Table 9.14). For the situation without any solution, the EAAP increases from 5,030 people for the current sea level up to 9,292-10,673 for time horizon 2100 under RCP 4.5 and 8.5. On average the EAAP increases 56 people per year, as a result of sea level rise. In this case, the quadratic effect as shown above for the EAD, when solutions are implemented, is not visible as no depth-damaged function is used. For example, alternative 1 resulted in a decrease of the EAAP of 3,256 people for the current sea level (from 5,030 to 1,774), which is quite similar to the decrease in EAAP when solutions are implemented. The development of EAD and EAAP in time is also shown in Figure 9.16 and Figure 9.17, for the current situation and alternative 1, for the two sea level rise scenarios considered.

Table 9.12 Adaptation options with costs and benefits.

#	Location	Revetment type	Length [km]	Costs [million $]	Decrease EAD [million $]	Decrease EAAP [people]	Ratio Decrease EAD/Costs [%]
1	Entire island of Ebeye	Standard	2000	$28.0	$0.71	3256	3%
2	Entire island of Ebeye	Berm	2000	$32.6	$0.70	3335	2%
3	Hotspot location 1	Standard	260	$3.6	$0.51	629	13%
4	Hotspot location 1	Berm	260	$4.2	$0.54	959	12%
5	Hotspot location 2	Standard	260	$3.6	$0.29	440	7%
6	Hotspot location 2	Berm	260	$4.2	$0.30	631	6%
7	Hotspot location 1 +2 and in between	Standard	1060	$14.8	$0.73	3437	5%
8	Hotspot location 1 +2 and in between	Berm	1060	$17.3	$0.70	3311	4%
9	Entire causeway	Standard	6000	$83.9	$1.00	0	1%
10	Entire causeway	Berm	6000	$97.9	$1.00	0	1%

Deltares

Figure 9.13 Inundation with a return period of 1/10 years for the current situation (left figure) and after the construction of revetment alternative 1 with the current sea level (right figure).

Figure 9.14 Inundation with a return period of 1/10 years for the current situation (left figure) and after the construction of revetment alternative 5 with the current sea level (right figure).
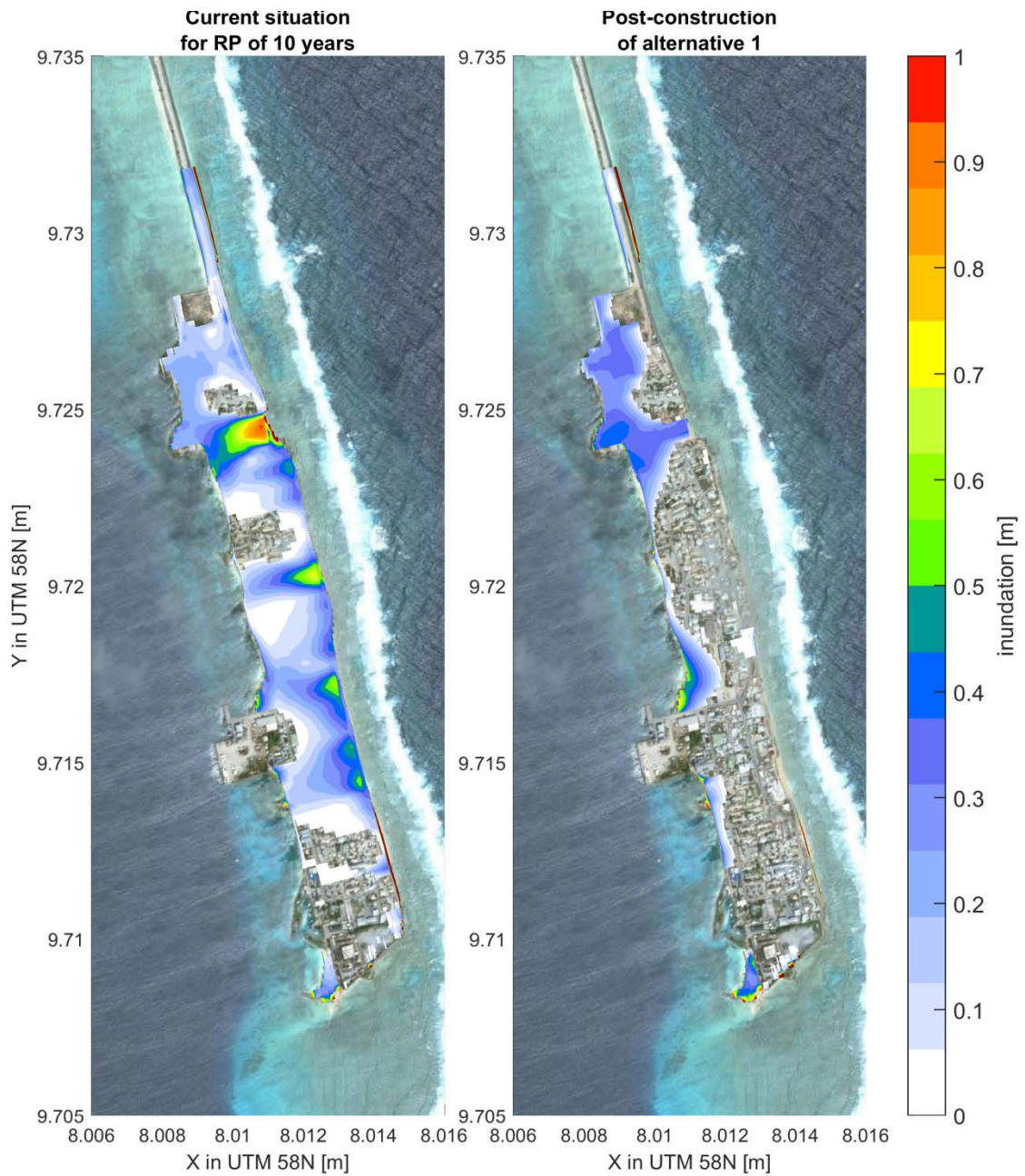
Figure 9.15 Inundation with a return period of 1/10 years for the current situation (left figure) and after the construction of revetment alternative 8 with the current sea level (right figure).
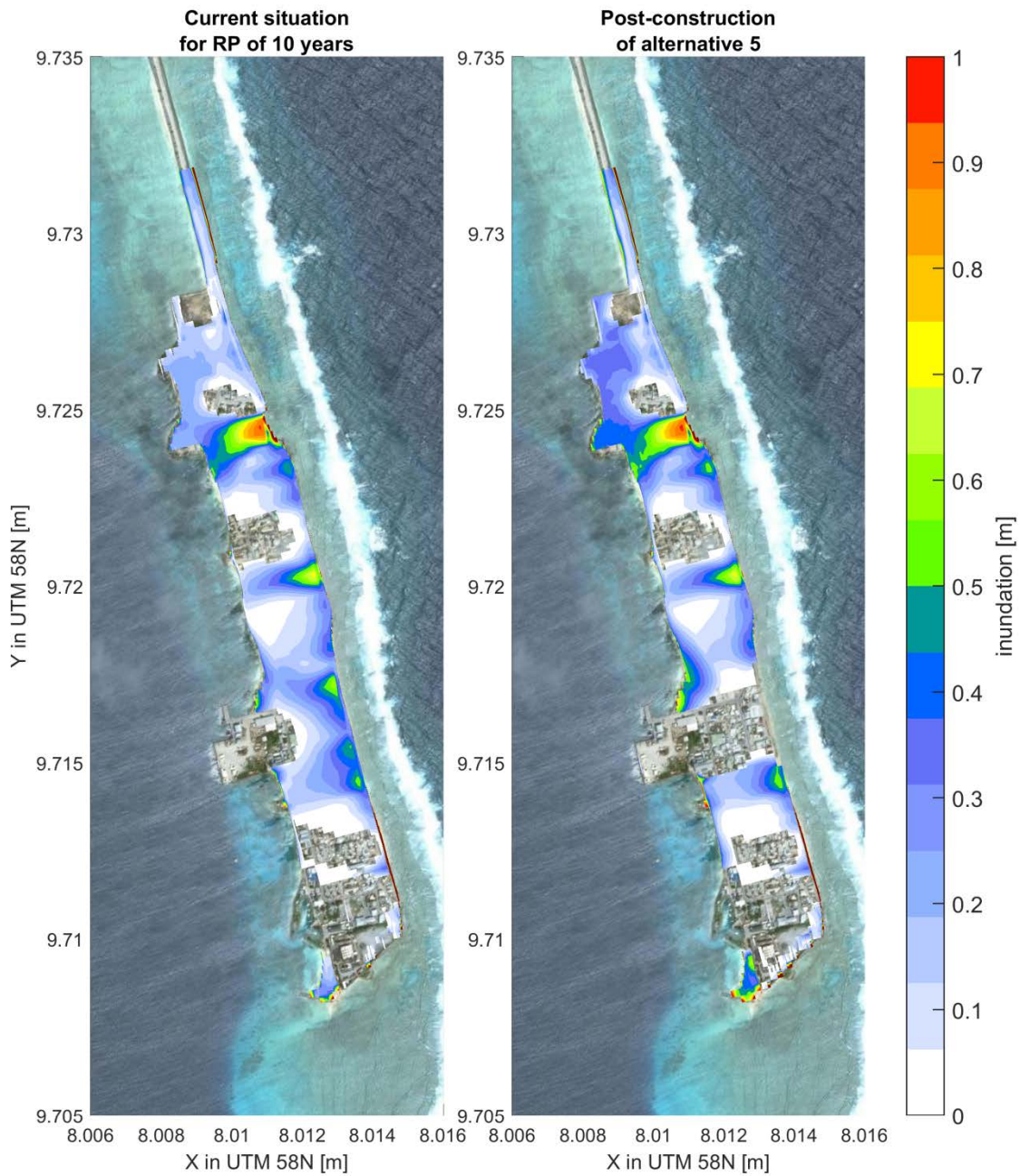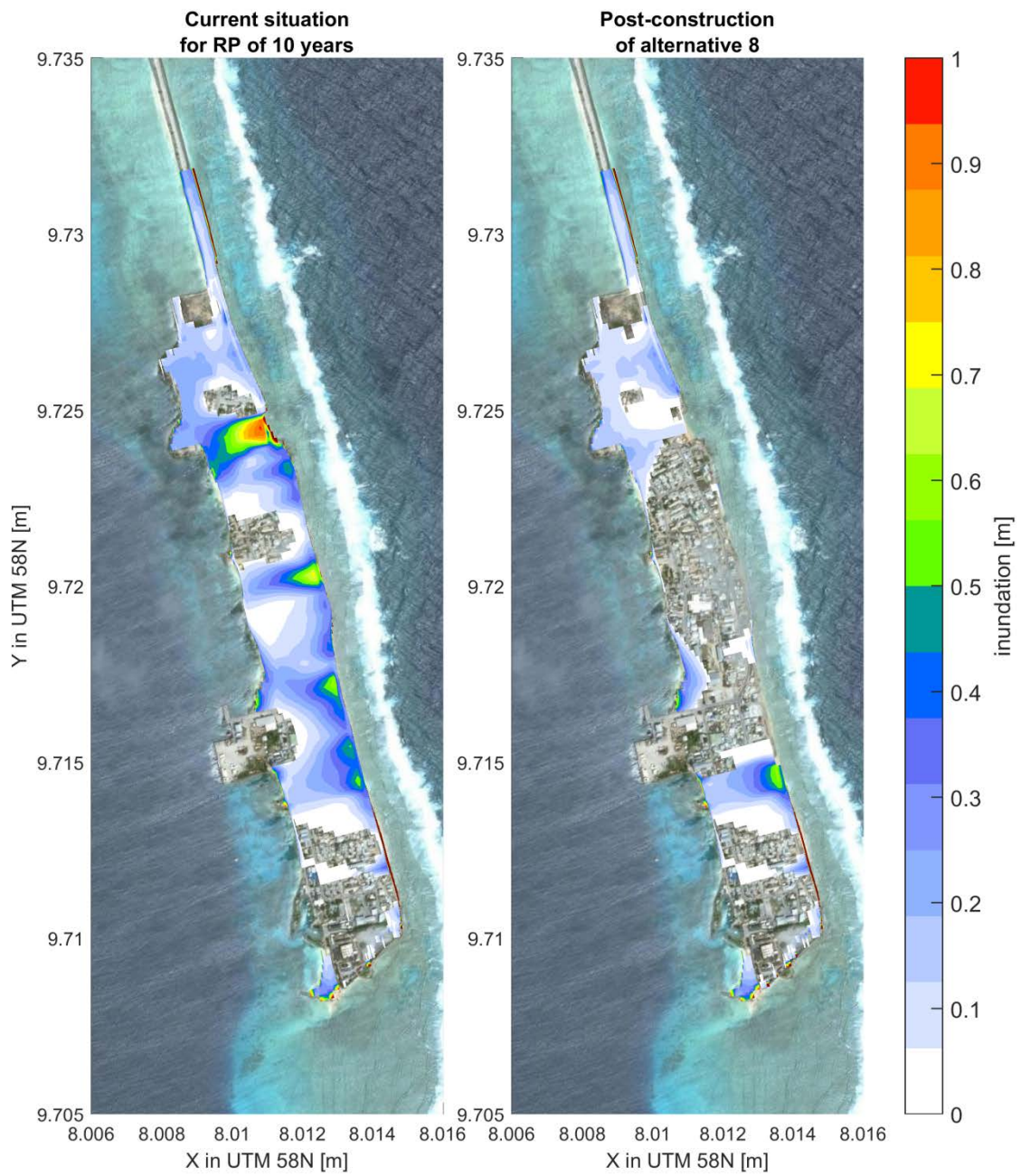
Table 9.13 EAD in million USD per year for different alternatives for different time horizons and RCP scenarios. [-] means this value is not determined.

A	Current	RCP 4.5			RCP 8.5		
		2030	2050	2100	2030	2050	2100
0	$2.4	$3.2	$3.9	$6.3	$3.3	$4.1	$9.1
1	$1.7	$2.1	$2.4	$3.8	$2.1	$2.5	$5.6
2	$1.7	$2.1	$2.4	$3.8	$2.1	$2.5	$5.6
3	$2.0	[-]	[-]	[-]	[-]	[-]	[-]
4	$1.9	[-]	[-]	[-]	[-]	[-]	[-]
5	$2.2	[-]	[-]	[-]	[-]	[-]	[-]
6	$2.2	[-]	[-]	[-]	[-]	[-]	[-]
7	$1.6	$2.4	$2.8	$4.6	$2.4	$3.0	$7.0
8	$1.7	$2.4	$2.9	$4.7	$2.4	$3.0	$7.1

Table 9.14 EAAP in people per year for different alternatives for different time horizons and RCP scenarios. [-] means this value is not determined.

A	Current	RCP 4.5			RCP 8.5		
		2030	2050	2100	2030	2050	2100
0	5030	6199	7174	9292	6283	7404	10673
1	1774	2659	3233	4963	2721	3414	6871
2	1695	2509	3076	4929	2554	3206	7368
3	4401	[-]	[-]	[-]	[-]	[-]	[-]
4	4071	[-]	[-]	[-]	[-]	[-]	[-]
5	4590	[-]	[-]	[-]	[-]	[-]	[-]
6	4399	[-]	[-]	[-]	[-]	[-]	[-]
7	1593	3171	3786	5753	3259	3925	8273
8	1719	3118	3799	5821	3184	3959	8373

Figure 9.16 Development of the EAD as function of the time horizon for the current situation and alternative 1. The width of the band represent the variability between the two sea level rise scenarios (RCP 4.5 and RCP 8.5).
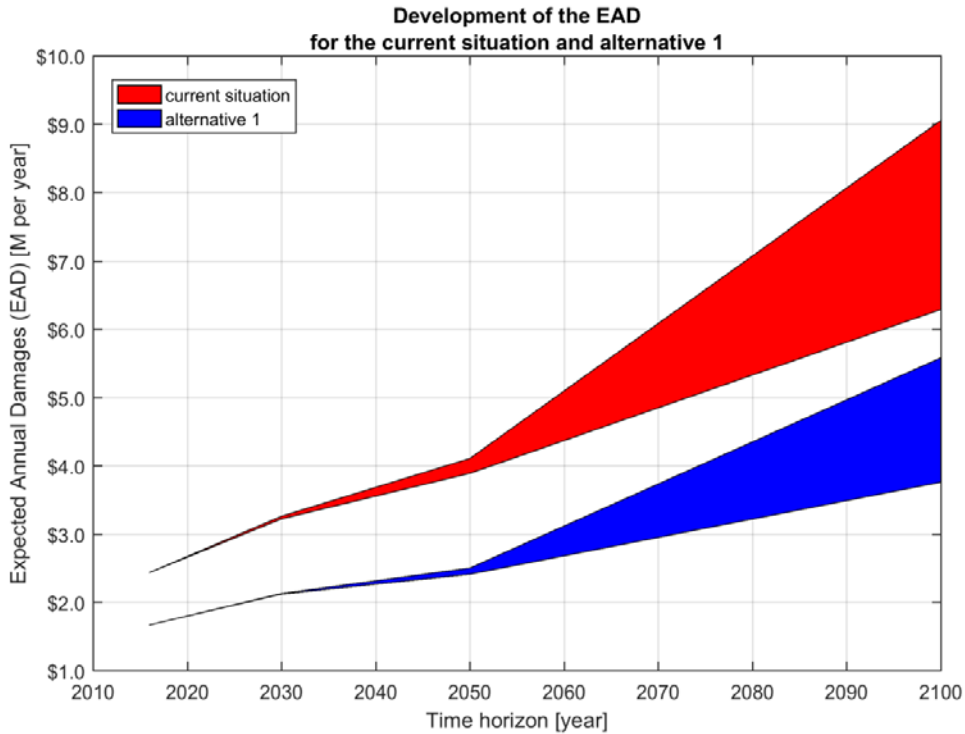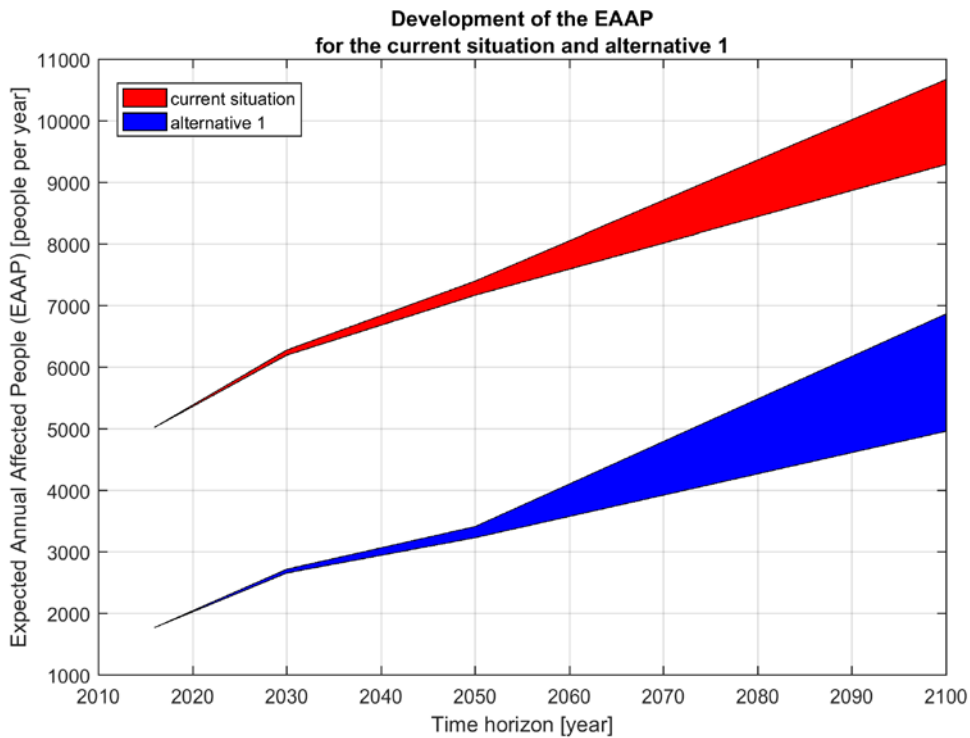

Figure 9.17 Development of the EAAP as function of the time horizon for the current situation and alternative 1. The width of the band represent the variability between the two sea level rise scenarios (RCP 4.5 and RCP 8.5).

9.6 Conclusions

In this chapter, different solutions have been identified, aiming at reducing the risks, at locations where those risks are the largest. In particular, two preferred conceptual designs have been presented, including a breakdown of costs per linear meter: one standard revetment and one berm-type revetment. The effectiveness of these interventions in reducing the hazards (i.e. inundation) is tested by means of numerical modelling simulations.

The cost-effectiveness of revetments at different locations and with different lengths have been assessed. Cost-effectiveness is defined as the ratio between construction costs and reduction in Expected Annual Damage (i.e. risk or EAD).

All the proposed intervention schemes aim at reducing the effects of hazards from the ocean side, which will lead to the highest risk reduction compared to hazards from the lagoon.

Constructing a revetment at the hotspot location is proven to be the most cost-effective solution. This is a result of decrease in damages to inundation and land loss due to erosion at locations where risks are the highest. Protecting the causeway is the least cost-effective due to the high construction costs compared to the decrease in risk, but could provide interesting options for long-term planning of the island (Section 10.2).

When budget constraints are not the limiting factor or in case costs for linear meter of revetment are lower, it is our advice to protect the entire ocean side of the island. This will avoid possible side effects induced by the revetment (e.g. local erosion).

Deltares

10 Discussion

10.1 Introduction
In this chapter, a number of discussion points have been analysed in more details. In particular:

- Alternative solutions for a long-term planning of the island of Ebeye (Section 10.2).
- Flexibility of the risk analysis framework to different conditions (Section 10.3).
- Factors of uncertainties and consequences on the final design (Section 10.4).

10.2 Long-term adaptive planning for Ebeye
In Section 9.2, a number of solutions have been proposed to mitigate the problems of flooding and the coastal erosion at Ebeye. These solutions have mainly considered options aiming at reducing risks at locations where those risks were higher (Section 8.5). Different alternatives have been tested, with an overall cost-estimate for each alternative as shown in Table 9.12. As discussed, these alternatives mainly aim at reducing the direct effects of coastal hazards from the ocean side. No solution is presented to mitigate the hazards from the lagoon side, as those hazards and risks score lower in the overall assessment.

However, risk is by definition the production of hazard, exposure and vulnerability (Section 2.1). Other options are generally available to reduce the risks, not by reducing the hazard component, but by lowering the exposure or vulnerability at the island. Some of these options are discussed in this section.

Also, as discussed in Section 9.2, the proposed designs will lead to a clear reduction of the flooding levels, as compared to the present situation. However, they will not completely protect the island from flooding for the most extreme events, already in the current situation (i.e. without considering the effect of sea level rise). On top of that, wave overtopping rates are likely to increase in the future as water level will increase due to sea level rise. As a consequence, higher waves will also approach the coast due to the larger water depth on the reef. As an example, a sea level rise of 12 cm by 2030, as shown in Table 6.8, may lead to an increase in overtopping rates of about 60-80%. These overtopping rates may increase up to about 300% in 2050, when considering a sea level rise of 25 cm.

Therefore, the solutions which have been presented in this study have to be seen as short- and medium-term solutions, rather than permanent solutions. In order to consider the possible effect of sea level rise, the conceptual designs proposed, have already included options that may be easily adaptable to higher sea level rise scenarios (e.g. berm solution in combination with revetment). Nevertheless, although practically possible from an engineering point of view, there will be a limit up to which the increase in height of the revetment will no longer be possible.

In this section, additional solutions are presented, which could be used in combination with the solutions presented in this study.

Additional short- and medium-term solutions (up to 30 years)
- Reduction of vulnerability for some of the properties on the island. This could be done for example by constructing some of the houses on poles (Figure 10.1). This is

especially important for houses located on the lagoon side, which are located ≈1.5 m above mean sea level.

Figure 10.1 Elevated houses in Majuro to prevent damage from waves and flooding (Hess et al., 2015).

- Protection of the causeway from both sides (ocean and lagoon), from Ebeye until Gugeegue. Although this option may not appear as the most cost-efficient in the short-term, it may offer very important opportunities as long-term solution (i.e. relocation towards Gugeegue, see next paragraph).
- Improvement of the present early warning system on the island, and in close cooperation with trained safeguards to deal with emergency situations (e.g. typhoons, extreme storms, tsunamis, etc.).
- The improvement of the drainage system is also advised. This will not only help draining the water during coastal flooding from waves and storm surges, but also from rainfall events. Flooding due to rainfall events happen on a regular base on the island (Figure 10.2).

Figure 10.2 Flooding on the road during a rainfall event.

Additional long-term solutions (30+ years)

- Relocation of part of the population from Ebeye towards Gugeegue (and islands in between). This should be part of a long-term adaptive plan of the island. The highest part of these islands should be chosen for resettlement. The topography of these islands is not available at present. However, Gugeegue has a surface comparable to Ebeye, therefore could offer potentially a very good alternative for relocation.
  The planning should include detailed calculations (supported by numerical modelling) of the risks levels at different part of the islands for different time horizons. If model simulations will show that the height of the island will not be sufficient to cope with future predicted coastal hazards, the best approach will be probably to increase artificially the height of these islands with material extracted from the lagoon, in combination with material extracted from other non-inhabited islands in the neighbourhood. Coastal protection works will also be required to protect the islands.
- The relocation of some of the population from Ebeye towards Gugeegue will also offer the opportunity to free some of the space (at higher risk) in Ebeye. The risks in these areas could then be lowered, for example, by raising the topography of the lower parts of the islands, with material extracted from the lagoon and/or in combination with material extracted from other non-inhabited outer islands. Alternatively, risks could be lowered by using alternative construction techniques for the houses located in these areas.
- Land reclamation may also be a possibility which should be explored, in order to gain additional space for the people living on the island. This is an option which is currently being considered for other islands in the Pacific (e.g Kiribati). The area north of Ebeye and west of the causeway, may be a good candidate to explore this option, given the very shallow bathymetry. However, further study would be required in order to further explore this option.

10.3 Flexibility of the methodology for risk analysis to different conditions

In this report, a generic methodology for risk analysis has been presented. The methodology, in general, is flexible and it allows for the use of input data from different sources: e.g. numerical modelling, measurements and/or other type of data or assumptions. In this study, for example, since no hydro-metrological data was recorded at Ebeye, data were derived mainly from numerical modelling calculations (see Chapter 7). Also, a number of assumptions had to be made in order to derive direct and indirect damages, since damage information after extreme events at Ebeye was extremely poor.

When new information will become available (e.g. better data to improve model calibration, detailed damage reports to improve depth-damage functions, etc.) the methodology will easily allow including this new information.

Another important point is that the risk calculation presented in the study has been derived assuming the current levels of exposure and vulnerability. In reality, in the future, not only the hazard will change (i.e. due to climate change and sea level rise) but also the levels of exposure (i.e. due to increase in population, new developments, etc.) and vulnerability (i.e. due to new building techniques). All these scenarios could be in principle included as part of the risk assessment, if scientifically information is available.

In the same way, the framework could also be applied to other islands. For example, the hazard assessment has been derived for the two islands of Majuro and Ebeye but, eventually,

the full risk assessment has only been carried out for Ebeye, where coastal protection works may be implemented in the near future. Nevertheless, the same procedure could also be applied to Majuro or other outer islands where protection works may also be expected. It is however important to mention that the accuracy of the results will be strictly dependent on the available data (see also Section 10.4 and 11.3).

10.4 Factors of uncertainties and consequences on the final design

A very important discussion point relates to the accuracy of the results in relation to the available data and the possible effects on the final designs and conclusions (see also Section 11.3).

For the present study, the main factors of uncertainties relate to the lack of:

- Detailed topographic map of the island
- Bathymetry data around the island
- Bed roughness information on the reef
- Wave data at the island (both from the ocean and the lagoon side)
- Water level data (both from the ocean and the lagoon side)
- Detailed damage reports from previous events
- Detailed flooding maps from previous events
- Depth-damage curves for the island

At the start of this study, none of the above mentioned datasets was available. By using global datasets, state-of-the-art numerical modelling techniques and data collected during the field visit, a basic dataset was constructed and which was used as a basis for the risk assessment analysis and the conceptual design of solutions. All the data used were first validated by comparing with data available at other neighbouring islands, where however conditions may be different from Ebeye.

Data availability, in relation to the purpose of the study, is a very important factor to consider during the interpretation of the results presented in this study. The usefulness of the study lies on the fact that it provides, in a relative sense, the locations where risks are higher, information which can be used for prioritizing possible interventions. Also, the scenarios developed for different time horizons can help estimating how these risks may change in the future due to climate change and sea level rise. Finally, the scenarios comparing the situation with and without interventions help quantifying the possible effect of different interventions in terms of risk reduction.

Nevertheless, the accuracy of the results (in an absolute sense) is clearly linked to the lack of the above mentioned data. For example, in Section 10.2 it is mentioned how an increase in sea level rise may affect that the overtopping rates (i.e. 25 cm of sea level rise may lead to an increase in overtopping rates of about 300%). In the same way, if predicted water levels are 25 cm higher than in reality, the predicted overtopping rates would be overestimated of 300%.

To deal with these uncertainties and due to the lack of data for model validation, in the present study, conservative choices have generally been made (e.g. use of a 20 s wave period for all swell conditions). These choices will also lead to design criteria which may be quite conservative. If the above mentioned datasets will become available, the conceptual designs presented in this study can be optimized.

11 Conclusions and recommendations for further work

11.1 Summary

In this study, a quantification of the coastal hazards for the islands of Ebeye and Majuro and a full coastal risk assessment for the island of Ebeye has been carried out. Among the coastal hazards, the following contributions have been quantified: swell-wave conditions from the ocean, typhoons, wind-waves from the lagoon, water levels (including the effects of tides, wind stress effect, inverse barometric effect and El Niño–Southern Oscillation (ENSO) effects), typhoons, tsunamis, climate change effects and sea level rise. (Chapter 5 and 6).

To translate offshore coastal hazards to impacts (i.e. inundation extent and coastal erosion) on the island, numerical modelling techniques have been used (i.e. the open-source XBeach model) in combination with simple formula's freely available via the SimpleCoast toolkit (www.simplecoast.com) (Chapter 7).

A coastal risk index has been designed, accounting for the contribution of coastal hazards, exposure and vulnerability affecting the different properties on the island. Also, indirect damages (i.e. socio-economic damages) have been included in the index based on assumptions and expert advice. This index was used as a basis for the coastal risk assessment. The index is flexible and can, in principle, be adapted in the future to include possible newly available/improved data which may become available.

The coastal risk assessment has been used to assess the difference in risks at different locations on the island, for different return periods and time horizons, also accounting for the effects of sea level rise and climate change. Also, the same procedure has been used as a basis for selections of priority areas of interventions, at location identified as high risk areas (Chapter 8).

Conceptual design of adaptation options were proposed, together with a cost-estimate of possible interventions, for the locations at higher risks. The effectiveness of the different solutions was estimated based on the same risk analysis methodology (Chapter 9).

11.2 Main conclusions

The main conclusions from this study have been summarized below under different categories:

Data collection and coastal hazards

▪ The data collected during the field visit at Ebeye was used for describing and understanding the main features and processing at the island i.e. reef geometry, bathymetry and topography. The island is low-lying, approximately between 0 and 3 m above mean sea level, and protected by a reef flat with a width of about 100 – 130 m. In general, the island topography at the ocean side is characterized by a higher elevation than the lagoon side (Section 5.2.2). This observation is consistent with topographic data from literature at most of similar atoll islands. The data have been used as input for the numerical modelling calculations, in combinations with data measured at other neighbouring islands and derived from global data-sets.

- The coastal hazard assessment based on numerical modelling has helped quantifying and prioritizing the different hazards on the island. Major hazards on the island are generated from the ocean; in particular: typhoons and swell waves. However, although of minor intensity, hazards from the lagoon can also lead to flooding due to the lower topography of the island on the lagoon side.

- Typhoons striking the Marshall islands are not yet fully developed. In particular, of all typhoon tracks analysed over the Marshall islands, only 30 tracks had a wind speed larger than 18 m/s (tropical storm or higher) (Section 6.4). Standard formulations from literature describing the shape of fully-developed cyclones have been adapted for this specific situation (Appendix A).

- According to literature, only minor impacts resulted from previous tsunami's events. The impact of the most recent and largest tsunami has been simulated as part of this study (Tohoku Earthquake of March 11, 2011; Section 6.5) and which resulted in minor flooding over the island.

Impacts of hazards on the island

- The maximum inundation areas and depths over the island are mainly determined by swell events, when considering events with return periods lower than 30 years, and by typhoon events when considering events with the largest return periods (Table 7.1 and Table 7.5). The maximum percentage of area inundated (with inundation depth larger than 20 cm; Table 7.7) increases from about 20%, for events with a return period of 5 years, to 90% for events with a return period of 50 years. This means that, during extreme events nearly the entire island is flooded already in the present situation.

- Areas and depths of inundation are likely to increase dramatically by the end of the century, for all sea level rise scenarios (Table 7.7). The highest relative increase will be especially noticeable for flooding events with the lower return periods, i.e. the island will experience recurrent flooding at short time intervals. The predicted increase in percentage of inundated area (with inundation depth larger than 20 cm) will be of a factor 3 – 4 for events with a return period of 5 years, depending on the sea level rise considered.

- Coastal erosion was estimated with simple empirical relationships. Land loss due to sea level rise will be the main source of erosion. The shoreline retreat may exceed the 2 meters by 2100, for the highest sea level rise scenario's and assuming that sufficient accommodation space is available.

Risk analysis and selection of priority areas for intervention

- A methodology for risk analysis, accounting for the contribution from the different hazards, vulnerability and exposure components has been implemented. The methodology is flexible so that assumptions and data can be updated when new data become available.

- Direct and indirect damages due to flooding and coastal erosion have been estimated. The main source of direct damages are damages to the houses and to the

causeway (Figure 8.3). The computed damages were verified versus real damages on the island after one specific extreme event.

- Estimated total damages may increase of about a factor 3 to 4 by the end of the century due to sea level rise, and depending on the sea level rise scenario considered (Section 8.3 and 8.4). More specifically, expected annual damages (EAD) may increase from about 2.5 million $ per year to over 9 million $ per year.

- The expected annual affected people (EAAP), defined as the number of people yearly affected by a flooding event with a water depth of at least 20 cm of water, may double by the year 2100.

- Hot-spots locations on the island at higher risks have been identified for the different time horizons. In particular, the risks in the present situation will be used as a basis to decide where interventions are required. Two hot-spots can be visible in the present situation, both located at the ocean side: one in the north and one in the central part of the island (Figure 8.8). These two locations stand out as locations at higher risks due to a combination of: high exposure and low topographic elevation.

Conceptual designs of adaptation options and cost-estimates

- Different types of interventions in order to reduce present and future risks on the island have been compared. Conceptual designs and cost-estimates have been provided for the best solutions (Section 9.2.4). Among all, the solution which is recommended as most suitable for the case of Ebeye is the revetment fronted by a berm (Figure 9.10) as it can more easily adapt in case of sea level rise. The recommended construction scheme, in order to reduce cost, is based on the use on the use of single-layer cubes, instead of rocks.

- Protect the island from flooding from the most extreme events and using standard overtopping normative would imply the construction of massive revetments with an height exceeding the 5 m above MSL (more than 2 m above the level of the island). In this study, designs have been proposed aiming at protecting the island from overtopping, considering yearly flooding conditions. On the other hand, the 1:50 year condition has been used as criteria for hydraulic stability. The proposed crest height of the revetment ranges between + 4m above MSL (in case of a revetment with berm) and +4.3 m above MSL (in case of simple revetment). The geometry of the proposed solutions should be verified and optimized after:

  a) The setting-up a long term continuous measurement campaign of the major forcing conditions, which will reduce uncertainties on the hazard component (i.e. waves and water levels).
  b) Detailed measurements of the topography of the island and bathymetry around the island (Section 11.3).
  c) After verifying the structure by means of physical modelling.

- Ranges of costs per linear meter for the construction of suitable revetment designs have been provided. These costs range between 16,000 up to 25,000 USD per linear meter, according to the material used for construction (respectively single-layer cubes or rocks). These values provide a first order indications and they assume the use of imported aggregates for constructions. Costs may vary largely depending on the

material and methods used for construction. Also, costs will depend on the final design of the structure.

▪ The final price per linear meter and the available budget will determine the length and location of the structure which can be built. Four options have been evaluated in the study, depending on the available budget (Figure 9.12):

    e) Revetment protecting the complete coastline at the ocean side
    f) Revetment protecting only the two hot-spots
    g) Revetment protecting the central part of the island
    h) Revetment protecting the causeway

The effectiveness of the four different options in terms of reduction in expected annual damages (EAD) has been tested by means of the same risk analysis procedure used to determine the hot-spot locations in the reference situation.

▪ The most effective solutions are the ones meant to protect directly the areas in front of the hot-spots. However, from an engineering point of view, it will be easier to construct a continuous revetment, including the hot-spots. Protecting the causeway score lower in terms of effectiveness buy it may provide interesting opportunities for long-term development of the island, including possible relocation of part of the population of Ebeye towards the island of Gugeegue (Table 9.12).

▪ The solution for coastal protection recommended in the study (i.e. revetment at the ocean side of the island) is however just one of the option for reducing risks. Other possible options are related to the reduction of the exposure and vulnerability components. The analysis and proposed methodology could be used as a basis for a long-term adaptive planning of the island (Section 10.2).

11.3 Recommendations for future work

A number of recommendations for future work are given below:

▪ <u>Data collection</u>:
Data availability at Ebeye is very scarce even after the data sourcing and collection performed in this study. In particular, none of the following data type was available at the start of the study: bathymetry data, topographic data, time series of wave data and water level data, flooding maps. All this information is crucial for proper calibration and validation of the numerical model used to estimate the impacts of the hazards on the islands and therefore to design proper solutions. Also, no damage report was available describing damages after the most extreme events, and which could be used for verification of the risk assessment calculations and to evaluate the efficiency of the different interventions. A basic dataset was collected during the first field mission and complemented with information from neighbouring measurements stations and global datasets, in order to achieve the primary objective of the present study (first risk assessment and conceptual design of adaptation options). However, it is very important that, at least, the following datasets will be collected, before proceeding to the detailed design of any solution:

- Detailed topography of the island.
- Detailed bathymetry around the island.

- Wave data time series (measurements to be collected for at least for one year).
- Water level data on the reef (measurements to be collected for at least for one year).
- Shoreline data (at least twice a year).
- Flooding maps after the most extreme events, mapping the areas which have been affected by flood.
- Damage reports after the most extreme events, indicating type of damages and costs resulting from the event.

- **Physical modelling:**
  In order to optimize the design of the proposed solutions, physical modelling is recommended. This is also important, as most of the formulation available in literature for the design of coastal structures have not been tested for these very specific physical conditions (i.e. coral reefs).

- **Availability of aggregates:**
  One of the biggest challenges, in the present situation, relates to the lack of available material for the implementation of suitable solutions.
  It is therefore recommended to explore the following possibilities:
  - Detailed survey of possible available sources of aggregates from the lagoon (i.e. mainly sand).
  - Opportunities to extract material (i.e. rocks) from inhabited outer islands.

Full cost-benefit analysis
  Once the design of the structure and construction materials have been finally defined, a revised cost-estimate is recommended and which should be the basis of a full cost-estimate analysis.

- **Other alternatives for risk reduction**
  The present study mainly focused on identifying the most effective solutions to reduce the overall risks, by reducing coastal hazards (i.e. by using the construction of a revetment on the lagoon side). However, other options should also be explored parallel to this alternative, and aiming at reducing: the vulnerability of some of the constructions (e.g. by using elevated houses on poles) or the exposure (e.g. by relocating people from the areas where risks are higher). Finally, all these options should be complemented by the use of early warning systems to alert people before the arrival of extreme events (e.g. swell waves, typhoons, tsunami's) which can be forecasted. Also, use of trained personnel and safeguards is advised to be able to deal with disaster and post-disaster situations.

- **Adaptive planning of the island:**
  The methodology and results provided in the report could be used as a basis for the design of a long-term adaptive planning of the island, possibly extended to other outer islands. This long-term planning should include different options for coastal adaptations (i.e. for different time horizons), as well as the future uncertainties e.g. related to future climate change scenarios, economic and demographic development of these islands, etc.

12 References

Allsop, A., Bruce, T., Pullen, T., Van der Meer, J. (2008). Direct hazards from wave overtopping - the forgotten aspect of coastal flood risk assessment?. Link: http://www.vandermeerconsulting.nl/downloads/risk_assessment/2008_allsop_bruce.pdf

Beca International Consultants Ltd, 2003. Ebeye Causeway Upgrade. Prepared for Republic of The Marshall Islands.

Brown, B.E. and Dunne, R.P., 1988. The impact of coral mining on coral reefs in the Maldives. Environmental Conservation, 15(2),159–165

Bruun, P., 1962. Sea level rise as a cause of shore erosion. Journal of Waterways and Harbour Divisions, ASCE 88, 117-130.

Budiyono, Y., Aerts, J., Brinkman, J., Marfai, M. A., & Ward, P. (2015). Flood risk assessment for delta mega-cities: a case study of Jakarta. Natural Hazards, 389–413. http://doi.org/10.1007/s11069-014-1327-9

Cooper, J. A. G., & Pilkey, O. H. (2004). Sea-level rise and shoreline retreat : time to abandon the Bruun Rule. Global and Planetary Change, 43, 157–171. http://doi.org/10.1016/j.gloplacha.2004.07.001

Cheriton, O. M., C. D. Storlazzi, and K. J. Rosenberger. (2016). Observations of wave transformation over a fringing coral reef and the importance of lowfrequency waves and offshore water levels to runup, overwash, and coastal flooding. Journal of Geophysical Research: Oceans, 121. http://doi.org/10.1002/2015JC011231

CSIRO, 2014. Climate variability, extremes and change in the Western Tropical Pacific: New Science and Updated Country Reports 2014. http://www.pacificclimatechangescience.org/publications/reports/climate-variability-extremes-and-change-in-the-western-tropical-pacific-2014/

Dee, D. P. and co-authors, 2011. The ERA-Interim reanalysis: configuration and performance of the data assimilation system, Q. J. R. Meteorol. Soc., 137 (656), 553-597, doi:10.1002/gj.828.

Delft Hydraulics (current Deltares), 2007. Physical model tests for Dubai Waterfront offshore islands 4 & 5. Report H4893.

Deltares, 2014. WES, Wind Enhance Scheme for cyclone modelling. User Manual. https://oss.deltares.nl/documents/183920/185723/Delft3D-WES_User_Manual.pdf

Egbert, G.D., and S.Y. Erofeeva. 2002. Effi cient inverse modeling of barotropic ocean tides. Journal of Atmospheric and Oceanic Technology 19:183-204.

Engineering, O. (2016). Modeling of tropical cyclone winds and waves for emergency management Modeling of tropical cyclone winds and waves for emergency management, (August). http://doi.org/10.1016/S0029-8018(02)00033-1

EurOtop, European Overtopping Manual - Wave overtopping of sea defences and related structures: Assessment manual (2007). Auteurs: Pullen, T. Allsop, N.W.H. Bruce, T. Kortenhaus, A. Schüttrumpf, H. Van der Meer, J.W.

Ferreira, O, 2016, C. Viavattene, J.A, Jiménez, CRAF Phase 1, a framework to identify coastal hotspots to storm impacts, Proceedings of the FloodRisk 2016 conference, Lyon, France.

Ford, M.R.; Becker, J.M., and Merrifield, M.A., 2013. Reef Flat wave processes and excavation pits: observations and implications for Majuro Atoll, Marshall Islands. Journal of Coastal Research, 29(3), 545–554. Coconut Creek (Florida), ISSN 0749-0208.

Fujita, T. (1952). Pressure Distribution Within Typhoon. Geophysical Magazine, 23, 437–451.

Gawehn, M., van Dongeren, A., van Rooijen, A., Storlazzi, C., Cheriton, O. M. and Reniers, A. (2016), Identification and classification of very-low frequency waves on a coral reef flat. J. Geophys. Res. Oceans. Accepted Author Manuscript. doi:10.1002/2016JC011834.

Geeraerts, J., P. Troch, J.De Rouck, H. Verhaeghe, J.J. Bouma. (2007) *Wave overtopping at coastal structures: prediction tools and related hazard analysis.* Elsevier, Journal of Cleaner Production, page 1514-1521.

Hein, J.R., Florence, L.W., Dan, L. M., 2007. Bathymetry of the Republic of the Marshall Islands and Vicinity. U.S. Geological Survey. http://pubs.usgs.gov/mf/1999/2324/.

Hemer, Mark A., Yalin Fan, Nobuhito Mori, Alvaro Semedo and Xiaolan L. Wang, (2013), Projected changes in wave climate from a multi-model ensemble. Nature Climate Change 3, 471–476, doi:10.1038/nclimate1791.

Hess, D., Hwang, D., Fellenius, K., Robertson, I., Stege, M., and Chutaro, B., 2015. Republic of the Marshall Islands Homeowner's Handbook to prepare for Natural Hazards. Published by University of Hawaii Sea Grant Program, June 2015, 81 p.

Holland, G. . (2008). A Revised Hurricane Pressure – Wind Model. Monthly Wearther Review, (2), 3432–3445. http://doi.org/10.1175/2008MWR2395.1

Holland, G., Belanger, J., & Fritz, A. (2010). A Revised Model for Radial Profiles of Hurricane Winds. American Meteorological Society, 4393–4401. http://doi.org/10.1175/2010MWR3317.1

Huang, Y., Weisberg, R. H., Zheng, L., & Zijlema, M. (2013). Gulf of Mexico hurricane wave simulations using SWAN : Bulk formula-based drag coefficient sensitivity for Hurricane Ike, 118(June), 1–23. http://doi.org/10.1002/jgrc.20283

IPCC, 2014. Fifth assessment Report of the Intergovernmental Panel on Climate Change (AR5). http://www.ipcc.ch/report/ar5/

Kron, W. (2005). Flood Risk = Hazard • Values • Vulnerability. Water International, 30(1), 58–68. http://doi.org/10.1080/02508060508691837

Lesser, G.R., Roelvink, J.A., van Kester, J.A.T.M., and Stelling, G.S., 2004. Development and validation of a three dimensional morphological model. Journal of Coastal Engineering 51: 883-915.

Liu, W. ., Katsaros, K. B., & Businger, J. A. (1979). Bulk parameterisation of air-sea exchanges of heat and water vapor including the molecular constraints at the interface. Journal of the Atmospheric Sciences, 36, 1722. Retrieved from http://journals.ametsoc.org/doi/pdf/10.1175/1520-0469(1979)036<1722:BPOASE>2.0.CO;2

Mori, N., T. Yasuda, H. Mase, T. Tom, and Y. Oku. (2010). Projection of extreme wave climate change under global warming. Hydrological Research Letters, 4, 15–19. http://doi.org/10.3178/hrl.4.15

NOAA. (1992). The 1992 Central Pacific Tropical Cyclone Season. Retrieved September 16, 1BC, from http://www.prh.noaa.gov/cphc/summaries/1992.php

Owen, S.D., Kench, P.S., Ford, M., 2016. Improving understanding of the spatial dimensions of biophysical change in atoll island countries and implications for island communities: A Marshall Islands' case study. Journal of Applied Geography. 72, 55-64.

Paulik, R. Smart, G., Turner, R., Bind, J. (2015). Development of Preliminary Depth-Damage Functions for Samoa Buildings. National Institute of Water and Atmospheric Research.

PCRAFI, 2015. Advancing Disaster Risk Financing & Insurance in the Pacific. https://www.gfdrr.org/sites/default/files/publication/2015.06.25_PCRAFI_Combined-%5BCompressed%5D-rev-0.9.pdf

Pistrika, A., Tsakiris, G., & Nalbantis, I. (2014). Flood Depth-Damage Functions for Built Environment, 553–572. http://doi.org/10.1007/s40710-014-0038-2

Pomeroy, A., R. J. Lowe, G. Symonds, A. R. Van Dongeren, and C. Moore (2012), The dynamics of infragravity wave transformation over a fringing reef, J. Geophys. Res., 117, C11022, doi:10.1029/2012JC008310.

Quataert, E., C. Storlazzi, A. van Rooijen, O. Cheriton, and A. van Dongeren (2015), The influence of coral reefs and climate change on wave-driven inundation of tropical coastlines, Geophys. Res. Lett., 42,6407–6415, doi:10.1002/2015GL064861.

Robertson, N., Hwang, D., 2015. Structural Survey of Shelters for Hurricane and Tsunami Evacuation – Majuro Atoll, Republic of the Marshall Islands. Conference Paper.

Roelvink, D., Reniers, A., Van Dongeren, A., Van Thiel de Vries, J., McCall, R., and Lescinksi, J., 2009. Modelling storm impacts on beaches, dunes and barrier islands. Journal of Coastal Engineering, 56, 1133-1152.

Ranasinghe, R., Callaghan, D., & Stive, M. J. F. (2012). Estimating coastal recession due to sea level rise : beyond the Bruun rule. Climatic Change, 561–574. doi.org/10.1007/s10584-011-0107-8

Ris, R.C, L.H. Holthuijsen and N. Booij, 1994, A spectral model for waves in the nearshore zone, 24th Int. Conf. Coastal Engineering, Kobe, Oct. 1994, pp. 68-78

Schwerdt, R. W., Ho, F. P., & Watkins, R. R. (1979). Meteorological criteria for standard project hurricane and probable maximum hurricane wind fields. Gulf and East Coasts of the United States. NOAA Tech. Rep. NWS 23, 317.

Sea Grant – University of Hawaii, 2013. A Rapid Assessment of Kili Island, Republic of The Marshal Islands, Following January 2011 Coastal Inundation: Implications for Future Vulnerability. Report.

Stelling, G. S., 1999. Internal note on Cyclone modelling. Tech. rep., WL | Delft Hydraulics, Delft, The Netherlands

Storlazzi, C. D., J. B. Shope, L. H. Erikson, C. A. Hegermiller, and P. L. Barnard. (2015). Future Wave and Wind Projections for United States and United States-Affiliated Pacific Islands. http://doi.org/http://dx.doi.org/10.3133/ofr20151001.

Symonds, G., Huntley, D.A., and Bowen, A., 1982. Two-Dimensional Surf Beat: Long Wave Generation by a Time-Varying Breakpoint. Journal of Geophysical Research, Vol. 87, No. C1, 492-498.

Thomas and Hall (1992). *Seawall Design.* CIRIA 1992. ISBN 0 7506 1053 0.

Tonkin+Taylor (2016). Affordable Coastal Protection. Desktop Review Report 121534-S86525.

USGS, 2015. Future Wave and Wind Projections for United States and Unites States-Affiliated Pacific Islands. By Curt D. Storlazzi, James, B. Shope, Li H. Erikson, Christie A. Hegermiller, and Patrick L. Barnard. Open File Report 2015-1001. http://pubs.usgs.gov/of/2015/1001/downloads/ofr2015-1001_report.pdf.

Van Dongeren, A. R., R. J. Lowe, A. Pomeroy, D. M. Trang, J. A. Roelvink, G. Symonds, and R. Ranasinghe (2013), Numerical modeling of low-frequency wave dynamics over a fringing coral reef, Coastal Eng., 73,178–190, doi:10.1016/j.coastaleng.2012.11.004.

Vickery, P. J., & Wadhera, D. (2008). Winds of Hurricanes from Flight-Level Pressure and H * Wind Data. Journal of Applied Meteorology and Climatology. http://doi.org/10.1175/2008JAMC1837.1

Willoughby, H. E., Darling, R. W. R., & Rahn, M. E. (2006). Parametric Representation of the Primary Hurricane Vortex . Part II : A New Family of Sectionally Continuous Profiles. Monthly Weather Review, 134, 1102–1120.

Wright, T. (2004). Tropical storm talas formation and impacts at Kwajalein atoll, 1–10.

Yao, Y., Becker, J.M., Ford, M.R., Merrifield, M.A., 2016. Modeling wave-processes over fringing reefs with an excavation pit. Journal of Coastal Engineering. 109, 9-19.

A Typhoons

A.1 Relationships for the generation of parametric hurricane surface fields

Hurricanes are among nature's most powerful and destructive phenomena. Numerical simulations can be used to identify the coastal hazards (i.e. wave height and surge levels) resulting from the high wind speeds and large pressure drops of these tropical storms. These simulations require input of a surface wind field and a pressure field (two-dimensional information). However, often only information about the track and a maximum sustained wind speeds (v_{max}) are available. Therefore, parametric relationships are used to estimate the wind and pressure fields. These relationships require as input parameters such as atmospheric pressure drop (Δp_c), the radius of maximum wind (*RMW*) and shape parameters.

This chapter describes how we have optimized and derived new relationships between maximum sustained winds, pressure, radius of maximum winds and wind profile specifically for the Marshall Islands based on data from the Joint Typhoon Warning Center (JTWC; https://metoc.ndbc.noaa.gov/en). This is needed in order to increase the accuracy of the surface wind fields which will be used to model the effect of hurricanes on wave heights and storm surge levels for The Marshall Islands case.

In particular, the following improvements have been made:
*   Improvement of the relationship between maximum wind speed and pressure drop. For the RMI this results in a largers pressure drop with a similar wind speed.
*   Improvement of the relationship between pressure drop and radius of maximum wind. For the RMI this results in wider (larger RMW) hurricanes for a given pressure drop.
*   New relationship for the maximum sustained wind speed and radius of 35 knots wind speed in order to fit the exponential decay of wind speeds in Holland (2010) and therefore more accurately reproduce the external wind structure.

A.1.1 Vmax – Δpc relation

A wide variety of relationships is available in literature to relate the minimum central pressure in the hurricane core and maximum surface winds just outside the core. These relationships provide a critical analysis tool for the assessment of maximum winds from a diverse set, since often only information about the maximum sustained wind speed and/or pressure is available.

Almost all pressure–wind models are of a (quadratic) form (Holland 2008), see Equation (1), in which *a*, *b* and *x* are fitting coefficients. Δp_c is the pressure drop defined from an external pressure (p_n) to the minimal pressure (p_c): $\Delta p_c = p_n - p_c$. Furthermore, the maximum sustained wind is defined with v_{max}.

$$v_{max} = a\Delta p_c{}^x$$
$$v_{max} = a\Delta p_c + b\Delta p_c{}^2$$

(1)

However, for the Marshall Island case, it was found that these relationships would overestimate the maximum wind speed for a certain pressure drop. This is because the existing formula of Holland (2008) has been derived for fully developed hurricanes, while around RMI typhoons are generally not yet fully developed (i.e. lower hurricane categories), see Chapter 5.2.5. For hurricanes active around the Marshall Islands the second quadratic

form has been fitted, based on data from the JTWC, resulting in new, slightly lower, fitting coefficients than used by Holland (2008). The fitting of the data points of the maximum sustained wind speed and the pressure drop is based on least square fit and presented in Figure A.1. The newly derived coefficients will result in a larger pressure drop for a given wind speed or lower wind speeds for a given pressure drop. Limited additional skill was found by including additional hurricane parameters such as intensity change, latitude, and translational speed. Therefore, the most simple equation for the pressure-wind relationship has been applied, improved based on the newly derived parameters.
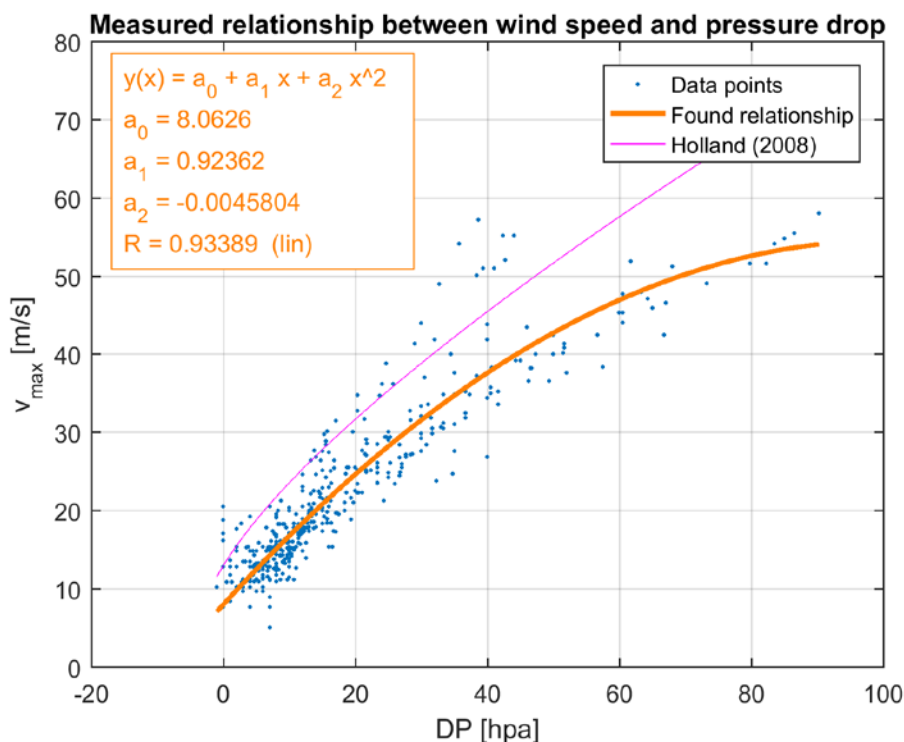

Figure A.1 Relationship between wind speed and pressure drop. Data points from the JTWC for maximum wind speed and pressure drop are shown by the blue dots, relationship between p_c and v_{max} based on Hollland (2008) is shown in pink, while the newly developed relationship based on least square fit on measurements points is shown in orange.

A.1.2   Radius of maximum wind (RMW)
The radius of maximum winds plays an important role in hurricane risk prediction since it determines part of the shape of the hurricane. However, empirical relationships to relate hurricane intensity with the radius of maximum winds are very scarce. Often the radius of maximum winds is related to the pressure drop and latitude.

Based on the exponential shape of Vickery and Waldhera (2008) and the data from the JTWC for the Pacific, a new equation has been derived to compute *RMW* (radius of maximum winds) as a function of Δp_c (pressure drop) and γ the latitude in degrees (Equation 2). The fitting of the data points of the pressure drop and radius of maximum winds is based on least square fit and presented in Figure A.2. Since the interest is reproducing tropical storms and hurricanes, a few data points with extremely large radii of maximum winds have been deleted. Very large radii of maximum winds are characteristic of (tropical) depressions and not of rapidly varying tropical storms. An arbitrary cut-off value of RMW > 250 km is used to fiter out these values. The relationship has a R^2 (statistical parameter that define how close the data are to the fitted regression line) of 0.86 and a RMSE (root-mean-square error) of 11.8

kilometres when compared with measured data. The newly derived relationship mainly results in wider (larger RMW) hurricanes during small pressure drops. The found relationship suggests a weaker correlation between the radius of maximum wind and latitude than Vickery and Waldhera (2008) and has a higher predictive skill for smaller hurricanes. For larger hurricanes (pressure drop > 40 mbar) the skill is similar.

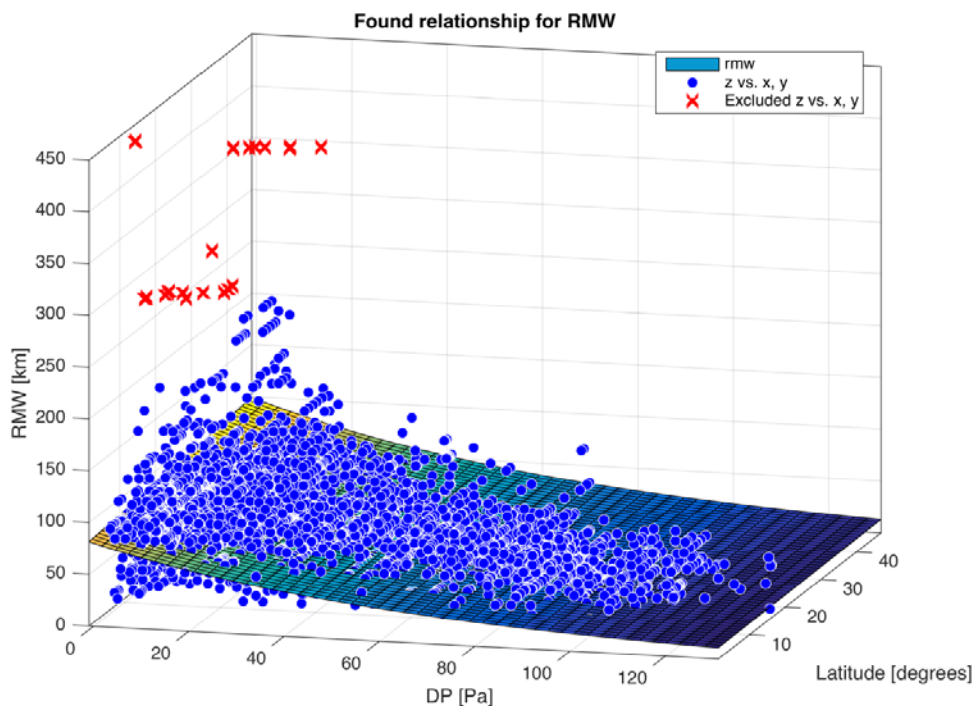$$\ln(RMW) = 4.446 - 0.01677 \cdot \Delta p_c + 0.00131\gamma \qquad (2)$$

Figure A.2 Modelled and observed Radius of Maximum Wind (RMW) versus pressure drop (DP) and latitude for all cyclones in the JTWC database. Each blue point is an observation point. The coloured surface represents the fitting relationship based on the least square fit. Extremely large RMW have been excluded from the analysis (red crosses).

A.1.3   Wind profile
Once the maximum sustained wind speed (v_{max}), pressure drop (Δp_c) and radius of maximum wind (*RMW*) of the hurricane track are available it is possible to create a surface wind field which is input for a numerical simulation.

A number of radial wind profiles exist (e.g., Willoughby et al. 2006; Fujita 1952); in this study Holland (2010) will be used. Holland (2010) revised the Holland (1980) parametric approach by applying additional information source for fitting purposes. In practice, this means that the exponential decay of the maximum wind speed after the radius of maximum wind is fitted with a source of additional information (e.g. hurricane archives, warning information or relationships).

In Holland (2010), the wind speed and pressure are determined by Equation (3) in which v_r is the sustained wind and p_r is the pressure both determined at a certain radius (*r*) compared to the radius of maximum winds (*RMW*). Reasoning from the eye of the hurricane, wind speeds

first increase till the *RMW* after that they start to decrease exponentially with the calibration factor *x* (default value: 0.5). The pressure increases exponentially from the eye. In the core of the hurricane core the pressure drop (Δp_c) is maximal. Further away from the eye the pressure starts to increase till the pressure of the soundings (p_n). Both the development of the wind speed and pressure are dependent of the Holland *b* parameter which is a combination of maximum wind speed, density of air and pressure drop.

$$v_r = v_{max} \left\{ \left(\frac{RMW}{r} \right)^b e^{\left[1 - \left(\frac{RMW}{r} \right)^b \right]} \right\}^x$$

$$p_r = p_n + \Delta p_c \exp\left(\frac{RMW}{r} \right)^b \qquad (3)$$

$$b = \frac{v_{max}^2 \cdot \rho_a * e}{100(p_n - p_c)}$$

Without additional information to fit the decay of the maximum sustained wind speed, a exponential decay by the power of 0.5 is used, because of the default value of the calibration factor *x,* see also Equation (3). When the wind profile is fitted with some additional information this calibration factor can either be larger than 0.5, which results in a slower decay further away from the core, or lower than 0.5, with the opposite effect. This calibration factor is therefore of great importance for the hurricane size and wind profile. Fitting of the parameter x is done according to Equation (4) in which x_n is the adjuected exponent at a observation radius r_n.

$$x = 0.5 + (r - RMW)\frac{x_n - 0.5}{r_n - RMW} \qquad (4)$$

In order to improve the accuracy of the surface wind fields created with Holland (2010), a relationship between the maximum sustained wind speed (v_{max}) and the radius of 35 knots wind speeds (*R35*) is derived based on the data from the JTWC for the Pacific. This relationship, see Figure A.3 is used to fit the wind profile of Holland (2010) and therefore determine an (improved) value for the calibration factor *x*. The result is Equation 5 in which $\Delta R35$ is dependent on the wind speed and latitude. The fit has a R^2 of 0.523, RMSE of 56 kilometres and it is only valid for the Pacific Ocean, since only track data from hurricanes in the Pacific Ocean is used. This relationship only describes the distances between the radius of maximum winds (RMW) and radius of 35 knots wind speeds (*R35*). In order to calculate (*R35*) one can apply Equation 6, since this describes the radius of 35 knots wind speeds from the eye instead of the distance from the RMW.

The effect can be seen in Figure A.4. For larger hurricanes the hurricane width is smaller with this relationship compared to Holland (2010), because the fit with R35 results in a faster decay, than without additional decay fitting.

$$\Delta R35 = 22.82 \cdot \left(v_{max} - 17.476 \right)^{0.4895} \cdot \left(1 + 0.02859 \cdot \gamma \right) \qquad (5)$$
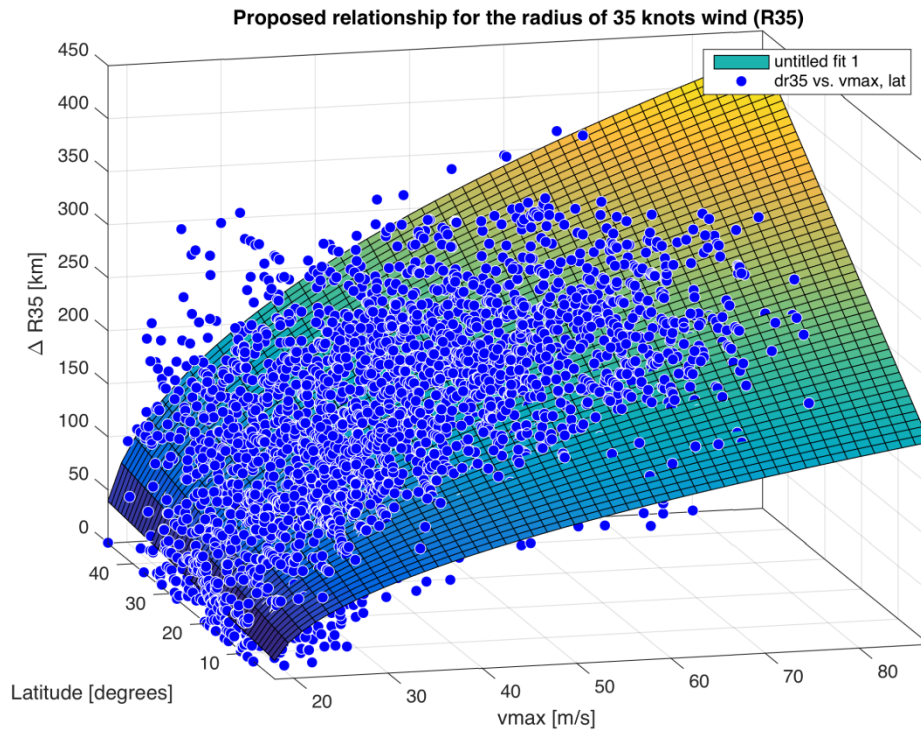
$$R35 = \Delta R35 + RMW \qquad (6)$$

Figure A.3 Modelled and observed R35 versus v_{max} and latitude for all hurricanes in the JTWC database. Each blue point is an observation point. The coloured surface represents the found relationship.
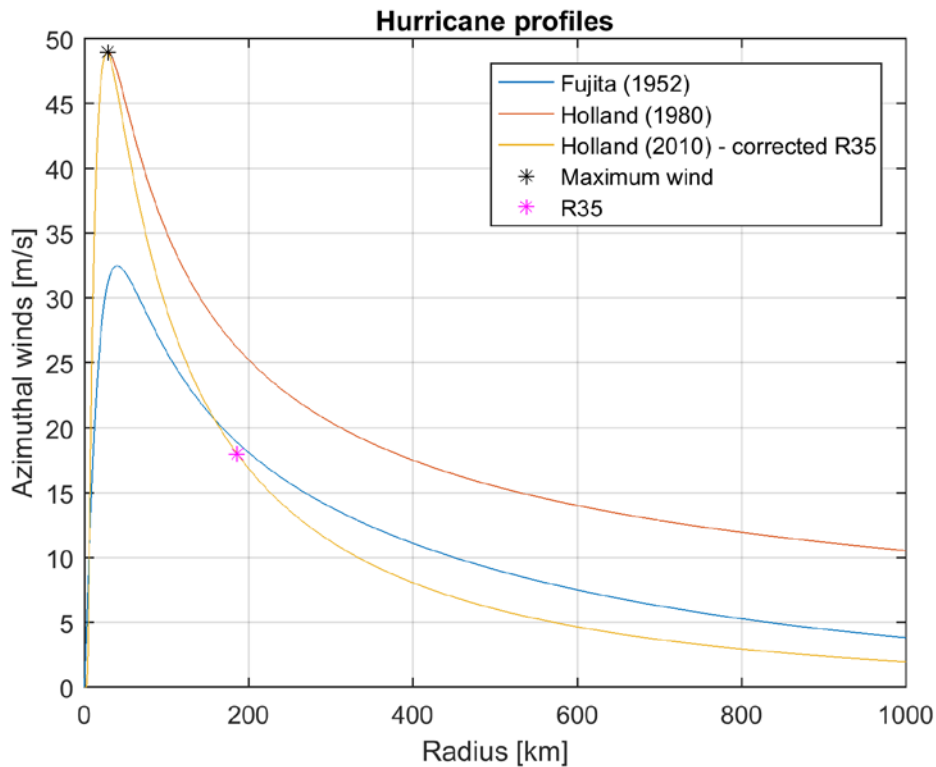

Figure A.4 Different wind profiles based on parametric relationships from literature (Fujita, 1952; Holland, 1980) and the newly derived relationship based on Holland 2010 and improved by using the R35 parameter.

A.1.4   Adjustments of modelled winds

Throughout this study a maximum sustained wind (v_{max}) is determined at a 10-m elevation over clear flat terrain and 1-minute averaged. The reason is to be consistent with the JTWC which also reports the maximum sustained surface winds in tropical disturbances in terms of 1-minute mean wind speed. Other nations, however, report maximum sustained surface winds averaged over a different time interval, which in many cases is 10-minutes.

Field observations are provided 10-minute averaged and converted to a standard 10-meter elevation. For height conversions Liu et al. (1979) is applied. For the conversion of 1-minute to 10-minute averaged wind speed, a conversion factor of 0.88 based on Holland (2008) is used.

This information is finally used in the Delft3D-Wave model based on the SWAN code (Ris et al.,1994) using 60-minute averaged wind speeds at a standard 10-meter elevation. A multiplication factor of 0.88 x 0.92 converts the 1-minute sustained wind speed to an hourly averaged wind speed.

A.1.5   Other relationships

Besides these relationships, the hurricane is described on a polar co-ordinate grid centred on the centre of the tropical cyclone, a so-called spiderweb (Stelling, 1999). The spider web included a number of settings related to the asymmetry of the storm but also physical and numerical constants:

- **Asymmetric structures** in wind speeds:
  – Asymmetry factor based on Schwerdt et al. (1979). Asymmetry is assumed to be the result from the forward motion of the storm
  – With a spatial distribution of asymmetry based on the factor *v/vmax* (i.e. letting it increase from 0 to RMW, and then decrease again)
- **Numerical settings**: 36 directional bins, 500 radial bins and maximum radius of 1000 km
- **Physical constants**: ρ_a of 1.05 kg/m^3 and p_c of 1012 mbar.

A.2   Validation: Hurricane Iniki (Hawaii, 1992)

A.2.1   Introduction

Hurricane Iniki was the most powerful hurricane to strike the U.S. state of Hawaii in recorded history. It formed on September 5, 1992, during the strong 1990–95 El Niño and attained tropical storm status on September 8. After turning north, see also Figure A.5, Iniki struck the island of Kauai on September 11 at peak intensity (category 4 on the Saffir–Simpson hurricane scale). It was the first hurricane to hit the state since Hurricane Iwa in the 1982 season, and the first major hurricane since Hurricane Dot in 1959. Iniki dissipated on September 13 about halfway between Hawaii and Alaska (NOAA, 1992).

In this study, Hurricane Iniki will be used to validate the newly derived parametric hurricane relations based on information about the track, maximum wind speed (v_{max}) and pressure (p_c) in reproducing wind speeds, pressure drops and wave height (in combination with SWAN) for several measurement locations available. Measurements of typhoons (i.e. generated winds and waves) are not available for the Marshall Islands; therefore this case study has been

used due to the large amount of available data and the fact that both Marshall and Hawaii are located in the same oceanic basin.
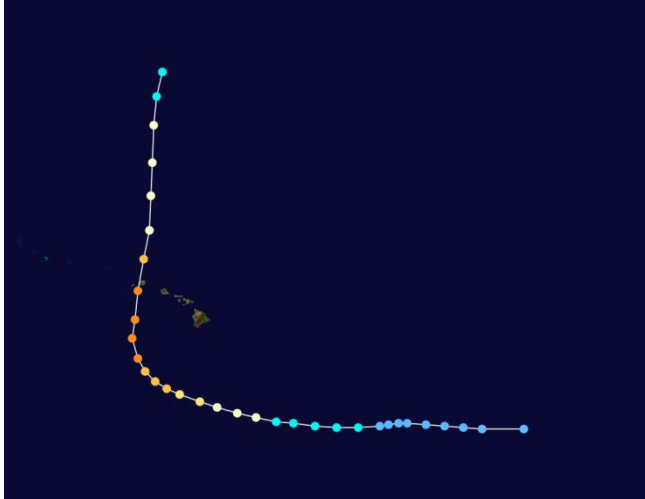

Figure A.5 Map with the track and intensity of the storm according to the Saffir–Simpson hurricane wind scale Red/yellow colours are hurricane categories (from yellow to red; increases intensity). Green is tropical storm category. Blue is a tropical depression.

A.2.2   Model setup

The hurricane track, wind speed and pressure are based on Joint Typhoon Warning Center (JTWC) accessed via the International Best Track Archive for Climate Stewardship (IBTrACS). The relationship from Section A.1 are applied to create a grid covering the hurricane surface field. Figure A.5 shows the best track with matching pressure and wind speed of Hurricane Iniki.

Two parametric wind models are applied. The first parametric wind field is based on the Holland (2010) <u>without</u> a fit for the wind profile which means the wind profile is similar to Holland (1980). The second parametric wind field is created <u>with</u> the use of a fit for the radius of 35 knots (*R35*) for Holland (2010) as described in Section A.1. The result is a more narrow wind profile.

Figure A.6 shows the location of two National Data Buoy Center (NDBC) moored buoys in the vicinity of the Hawaiian Islands during Hurricane Iniki. The storm passed within 250 and 73 km, respectively, of NDBC buoy 51002 and 51003, providing surface wind, pressure and wave measurements on the left and right side of the storm track. On top of that there are 3 stations on the Hawaiian Islands that recorded surface wind, pressure and water levels.

Table A.1   Applied best track with pressure, wind speed and classification.

Date/Time	Latitude	Longitude	Pressure	Wind Speed
(UTC)	(N)	(W)	(mb)	(m/s)
09/06/1800	12.2	140.0	1008	15.4
09/07/0000	12.3	141.1	1008	12.9
09/07/0600	12.3	141.7	1007	12.9
09/07/1200	12.2	142.4	1006	15.4
09/07/1800	12.1	143.0	1004	15.4
09/08/0000	12.0	144.5	1002	18.0
09/08/0600	12.0	146.0	1000	20.6
09/08/1200	12.1	147.5	1000	20.6
09/08/1800	12.3	149.0	996	25.7
09/09/0000	12.4	150.2	996	30.8
09/09/0600	12.7	151.6	992	33.4
09/09/1200	13.0	152.9	992	33.4
09/09/1800	13.4	154.3	984	41.1
09/10/0000	13.8	155.5	980	43.7
09/10/0600	14.3	156.9	960	46.3
09/10/1200	14.7	157.8	960	51.4
09/10/1800	15.2	158.6	951	51.4
09/11/0000	15.9	159.3	948	56.5
09/11/0600	16.8	159.8	947	59.1
09/11/1200	18.2	160.2	939	61.7
09/11/1800	19.5	160.0	938	64.3
09/12/0000	21.5	159.8	945	59.1
09/12/0600	23.7	159.4	959	51.4
09/12/1200	25.7	159.0	980	41.1
09/12/1800	28.1	158.9	980	41.1
09/13/0000	30.4	158.8	990	33.4
09/13/0600	33.0	158.7	990	33.4
09/13/1200	35.0	158.5	1000	25.7
09/13/1800	36.7	158.1	1002	20.6

A.2.3   Numerical model

A Delft3D-FLOW and WAVE model of the area of interest (Northing: 12 till 32 degrees, Easting: -170 till -150 degrees) has been created. The Delft3D-FLOW grid contains of 200 x 200 grid cells. In Figure A.6 the model grid and bathymetry are shown.
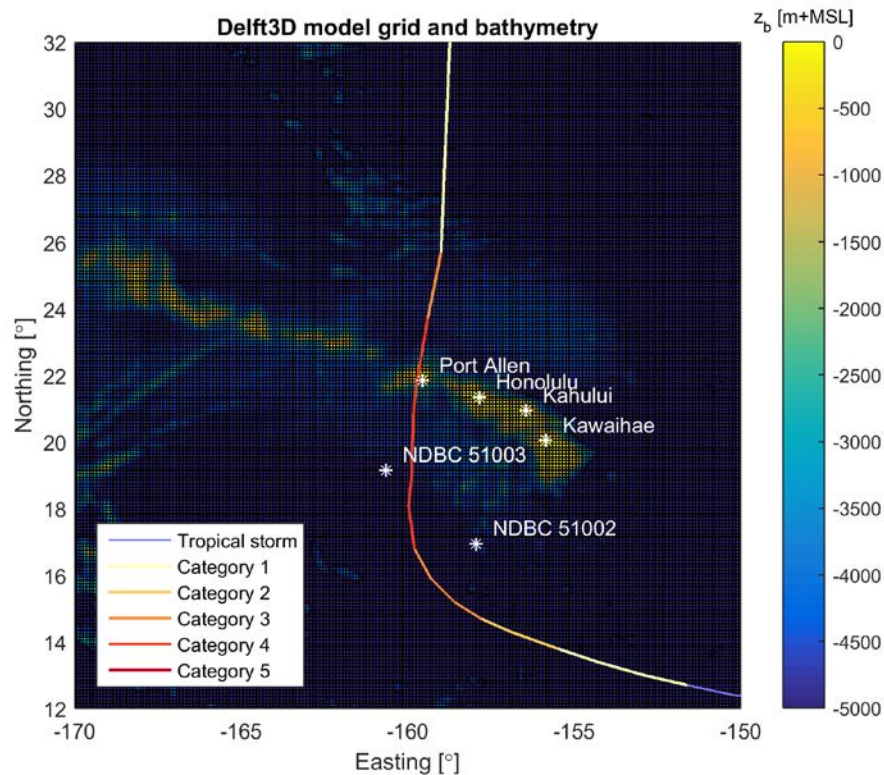
Figure A.6 Model setup: grid and bathymetry as used in the Delft3D model. The hurricane track is indicated with the coloured line. The buoy locations are also indicated in white.

A.2.4   Model results

<u>Wind speed and atmospheric pressure</u>
For meteorological observations (i.e. wind speed and pressure) five stations in the area can be used. First of all, two NDBC buoys south of Hawaii. Secondly, there are three stations on different islands of Hawaii. Port Allen was the only station on land strongly affected by Hurricane Iniki.

Port Allen was located (almost) in the eye of the storm. It is therefore expected that the applied maximum sustained wind and pressure provided by the JTWC would match the observations fairly closely. However, modelled wind speeds were substantially higher than the observed wind speeds (45 m/s modelled versus 30 m/s observed) (Figure A.7). It is hypothesised that this is related to the impact of the rough, irregular ground on the island since the data from JTWC are determined over clear flat terrain. The difference between the wind speeds modelled with and without R35 relationship are small for the maximum observed wind speed. For the winds some hours before and some hours after impact, one can see that the wind speeds are overestimated without R35 correction.

For atmospheric pressure at Port Allen there is an overestimation of the pressure (p_c), see Figure A.8, of about 5 mbar (underestimation of the pressure drop of +/- 10%) and there is no difference between the two parametric pressure fields. This is because the fitting coefficient x is only affecting the wind profile and not the distribution of the atmospheric pressure. For the atmospheric measurements at Honolulu there is little pressure drop observed and this small

effect is captured by the model, as can be seen in the upper left panel of Figure A.8. This gives confidence in the distribution of the atmospheric pressure.

For the two NDBC buoys (51002 and 51003) the atmospheric pressure is overestimated. For the modelled pressure drop is 5 and 12 mbar, the measured drop is 13 and 17 mbar for respectively buoy 51002 and 51003. For the wind speeds modelled with the R35 relationship (yellow line) there is an underestimation of 51002 (east of the track; +/- 2 m/s too low) and an overestimation of 51003 (west of the track; +/- 10 m/s too high), see also Figure A.6. This incorrect reproduction of the pressure and wind speed could be related to a number of reasons (i.e. incorrect track / intensity / parametric relationships, etc.), however the improvement of the parametric surface wind field by applying the R35 relationship is clear. Especially for buoy 51002, which is further away from the eye, there is a substantially more accurate reproduction of the wind speed. When applying Holland (2010) without this correction wind speeds further away from the core tend to be overestimated.

In Figure A.9 and Figure A.10 the maximum modelled wind speed is presented. In these Figures one can see that mainly the island of Kauai is influenced by wind speeds larger than 25 m/s. Winds at the east-side of the core tend to be higher, due to the asymmetry in the hurricane. Without the R35 correction (Figure A.9) the wind speed at the Hawaiian Islands would be strongly overestimated, as can be seen by the difference between the surface plot and the observation circles. With this R35 relationship (Figure A.10) maximum wind speeds are more in line with observations, however the observation at Port Allen is not in line with the modelled wind speeds. It is hypothesised that this is related to the impact of the rough, irregular ground on the island.

The applied meteorological forcing is based on a set of parametric relationships and therefore, logically, not fully in line with observations since hurricanes do not follow these relationships one-on-one (i.e. there is quite some natural spreading between different hurricanes). The overall patterns are however captured with the applied forcing. However, it is expected a priori that the errors in the applied wind field may result in (additional) errors in the modelled waves, despite the improved relationship will try to minimize these errors.
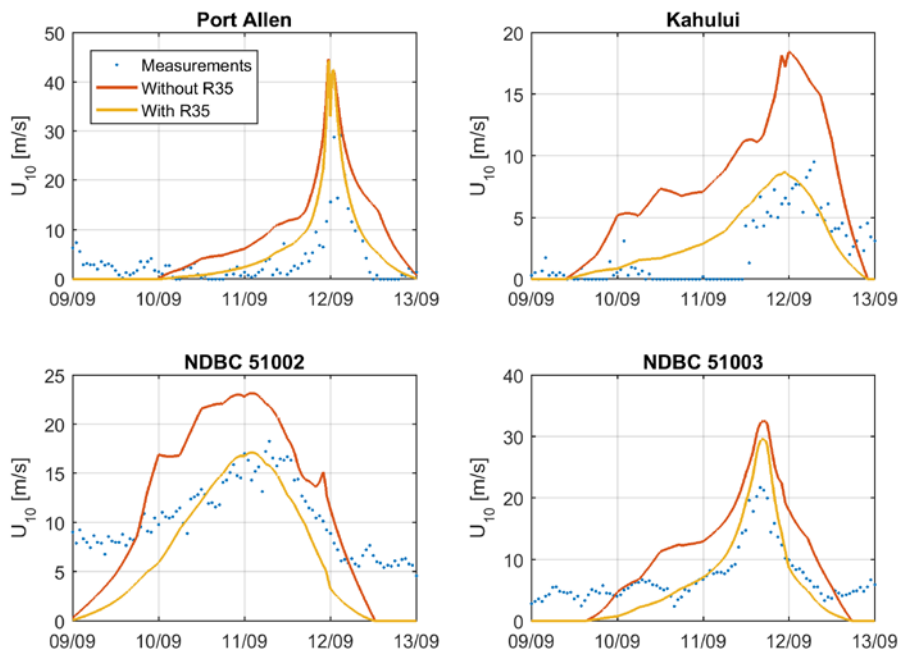
Figure A.7   Time series of measured and modelled 10-minute averaged wind speeds 10 m above sea surface. The dark brown line shows the modelled wind speed computed using the default Holland (2010) relationship; the light brown line the wind speed computed based on the improved Holland (2010) relationship by using the R35 information in Section A.1.3.
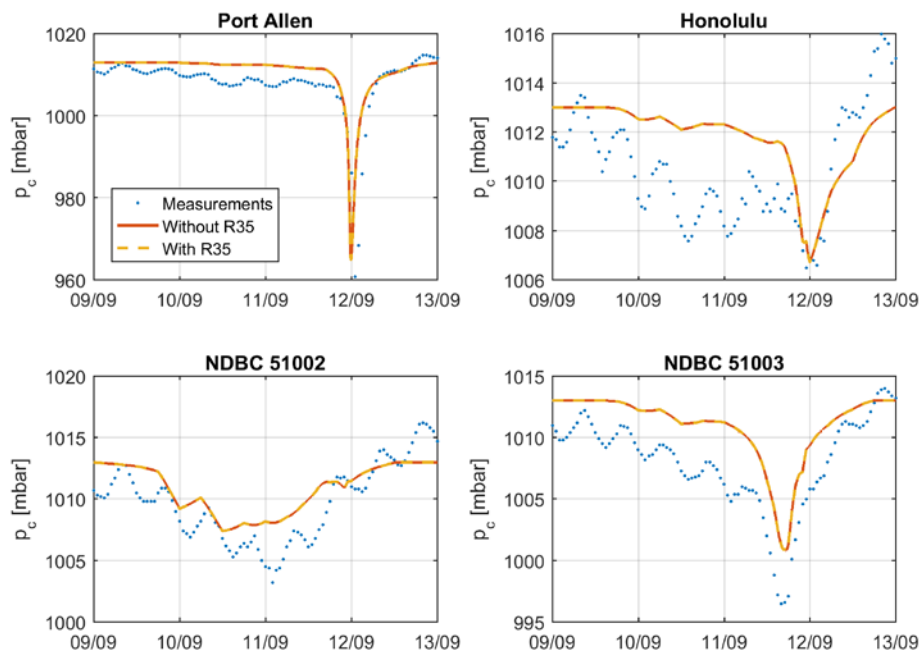

Figure A.8   Time series of modelled at measured atmospheric pressure in mbar. The dark brown line shows the modelled atmospheric pressure computed using the default Holland (2010) relationship; the light brown line the wind speed computed based on the improved Holland (2010) relationship by using the R35 information in Section A.1.3.
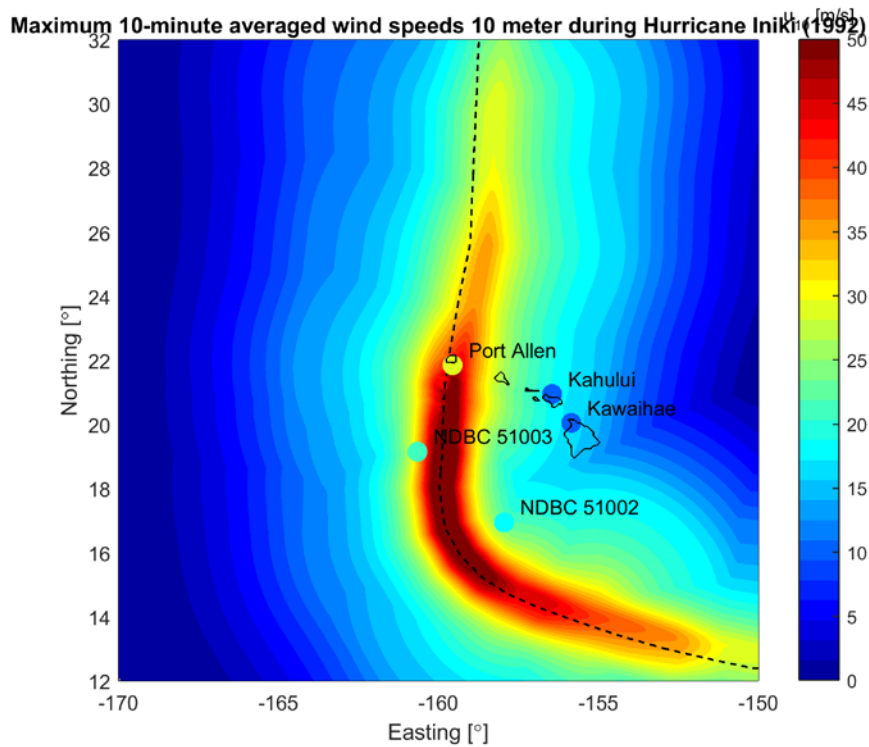
Figure A.9 Maximum measured (dots) and modelled (field) 10-minute averaged wind speed 10 m above sea surface during Hurricane Iniki (1992) without R35 correction.
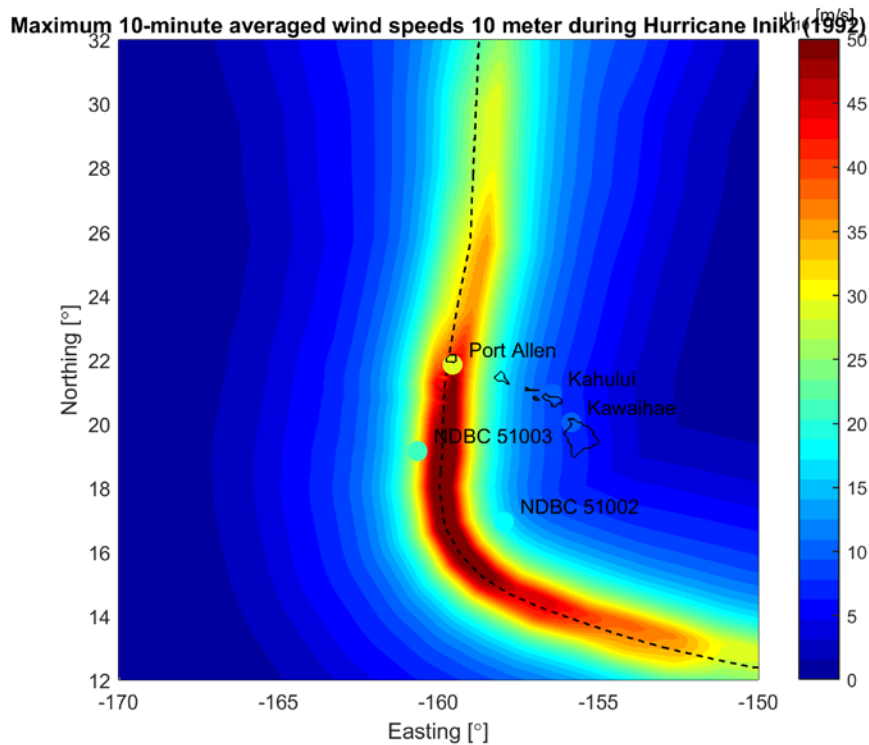

Figure A.10 Maximum measured (dots) and modelled (field) 10-minute averaged wind speed 10 m above sea surface during Hurricane Iniki (1992) with R35 correction.

Wave height

For validation of the computed wave parameters (i.e. wave height), wave observations at the two NDBC buoys were used. Both buoys were not severely impacted by Hurricane Iniki (Hs < 6.0 meters) since the distance to the eye was respectively 250 (buoy 51002) and 73 kilometres (buoy 51003). However, the information from these buoys is important to validate the computation of the maximum significant wave height observed.

For buoy 51002, without the R35 correction, wave heights are strongly overestimated (modelled: Hs > 8 meters and observed: Hs = 6 meter) (Figure A.11). This is directly related to the overestimation of the wind speed and the width of hurricane (i.e. wind fetch). Hence, a larger fetch and higher wind speed will results in a higher significant wave height. With the R35 relationship the wave heights are slightly underestimated, of a similar magnitude as the underestimation of the wind speed (variation in wind speeds and wave heights of +/- 10-20%).

For buoy 51003 there is a (large) overestimation. Wave heights did not exceed the 6 meter in the measurements, but in the SWAN model the waves are much higher (8 - 9 meters). The R35 relationship has less impact compared to buoy 51002 since this buoy is closer to the core of the hurricane and therefore are less influenced by the fitting parameter *x* in Holland (2010). Again, the overestimation in the wind speed leads to an overestimation of the wave height (variation in wind speeds and wave heights of +/- 30-40 %).
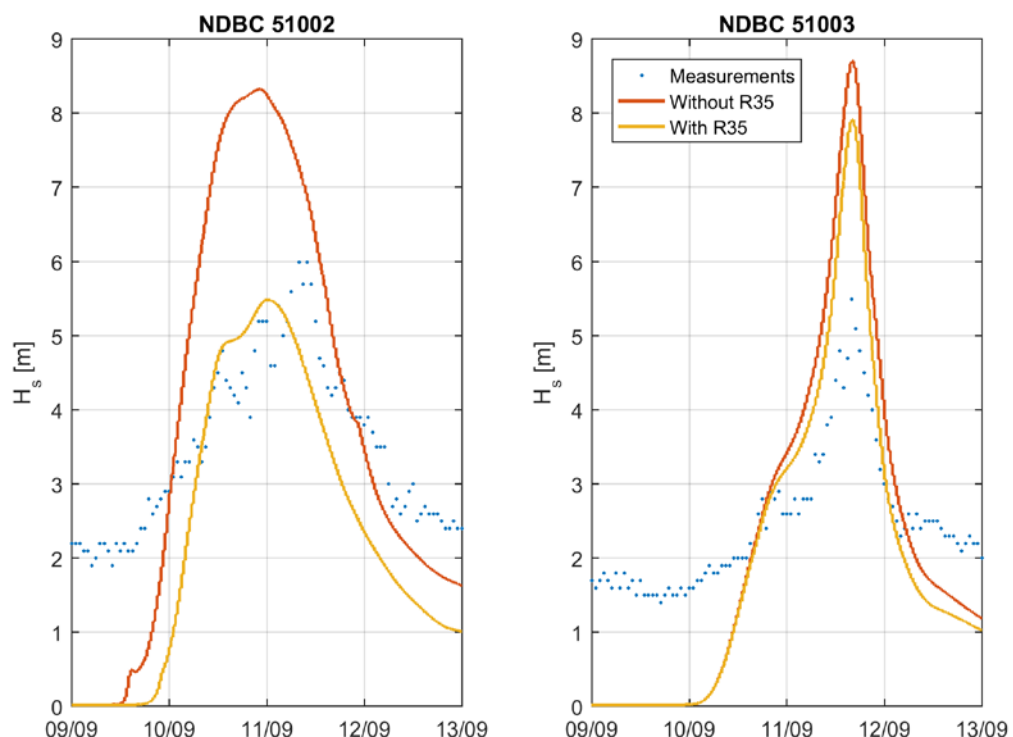

Figure A.11 Time series of modelled at measured wave height in meters.

<u>Water levels</u>
For water level observations the two NOAA buoys at the Hawaiian Island of Kauai and Oahu have been used, see Figure A.6 at Port Allen and Honolulu. Port Allen recorded water levels of around 1.44 meter +MSL. Honolulu was less impacted and the recorded high water was about 0.73 meter +MSL.

In Figure A.12 the model results are presented. The water level is underestimated quite significantly (Port Allen: modelled: 0.9 m +MSL, measured: 1.4 m +MSL). As modelled, the water level elevation consists of the astronomical tide, the atmospheric pressure drop and wind driven surge. Compensating for the incorrect pressure (5 mbar more pressure drop) will result in a +/- 5 centimetres higher surge level and is thus not enough to compensate the difference between the measurements. The hypothesis is that the difference between the model and observation is in large part due to the effect of wave-driven setup especially since observation point is located in a sheltered port. This is not taken into account in the model since this would require a higher resolution model.

For Honolulu something similar is observed. The underestimation is however a factor 2 less (modelled: 0.4 m +MSL, measured: 0.7 m +MSL), but also the simulated wave height is factor 2 lower. This supports the hypothesis that wave set-up could be reasonable for the observed difference in the model and measurement. In the Ebeye model, the Delft3D results will be used to drive the higher resolution XBeach model which does include wave-induced setup.
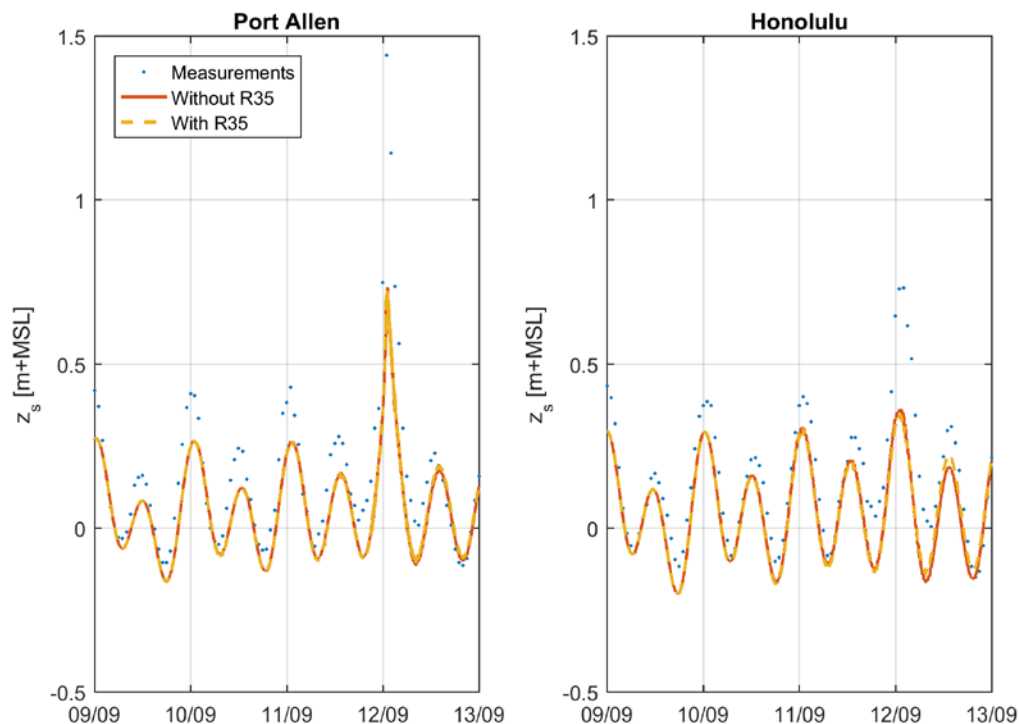

Figure A.12 Time series of modelled at measured water level in meters + MSL.

A.2.5   Conclusions
The performance of two Holland wind profile models described in Section A.1 to reproduce the wind measurements at land and at two buoys has been evaluated. The parametric wind field based on Holland (2010) including a fit for the radius of 35 knots wind (R35) resulted in a significant improvement in reproducing the observed wind speeds and wave height.

When applying Holland (2010) without an additional fit it is not possible to accurately reproduce both the core and external wind structure in hurricanes. The effect will be an overestimation further away from the eye. Applying a fit on the wind profile reproduction of the external wind structure greatly improved the results since the maximum sustained wind speed decreases more quickly further away from the core, also resulting in an improvement of the wave height prediction. Surge levels were underestimated; it is hypothesised that this is related to wave-induced setup. In fact, measurements were obtained within a harbour, while the model does not have the sufficient accuracy to resolve these shallow water processes.

B   On the effects of mining pits

B.1   Introduction

Several stretches of reef surrounding Kwajalein Atoll, such as the reefs fronting Ebeye and Kwajalein, show signs of human interventions. Reef flats have been mined for coral rock, leaving pits behind with depths of typically 1-4 m (Figure B.1; a-c). Exploration of these borrow pits during the field visit showed that, although some of them are used as dumping ground for waste (Figure B.1; d), others are also host to an abundance of new corals and sea-life (Figure B.1; e,f). This indicates that the reefs are able to, at least partially, recover from mining activities. The recovery of reefs after such interventions is known to be problematic and can take more than 50 years, which is why coral rock mining is mostly associated with reef degradation and the loss of ecosystem complexity (Brown and Dunne, 1988).

Only little research has been carried out on the effects of borrow pits on reef hydrodynamics. For an 80 m wide fringing reef flat at Majuro Atoll, Ford et al., (2013) conducted an experimental field study on the effects of borrow pits on wave heights in the near shore region. They found that wave heights near the coastline had decreased by 8% in presence of a borrow pit. This was mainly a result of less infragravity (i.e. long wave) energy, as short wave heights were slightly higher than measured at a comparable location without borrow pit. Since these conclusions are based on measurements at a single site they can not be generalized for other reefs, where the effect of borrow pits on reef hydrodynamics may be different (Ford et al. 2013; Yao et al., 2016).

In this annex, the XBeach model used to assess the coastal risks at Ebeye (Chapter 7) was applied to investigate the possible effects of mining pits on short and long wave heights towards the coast. This activity, although not directly part of the project, has been carried as side investigation during the project upon client request. Therefore, results are only presented for a limited number of conditions. For more general results, a full modelling study on the effects of mining pits of different geometries and in different conditions, on the local hydrodynamics and sediment transport would be required.
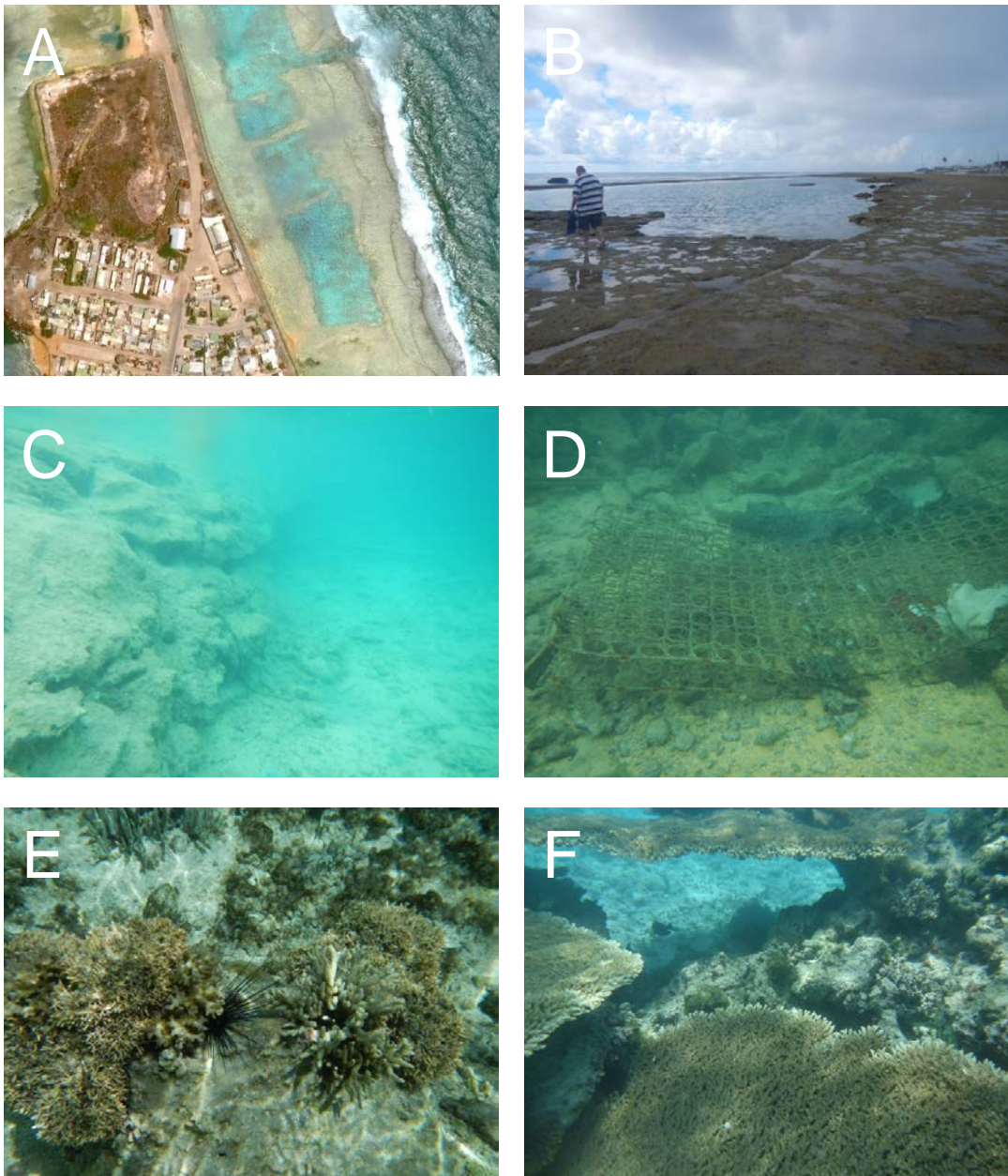
Figure B.1   Aerial view and photographs of mining pits at Ebeye island.

B.2   Effect of mining pits on wave conditions at Ebeye

For an assessment of the possible effects of mining pits at the study site of Ebeye, the results from the XBeach model simulations, considering large swell conditions and with different return periods, were used (Section 6.3.1). Wave heights and water levels were compared at different cross-shore transects located in the north and north-east of the island. In particular, transects at which mining pits were present (Figure B.2 a, red lines) and transects just next to these pits Figure B.2 a, black lines). In particular, the figures refer to a swell event with a return period of 10 years. However, similar results were obtained for events with different return periods.

Figure B.2 b shows that wave-induced setup (green line) is hardly influenced by the presence of the mining pits. Nevertheless, the mining pits have an effect on the short (Hs_{hf}, blue line) and long (Hs_{lf}, red line) wave height. Most of the short wave dissipation occurs in the region of wave breaking at the outer reef edge, after which dissipation continues, at slower rate, over the reef flat. For a standard profile (with no mining pit), the short wave dissipation over the reef continues. However, in the presence of a borrow pit, the short wave dissipation is almost zero due to the reduced effect of bottom friction at higher water depths, which in turn results in higher wave energy at the coastline. This is consistent with the findings from Ford et al., 2013 and Yao et al., 2016.

On the other hand, long wave heights are lower in the case of a borrow pit. Generally, long waves on a reef flat grow by the release of momentum from the breaking of short waves (Symonds et al., 1982; Pomeroy et al., 2012). Hence, the reason for long wave heights being lower, is that less short wave energy is dissipated and transferred to the lower wave frequencies.

Figure B.2 c shows short and long wave heights at all different transects, with and without borrow pit (respectively black and pink circles). The average values of the two clouds of points are also indicated by the two stars. In general, it is clear how the pits lead to a shift towards higher short wave heights and towards lower long wave heights. On average, significant short wave heights at the coastline for cases with a borrow pit were ca. 20% higher ($\approx$ 10-12 cm depending on the offshore swell return period), while long wave heights were 4% lower.

However, it is important to keep in mind that the construction of mining pits may also have additional side effects, with possible negative consequences. One possible effect could be the local focussing and defocusing in wave energy due to wave diffraction over the reef. This may generate gradients in alongshore wave energy, which may lead to local hot spots of erosion. Furthermore, waves may become trapped between the coast and the borrow pit and start to resonate, which leads to high water levels. Moreover, local alongshore gradients in wave breaking over the reef may also lead to difference in water level set-up and possible return currents over the reef, under specific wave angles and wave height conditions. Return currents can lead to an offshore transport of sediments inside the mining pits which will be removed from the coastal system, also leading to erosion. These aspects were also mentioned among additional implications of mining pits by Ford et al. (2013).

However, in order to investigate the complete range of all these aspects and draw general conclusions, a full modelling study on the effects of mining pits would be required. This study should include the simulation of the effects of mining pits under different wave conditions (i.e. wave heights, wave angles and periods), under different water levels, and for mining pits with a different geometry (i.e. depth and distance from the coastline).
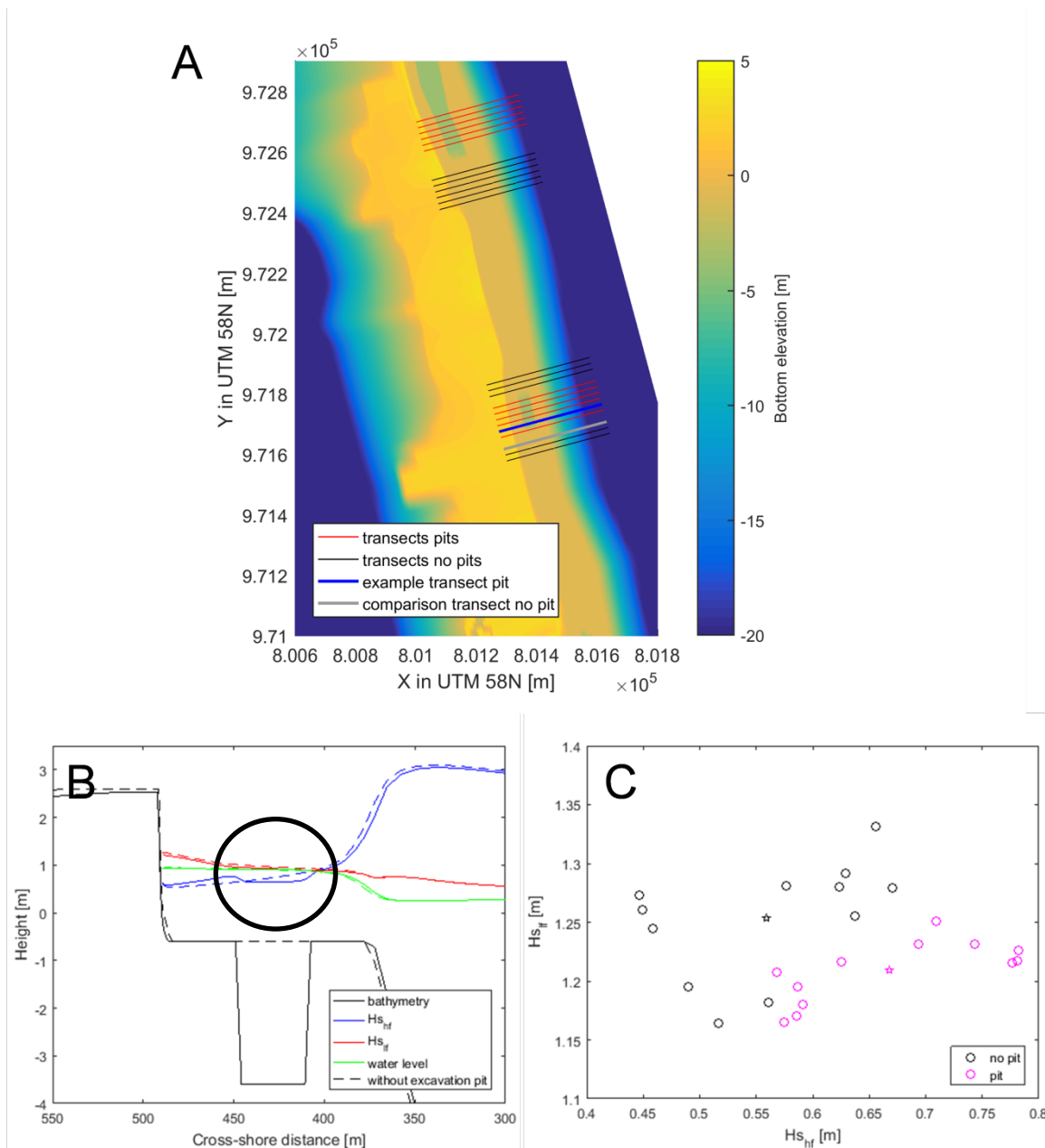
Figure B.2 Effect of excavation pits on wave heights and water levels at Ebeye. (A) Transects used for the analysis: red transects cross borrow pits whereas black transects are located next to borrow pits. The two transects that are highlighted blue (borrow pit) and grey (no borrow pit) indicate the location of the example data used in subfigure b). (B) Cross section of bathymetry (black), significant short wave heights (Hs$_{hf}$;blue), significant long wave heights (Hs$_{lf}$;red) and water levels (green) for a wave height with return period of 10 years and in presence of an excavation pit. The same parameters are plotted with dashed lines for the reference transect without borrow pit that was used for comparison (see grey transect in subfigure a). (C) Hs$_{hf}$ and Hs$_{lf}$ at the coastline for all the transects with borrow pit (magenta) and without borrow pit (black) and for an offshore wave height return period of 10 years. Stars resemble the averages of the point clouds.

C Alternative (temporary) designs

During the preparation process of the PREP, the government expressed its strong preference to make sure that the largest portion of the coast at the ocean side would be protected. Therefore, alternative designs which would reduce the overall quantity of the required material as well as the costs per linear meter have been explored.

To address this request by the government, the following design (i.e. tandem breakwater) was elaborated (Figure C.1) and discussed during the appraisal mission of the project (February 2017). The design includes a breakwater and a revetment. The general philosophy of this design is that it could be used as temporary solution before funds will become available to complete the structure by adding the berm between the breakwater and the revetment, as discussed in Chapter 9.

However, it has to be noted that this temporary design will result in more damages and higher overtopping rates until the structure is not completed.
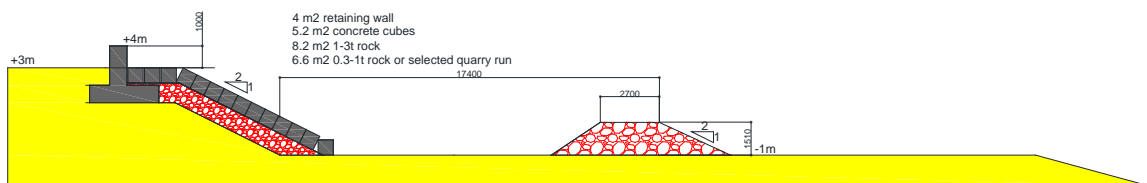

Figure C.1 Tandem breakwater (temporary design).

This design will result in a reduction of almost 35% of the costs for a berm breakwater. Physical modeling should reveal if the effect (inducing wave breaking) of the first low crested breakwater is sufficient or whether a slightly higher mound is needed. Moreover, it will be important to test and evaluate the number of concrete blocks required at the toe of the revetment in order to grant the stability of the structure.

Table C.1 Costs for tandem breakwater per linear meter.

	Tandem breakwater cube armour 1	
	Volume m^3/m	Costs USD
Armour rock 3-6t m^3		-
Armour rock 1-3t m^3	8.2	992
Aggregate/Underlayer 0.3-1t or selected QR m^3	6.6	426
Mass Concrete (Standard 30Mpa) including formwork m^3	4	1,935
Mass Concrete (Standard 30Mpa) including formwork m^3	5.2	2,516
Local transport	15.8	1,911
Primary port transport	8.2	3,306
Costs per running meter USD		**11,085**

Another option for reducing overall costs could be for instance to decrease the width of the berm by 5 m, which could result in a cost reduction of 2,500 USD per linear meter with respect to the design as presented in Chapter 9 (i.e. approx. 14,000 USD per linear meter breakwater; Figure C.2). Also in this case, physical modeling is required to get a better understanding of the wave breaking process (i.e. at which cross-shore location wave breaking takes place) as well as for the optimization of the design.

A summary table with indicative costs for the different designs and for different lengths is provided (Table C.2), additional to Table 9.12 as in the report. In the table, the last two columns to the right does not correspond to any of the alternatives as presented in the report, but they have been added as cost values roughly correspond to the budget which would become available through the GCF proposal (i.e. ≈ US$ 20 million).
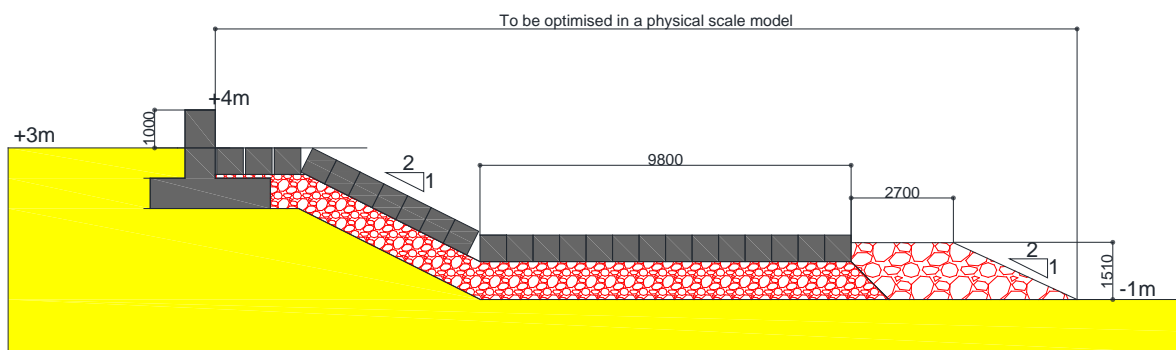

Figure C.2 Breakwater with reduced berm width.

Table C.2 Summary table with indicative costs for the different design options and for the different alternatives. Values in the table provide costs in million US$.

Length (m)	2,000 (Alternative 1,2)	1,060 (Alternative 7,8)	1,440	1,800
Standard option	28.0	14.8	20.2	25.2
Berm option	32.6	17.3	23.5	29.4
Tandem breakwater	22.2	11.8	16.0	**20.0**
Breakwater with reduced berm width	27.7	14.7	**19.9**	24.9

Deltares